

Design and Synthesis of Novel Lanthanide  
Chelates for use in Magnetic Resonance  
Imaging (MRI)

Thesis Submitted for the Degree of  
Doctor of Philosophy  
at the University of Leicester

by

Graeme James Stasiuk MChem (Leicester)  
Department of Chemistry  
University of Leicester

May 2010

## Abstract

This thesis reports a series of novel Ln-DO3A based complexes, modulation of emission intensity (Eu and Tb) has been achieved and relaxivity,  $r_1$ , (Gd) has been shown.

Propargyl-appended lanthanide complexes derived from DO3A, has a hydration state,  $q = 2$ . They undergo Cu(I) catalysed cycloaddition reactions with azides to form 1,2,3-triazole appended complexes: coordination of one of the triazole nitrogen atoms to the metal centre changes the local coordination environment and luminescence studies indicate a hydration state of  $q = 1$ .

Propargyl-appended Ln(III) complexes show unanticipated reactivity towards  $\text{NaN}_3$  in the Cu(I) catalysed ‘click’ reaction yielding an unsubstituted 1,2,3-triazole. The resulting Eu(III) complex exhibits pH-responsive  $^1\text{H}$  NMR and Ln(III) luminescence behaviour in the physiological pH range, consistent with deprotonation of the NH-acidic bound triazole. The coordination mode of the NH-triazole switches from NH-triazole bound in a pyridinic manner to bound in an anionic manner as a triazolide, while retaining a  $q = 1$ . This was demonstrated in luminescent studies of Eu(III) and Tb(III) complexes with a  $\text{p}K_a \sim 7.5$ . Relaxation measurements on the Gd(III) analogue show a  $q = 1$  throughout the pH range, *i.e.* no change in hydration state.

To overcome the unanticipated reactivity of  $\text{NaN}_3$  with propargyl-appended Ln(III) complexes, *p*-ethynylbenzyl-appended Ln(III) complexes were synthesised. These show promise as precursors for multimeric, self-associating and *d-f* hybrid complexes, *via* the Cu(I) catalysed cycloaddition or ‘click’ reaction. Luminescent studies show evidence of the formation of 1,2,3-triazoles that do not bind to the Ln(III) metal centre, with a hydration state  $q = 1$ . These complexes have been applied in the synthesis of multimeric, self-associating and *d-f* hybrid compounds.

Uridine was attached to a EuDO3A chelate *via* four different linkers. These complexes are precursors for an accumulation and activation strategy, developed as enzyme activated contrast agents. Neutral  $q = 1$  Eu(III) uridine-DO3A based complexes were successfully synthesised and linked *via* a propyl, amide or 1,2,3-triazole unit.

## **Acknowledgements**

Firstly, I would like to say thanks to my supervisor Dr Mark Lowe, for all his support and guidance during my PhD, as well as previous members of the group: Dr Jackie Hamblin, Dr Marco Giardiello, Dr Rowena Griffin, Mark Walton and Joseph Philips. A big thank you to all the other members of the lab group, as well as Dr Gerry Griffith for the NMR analysis, Dr Graham Eaton for the mass spectrometry and Kuldip Singh for X-ray Crystallography.

Secondly, I'd like to acknowledge Prof. Mauro Botta at the Università del Piemonte Orientale, Italy and the rest of his research group: especially, Stefano Avedano and Dr Filip Kielar for hosting me in Alessandria and allowing me to run and collect all the relaxation measurements and data.

Also, thanks to my Mum, Dad and my brothers for their support throughout my PhD, as well as all my friends, especially Tim, John, Sophie, Chris, Rob, Phil and Youcef who helped to take my mind off work. I would also like to say a special thank you to Emily for all her love and support throughout my PhD.

Finally, I'd like to thank the EPSRC and The University of Leicester for funding.

## Abbreviations

Å	Angstroms
aDO3A	1,4,7-tris[(4'-(carboxyl)-1'-carboxybutyl)-1,4,7,10-tetraazacyclododecane
a.u.	Arbitrary units
B <sub>0</sub>	magnetic field
BFP	Blue fluorescent protein
B.M.	Bohr Magnetron
Bp	Boiling Point
BPCA	Blood Pool Contrast Agent
<i>C</i>	Molar concentration of paramagnetic compound
Calcd	Calculated
CD	Cyclodextrin
CEST	Chemical Exchange Saturation Transfer
<i>Cf.</i>	confer (compare)
cm <sup>-1</sup>	Per centimetre
C.N.	Coordination number
COSY	Correlation spectroscopy
CT	Computed tomography
Cyclen	1,4,7,10-tetraazacyclododecane
°C	Degrees Centigrade
δ	Delta (NMR Chemical Shift)
δ	Delta (Chelate Ring Helicity) Right Hand
Δ	Delta (Change in) or Configurational Chirality, Right Hand
Da	Dalton
DAB	Diaminobutane
Δ <i>G</i>	Gibbs Free Energy Change
Δ <i>H</i>	Enthalpy Change
Δ <i>S</i>	Entropy Change
DCM	Dichloromethane
DFT	Density Functional Theory
DMAP	Dimethylaminopyridine
DO3A	1,4,7-tris(carboxymethyl)-1,4,7,10-tetraazacyclododecane

DO3MA	1,4,7-tris(1'-carboxyethyl)-1,4,7,10-tetraazacyclododecane
DOTA	1,4,7,10-tetraazacyclododecane-1,4,7,10-tetraacetic acid
DOTAM	1,4,7,10-tetraazacyclododecane-1,4,7,10-tetraacetamide
DMF	Dimethyl formamide
DNA	Deoxyribonucleic acid
DTPA	Diethylenetriaminepentaacetic acid
DTTA	Diethylene Triamine Tetraacetic Acid
ED	Electrical Dipole
EDTA	Ethylenediaminetetraacetic acid
<i>e.g.</i>	<i>exempli gratia</i> (for example)
ENDOR	Electron-nuclear double-resonance
ESMS	Electrospray Mass Spectrometry
EtOH	Ethanol
eV	Electronvolts
Exp	Experimental
<sup>18</sup> F-FDG	<sup>18</sup> F-labelled glucose (fluorodeoxy glucose)
FAB	Fast Atom Bombardment
FHBG	9-(4-[ <sup>18</sup> F]-fluoro-3-hydroxymethylbutyl)-guanine
FID	Free Induced Decay
FIAU	5-iodo-2'-fluoro-2'-deoxy-1-β-D-arabino-furanosyl-5-iodouracil
g	Grams
GIST	Gastrointestinal Stromal Tumours
gDO3A	1,4,7-tris[(3'-(carboxyl)-1'-carboxypropyl)-1,4,7,10-tetraazacyclododecane
gDOTA	1,4,7,10-tetra-azacyclododecane-1,4,7,10-tetraglutamic acid
GFP	Green fluorescent protein
HIV	<i>Human immunodeficiency virus</i>
HOPO	Hydroxypyridonato
HPLC	High-performance liquid chromatography
HSA	Human Serum Albumin
HSV-TK	Herpes Simplex Virus 1 Thymidine Kinase
Hz	Hertz
<i>I</i>	Spin (quantum number of a nucleus)
$\gamma$	Gyromagnetic Ratio

ICP-MS	Inductively Coupled Plasma Mass Spectrometry
<i>i.e.</i>	id est (that is)
<i>in vitro</i>	In an artificial environment outside a living organism
<i>in vivo</i>	Within a living organism
IR	Infrared
ISC	Intersystem Crossing
<i>in situ</i>	in the reaction mixture
K	Kelvin
KJ mol <sup>-1</sup>	Kilojoules Per Mole
$\lambda$	Lambda (Chelate Ring Helicity) Left Hand
$\Lambda$	Lambda Configurational Chirality, Left Hand
$k_{ex}$	Water exchange rate
$k_{H_2O/D_2O}$	Rate constant in H <sub>2</sub> O/D <sub>2</sub> O
$\lambda_{ex}$	Wavelength of Excitation
$\lambda_{em}$	Wavelength of Emission
$\lambda_{max}$	Wavelength of Maximum Emission/Absorption
LIS	Lanthanide Induced Shift
LMCT	Ligand to Metal Charge Transfer
M	Molar
M <sup>-1</sup>	Per Molar
$\mu$ g	Microgram
$\mu$ l	Microlitre
$\mu$ M	Micromolar
$\mu$ mol	Micromole
mg	Milligram
cm <sup>3</sup>	Millilitre
mM	Millimolar
mM <sup>-1</sup> s <sup>-1</sup>	Per Millimolar Per Second (units of relaxivity)
mmol	Millimole
ms	Millisecond
ms <sup>-1</sup>	Per Millisecond
MALDI	Matrix Assisted Laser Desorption Ionisation
MD	Magnetic Dipole

MeCN	Acetonitrile
MeOH	Methanol
MHz	Megahertz
MLCT	Metal to Ligand Charge Transfer
MR	Magnetic resonance
MRA	Magnetic Resonance Angiography
MRI	Magnetic resonance imaging
$N_{\text{eff}}$	Effective magnetic moment
nm	Nanometres
NMR	Nuclear magnetic resonance
NMRD	Nuclear Magnetic Resonance Dispersion
NOE	Nuclear Overhauser Effect
ns	Nanosecond
PAMAM	Polyamidoamide
PARACEST	Paramagnetic Chemical Exchange Saturation Transfer
PBS	Phosphate Buffered Saline
PEG	Polyethylene Glycol
PGA	Poly(L-glutamic Acid)
PET	Positron emission tomography
ppm	Parts per million
ps	Picosecond
$q$	Number of inner sphere water molecules/ hydration state
QD	Quantum Dot
$r_1$	Relaxivity
$R_1$	Longitudinal relaxation rate of water protons
rad s <sup>-1</sup>	Radians Per Second
Rf	Retention fraction
RIME	Receptor induced Magnetisation Enhancement
RF	Radio frequency
S	Singlet electronic state
SAP	Square Antiprismatic
SPECT	Single photon emission computed tomography
T	Tesla

$T_1$	Triplet electronic state
$T_1$	Longitudinal relaxation time
$T_2$	Transverse relaxation time
TAFI	Thrombin-Activatable Fibrinolysis Inhibitor
<sup>t</sup> BuDO3A	1,4,7-tris(tert-butoxycarbonylmethyl)-1,4,7,10-tetraazacyclododecane
TFA	Trifluoroacetic acid
THF	Tetrahydrofuran
TMS	Tetramethylsilane
tri	NH-1,2,3-triazole
tri <sup>-</sup>	deprotonated 1,2,3-triazole
TRITC	Tetramethylrhodamine-5-isothiocyanate
TSAP	Twisted Square Antiprismatic
$\tau_m$	Mean residence lifetime of a water molecule coordinated to a metal ion
$\tau_R$	Molecular reorientation time
$\mu$	Magnetic moment
UV	Ultraviolet
<i>via</i>	By means of
$\nu_{max}$	Maximum Vibrational Frequency
<i>vs.</i>	Versus
VT	Variable Temperature
$\omega_L$	angular velocity
$\omega_o$	angular frequency
Wt	Weight
ZFS	Zero Field Splitting

# Contents

Abstract	I
Acknowledgments	II
Abbreviations	III
Contents	VIII
<b>Chapter 1 Introduction</b>	<b>1</b>
<b>1.1 Molecular Imaging</b>	<b>1</b>
1.1.1 <i>In-Vivo Molecular Imaging</i>	1
<b>1.2 Magnetic Resonance Imaging</b>	<b>2</b>
1.2.1 <i>Principles of Magnetic Resonance Imaging</i>	3
1.2.2 <i>Principles of NMR</i>	4
1.2.3 <i>NMR Signal</i>	7
1.2.4 <i>Longitudinal (Spin-Lattice) Relaxation Time, <math>T_1</math></i>	9
1.2.5 <i>Measurement of <math>T_1</math>: the Inversion Recovery Experiment</i>	9
1.2.6 <i>Transverse (Spin-Spin) Relaxation Time, <math>T_2</math></i>	10
1.2.7 <i>Measurement of <math>T_2</math>: The Hahn Spin Echo Experiment</i>	11
1.2.8 <i>Magnetic Field Gradients</i>	13
1.2.9 <i>Inversion Recovery Imaging</i>	13
1.2.10 <i>Spin Echo Imaging</i>	14
<b>1.3 Contrast Agents</b>	<b>15</b>
1.3.1 <i>Gd(III)-based Contrast agents</i>	15
1.3.2 <i>Water Proton Relaxivity, <math>r_1</math></i>	19
1.3.3 <i>Hydration State, <math>q</math></i>	20
1.3.4 <i>Inner-Sphere Water Proton Relaxation</i>	22
1.3.5 <i>Gd(III)-Water Distance, <math>r_{GdH}</math></i>	23
1.3.6 <i>Rotational Correlation Time, <math>\tau_R</math></i>	23
1.3.7 <i>Electronic Relaxation Time, <math>T_{1e}</math></i>	24
1.3.8 <i>Outer Sphere Water Proton Relaxation</i>	25
1.3.9 <i>Water Exchange Lifetime, <math>\tau_m</math></i>	25
<b>1.4 Contrast Agent Enhancement</b>	<b>28</b>
1.4.1 <i>Shortening of the Water Exchange Lifetime, <math>\tau_m</math></i>	29

1.4.2	<i>Lengthening the Rotational Correlation Time, <math>\tau_R</math></i>	33
<b>1.5</b>	<b>Second Generation Contrast Agents</b>	35
<b>1.6</b>	<b>Lanthanides</b>	39
1.6.1	<i>Properties of the Lanthanides</i>	39
1.6.2	<i>Coordination Chemistry of the Lanthanides</i>	40
1.6.3	<i>Luminescence Studies</i>	41
1.6.4	<i>Lanthanide luminescence</i>	41
1.6.5	<i>Sensitised Emission</i>	43
1.6.6	<i>Determination of Hydration state, q: Luminescent Lifetime Studies</i>	47
<b>1.7</b>	<b>Thesis Outline</b>	49
<b>1.8</b>	<b>References</b>	50
<b>Chapter 2</b>	<b>'Click' Chemistry with Lanthanide Chelates</b>	56
<b>2.1</b>	<b>Introduction</b>	56
2.1.1	<i>In situ generation of azides</i>	57
2.1.2	<i>'Click' Chemistry and Biological Molecules</i>	58
2.1.3	<i>'Click' Chemistry on Metal Chelates</i>	59
2.1.4	<i>1,2,3-Triazole Appended Lanthanide Complexes</i>	61
2.1.5	<i>Target Lanthanide compounds</i>	62
<b>2.2</b>	<b>Macrocyclic Synthesis</b>	64
2.2.1	<i>Formation of 1,4,7-tris(tert-butoxycarbonylmethyl)-10-(prop-2-ynyl)-1,4,7,10-tetraazacyclododecane. (2)</i>	64
2.2.2	<i>1,2,3-Triazole Formation Before Ln(III) Coordination</i>	65
2.2.3	<i>Formation of 1,4,7-tris(tert-butoxycarbonylmethyl)-10-((1H-1,2,3-triazol-4-yl)methyl)-1,4,7,10-tetraazacyclododecane. (3c)</i>	67
2.2.4	<i>Cleavage of tert-butyl Esters</i>	68
2.2.5	<i>Formation of 1,4,7-tris(carbonylmethyl)-10-(prop-2-ynyl)-1,4,7,10-tetraazacyclododecane. (4)</i>	69
<b>2.3</b>	<b>Lanthanide Complex Preparation</b>	69
<b>2.4</b>	<b>Luminescence Studies of Pendant Alkyne Complexes Ln.4</b>	70
2.4.1	<i>Characterisation of <b>Eu.4</b></i>	70
2.4.2	<i>Characterisation of <b>Tb.4</b></i>	72
<b>2.5</b>	<b>Triazole-appended Lanthanide Complexes</b>	74
2.5.1	<i>1,2,3-Triazole-3-benzyl appended lanthanide complexes (<b>Ln.5a</b>)</i>	75
<b>2.6</b>	<b>Characterisation and luminescence studies of Ln.5a</b>	75
2.6.1	<i>Characterisation of <b>Eu.5a</b></i>	75
2.6.2	<i>Eu(III) Emission Intensity vs. pH for <b>Eu.5a</b></i>	77
		IX

2.6.3. <i>Characterisation of Tb.5a</i>	79
<b>2.7 Unsubstituted 1,2,3-triazole appended lanthanide complexes</b>	80
2.7.1 <i>Characterisation of Eu.5c</i>	82
2.7.2 <i>pH responsive behaviour of Eu.5c</i>	82
2.7.3 <i>Eu(III) Emission Intensity vs. pH for Eu.5c</i>	84
<b>2.8 Characterisation of Tb.5c</b>	87
2.8.1 <i>Tb(III) Emission Intensity vs. pH for Tb.5c</i>	87
<b>2.9 N<sub>3</sub><sup>-</sup> binding studies upon Eu.4</b>	90
<b>2.10 Relaxometric Investigation of Gd(III) Triazole Complexes</b>	92
2.10.1 <i>Relaxivity vs. [carbonate] studies of Gd.4</i>	92
2.10.2 <i>Relaxivity vs. pH for Gd.5a</i>	94
2.10.3 <i>Relaxivity vs. pH for Gd.5c</i>	95
2.10.4 <i>NMRD: Rotational correlation time, <math>\tau_R</math>, for Gd.4 – 5d</i>	96
2.10.5 <i><sup>17</sup>O variable temperature of Gd.5c</i>	97
<b>2.11 Summary and conclusions</b>	99
<b>2.12 References</b>	100
<b>Chapter 3 ‘Click’ Chemistry as a Route to Multimeric MRI Contrast Agents</b>	103
<b>3.1 Introduction</b>	103
3.1.1 <i>Using ‘Click’ Chemistry to Generate Multimeric Contrast Agents</i>	105
<b>3.2 Target Multimeric MRI Contrast Agent</b>	107
<b>3.3 Synthesis of Ln.8</b>	111
<b>3.4 Luminescence Studies of Lanthanide Complexes Bearing a Pendant <i>p</i>-Ethynylbenzyl Ln.8</b>	112
3.4.1 <i>Characterisation of Eu.8</i>	112
3.4.2 <i>Characterisation of Tb.8</i>	114
3.4.3 <i>Characterisation of Y.8</i>	116
<b>3.5 Synthesis of Ln.12</b>	116
3.5.1 <i>Synthesis of precursors for Ln.12</i>	117
3.5.2 <i>Formation of Eu.12</i>	119
3.5.3 <i>Characterisation of Eu.12</i>	120
<b>3.6 Synthesis of Trimeric Lanthanide Complexes Ln.13</b>	122
3.6.1 <i>Characterisation of Eu.13</i>	122
<b>3.7 Synthesis of Hexameric Compounds Using ‘Click’ Chemistry Ln.14</b>	125
3.7.1 <i>Characterisation of Eu.14</i>	126

<b>3.8 Summary and conclusions</b>	129
<b>3.9 References</b>	131
<b>Chapter 4 ‘Click’ Chemistry as a Route to Dual Modal Contrast Agents</b>	<b>133</b>
<b>4.1 Introduction</b>	133
<i>4.1.1 MR/Optical Imaging Agents</i>	133
<i>4.1.2 PET/Optical Imaging Agents</i>	135
<i>4.1.3 Rhenium as an Optical Probe</i>	136
<i>4.1.4 Synthesis of a Potential Dual Modal MR/Optical Imaging Agent</i>	137
<b>4.2 Attempted Synthesis of <b>14</b></b>	139
<b>4.3 Synthesis of Ln.<b>15</b></b>	142
<i>4.3.1 Luminescence studies of <b>Eu.15</b></i>	143
<i>4.3.2 Luminescence studies of <b>Tb.15</b></i>	146
<i>4.3.3 Characterisation of <b>Y.15</b></i>	148
<b>4.4 Bimetallic Lanthanide Rhenium Complexes</b>	149
<i>4.4.1 Luminescence studies of <b>Eu. Re.16</b></i>	150
<i>4.4.2 Characterisation of <b>Tb.Re.16</b></i>	151
<i>4.4.3 Characterisation of <b>Y.Re.16</b></i>	152
<b>4.5 p-Benzyl Appended Gd(III) Complexes</b>	153
<b>4.6 Summary and Conclusions</b>	154
<b>4.7 References</b>	155
<b>Chapter 5 Towards MR Contrast Agents for Imaging Gene Expressions</b>	<b>157</b>
<b>5.1 Introduction</b>	157
<i>5.1.1 Gene therapy</i>	161
<i>5.1.2 Herpes Simplex Virus 1 Thymidine Kinase Reporter Gene</i>	163
<i>5.1.3 Target Complexes</i>	164
<b>5.2 Uridine Transformations</b>	167
<i>5.2.1 Formation of 5-trityl-2-deoxyuridine (<b>17</b>)</i>	168
<i>5.2.2 Retention of stereochemistry of the Uridine</i>	168
<i>5.2.3 Formation of 3'-O-methanesulfonyl-5'-O-trityl-2'-deoxyuridine (<b>18</b>)</i>	169
<i>5.2.4 Formation of 1-[2-deoxy-5-O-(triphenylmethyl)-<math>\beta</math>-D-threo-pento-furanosyl]-uracil (<b>19</b>)</i>	169

5.2.5	<i>Formation of 1-[2-deoxy-3-O-methanesulfonyl-5-O-(triphenylmethyl)-β-D-threo-pentofuranosyl]uracil (20)</i>	169
5.2.6	<i>Formation of 3-azido-5-O-trityl-2,3-dideoxyuridine uracil (21)</i>	170
5.2.7	<i>Formation of 3-amino-5-O-trityl-2,3-dideoxyuridine uracil (22)</i>	170
<b>5.3</b>	<b>Linking Uridine to Macrocycles</b>	170
5.3.1	<i>Formation of 3-chloroacetamide-5-O-trityl-2,3-dideoxyuridine (23)</i>	171
5.3.2	<i>Formation of 3-azido-2,3-dideoxyuridine (24)</i>	171
5.3.3	<i>Formation of 5-trityl-2-(-3-chloropropoxy)-uridine (25)</i>	171
<b>5.4</b>	<b>Macrocycle Synthesis</b>	173
5.4.1	<i>Formation 1,4,7-tris(carbonylmethyl)-10-(3-acetamide-5-hydroxy-2,3-dideoxyuridine)-1,4,7,10-tetraazacyclododecane (28)</i>	174
5.4.2	<i>Formation 1,4,7-tris(carbonylmethyl)-10-(5-hydroxy-2-(-3-chloropropoxy)-uridine)-1,4,7,10-tetraazacyclododecane (29)</i>	175
<b>5.5</b>	<b>Synthesis of Lanthanide Complexes</b>	175
5.5.1	<i>Luminescence studies of Eu.28</i>	175
5.5.2	<i>Luminescence studies of Eu.29</i>	177
<b>5.6</b>	<b>'Click' Chemistry with Nucleoside Bases</b>	179
5.6.1	<i>Luminescent studies of Eu.30</i>	180
5.6.2	<i>Luminescence studies of Eu.31</i>	182
<b>5.7</b>	<b>Summary and conclusions</b>	184
<b>5.8</b>	<b>References</b>	185
<b>Chapter 6</b>	<b>Conclusions and Future Work</b>	187
6.1	<b>'Click' chemistry with lanthanide chelates</b>	187
6.2	<b>'Click' Chemistry as a Route to Multimeric MRI Contrast Agents</b>	190
6.3	<b>'Click' Chemistry as a Route to Dual Modal Contrast Agents</b>	192
6.4	<b>Enzyme Activated Contrast Agents</b>	193
<b>Chapter 7</b>	<b>Experimental</b>	196
7.1	<b>Materials and Methods</b>	196
7.1.1	<i>Reagents</i>	196
7.1.2	<i>Chromatography</i>	196
7.1.3	<i>Spectroscopy</i>	196
7.1.4	<i>Luminescence Spectroscopy</i>	197
7.1.5	<i>Hydration State, q, Determination</i>	197
7.1.6	<i><sup>1</sup>H Relaxation Data</i>	198
7.1.7	<i>pH Titrations</i>	199

7.1.8	<i>Azide Binding Studies</i>	199
7.1.9	<i>Concentration Determination via Mineralisation with Nitric Acid</i>	200
7.1.10	<i>Xylenol Orange Calibrations</i>	201
<b>7.2</b>	<b>Phenyl Triazole synthesis</b>	201
7.2.1	<i>1-(Chloromethyl)-4-ethynylbenzene (6a)</i>	201
7.2.2	<i>1-(Bromomethyl)-4-ethynylbenzene (6b)</i>	202
7.2.3	<i>1-(Hydroxymethyl)-4-(1-phenyl-1,2,3-triazo-4-yl)-benzene (9)</i>	202
7.2.4	<i>1-(Chloromethyl)-4-(1-phenyl-1,2,3-triazo-4-yl)-benzene (HCl salt)(10)</i>	203
7.2.5	<i>1-Ethyl-4-phenyl-1,2,3-triazole (13)</i>	203
7.2.6	<i>Benzyl Azide</i>	204
<b>7.3</b>	<b>Uridine Transformations</b>	205
7.3.1	<i>5-Trityl-2-deoxyuridine (17)</i>	205
7.3.2	<i>3'-O-Methanesulfonyl-5'-O-trityl-2'-deoxyuridine (18)</i>	206
7.3.3	<i>1-[2-Deoxy-5-O-(triphenylmethyl)-<math>\beta</math>-D-threo-pento-furanosyl]-uracil (19)</i>	206
7.3.4	<i>1-[2-Deoxy-3-O-methanesulfonyl-5-O-(triphenylmethyl)-<math>\beta</math>-D-threo-pentofuranosyl]uracil (20)</i>	207
7.3.5	<i>3-Azido-5-O-trityl-2,3-dideoxyuridine (21)</i>	208
7.3.6	<i>3-Amino-5-O-trityl-2,3-dideoxyuridine (22)</i>	209
7.3.7	<i>3-Chloroacetamide-5-O-trityl-2,3-dideoxyuridine (23)</i>	209
7.3.8	<i>3-Azido-2,3-dideoxyuridine (24)</i>	210
7.3.9	<i>5-Trityl-2-(-3-chloropropoxy)-uridine (25)</i>	211
<b>7.4</b>	<b>Macrocycle synthesis</b>	212
7.4.1	<i>1,4,7-Tris(tert-butoxycarbonylmethyl)-1,4,7,10-tetraazacyclododecane, (<sup>t</sup>BuDO3A) (1)</i>	212
7.4.2	<i>1,4,7-Tris(tert-butoxycarbonylmethyl)-10-(prop-2-ynyl)-1,4,7,10-tetraazacyclododecane (2)</i>	213
7.4.3	<i>1,4,7-Tris(tert-butoxycarbonylmethyl)-10-((1H-1,2,3-triazol-4-yl)methyl)-, -1,4,7,10-tetraazacyclododecane (3c)</i>	213
7.4.4	<i>1,4,7-Tris(tert-butoxycarbonylmethyl)-10-(1-methyl-4-ethynylbenzene)-1,4,7,10-tetraazacyclododecane (7)</i>	214
7.4.5	<i>1,4,7-tris(tert-butoxycarbonylmethyl)-10-(1-methyl-4-(1-phenyl-1,2,3-triazo-4-yl)-benzene)-1,4,7,10-tetraazacyclododecane (11)</i>	215
7.4.6	<i>1,4,7-Tris(tert-butoxycarbonylmethyl)-10-(3-acetamide-5-O-trityl-2,3-dideoxyuridine)-1,4,7,10-tetraazacyclododecane (26)</i>	216
7.4.7	<i>1,4,7-Tris(tert-butoxycarbonylmethyl)-10-(5-trityl-2-(-3-chloropropoxy)-uridine)-1,4,7,10-tetraazacyclododecane (27)</i>	217

<b>7.5 Proligand Synthesis</b>	218
7.5.1 1,4,7-Tris(carbonylmethyl)-10-(prop-2-ynl)-1,4,7,10-tetraazacyclododecane ( <b>4</b> )	218
7.5.2 1,4,7-Tris(carbonylmethyl)-10-((1H-1,2,3-triazol-4-yl)methyl)-,)-1,4,7,10-tetraazacyclododecane ( <b>5c</b> )	218
7.5.3 1,4,7-Tris(carboxymethyl)-10-(1-methyl-4-ethynylbenzene)-1,4,7,10-tetraazacyclododecane ( <b>8</b> )	219
7.5.4 1,4,7-Tris(carboxymethyl)-10-(1-methyl-4-(1-phenyl-1,2,3-triazo-4-yl)-benzene)-1,4,7,10-tetraazacyclododecane ( <b>12</b> )	219
7.5.5 1,4,7-Tris(carbonylmethyl)-10-(3-acetamide-5-hydroxy-2,3-dideoxyuridine)-1,4,7,10-tetraazacyclododecane ( <b>28</b> )	220
7.5.6 1,4,7-Tris(carbonylmethyl)-10-(5-hydroxy-2-(-3-chloropropoxy)-uridine)-1,4,7,10-tetraazacyclododecane ( <b>29</b> )	221
<b>7.6 Lanthanide Complexation</b>	221
7.6.1 Europium (III) 1,4,7-tris(carbonylmethyl)-10-(prop-2-ynl)-1,4,7,10-tetraazacyclododecane, ( <b>Eu.4</b> )	222
7.6.2 Terbium (III) 1,4,7-tris(carbonylmethyl)-10-(prop-2-ynl)-1,4,7,10-tetraazacyclododecane, ( <b>Tb.4</b> )	222
7.6.3 Gadolinium (III) 1,4,7-tris(carbonylmethyl)-10-(prop-2-ynl)-1,4,7,10-tetraazacyclododecane, ( <b>Gd.4</b> )	223
7.6.4 Europium (III) 1,4,7-tris(carboxymethyl)-10-(1-methyl-4-ethynylbenzene)-1,4,7,10-tetraazacyclododecane ( <b>Eu.8</b> )	223
7.6.5 Terbium (III) 1,4,7-tris(carboxymethyl)-10-(1-methyl-4-ethynylbenzene)-1,4,7,10-tetraazacyclododecane ( <b>Tb.8</b> )	224
7.6.6 Gadolinium (III) 1,4,7-tris(carboxymethyl)-10-(1-methyl-4-ethynylbenzene)-1,4,7,10-tetraazacyclododecane ( <b>Gd.8</b> )	224
7.6.7 Yttrium (III) 1,4,7-tris(carboxymethyl)-10-(1-methyl-4-ethynylbenzene)-1,4,7,10-tetraazacyclododecane ( <b>Y.8</b> )	224
7.6.8 Europium (III) 1,4,7-tris(carbonylmethyl)-10-(3-acetamide-5-hydroxy-2,3-dideoxyuridine)-1,4,7,10-tetraazacyclododecane ( <b>Eu.28</b> )	225
7.6.9 Europium (III) 1,4,7-tris(carbonylmethyl)-10-(5-hydroxy-2-(-3-chloropropoxy)-uridine)-1,4,7,10-tetraazacyclododecane ( <b>Eu.29</b> )	225
<b>7.7 ‘Click’ chemistry synthesis</b>	226
7.7.1 Europium (III) 1,4,7-tris(carbonylmethyl)-10-((1-benzyl-1,2,3-triazol-4-yl)methyl)-,)-1,4,7,10-tetraazacyclododecane ( <b>Eu.5a</b> )	226
7.7.2 Terbium (III) 1,4,7-tris(carbonylmethyl)-10-((1-benzyl-1,2,3-triazol-4-yl)methyl)-,)-1,4,7,10-tetraazacyclododecane ( <b>Tb.5a</b> )	226

7.7.3	<i>Gadolinium (III) 1,4,7-tris(carbonylmethyl)-10-((1-benzyl-1,2,3-triazol-4-yl)methyl)-,)-1,4,7,10-tetraazacyclododecane (Gd.5a)</i>	227
7.7.4	<i>Europium (III) 1,4,7-tris(carbonylmethyl)-10-((1H-1,2,3-triazol-4-yl)methyl)-,)-1,4,7,10-tetraazacyclododecane (Eu.5c)</i>	227
7.7.5	<i>Terbium (III) 1,4,7-tris(carbonylmethyl)-10-((1H-1,2,3-triazol-4-yl)methyl)-,)-1,4,7,10-tetraazacyclododecane (Tb.5c)</i>	228
7.7.6	<i>Gadolinium (III) 1,4,7-tris(carbonylmethyl)-10-((1H-1,2,3-triazol-4-yl)methyl)-,)-1,4,7,10-tetraazacyclododecane (Gd.5c)</i>	228
7.7.7	<i>Gadolinium (III) 1,4,7-tris(carbonylmethyl)-10-((1-naphthyl-1,2,3-triazol-4-yl)methyl)-,)-1,4,7,10-tetraazacyclododecane (Gd.5d)</i>	229
7.7.8	<i>Europium (III) 1,4,7-tris(carboxymethyl)-10-(1-methyl-4-(1-phenyl-1,2,3-triazo-4-yl)-benzene)-1,4,7,10-tetraazacyclododecane. (Eu.12)</i>	229
7.7.9	<i>Europium (III) 1,4,7-tris(carboxymethyl)-10-(1-methyl-4-(1-ethyl-1,2,3-triazo-4-yl)-benzene)-1,4,7,10-tetraazacyclododecane. (Eu.15)</i>	230
7.7.10	<i>Terbium (III) 1,4,7-tris(carboxymethyl)-10-(1-methyl-4-(1-ethyl-1,2,3-triazo-4-yl)-benzene)-1,4,7,10-tetraazacyclododecane (Tb.15)</i>	230
7.7.11	<i>Gadolinium (III) 1,4,7-tris(carboxymethyl)-10-(1-methyl-4-(1-ethyl-1,2,3-triazo-4-yl)-benzene)-1,4,7,10-tetraazacyclododecane (Gd.15)</i>	231
7.7.12	<i>Yttrium (III) 1,4,7-tris(carboxymethyl)-10-(1-methyl-4-(1-ethyl-1,2,3-triazo-4-yl)-benzene)-1,4,7,10-tetraazacyclododecane (Y.15)</i>	231
7.7.13	<i>Europium(III)1,4,7-tris(carbonylmethyl)-10-((1-2,3-dideoxyuridine-1,2,3-triazol-4-yl)methyl)-,)-1,4,7,10-tetraazacyclododecane (Eu.30)</i>	232
7.7.14	<i>Europium(III)1,4,7-tris(carbonylmethyl)-10-(4-(2,3-dideoxyuridine-1,2,3-triazol-4-yl)-1-methyl-benzene)-,)-1,4,7,10-tetraazacyclododecane (Eu.31)</i>	232
<b>7.8</b>	<b>Synthesis of Multimeric Compounds</b>	233
7.8.1	<i>1,3,5-Tris((Europium (III) 1,4,7-tris(carboxymethyl)-10-(1-methyl-4-(1,2,3-triazo-4-yl)-benzene)-1,4,7,10-tetraazacyclododecane)-methyl)-2,4,6- tris (methyl), benzene (Eu.13)</i>	233
7.8.2	<i>1,2,3,4,5,6-Hexa-((Europium (III) 1,4,7-tris(carboxymethyl)-10-(1-methyl-4-(1,2,3-triazo-4-yl)-benzene)-1,4,7,10-tetraazacyclododecane)-methyl)-benzene. (Eu.14)</i>	234
<b>7.9</b>	<b>Rhenium Complexation</b>	235
7.9.1	<i>Synthesis of 14c</i>	235
7.9.2	<i>Europium (III) 1,4,7-tris(carboxymethyl)-10-(1-methyl-4-(1-ethyl-2,3-rhenium-hexacarbonyl-dichloride-1,2,3-triazo-4-yl)-benzene)-1,4,7,10-tetraazacyclododecane. (Eu.Re.16)</i>	236

7.9.3	<i>Terbium (III) 1,4,7-tris(carboxymethyl)-10-(1-methyl-4-(1-ethyl-2,3-rhenium-hexacarbonyl-dichloride-1,2,3-triazo-4-yl)-benzene)-1,4,7,10-tetraazacyclododecane (Tb.Re.16)</i>	236
7.9.4	<i>Gadolinium (III) 1,4,7-tris(carboxymethyl)-10-(1-methyl-4-(1-ethyl-2,3-rhenium-hexacarbonyl-dichloride-1,2,3-triazo-4-yl)-benzene)-1,4,7,10-tetraazacyclododecane (Gd.Re.16)</i>	237
7.9.5	<i>Yttrium (III) 1,4,7-tris(carboxymethyl)-10-(1-methyl-4-(1-ethyl-2,3-rhenium-hexacarbonyl-dichloride-1,2,3-triazo-4-yl)-benzene)-1,4,7,10-tetraazacyclododecane (Y.Re.16)</i>	237
<b>7.10</b>	<b>References</b>	238
	<b>Chapter 8 Appendix</b>	239
<b>8.1</b>	<b>Courses and Conferences</b>	239
8.1.1	<i>Lecture Courses</i>	239
8.1.2	<i>Training Courses</i>	239
8.1.3	<i>Conferences Attended</i>	239
8.1.3.1	<i>Oral Communication</i>	239
8.1.3.2	<i>Posters Presentations</i>	240
8.1.4	<i>Publications</i>	240
8.1.5	<i>Demonstrating</i>	240
8.1.6	<i>Seminars Attended</i>	241
<b>8.2</b>	<b>X-ray Crystallography Data</b>	243
8.2.1	<i>X ray Data for 3c</i>	243
8.2.2	<i>X ray Data for 14c</i>	245

# Chapter 1

## Introduction

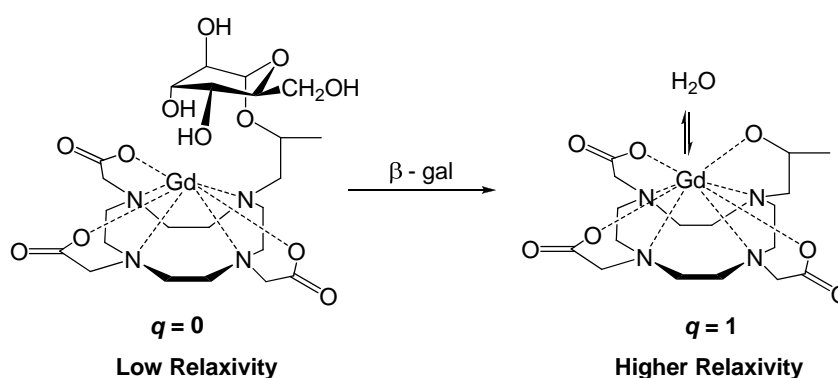
### 1.1 Molecular Imaging

Molecular imaging provides a view of the body at the cellular level, it enables the visualization of key biological processes as they happen within the cell. This has only been possible due to the astonishing increase in knowledge of genetics and molecular biology of human disease. Significant progress has been made in the understanding of molecular-genetic mechanism of many diseases; this has been achieved with the modern molecular-biological assay.<sup>1</sup> A range of diagnostic imaging modalities are currently being applied in the field of molecular imaging, such as positron emission tomography (PET), single photon emission computed tomography (SPECT), X-ray computed tomography (CT), ultrasound, near-IR fluorescence mediated tomography and magnetic resonance (MR) imaging.<sup>2</sup>

#### 1.1.1 *In-Vivo Molecular Imaging*

Molecular imaging employs three strategies: direct, indirect and biomarker imaging. Direct imaging is based upon imaging the target directly, usually with a target-specific probe, *i.e.* linking a probe to a protein or antibody that is specific for cell surface receptors. These strategies have been established using optical, nuclear and MR imaging. The image of probe localisation and concentration (signal intensity) is directly related to its interaction with the target.<sup>1</sup> In nuclear imaging of tumour vasculature, the  $\alpha_v\beta_3$  integrin, which is highly expressed and plays an important role in metastasis and tumour induced angiogenesis is a target. The imaging and targeting of the  $\alpha_v\beta_3$  integrin with a <sup>18</sup>F-labeled glycosylated RGD-containing peptides are being developed by Hauberner *et al.*<sup>3</sup> Indirect imaging is more complicated; the most widely used indirect imaging is “reporter gene imaging”. This requires the reporter gene to be delivered to the target cell/tissue (“pre-targeting”) usually by vector transfection/transduction. The reporter gene includes transcription factors that function as “molecular-genetic sensors” and initiate reporter gene expression.<sup>1</sup> This protein can be an optical imaging probe; such as green fluorescent protein (GFP) or blue fluorescent protein (BFP), these proteins are not used for imaging within the

body, as the emission wavelength will not penetrate tissue, these proteins are used for *in vitro* studies. For nuclear and MR imaging, the reporter gene requires a specific probe that interacts with the reporter gene product in order to produce an image; the target molecule is not imaged directly. For example, enzyme-mediated MR gene expression has been proposed by Meade and co-workers; on entering the target cell expressing the reporter gene product,  $\beta$ -galactosidase a  $\beta$ -galactose unit bound to a Gd(III) complex, is cleaved from the MR agent, changing the hydration state and increasing signal intensity (Scheme 1.1).<sup>4</sup>



Scheme 1.1

Biomarker or surrogate marker imaging is used to assess downstream effects of one or more endogenous molecular-genetic process. This can be used to look at downstream effects of genetic disease pathways such as those in cancer. An example of clinically useful biomarker imaging for “early” assessment of treatment is  $^{18}F$ -FDG ( $^{18}F$ -labelled glucose) PET imaging of gastrointestinal stromal tumours (GIST) pre- and post-STI1571 (Gleevec) treatment.<sup>5,6</sup> This reports on downstream effects of receptor mediated glucose uptake, and monitors the protein that regulates glucose uptake and metabolism in GIST.

## 1.2 Magnetic Resonance Imaging

Magnetic resonance imaging (MRI) is a non-invasive diagnostic tool in clinical medicine. MRI provides highly detailed three-dimensional images of *e.g.* organs, tissues and blood flow within the human body. The technique visualizes water protons within the body. As a result of the high abundance of water molecules in biological systems, it is used

to detect a wide variety of pathological conditions throughout the body, such as heart disease, cancer and musculoskeletal disorders.

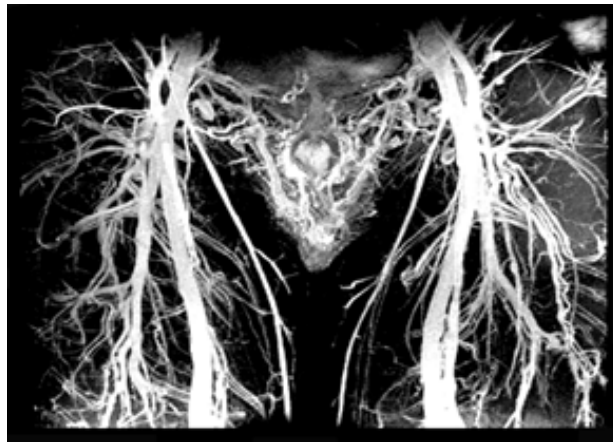


Figure 1.1 MR image angiogram of the thighs and groin.<sup>7</sup>

The concept of MRI was developed in 1972 by Paul Lauterbur at the University of Illinois, USA, and Sir Peter Mansfield at the University of Nottingham, UK, joint winners of the Nobel Prize for Physiology or Medicine in 2003.<sup>8,9</sup>

MRI is essentially an elaborate proton nuclear magnetic resonance (NMR) experiment, which employs low intensity radio frequency (RF) waves and gradient magnetic fields. By using tailored pulse sequences and field gradients the technique provides excellent contrast between different types of tissue in the body, due to both the different concentrations of water protons, and the variation in  $T_1$  relaxation times of water protons in different environments.

### *1.2.1 Principles of Magnetic Resonance Imaging*

MRI functions by visualizing spin active nuclei, such as protons, which have a nuclear spin quantum number,  $I = \frac{1}{2}$ . The human body is mainly composed of water and fat, both containing many hydrogen atoms. This means that the body is made up of approximately 63% hydrogen atoms.<sup>10</sup> MRI provides information on the distribution and quantity of protons within biological systems.

The body is placed in a magnetic field ( $B_0$ ) which partially polarizes the nuclei, aligning either parallel or antiparallel to the magnetic field. The parallel alignment is the

favourable position as it is the lowest energy state. The nuclei are exposed to a sequence of RF pulses, this excites from the parallel lower energy state to the antiparallel higher energy state. The RF pulses are turned off and the nuclei relax back to the ground state (parallel) this relaxation re-emits RF radiation at their Larmor frequency. The signal is detected and turned into an image, showing proton nuclei within a body: the faster the longitudinal relaxation rate,  $R_1$ , the more intense the signal. Organs and tissues in the body contain varying amounts of water molecules; a higher concentration of water molecules provides a more intense signal. Tissues in the body also have different environments, this can affect the rate at which water protons relax, *i.e.* they have different longitudinal relaxation times ( $T_1$ ). As  $T_1$  is decreased, signal intensity increases, the various environments cause signal intensity to differ within the body. The contrast observed is due to the difference of  $T_1$ , between different water protons. Contrast agents have been produced to exploit this concept by varying  $T_1$ , around one third of clinical scans employ the use of a contrast agent.<sup>10</sup>

### 1.2.2 Principles of NMR

Nuclear spin is the fundamental term which will determine if nuclei are observable by NMR spectroscopy. The spin quantum number,  $I$ , is composed of the sum of the individual contributions of each of the unpaired protons and neutrons, possessing spin of  $\pm 1/2$ . In order to be observable by NMR spectroscopy the nuclei must possess a non zero value of  $I$ . The properties of nuclei commonly observed in NMR experiments are shown in Table 1.1.<sup>11</sup>

The spin of any nuclide is proportional to its magnetic moment,  $\mu$  where  $\gamma$  is the gyromagnetic ratio. Each value of  $m_I$  corresponds to a different orientation of nuclear spin, and therefore, nuclear magnetic moment (Equation 1). When placed in a magnetic field, nuclei with spin angular momentum will behave as bar magnets and will align along the external magnetic field,  $B_o$ , which by convention is oriented along the  $z$ -axis. The  $z$ -components of the magnetic moment will align either parallel or antiparallel with the magnetic field (Figure 1.2). The magnitude of the magnetic moment in the  $z$ -direction,  $\mu_z$  (Equation 2).

Nuclide	Spin	Magnetic Moment	Gyromagnetic Ratio
	$I$	$\mu / \mu_N$	$\gamma$ ( $10^7 \text{ T}^{-1}\text{s}^{-1}$ )
$^1\text{H}$	$\frac{1}{2}$	2.79285	26.752
$^2\text{H}$	1	0.85745	4.1067
$^{13}\text{C}$	$\frac{1}{2}$	0.7023	6.7272
$^{14}\text{N}$	1	0.40356	1.9328
$^{31}\text{P}$	$\frac{1}{2}$	1.1317	10.84

Table 1.1 Magnetic properties of nuclei commonly observed by NMR spectroscopy (where  $\mu_N$  is the nuclear magneton,  $5.05079 \times 10^{-27} \text{ J T}^{-1}$ )

$$\mu = \gamma \vec{I} \quad (1)$$

$$\mu_z = \gamma I_z = m_I \gamma \hbar \quad (2)$$

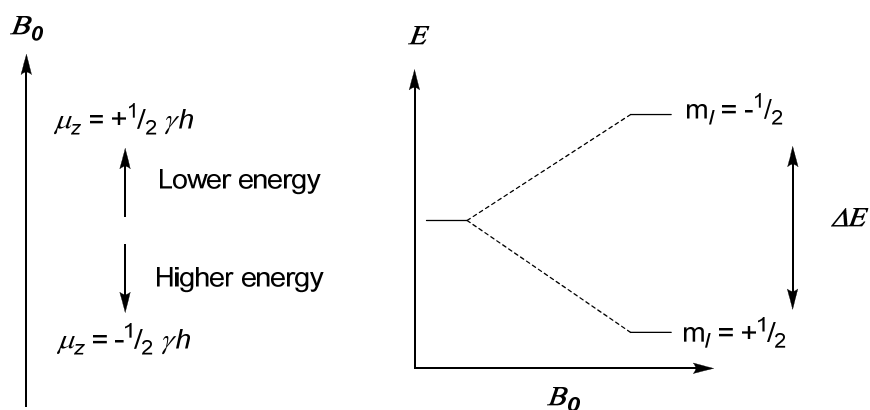


Figure 1.2 Alignment of magnetic moments,  $\mu_z$ , in a magnetic field,  $B_0$ .

An important factor in understanding NMR spectroscopy is the concept of angular momentum. Angular momentum refers to an object moving on a circular path around a reference point. This is related to nuclei as spin angular momentum, the magnitude of which  $|I|$  is defined in Equation 3, where  $h$  is Planck's constant and  $I$  is the spin quantum number.

$$|I| = \hbar\sqrt{I(I+1)}, \quad \hbar = \frac{h}{2\pi} \quad (3)$$

The most commonly observed nuclide by NMR is the spin  $\frac{1}{2}$   $^1\text{H}$ . The angular momentum is arbitrarily quantised along the  $z$ -axis of an orthogonal coordination system. Figure 1.3 shows the possible orientations of the spin angular momentum around the  $z$ -axis for a spin  $\frac{1}{2}$  nuclei, where  $m_I$ , the magnetic quantum number, is equal to  $-I, -I + 1, \dots, I$  totalling  $2I + 1$ ; the total number of orientations.

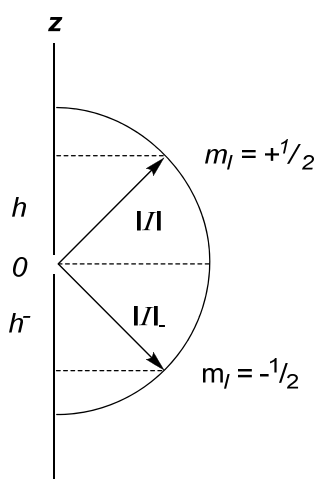


Figure 1.3 Orientation of  $m_I$  around the  $z$ -axis for an  $I = \frac{1}{2}$  nucleus. There are two possible orientations for an  $I = \frac{1}{2}$  nucleus;  $+\frac{1}{2}$  and  $-\frac{1}{2}$ .

$$E = -\mu_z B_o = -m_I \hbar \gamma B_o \quad (4)$$

$$\Delta m_I = \pm 1 \quad (5)$$

$$\Delta E = \gamma \hbar B_o \quad (6)$$

The magnetic energy of a nucleus placed in a magnetic field is derived from Equation 4. The selection rule for an NMR transition between the  $m_I$ -states is shown in Equation 5. The energy difference between two  $m_I$ -states is in Equation 6 and is therefore proportional to the magnetic field strength. The nucleus must be supplied with the required energy,  $\Delta E$ , in the form of electromagnetic radiation in order for a transition into a higher energy state to occur. Likewise, if a transition is to a lower energy state electromagnetic radiation equal to the energy difference  $\Delta E$ , is emitted.

The angular frequency for the electromagnetic radiation of an  $m_I$ -state transition is expressed by Equation 7.

$$\omega_o = \gamma B_o \quad (7)$$

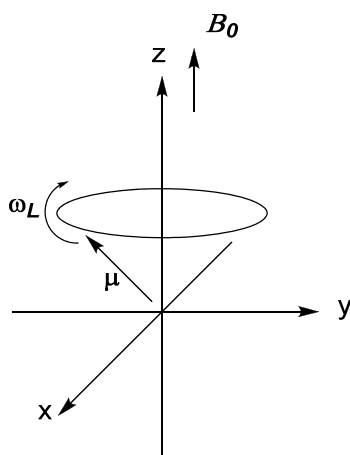


Figure 1.4 Angular velocity of nuclei.

In a magnetic field,  $\mu$  revolves around  $B_o$  with angular velocity,  $\omega_L$  (Figure 1.4).

$$\omega_L = -\gamma B_o \quad (8)$$

The angular velocity ( $\omega_L$ ), is known as the Larmor frequency, and is identical to the angular frequency ( $\omega_o$ ), required for an energy transition to take place. For this reason, angular frequency is also known as Larmor frequency.<sup>12</sup>

### 1.2.3 NMR Signal

An NMR signal arises from the difference in energy absorbed or emitted during transitions between two  $m_I$ -states. Boltzmann distribution is employed in order to calculate the relative populations of the lower energy,  $N^+$ , and higher energy,  $N^-$ ,  $m_I$ -states (Equation 9)

$$\frac{N^+}{N^-} = e^{\frac{-\Delta E}{kT}} \quad (9)$$

$\Delta E$  is the energy difference between the  $m_I$ -states,  $T$  is the temperature in Kelvin and  $k$  is the Boltzmann constant ( $1.3806 \times 10^{-23} \text{ J K}^{-1}$ ). According to the Boltzmann distribution the most populated state is the lower energy,  $N^+$   $m_I$ -state, in the absence of a magnetic field. The individual spins rotate at random phases around the  $x,y$ -plane when placed in a magnetic field. Application of a  $90^\circ$  radio frequency (RF) pulse,  $B_1$ , equivalent to the Larmor frequency along the  $x,y$ -plane will cause bunching of the individual spins, known as coherence. If the RF field is applied for a long enough time the net magnetisation,  $M$ , will flip onto the  $x,y$ -plane. All the spins are now in the same phase and precess around  $B_o$  at the Larmor frequency (Figure 1.5). Application of a  $90^\circ$  RF pulse causes the  $m_I$ -states to be equally populated as longitudinal magnetisation has been converted to transverse magnetisation. After a  $180^\circ$  RF pulse has been applied the Boltzmann distribution is inverted. The spins will continue to precess around  $B_o$  until the RF field is removed, at which point spin relaxation processes will cause loss of coherence as magnetisation returns to its equilibrium position. The individual spins begin to precess about the  $x,y$ -plane at different resonant frequencies, inducing a radiofrequency in the NMR spectrometer detector coils, which detects only transverse magnetisation. As equilibrium is re-established the coils detect a loss in radiofrequency known as free induced decay (FID), which is transformed into an NMR spectrum by the mathematical technique Fourier Transformation.

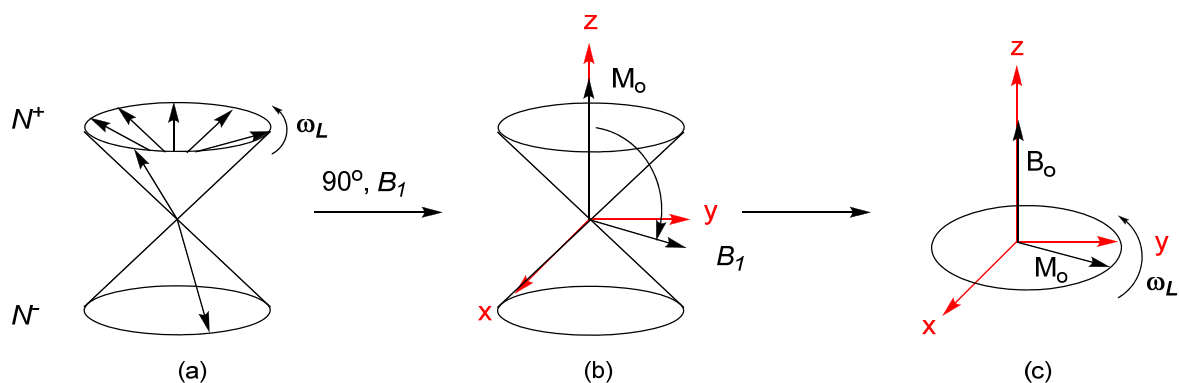


Figure 1.5 Coherence of individual spins following a  $90^\circ$  RF pulse. (a) the equilibrium Boltzmann distribution of spins when nuclei are placed in a magnetic field. (b) the net magnetisation,  $M$ , flips  $90^\circ$  onto the  $x,y$  plane. (c) the  $m_I$ -states are now all in the same phase and precess around the magnetic field,  $B_o$ , at Larmor frequency,  $\omega_L$ .

#### 1.2.4 Longitudinal (Spin-Lattice) Relaxation Time, $T_1$

Figure 1.6 shows that at equilibrium the net magnetisation,  $M_o$ , is in line with the applied magnetic field,  $B_o$ , and, therefore, the  $z$ -component of magnetisation,  $M_z$ , is equal to  $M_o$ , and is referred to as the longitudinal magnetization. Following a  $90^\circ$  RF pulse, the longitudinal magnetisation is converted to transverse as the spins revolve about the  $x,y$ -plane and thus  $M_z = 0$ . The time taken for  $M_z$  to return to its equilibrium value is known as the longitudinal relaxation time,  $T_1$ . The motions of molecules in the surroundings (the lattice) cause fluctuations in the local magnetic field, re-establishing Boltzmann distribution of the  $m_I$ -states. The equation for the return to equilibrium following this process is shown in Equation 10, where  $\tau$  is the delay time following the  $90^\circ$  RF pulse.

If a  $180^\circ$  RF pulse is applied, the net magnetisation will be inverted along the  $z$ -axis.  $M_z$  will then return back to its equilibrium position along the  $z$ -axis at a rate governed by  $T_1$ . The equation for the return to equilibrium following this process is shown in Equation 11, where  $\tau$  is the delay time following the  $180^\circ$  RF pulse.

$$M_z = M_o (1 - e^{-\tau/T_1}) \quad (10)$$

$$M_z = M_o (1 - 2e^{-\tau/T_1}) \quad (11)$$

#### 1.2.5 Measurement of $T_1$ : the Inversion Recovery Experiment

$T_1$  can be accurately measured by a pulsed NMR technique known as inversion recovery. Nuclei are subjected to a  $180^\circ$  RF pulse and are allowed to relax back towards equilibrium for a delay time,  $\tau$ , after which a  $90^\circ$  RF pulse is employed and a FID is detected and the intensity of the signal is determined (Figure 1.6). The sequence is repeated for a series of  $\tau$ . Equation 10 shows that by plotting  $\ln[I(\infty) - I(\tau)]$  vs.  $\tau$ ,  $T_1$  can be determined (where  $\ln I(\infty)$  is the intensity of the fully relaxed sample).

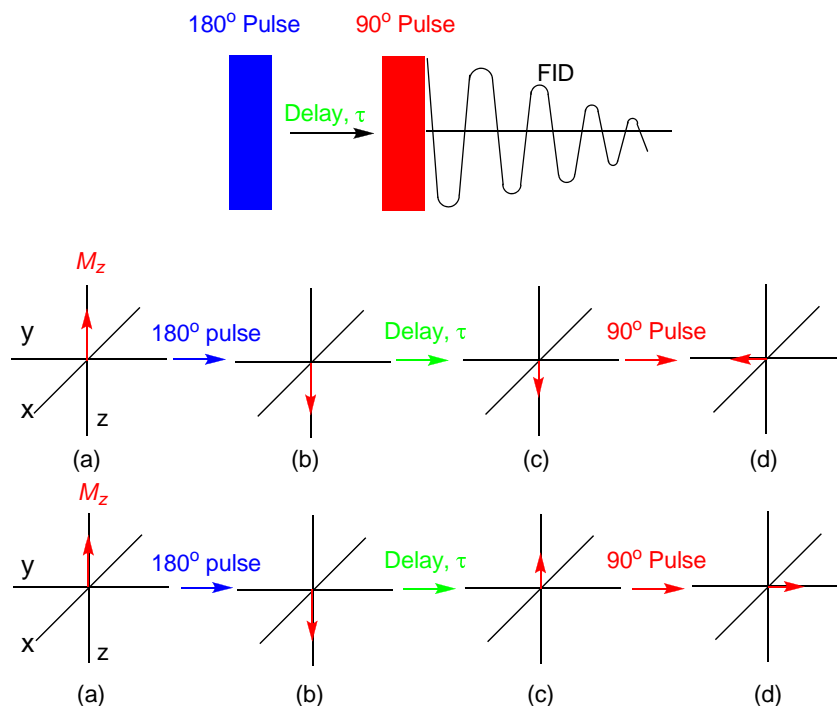


Figure 1.6 The inversion recovery experiment. (a) the  $M_z$  component of the net magnetisation is in line with the magnetic field,  $B_0$ , and, thus  $M_o = M_z$ . (b)  $M_z$  flipped across the  $z$ -axis following a  $180^\circ$  RF pulse. (c) the  $M_z$  returning to equilibrium following a delay time,  $\tau$ , where above shorter delay is employed,  $\tau_1$ , compared to the longer  $\tau_2$  below. (d)  $M_z$  to be flipped onto the  $x,y$ -plane following a  $90^\circ$  RF pulse, from where a FID is detected and the signal intensity is recorded.

### 1.2.6 Transverse (Spin-Spin) Relaxation Time, $T_2$

Following a  $90^\circ$  RF pulse, the spins precess coherently around the  $x,y$ -plane. Coherence is lost as each of the individual spins return to equilibrium and “fan out” around the  $x,y$ -plane, re-establishing transverse magnetisation,  $M_{xy}$  (Figure 1.7). The process for  $M_{xy}$  to return to its equilibrium value is known as transverse relaxation time,  $T_2$ . Transverse relaxation occurs at the same time as longitudinal relaxation; however  $T_2$  is always shorter than or equal to  $T_1$ .

$$M_{xy} = M_{xyo} e^{-\tau/T_2} \quad (12)$$

Determination of  $T_2$  can be carried out by measurement of spectral line width at half height. The length of transverse relaxation time has an effect on the line broadening of NMR spectra. The line width at half height is governed by Equation 13, where  $\Delta\nu_{1/2}$  is the

frequency, in Hertz, at half height. Therefore, as  $T_2$  increases, line widths become narrower in NMR spectra.

$$\Delta\nu_{1/2} = \frac{1}{\pi T_2} \quad (13)$$

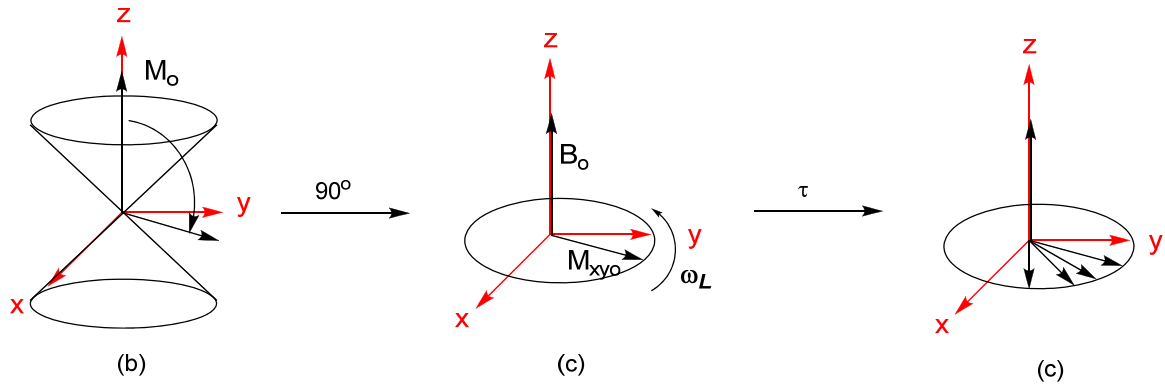


Figure 1.7 Transverse relaxation,  $T_2$ . (a) the spins are flipped onto the  $x,y$ -plane following a  $90^\circ$  RF pulse. (b) the net magnetisation precesses around the  $x,y$ -plane at Larmor frequency. (c) the spins start to return to equilibrium, restoring transverse magnetization  $M_{xy}$ , as they “fan out” around the  $x,y$ -plane.

So far it has been assumed that the varying frequencies of the spins away from Larmor frequencies arise solely due to interactions within the sample. It is important, however, to bear in mind the bulk inhomogeneity of the magnet,  $\Delta B_0$ , *i.e.* the field varies at different locations of the sample, and contributes to the observed transverse relaxation time in an NMR signal,  $T_2^*$ .

$$\frac{1}{T_2^*} = \frac{1}{T_2} + \gamma \Delta B_0 \quad (14)$$

### 1.2.7 Measurement of $T_2$ : The Hahn Spin Echo Experiment

Measurement of spectral line width may not necessarily be a very accurate way to measure  $T_2$  as  $T_1$  and magnet inhomogeneity each have an effect.  $T_2$  can be accurately determined *via* the Hahn Spin Echo experiment, a pulsed NMR technique. Following a  $90^\circ$  RF pulse, there is loss of phase coherence around the  $x,y$ -plane. The spins precess at differing frequencies due to both the true  $T_2$  effect and the inhomogeneity effects. A  $90^\circ$  pulse is applied followed by a delay time,  $\tau$ , and the spins begin to fan out. Application of a

180° RF pulse, along the  $x,y$ -plane, followed by a delay time,  $\tau$ , will re-focus the spins such that they are all in phase. The true  $T_2$  process, however, will cause a reduction in the transverse magnetisation that cannot be re-focused following a 180° RF pulse. A FID is measured and the experiment is repeated for several values of  $\tau$  (Figure 1.8).

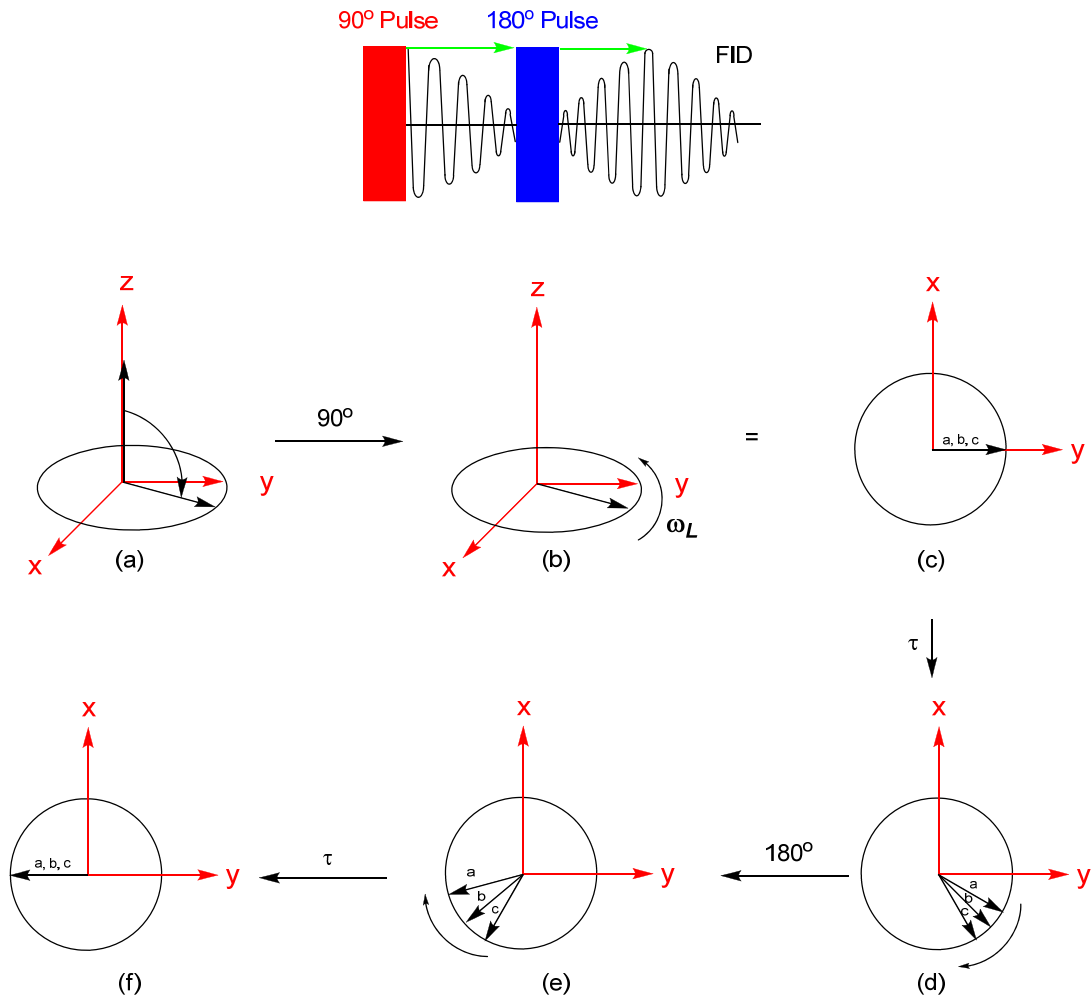


Figure 1.8 The Hahn Spin Echo Experiment. (a) the spins are inverted onto the  $x,y$ -plane and (b) and (c) they precess at Larmor frequency. (d) shows that after delay time,  $\tau$ , the spins precess at differing frequencies where a is the slowest and c is the fastest. The spins are inverted along the  $x,y$ -plane following a 180° pulse, (e), and phase coherence is re-established after delay time,  $\tau$ , (f).

The relaxation occurs over time  $2\tau$  and, therefore, using Equation 13 the NMR signal intensity is defined (Equation 15) and, therefore, a plot of  $\ln I_{2\tau}$  vs.  $\tau$  will give  $T_2$ .

$$I_{2\tau} = I_0 e^{-2\tau/T_2} \quad (15)$$

### 1.2.8 Magnetic Field Gradients

In order to produce three-dimensional images of the body MRI scanners employ a series of magnetic field gradients in order to spatially encode observed nuclear spin densities, allowing for slices of the body to be identified. Consider the two solid blocks in Figure 1.9. Projection of the proton spin density onto the  $x$ -axis alone would give the same readout for each sample and therefore the same image.

In order to determine the proton spin density dispersion three-dimensionally measurements must be made along the  $x$ ,  $y$  and  $z$ -axis together. Gradient field detection along each axis is, therefore, carried out and the results combined to produce a three-dimensional image.

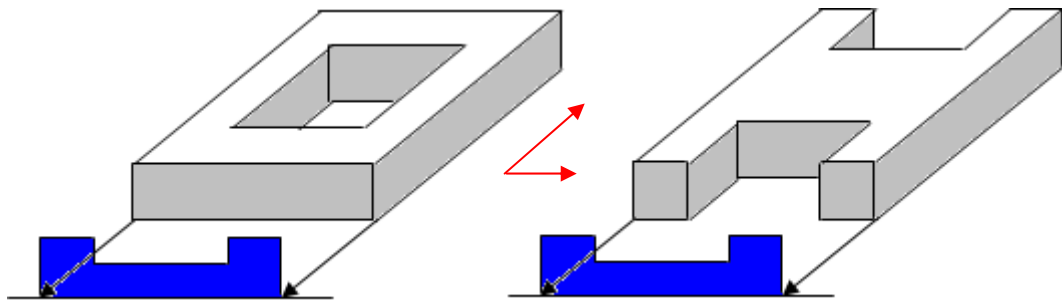


Figure 1.9 Proton spin density. The spin density readout (blue) along the  $x$ -axis only shows both three-dimensional objects (a) and (b) to appear identical.

### 1.2.9 Inversion Recovery Imaging

The mechanisms of the inversion recovery experiment have been previously discussed (Section 1.2.5). Application of this technique can provide highly detailed images based on longitudinal relaxation times. Following a  $180^\circ$  pulse, in tissue types where water proton  $T_1$  is short,  $M_z$  will be re-established quickly after the delay time,  $\tau$ , and therefore following the  $90^\circ$  pulse, more bulk magnetisation will be flipped onto the  $x,y$  plane, *c.f.* longer water proton  $T_1$  times. This leads to a higher intensity transverse magnetisation signal being detected. Therefore, tissue types with shorter water proton longitudinal relaxation times will provide higher signal intensities and, thus, appear brighter in MR

images. An advantage of short  $T_1$  is that the delay time can be quite short and, therefore, many more scans can be accumulated within a short time, allowing for a higher signal to noise ratio and clearer images (Figure 1.10).

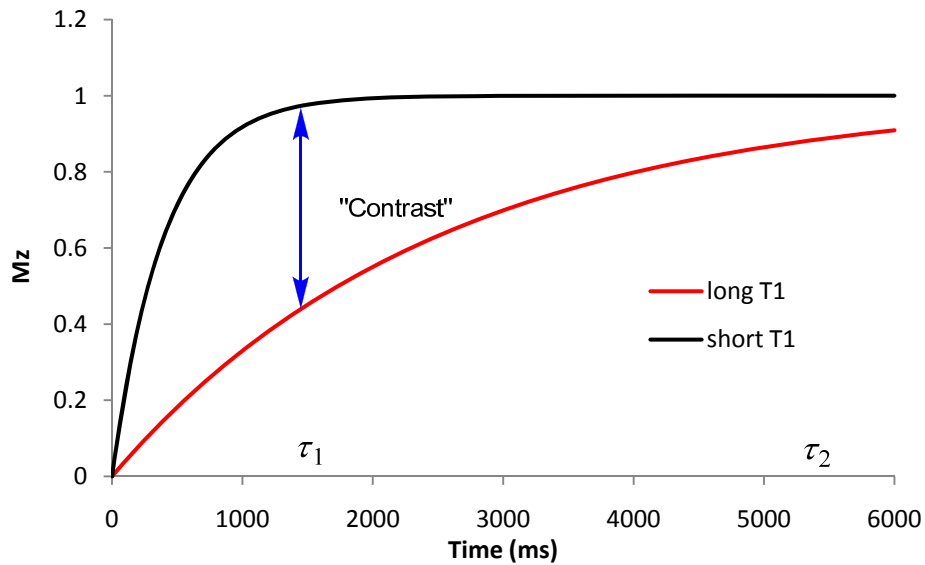


Figure 1.10 Contrast between  $T_1$  relaxations of different tissue types

Figure 1.10 represents the difference between a short  $T_1$  and long  $T_1$  and the ability to create contrast, *i.e.* if delay before the next pulse is  $\tau_1$  then only the faster relaxing proton has regained 100% magnetisation and the slower one has not, therefore contrast is observed, if the delay is  $\tau_2$  both protons will appear at similar intensity, as both have regained magnetisation in the z direction before the next pulse. Exploiting this difference in  $T_1$  gives rise to contrast between different tissue types in an MRI scan.

### 1.2.10 Spin Echo Imaging

$T_1$  varies from tissue to tissue; this degree of variation may not be large enough in some cases to provide clear contrast between tissue types, *i.e.* if  $T_1$  is very fast in two tissues. As  $T_2$  is always shorter or equal to  $T_1$ , imaging based on transverse relaxation times,  $T_2$ , can be employed in order to show contrast between the fast  $T_1$  tissues. The spin echo experiment has been previously discussed (Section 1.2.7). As  $T_2$  results in a loss of coherence about the  $x,y$ -plane, transverse magnetisation is therefore lost. Thus, the faster the transverse relaxation the lower the signal intensity resulting in darker MR images.

### 1.3 Contrast Agents

As discussed in section 1.2.9 and 1.2.10 contrast between tissue types is, determined by the longitudinal and transverse relaxation times of the water protons present. Enhancement of image contrast results from enhancement of the water proton relaxation processes. This is achieved by administering agents to the patient, which have an effect on the water proton relaxation times. Contrast agents that are designed to shorten  $T_1$  and give ‘positive’ contrast are known as  $T_1$  agents, those that are designed to shorten  $T_2$  and give ‘negative’ contrast are known as  $T_2$  agents.

Contrast agents are the magnetic resonance equivalent of a dye which is injected into the body to improve the contrast between healthy and diseased tissue, to show physiological function or blood flow.<sup>7</sup> It is not the contrast agent that is observed, rather the effect on the longitudinal relaxation ( $T_1$ ) and the transverse relaxation times ( $T_2$ ) of the surrounding water proton nuclei.<sup>13</sup> Most  $T_1$  contrast agents consist of paramagnetic metal complexes of gadolinium (Gd(III)), which increase localized signal intensity by lowering  $T_1$  of bound water protons, these waters exchange with bulk water at rates  $> 10^6 \text{ s}^{-1}$  and pass on the effect to surrounding water molecules (the seminal review by Lauffer in 1987 illustrated the use of Gd(III) complexes as contrast agents, renewing interest in the chemistry of Gd(III) and of lanthanides in general).<sup>14</sup> One of the reasons for the interest in lanthanides, in particular Gd(III), is their unique magnetic properties. Gd(III) has seven unpaired  $f$ -electrons; it is one of the most paramagnetic ions. Its relatively slow electron spin relaxation rate, and its large effective magnetic moment,  $\mu_{\text{eff}} = 7.94 \text{ B.M.}$ ,<sup>15</sup> leads to a metal ion with almost ideal magnetic properties for a contrast agent.<sup>7</sup> At present approximately 30% of MRI scans use a Gd(III)-based contrast agent,<sup>16</sup> and the latest data has shown that in 2005 around 10 million MRI scans used a contrast agent.<sup>17</sup>

#### 1.3.1 Gd(III)-based Contrast agents

The primary concern when preparing Gd(III)-based contrast agents is to ensure the metal ion complex is stable with respect to loss of Gd(III). Gd(III) has a similar ionic radii to that of Ca(II),  $1.05\text{\AA}$  and  $1.12\text{\AA}$  respectively (C.N. =8).<sup>18,19</sup> Due to the greater charge density of Gd(III) there is a greater affinity for Ca(II) binding sites on biological molecules.

This can lead to the inhibition of calcium transfer processes in biological systems, *e.g.* bone-deposition, the inhibition of calmodulin a calcium binding protein that modulates many processes within the cell,<sup>20</sup> skeletal, smooth and cardiac muscle contraction by blocking the  $\text{Na}^+/\text{Ca}^{2+}$  synaptic membrane.<sup>21</sup>

The first generation of Gd(III)-based contrast agent development involves complexation of the metal ion with derivatives of either diethylenetriamine pentaacetate (DTPA)<sup>22,23</sup> or 1,4,7,10-tetraazacyclododecane-1,4,7,10-tetraacetic acid (DOTA) (Figure 1.11).<sup>24</sup> The commercially available Gd(III)-based contrast agents are the anionic complexes  $[\text{Gd-DOTA}]^-$  (Dotarem, Guerbert S.A., France, 1989), and  $[\text{Gd-DTPA}]^{2-}$  (Magnevist, Scherring, A.G., Germany, 1988), the neutral complexes Gd-HP-DO3A (Prohance, Bracco Diagnostics, Italy, 1992),  $[\text{Gd-DO3A-butrol}]$  (Gadovist, Scherring A.G., Germany, 1999), Gd-DTPA-BMA (Omniscan, Winthrop University Laboratories, U.S.A., 1993) and Gd-DTPA-BMEA (OptiMARK, Mallinckrodt, U.S.A., 1998) and the blood pool contrast agent MS-325 (Vasovist, Scherring A.G., Germany, 2005). All of these complexes show high *in vivo* kinetic stability (Table 1.2, shows thermodynamic stability constants and acid dissociation rate constants), each of the ligands form a highly stable octadentate complex with Gd(III) ion, allowing one free coordination site to bind exchanging water molecules. It has recently been suggested that Gd-DTPA-BMA has been found to be unstable in patients with severe renal impairment,<sup>25</sup> this instability is thought to be due to the kinetic instability of the complex under acidic conditions, such as that of the kidneys of renally impaired patients.

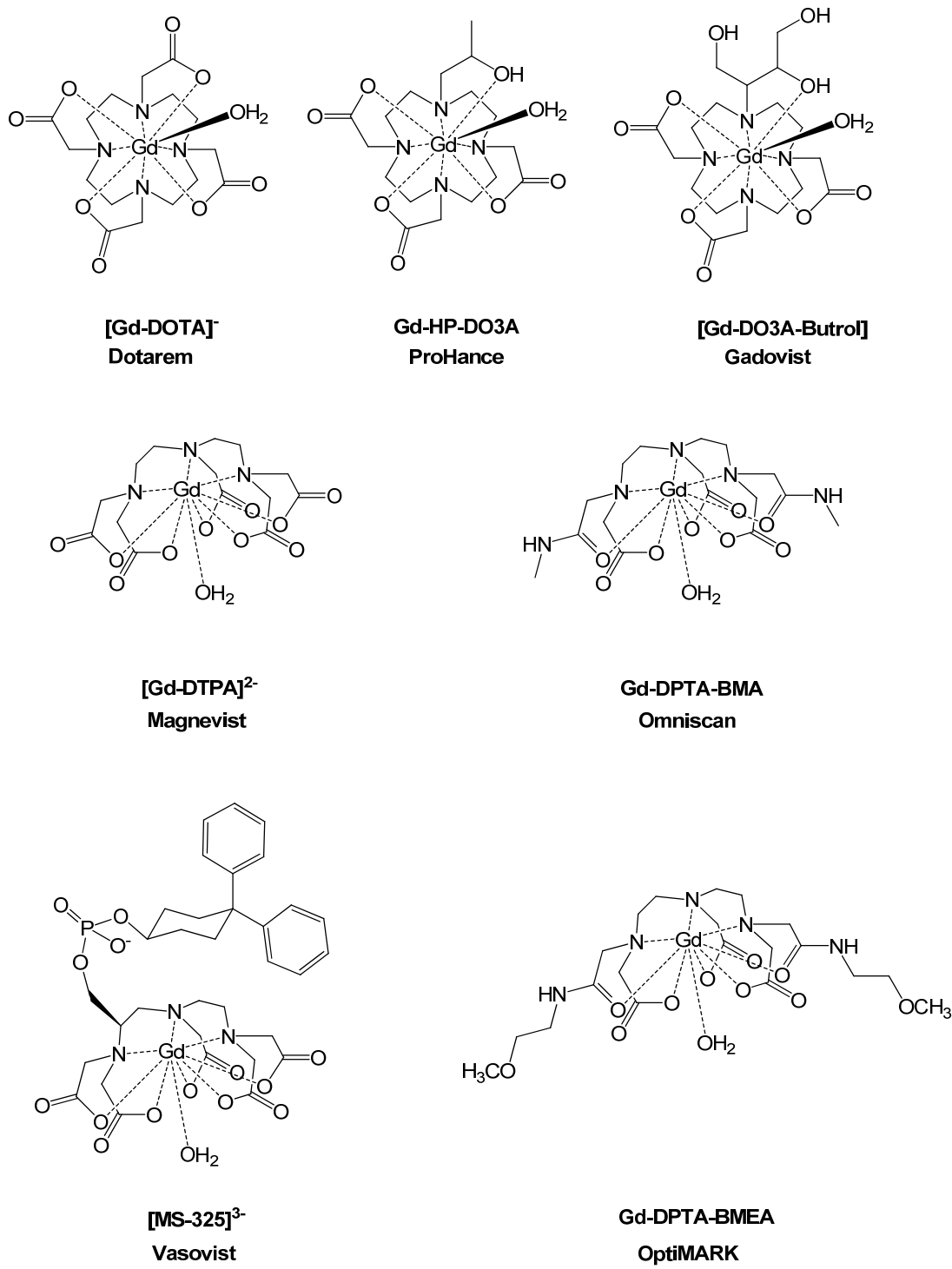


Figure 1.11 First generation magnetic resonance contrast agents.

Contrast Agent	Chemical Name	$\log K_{ML}^{26-31}$	$k_{obs} (10^3 s^{-1})^{32}$
Dotarem <sup>®</sup>	[Gd-DOTA] <sup>-</sup>	25.3	0.021
ProHance <sup>®</sup>	Gd-HP-DO3A	23.8	0.064
Gadovist <sup>®</sup>	[Gd-DO3A-butrol] <sup>2-</sup>	21.8	-
Magnevist <sup>®</sup>	[Gd-DTPA] <sup>2-</sup>	22.46	1.2
Omniscan <sup>®</sup>	Gd-DTPA-BMA	16.85	> 20
OptiMARK <sup>®</sup>	Gd-DTPA-BMEA	16.84	-

Table 1.2 Association constants,  $\log K_{ML}$ , and acid dissociation rate constants ( $[H^+] = 0.1 M$ ),  $k_{obs}$ , for the commercially available Gd(III) contrast agents.

The association (equilibrium) constant,  $K_{ML}$ , is defined in Equation 16. The large  $K_{ML}$  values observed in Table 1.2 show the equilibrium very much to the side of the metal-ligand complex, hence very little free metal ion in solution

$$K_{ML} = \frac{[ML]}{[M][L]} \quad (16)$$

The kinetic inertness of the ligands is demonstrated by the low acid dissociation rate constants,  $k_{obs}$ . Unsurprisingly, DOTA exhibits more kinetic stability than DTPA, which can be attributed to the macrocyclic effect of addition of a cyclic chelating ligand such as DOTA as opposed to the linear DTPA.

Transmetallation studies have also been carried out to assess the preferential binding selectivity for Gd(III),  $K_{sel}$ , over other physiologically present metal ions a more useful indicator of thermodynamic stability;<sup>31-36</sup> Cu(II), Ca(II) and Zn(II), as well as  $H^+$ . Table 1.3 shows the calculated  $K_{sel}$  values for each complex are high and, therefore, preferential selectivity for Gd(III) is exhibited.

$$K_{sel} = K_{ML} \left( \frac{K_{H^+L}}{[H^+]} + \frac{K_{CaL}}{[Ca^{2+}]} + \frac{K_{CuL}}{[Cu^{2+}]} + \frac{K_{ZnL}}{[Zn^{2+}]} \right) \quad (17)$$

Contrast Agent	Ligand	log $K_{sel}$	log $K_{CaL}$	log $K_{CuL}$	log $K_{ZnL}$
Dotarem <sup>®</sup>	DOTA	8.3	17.23	22.63	21.05
ProHance <sup>®</sup>	Gd-HP-DO3A	6.95	14.83	22.84	19.37
Gadovist <sup>®</sup>	Gd-DO3A- butrol	4.13	11.74	22.87	19.26
Magnevist <sup>®</sup>	DTPA	7.04	10.75	21.38	18.29
Omniscan <sup>®</sup>	DTPA-BMA	9.04	7.17	13.03	12.04
OptiMARK <sup>®</sup>	DTPA-BMEA	-	-	-	-

Table 1.3 Association constants for the commercially available contrast agent ligands with selected metal ions.

### 1.3.2 Water Proton Relaxivity, $r_1$

Contrast agents increase signal intensity *e.g.* in order to show blood flow around the body, they also provide contrast between diseased and normal tissue. The signal intensity depends upon the longitudinal relaxation rate of water protons ( $R_1 = 1/T_1$  ( $s^{-1}$ )). Increasing the relaxation rate will increase the signal intensity.<sup>7</sup> Increasing the relaxation rate by only 10-20% is sufficient to be identified by NMR imaging.<sup>14</sup>

The longitudinal paramagnetic relaxation rate enhancement of free water protons,  $R_{1p}$ , is made up of contributions from the inner-sphere (water molecules coordinated directly to the metal centre) relaxation mechanism,  $R_{1p}^{IS}$ , and the outer-sphere (closely diffusing water molecules in the bulk) relaxation mechanism,  $R_{1p}^{OS}$  (Equation 18). The efficiency of a contrast agent is defined by its relaxivity,  $r_1$ : the total paramagnetic relaxation rate enhancement of the water protons per unit concentration of the contrast agent ( $mM^{-1}s^{-1}$ ) (Equation 19).<sup>7</sup> Contrast agent ligands are designed so that one or two coordination sites of the nine-coordinate Gd(III) ion are left free to allow water molecules to bind and exchange with bulk water. The predominant relaxation contribution for contrast agents is that of the inner-sphere protons. It is the contribution that can be more readily controlled by careful contrast agent design.

$$R_{1p} = R_{1p}^{IS} + R_{1p}^{OS} \quad (18)$$

$$r_1 = R_{1p}/[Gd] \quad (19)$$

$$R_{1p}^{IS} = \frac{Cq}{55.6} \frac{1}{T_{1M} + \tau_m} \quad (20)$$

The longitudinal paramagnetic inner-sphere relaxation rate is expressed by Equation 20.<sup>7</sup> Where  $C$  is the concentration of paramagnetic ion,  $q$  is the number of coordinated water molecules,  $T_{1M}$  is the longitudinal relaxation time of the inner sphere waters and  $\tau_m$  is the water exchange lifetime. Equation 20 shows that increasing  $q$ , the hydration state of the complex, will increase the overall relaxivity. An increase in the water exchange rate,  $k_{ex}$  ( $1/\tau_m$ ), will allow more water molecules from the bulk to feel the paramagnetic effects as they come in contact with the Gd(III) ion.<sup>37</sup>

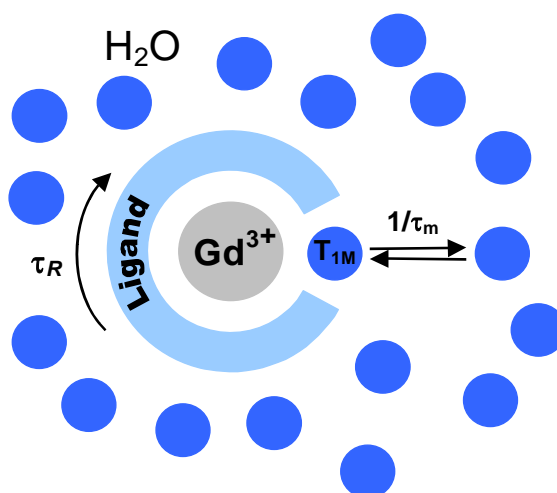


Figure 1.12 Schematic representation of a contrast agent.<sup>37</sup>

Figure 1.12 shows a representation of the outer-sphere and inner-sphere contributions influencing the relaxivity of a contrast agent. The rotational correlation time,  $\tau_R$ , provides further contribution to water proton relaxation and discussed in Section 1.3.6.

### 1.3.3 Hydration State, $q$

Contrast agents that are administered to a human must be safe; the ligand should form a stable complex so that the Gd(III) ion is not released into the body. This safety

concern limits the ability to increase  $q$  to increase relaxivity.<sup>17</sup> The focus of much contrast agent development has been the variation in  $q$ , making sure that the thermodynamic stability of the complex does not decrease sufficiently that the Gd(III) ion becomes labile.

[Gd-DOTA]<sup>-</sup> has been modified to increase  $q = 1$  to  $q = 2$ , by the removal of an acetate group creating a seven coordinate complex [Gd-DO3A]. The relaxivity of [Gd-DO3A] is  $r_1 = 4.8 \text{ mM}^{-1}\text{s}^{-1}$  (20 MHz, 40°C). Under the same conditions [Gd-DOTA]<sup>-</sup> has a relaxivity  $r_1 = 3.5 \text{ mM}^{-1}\text{s}^{-1}$ . The difference is attributed to the difference in hydration states.<sup>37</sup> The stability constant,  $\log K_{ML}$ , for [Gd-DOTA]<sup>-</sup> has been measured at 25.30, the  $\log K_{ML}$ , for [Gd-DO3A] is a much lower value at 21.00.<sup>32, 27</sup> Showing that as  $q$  is increased, there is a considerable loss of thermodynamic stability by the removal of a donor atom. When there is an  $\alpha$ -substituent (Figure 1.13), in this position it slows or ‘locks’ arm-rotation, this boosts kinetic stability, with respect to acid- or metal- ion<sup>-</sup> catalysed Gd loss ([Gd-DO3A] is not kinetically stable enough to use *in vivo* as the Gd(III) ion loss is too great). There is an inherent problem for such DO3A-based  $q = 2$  complexes; they allow the coordination of endogenous ligands such as bicarbonate, citrate, lactate and phosphate, which decrease relaxivity by displacing coordinated water molecules.

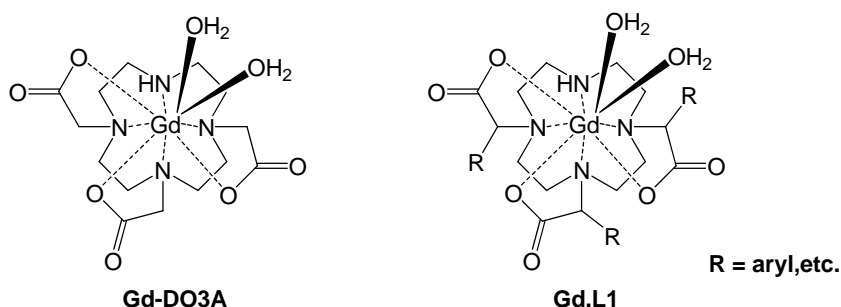


Figure 1.13 Examples of seven-coordinate DO3A-based complexes

The hydroxypyridinone (HOPO) class of compounds developed by Raymond *et al.* appear to be stable  $q = 2$  complexes resistant to anion coordination.<sup>38</sup> **Gd.L2** has a  $\log K_{ML}$  of 18.25 and a relaxivity of  $r_1 = 10.50 \text{ mM}^{-1}\text{s}^{-1}$  (20 MHz, 37°C). The stability is comparable to those in clinical use and ligand development in order to increase stability is ongoing.<sup>38</sup>

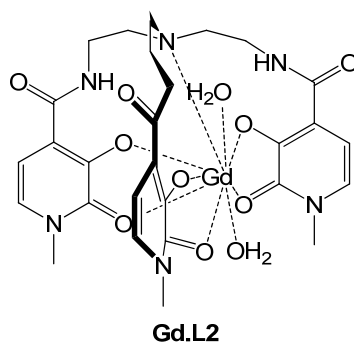


Figure 1.14 Hydroxypyridinone (HOPO) Gd(III) complex.

Contrast Agent	Chemical Name	$q$	$\log K_{ML}$	$r_1$ (mM <sup>-1</sup> s <sup>-1</sup> ) <sup>39, 38</sup>
Dotarem <sup>®</sup>	[Gd-DOTA] <sup>-</sup>	1	25.3	4.20 <sup>a</sup>
ProHance <sup>®</sup>	Gd-HP-DO3A	1	23.8	3.70 <sup>c</sup>
Gadovist <sup>®</sup>	[Gd-DO3A-butrol]	1	21.8	3.60 <sup>c</sup>
Magnevist <sup>®</sup>	[Gd-DTPA] <sup>2</sup>	1	22.46	4.30 <sup>a</sup>
Omniscan <sup>®</sup>	Gd-DTPA-BMA	1	16.85	4.39 <sup>a</sup>
OtiMARK <sup>®</sup>	Gd-DTPA-BMEA	1	16.84	4.70 <sup>b</sup>
<b>Gd.L2</b>		2	18.25*	10.50 <sup>c</sup>

Table 1.4 Hydration state values,  $q$ , stability constants,  $\log K_{ML}$  (\* determined from the  $pM$  value of 19.2 ( $-\log[\text{free Gd(III)}]$  at pH 7.4 where  $[\text{Gd(III)}] = 1 \times 10^{-6}$  M, and  $[\text{L}] = 1 \times 10^{-5}$  M)<sup>40</sup>), and relaxivity values,  $r_1$  (20 MHz at 25°C<sup>a</sup>, 40°C<sup>b</sup> or 37°C<sup>c</sup>), for each of the commercially available MRI contrast agents and of **Gd.L2**

### 1.3.4 Inner-Sphere Water Proton Relaxation

Inner-sphere proton relaxation,  $R_{1p}^{IS}$ , is controlled by a number of factors as shown in Equation 20. The most noticeable, the longitudinal relaxation time,  $T_{1M}$  and the water exchange lifetime,  $\tau_m$ , of the bound water molecules. The first generation contrast agents have a  $T_{1M}$ , which is much greater than  $\tau_m$ , therefore,  $T_{1M}$  is the limiting factor in contrast agent development.<sup>17</sup>

$$\frac{1}{T_{1M}} = \frac{2}{15} \frac{\gamma_H^2 g_e^2 \mu_B^2 S(S+1)}{r_{GdH}^6} \left[ \frac{7\tau_{c2}}{1 + \omega_S^2 \tau_{c2}^2} + \frac{3\tau_{c1}}{1 + \omega_H^2 \tau_{c1}^2} \right] \quad (21)$$

Equation 21, where  $\gamma_H$  is the proton gyromagnetic ratio,  $g_e$  is the electron  $g$ -factor,  $\mu_B$  is the Bohr magneton and  $S$  is the spin quantum number (7/2 for Gd(III)). Shows that relaxation depends on the Gd-H distance  $r_{GdH}$ , the proton Larmor frequency,  $\omega_H$  (in rad/s), the electron Larmor frequency,  $\omega_S$  ( $\omega_S = 658 \omega_H$ ), and the correlation times  $\tau_{c1}$  and  $\tau_{c2}$ . Which themselves are comprised of the rotational correlation time,  $\tau_R$ , the water exchange lifetime,  $\tau_m$ , and the electronic relaxation time of the metal Gd(III) ion,  $T_{1e}$ ,<sup>17</sup> shown in Equation 22.

$$\frac{1}{\tau_{ci}} = \frac{1}{\tau_m} + \frac{1}{\tau_R} + \frac{1}{T_{1e}}; \quad i = 1, 2 \quad (22)$$

Optimisation of contrast agent relaxivity can therefore be achieved by increasing the water exchange rate, decreasing the Gd-H distance, increasing the electronic relaxation rate and slowing down the rotational motion of the complex.

### 1.3.5 Gd(III)-Water Distance, $r_{GdH}$

Varying the Gd(III)-water distance could lead to large enhancement of relaxivity as,  $T_{1M}$  dependence is proportional to  $1/r^6$ , a decrease in distance of about 0.2Å would increase relaxivity by about 50%. Gd-H distances are generally reported within the range 2.5Å to 3.3Å, which have been determined by X-ray diffraction or calculated indirectly by relaxivity studies. More recently the Gd-H distance has been determined as  $3.1 \pm 0.1$ Å for several DOTA and DPTA derivatives by ENDOR spectroscopy.<sup>41, 42</sup>

### 1.3.6 Rotational Correlation Time, $\tau_R$

Most clinical MRI scanners operate at magnetic field strengths 0.5-1.5T (20-60MHz); at these frequencies the longitudinal relaxation time of the water molecules bound,  $T_{1M}$ , is dominated by the molecular reorientation (rotational correlation) time,  $\tau_R$ . The slower the Gd(III) complex tumbles, the longer the correlation time leading to faster relaxation rates and higher relaxivities. A number of approaches have been taken to lengthen  $\tau_R$ . The most common approach is to attach a slowly tumbling macromolecule to a Gd(III) complex. For example binding to a protein, a dendrimer, and polysaccharide or by aggregation of amphiphilic complexes.<sup>7</sup> A method resulting in impressive results is the formation of host-guest, non-covalent interactions between the Gd(III) complex and a slow tumbling macromolecule, *i.e.* the design of complexes bearing hydrophobic moieties that can bind the protein Human Serum Albumin (HSA).<sup>7</sup> As Clinical MRI machines go to higher magnetic field strengths this effect decreases and becomes less important to increasing relaxivity.

At the frequencies of clinical MRI scanners, relaxivity is therefore dominated by contrast agent rotational correlation time; slowing down molecular tumbling causes an increase in the rotational correlation time, which in turn increases  $\tau_c$  and enhances relaxivity.<sup>43</sup> The simulated NMRD (Nuclear Magnetic Resonance Dispersion) profiles in

Figure 1.15 show a dramatic increase in relaxivity at the field frequency range 0.5-1.5 T (20-60 MHz) upon increase of a molecules rotational correlation time.

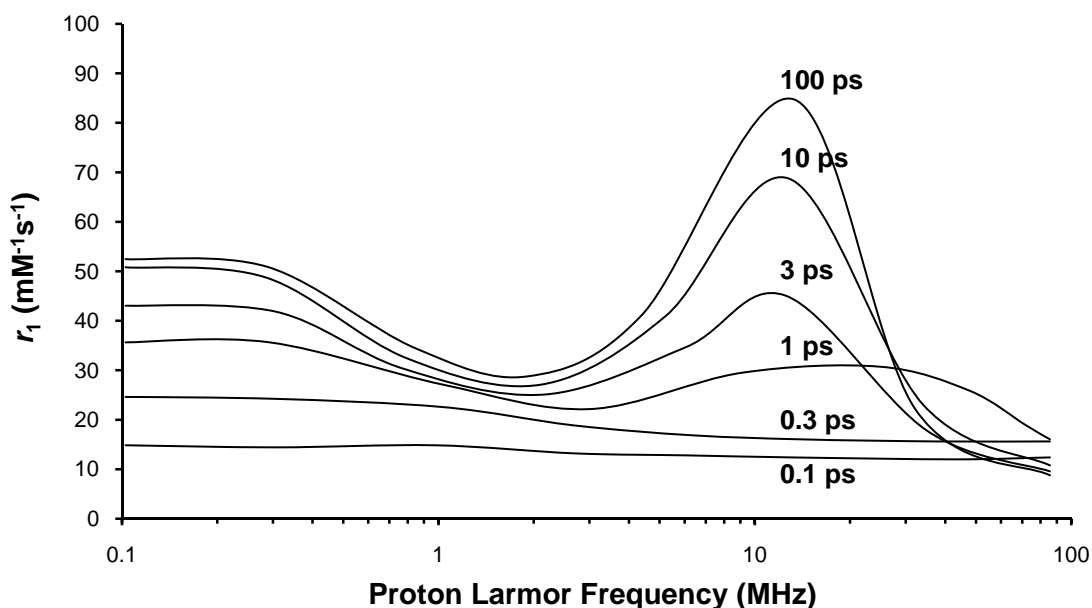


Figure 1.15 NMRD profiles of hypothetical complexes with varying  $\tau_R$  of 0.1 to 100 ps.

It is possible to use data calculated from an NMRD profile to determine the rotational correlation time by fitting the parameters from Equation 21 as well as those obtained from the closely diffusing outer sphere contribution, (discussed in Section 1.3.7).

### 1.3.7 Electronic Relaxation Time, $T_{1e}$

The relaxation rate is affected by the imposing magnetic fields strength. For Gd(III) complexes,  $T_{1e}$  is related to the change of zero field splitting (ZFS) of the electronic spin states, which arise from dynamic distortions of the ligand field interaction.<sup>44</sup> As magnetic field frequency increases both proton and electron Larmor frequencies increase as well. The electron Larmor frequency,  $\omega_S$ , is 658 times greater than  $\omega_H$ , the proton Larmor frequency. In Equation 21 the first term in square brackets, the ‘7 term’ ( $\omega_S$ ) disperses at lower fields than the second term, the ‘3 term’ ( $\omega_H$ ).<sup>18</sup> At higher frequencies there is complete dispersion of the effects of  $T_{1e}$ , as the proton Larmor contribution becomes negligible.

### 1.3.8 Outer Sphere Water Proton Relaxation

The outer sphere contribution accounts for around 40% of the overall relaxivity of monoaqua Gd(III) complexes at imaging fields.<sup>45</sup> It arises from the diffusion of bulk water molecules exchanging with the inner sphere bound water molecules of the nearby paramagnetic complex, and is expressed by Equation 23.

$$R_{1p}^{OS} = C^{OS} \left( \frac{1}{aD} \right) [7J(\omega_s) + 3J(\omega_H)] \quad (23)$$

$$J(\omega) = R_e \left[ \frac{1 + 1/4 \left( i\omega\tau_d + \frac{\tau_d}{\tau_{sj}} \right)^{1/2}}{I + \left( i\omega\tau_d + \frac{\tau_d}{\tau_{sj}} \right)^{1/2} + 4/9 \left( i\omega\tau_d + \frac{\tau_d}{\tau_{sj}} \right) + 1/9 \left( i\omega\tau_d + \frac{\tau_d}{\tau_{sj}} \right)^{3/2}} \right] \quad (24)$$

$$j = 1, 2; \quad \tau_d \frac{a^2}{D}$$

where  $C^{OS}$  is a constant ( $5.8 \times 10^{-13} \text{ s}^{-1} \text{ M}^{-1}$ ),  $J(\omega)$  is the non-Lorentzian spectral density, which is dependent on  $\tau_s$ , the electronic correlation time,  $a$  is the shortest distance of approach (i.e. the radius of the outer sphere) and  $D$  is the diffusion coefficient of the solvent.<sup>46</sup>

### 1.3.9 Water Exchange Lifetime, $\tau_m$

A contrast agent must have at least one water molecule bound; fast water exchange is essential so as to allow more water molecules from the bulk to coordinate to the paramagnetic metal centre enhancing the overall water proton relaxation rates. The charge of a complex plays a big effect on the rate of exchange,  $k_{ex}$  ( $1/\tau_m$ ), water exchange on a positively charged complex is far slower than on a neutral complex, which in turn is slower than on a negatively charged complex.<sup>7</sup> An alternative approach is to change the hydrophobicity (surface area) of the ligand. The water exchange lifetime cannot be too

short, however, as Equation 22 shows,  $\tau_m$  contributes to  $\tau_c$ , a decrease of which would result in a reduction of relaxation rates.  $\tau_m$ , depends on the number of water molecules in the outer-sphere. For a complex with a large surface area/ high hydrophobicity, nearby water molecules may be obstructed from interacting with the complex, in turn causing an increase in  $\tau_m$ , therefore an efficient contrast agent would have a small surface area and be less hydrophobic.<sup>7</sup>

Measurement of  $\tau_m$  is carried out by variable temperature  $^{17}\text{O}$  NMR spectroscopy, in which the temperature dependence of the paramagnetic contribution,  $R_{2p}^O$ , to the observed transverse relaxation rate,  $R_{2obs}^O$ , of water  $^{17}\text{O}$  nuclei is observed

$$R_{2p}^O = R_{2obs}^O - R_{2d}^O \quad (25)$$

where the paramagnetic term  $R_{2d}^O$  is determined from a solution containing a diamagnetic analogue of the chelate being studied.<sup>47</sup>

$R_{2p}^O$  is related to  $\tau_m^O$ , via the  $^{17}\text{O}$  chemical shift difference between coordinated and bulk water molecules,  $\Delta\omega_m^O$ , and the transverse relaxation rate of the coordinated water  $^{17}\text{O}$ ,  $R_{2m}^O$ , following the Swift and Connick theory,<sup>48</sup> and is expressed by

$$R_{2p}^O = \frac{qC}{55.6} \tau_m^{O-1} \frac{R_{2m}^{O2} + \tau_m^{O-1} R_{2m}^O + \Delta\omega_m^{O2}}{\left(R_{2m}^O + \tau_m^{O-1}\right)^2 + \Delta\omega_m^{O2}} \quad (26)$$

where  $R_{2m}^O$  is determined in Equation 27.<sup>49</sup>

$$R_{2m}^O = \frac{1}{3} \left( \frac{A}{\hbar} \right)^2 S(S+1) \left( \tau_{e1} + \frac{\tau_{e2}}{1 + \omega_s^2 \tau_{e2}^2} \right) \quad (27)$$

$$\frac{1}{\tau_{ei}} = \frac{1}{\tau_m^O} + \frac{1}{T_{1e}}$$

where  $S$  is the electronic spin quantum number (7/2 for Gd(III)),  $(A/\hbar)$  is the Gd-O scalar coupling constant (approx  $-3.8 \times 10^6 \text{ rad s}^{-1}$ ),<sup>50</sup>  $\tau_{ei}$  ( $i = 1, 2$ ) is the correlation times of modulating the scalar interaction and  $T_{1e}$  is the electronic relaxation time.

The temperature dependence of  $\Delta\omega_m^O$  is expressed by Equation 28, where  $B_o$  is the magnetic field strength and  $k_B$  is the Boltzmann constant.<sup>49</sup>

$$\Delta\omega_m^O = \frac{g_e \mu_B S(S+1) B_o}{3k_B T} \frac{A}{\hbar} \quad (28)$$

The temperature dependence of  $R_{2p}^O$  is expressed in terms of the  $^{17}\text{O}$  water exchange lifetime,  $\tau_m^O$ , and to  $\tau_v$  (the correlation time for modulation of the ZFS) by the Eyring equation, (Equation 29)

$$\frac{1}{\tau_j} = \frac{k_B T}{h} \exp\left(\frac{\Delta S_j^\ddagger}{R} - \frac{\Delta H_j^\ddagger}{RT}\right) = \frac{(\tau_i^{-1})^{298.15} T}{298.15} \exp\left(\frac{\Delta H_j^\ddagger}{R} \left(\frac{1}{298.15} - \frac{1}{T}\right)\right) \quad (29)$$

where the suffix  $j$  refers to the different correlation times ( $m, v$ ),  $\Delta S^\ddagger$  and  $\Delta H^\ddagger$  are the entropy and enthalpy of activation for the corresponding dynamic process respectively and  $(\tau_j^{-1})^{298.15}$  is the rate at 298.15 K.<sup>51</sup> Water exchange rate,  $k_{ex}$ , can be expressed in terms of the inverse of the water exchange lifetime,  $\tau_m^O$ .

The paramagnetic contribution to the  $^{17}\text{O}$  transverse relaxation rate,  $R_{2p}^O$ , increases with temperature in the slow kinetic region (*i.e.* when temperatures are low) and is directly determined by  $k_{ex}$  ( $1/\tau_m^O$ ). In the fast exchange region (*i.e.* when temperatures are high) the water exchange lifetime,  $\tau_m^O$ , becomes short enough with respect to the relaxation rate of the coordinated water  $^{17}\text{O}$ ,  $R_{2m}^O$ , resulting in a decrease in  $R_{2p}^O$ .<sup>52</sup>

The plot maximum shows the change over from the slow to fast regions, which shifts to lower temperatures with increasing water exchange rates. The plot maxima of the bell-shaped curves move to lower temperatures as the water exchange rate of the complex increases, as shown in Figure 1.16. Variable temperature  $^{17}\text{O}$  NMR profiles can be fitted by

utilising Equations 29-32 to yield the water exchange lifetime,  $\tau_m$ , as well as  $\tau_v$  and the activation entropy and enthalpy,  $\Delta S^\ddagger$  and  $\Delta H^\ddagger$  respectively.

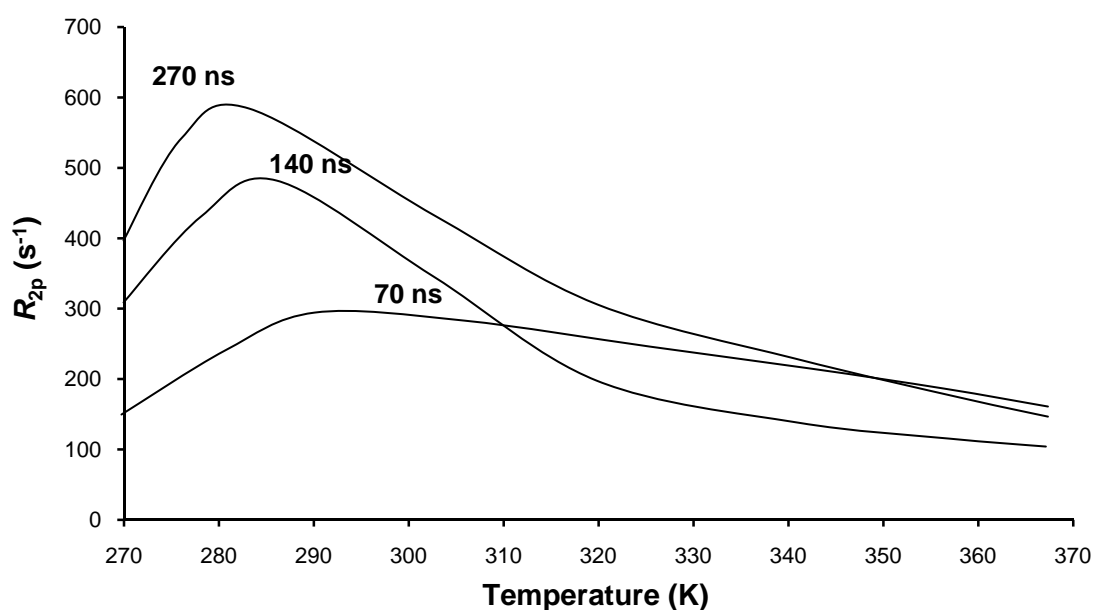


Figure 1.16 Variable temperature  $^{17}\text{O}$  NMR profile of a hypothetical  $[\text{Gd-DOTA}]^-$  complex with  $\tau_m$  ranging from 70-270 ns.

#### 1.4 Contrast Agent Enhancement

The focus of contrast agent research in recent years has centred on the exploitation of the water exchange lifetime and rotational correlation time contributions to overall relaxivity. Table 5 shows the  $\tau_m$  and  $\tau_R$  values for  $[\text{Gd-DTPA}]^{2-}$ ,  $[\text{Gd-DOTA}]^-$  and Gd-DO3A.<sup>50, 53</sup>

Contrast Agent	Chemical Name	$\tau_m$ (ns)	$\tau_R$ (ps)
Dotarem <sup>®</sup>	$[\text{Gd-DOTA}]^-$	244 <sup>a</sup>	77 <sup>a</sup>
	Gd-DO3A	160 <sup>b</sup>	66 <sup>b</sup>
Magnevist <sup>®</sup>	$[\text{Gd-DTPA}]^{2-}$	303 <sup>a</sup>	58 <sup>a</sup>

Table 1.5 Water exchange lifetime,  $\tau_m$ , and rotational correlation time,  $\tau_R$ , for  $[\text{Gd-DTPA}]^{2-}$ ,  $[\text{Gd-DOTA}]^-$  and Gd-DO3A. a = 25°C, 9.4 T ( $^{17}\text{O}$ )<sup>53</sup>, b = 25°C, 2.1 T ( $^{17}\text{O}$ )<sup>50</sup>.

#### 1.4.1 Shortening of the Water Exchange Lifetime, $\tau_m$

Manipulation of the water exchange dynamics of Gd(III) chelates has been achieved by either manipulation of the steric compression surrounding the Gd(III) centre or by the modification of pendant groups to the chelate.

The former was achieved by Merbach and co-workers who increased the steric crowding of monoaqua  $[\text{Gd-DTPA}]^{2-}$  and  $[\text{Gd-DOTA}]^-$  chelates by replacing one or two of the ethylene bridges of the chelates with propylene bridges.<sup>54, 55</sup> Despite the slight loss in stability of the chelates, the induced steric compression around the Gd(III) centre facilitated the leaving of the Gd(III) bound water. Water exchange rates were increased from  $\sim 30$ -50 fold for the  $[\text{Gd-DOTA}]^-$  analogues and  $\sim 45$ -100 fold for the  $[\text{Gd-DTPA}]^{2-}$  analogues.

It is well known that  $[\text{Ln-DOTA}]^-$  exists in solution as four interchangeable stereoisomeric complexes, related as two enantiomeric pairs: the mono-capped square antiprismatic geometry (SAP) and the mono-capped twisted square antiprismatic geometry (TSAP) (Figure 1.17).<sup>56</sup> Each possesses a  $C_4$ -rotation axis perpendicular to the plane through the four nitrogens of the cyclen ring, capped by the water oxygen atom.<sup>57</sup>

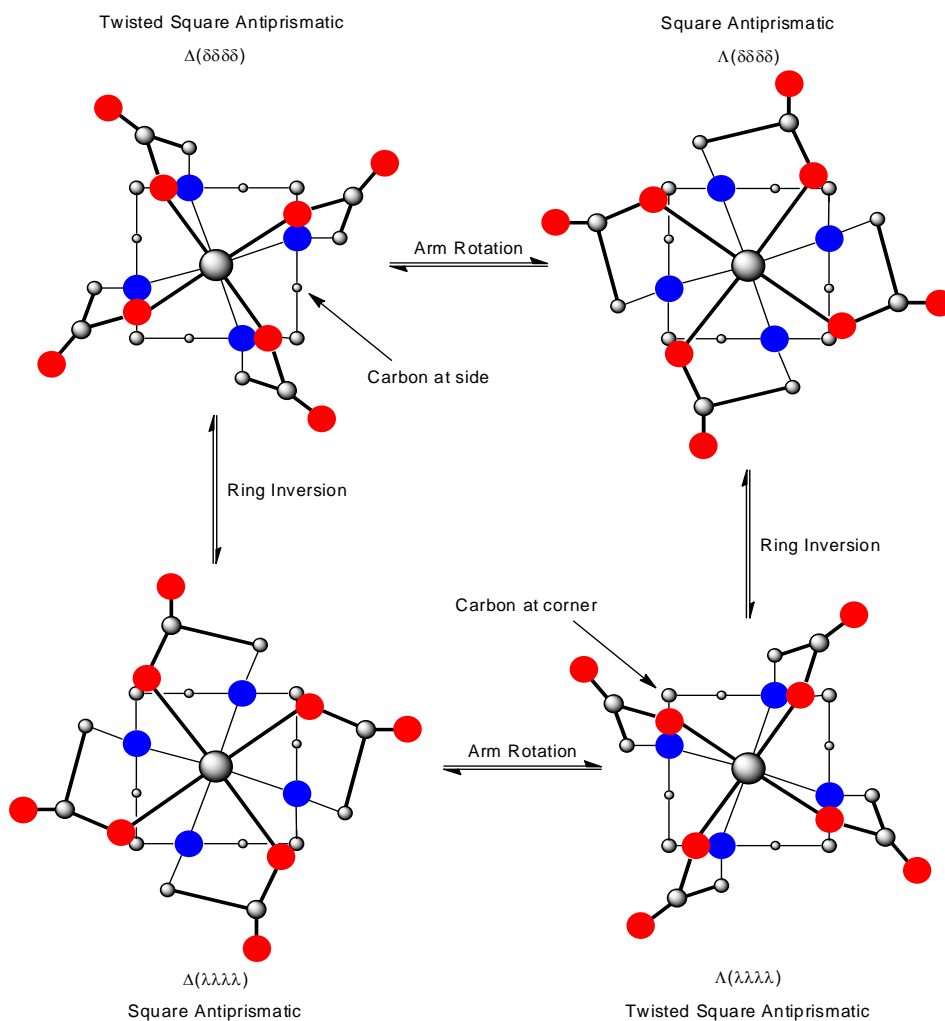


Figure 1.17 [Ln-DOTA]<sup>-</sup> stereoisomeric structures present in solution.<sup>56</sup>

Figure 1.17 shows that the interconversion between the two isomers, SAP and TSAP, occurs either by cooperative ring inversion ( $\lambda$  to  $\delta$ ) or by concerted arm rotation ( $\Delta$  to  $\Lambda$ ).<sup>58</sup> The activation energy for the inversion of SAP to TSAP is greater, at  $\Delta G^\ddagger = 65.6 \text{ kJ mol}^{-1}$  compared to the reverse inversion,  $\Delta G^\ddagger = 61.4 \text{ kJ mol}^{-1}$ , causing the SAP geometry to be the major isomer in solution for Eu(III) complexes.<sup>59, 60</sup> The minor TSAP isomer possesses greater steric crowding about the Eu(III) centre, which is the cause of its decreased presence in solution. The increased steric crowding, however, facilitates the release of the Ln(III) bound waters, lowering the water exchange lifetime from  $\tau_m = 1.88 \times 10^{-5} \text{ s}$  (SAP) to  $\tau_m = 4.16 \times 10^{-3} \text{ s}$  (TSAP) ([Eu-DOTA]<sup>-</sup>, 400 MHz <sup>1</sup>H NMR spectrometry, CD<sub>3</sub>CN, 298 K).<sup>61, 62</sup> The faster observed water exchange has led to the production of DOTA chelates incorporating pendant side chains designed to lock the species in the minor TSAP form in solution.

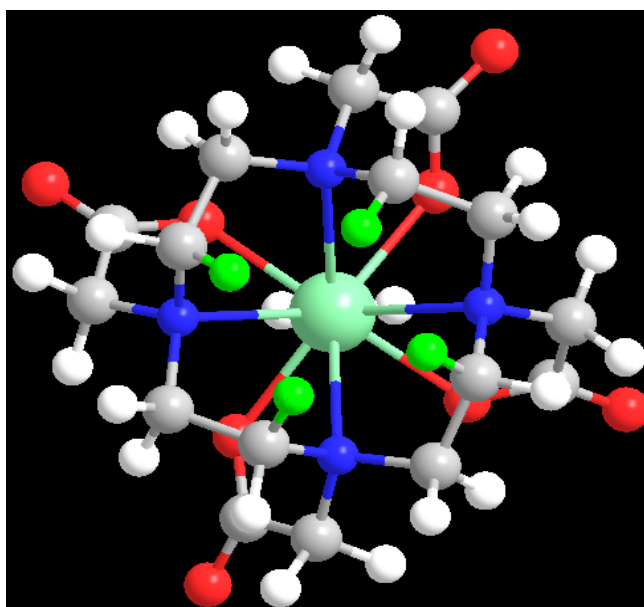


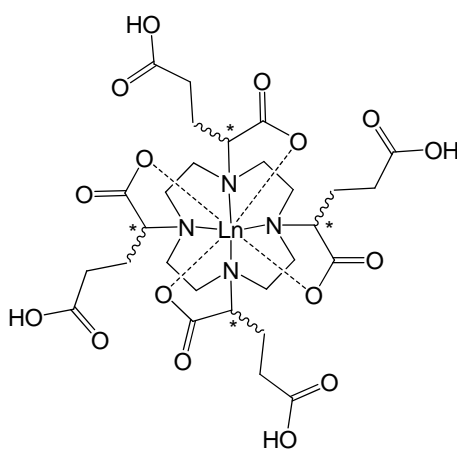
Figure 1.18 Three-dimensional view of  $[\text{Eu-DOTA}]^-$  in the SAP isomeric form showing the axial protons (green) oriented towards the Eu(III).

$^1\text{H}$  NMR spectroscopy is an extremely useful tool in determining the abundance of each isomer in solution as the inversion process is slowed at lower NMR operating temperatures. It is worth noting at this point that the above water exchange rate was measured from  $^1\text{H}$  NMR spectra of the  $[\text{Eu-DOTA}]^-$  analogue, where the observed Eu(III) bound water resonances vary upon increasing temperature, allowing for exchange rate determination. Comparison between the isomeric water molecules was made easier by the large chemical shift difference between the Eu(III) bound water proton resonance of the TSAP isomer at  $\delta \sim 9$  ppm compared to SAP isomer at  $\delta \sim 82$  ppm.<sup>61</sup> The same trend is observed when comparing the axial proton shifts of the cyclododecane ring of the DOTA chelate. When coordinated to the Eu(III) ion, four of the axial protons are in close proximity with the highly paramagnetic metal ion, inducing a large chemical shift to  $\sim 25$ - $35$  ppm, in the  $^1\text{H}$  NMR spectrum. The chemical shifts of the axial protons on the ring of the macrocycle are observed for both isomers, which invert from the SAP to TSAP isomer, causing a reorientation of the associated axial protons with respect to the Eu(III) centre.<sup>54</sup>

Figure 1.18 shows in green, the axial protons which are oriented towards the Eu(III) centre of the  $[\text{Eu-DOTA}]^-$  complex, under the plane of the four nitrogens. Axial proton resonances are observed at  $\sim 15$ - $25$  ppm for TSAP isomers, while the same axial protons

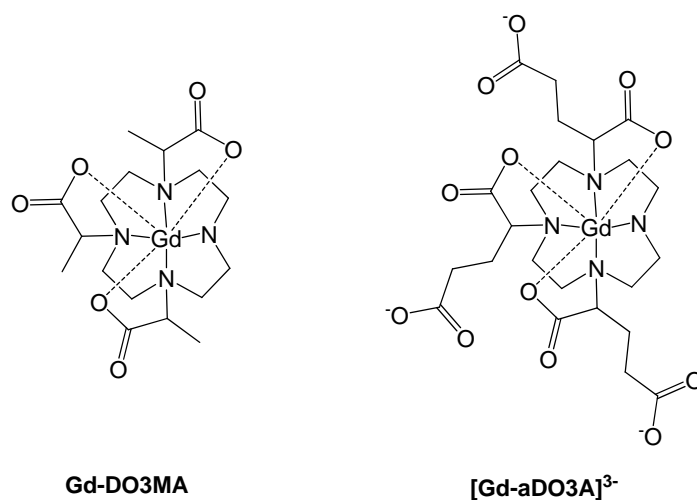
appear at  $\sim 30$ -50 ppm for SAP isomers, showing a clear distinction between the two isomeric forms.<sup>58</sup>

The introduction of substituents in the  $\alpha$ -carbon positions, such as the addition of glutaric acid groups as in Ln-gDOTA, brings about increased rigidity, particularly inhibiting arm rotation and sterically locking the complex.<sup>63</sup> The addition of such substituents results in the formation of two diastereoisomeric pairs, rather than enantiomeric pairs,<sup>64</sup> and gives rise to six possible stereoisomeric configurations in solution with respect to the aliphatic substituents; *RRRR*, *SSSS*, *RSSS*, *SRRR*, *RSRS*, *RRSS*, defined by the absolute configuration at the  $\alpha$ -carbon.<sup>63</sup>



**Ln-gDOTA**

Pendant group modification is also used as a strategy to enhance water exchange rate. The variation of structure and charge of such moieties leads to organisation of the solvent spheres, providing lower energy routes to more efficient water exchange. The incorporation of negative charge by the substitution of the  $\alpha$ -carbon methyl groups of DO3MA with adipic acid gave rise to a five-fold reduction in the water exchange lifetime and  $\sim 100\%$  increase in relaxivity from the resulting ligand aDO3A;  $\tau_m = 160$  ns and  $\tau_m = 30$  ns (0.5 T);  $r_1 = 6.0$  mM<sup>-1</sup>s<sup>-1</sup> and  $r_{1p} = 12.3$  mM<sup>-1</sup>s<sup>-1</sup> for [Gd-DO3MA] and [Gd-aDO3A]<sup>3-</sup> respectively (25°C, 20 MHz).<sup>66</sup>



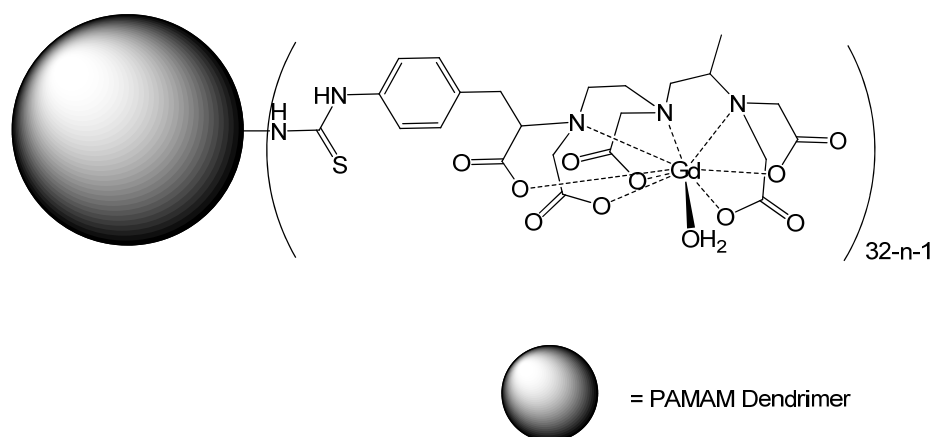
#### 1.4.2 Lengthening the Rotational Correlation Time, $\tau_R$

As discussed in Section 1.3.6, at clinical MRI frequencies  $T_{1m}$  is dominated by the rotational correlation time,  $\tau_R$ ; the lengthening of which results in an increase in relaxivity and enhancement of image intensity. The rotational correlation time of contrast agents has been lengthened by the preparation of slowly tumbling Gd(III) macromolecules, with the incorporation of several pendant groups, such as tris(hydroxymethyl)aminomethanes<sup>67</sup> and cyclams.<sup>68</sup> The increase of the molecular weight reduces the motional tumbling of the Gd(III) complex, increasing  $\tau_R$ .

The preparation of high molecular weight dendrimeric macromolecules has been of considerable interest in the production of MRI contrast agents.<sup>69,70</sup> The incorporation of several Gd(III) chelates into large molecular weight spherical macromolecules bearing polymeric cores has led to the production of contrast agents which display high MR image contrast with a much lower dosage administered to the patient. Two such polymer core based dendrimers are the commercially available diaminobutane (DAB) and polyamidoamide (PAMAM),<sup>71</sup> each highly water-soluble spherical molecules bearing primary amino acid groups exposed on their surface, capable of Gd(III) chelation. The incorporation of lanthanide based chelates into PAMAM dendrimers has been extensively researched in recent years.<sup>72, 73</sup>

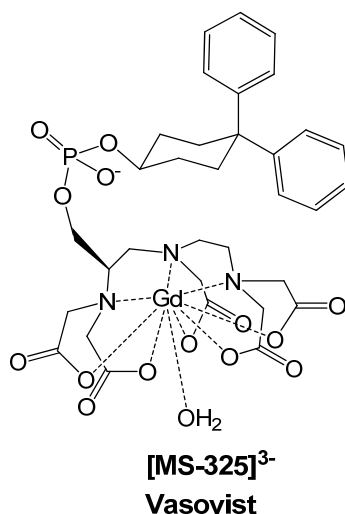
Hermann and co-workers recently developed a series of G2-, G3- and G4-PAMAM dendrimers incorporating monophosphinated Gd-DOTA based chelates.<sup>74,75</sup> The dendrimers are denoted G2- G3- and G4-, which refers to the number of exposed primary

amino groups on the surface the macrocycle (8 amino groups for G1-, 16 for G2-, 32 for G3- and 64 for G4-) surrounding the PAMAM backbone. This allows for the production of increasing molecular weight macromolecules containing increasing numbers of Gd(III) chelates. The measured relaxivities for each of the generated dendrimeric species increased with increasing size;  $r_1 = 10.1 \text{ mM}^{-1}\text{s}^{-1}$ ,  $r_1 = 14.1 \text{ mM}^{-1}\text{s}^{-1}$  and  $r_1 = 18.1 \text{ mM}^{-1}\text{s}^{-1}$  (37°C, pH 7.5, 20 MHz), attributed to the increasing global rotational correlation time of the dendrimers;  $\tau_{Rg} = 1,560 \pm 280 \text{ ps}$ ,  $2,690 \pm 270 \text{ ps}$  and  $3,140 \pm 210 \text{ ps}$  (25°C, pH 7.5) for G1-8 Gd(III), G2-16 Gd(III) and G4-59 Gd(III) respectively. The relaxivity enhancement was not as great as was hoped due to the low rigidity factor,  $S^2 \sim 0.26$ , causing fluctuations within the molecule and lowering the effective rotational correlation time;  $\tau_R = 115 \pm 4 \text{ ps}$ ,  $100 \pm 3 \text{ ps}$  and  $133 \pm 4 \text{ ps}$  (25°C, pH 7.5) for G1-8 Gd(III), G2-16 Gd(III) and G4-59Gd(III) respectively.



The lengthening of the rotational correlation time,  $\tau_R$ , has also been achieved by the receptor induced magnetisation enhancement (RIME) strategy in which pendant groups are attached to the Gd(III) chelate enabling binding to slowly tumbling molecules, such as serum proteins.<sup>76</sup> The attachment of hydrophobic moieties has led, for example, to the development of contrast agents which bind non-covalently to the plasma protein human serum albumin (HSA), Lauffer and coworkers have developed a blood pool agent, [MS-325]<sup>3-</sup>, commercially known as Vasovist, a DTPA-based Gd complex, which binds HSA *via* the hydrophobic diphenyl cyclobenzyl moiety, showing an increase in relaxivity from  $r_1 = 6 \text{ mM}^{-1}\text{s}^{-1}$  (35°C, 20 MHz) to  $r_1 = \sim 45 \text{ mM}^{-1}\text{s}^{-1}$  (35°C, 20 MHz), when bound to HSA.<sup>77</sup> This shows a 7-fold increase in relaxivity, giving a 7-fold increase in image intensity. A second strategy is the incorporation of amphiphilic, hydrophobic side chains allowing for

the incorporation of several Gd(III) chelates into slowly tumbling liposomes either within the liposome vesicle or immobilized in the membrane.<sup>78</sup>



### 1.5 Second Generation Contrast Agents

Whilst MRI in general provides good resolution, producing highly detailed images of the whole body, even using cutting-edge MRI scanners and contrast agents, the poor sensitivity of the NMR phenomenon makes it less than ideal for use in detecting cellular and molecular processes. At present, commercial contrast agents are administered in dosages of around  $0.1 \text{ mmolkg}^{-1}$  to the patient to overcome the inherent insensitivity. One approach to solve the problem has been to localise the contrast agent *via* an interaction with a particular target molecule, which can be either extra- or intracellular. Extracellular imaging, for example involves linking the Gd(III) chelate to a protein or antibody that is specific for a cell surface receptor. The exploitation of avidins high affinity for biotin (labelled antibody) ( $K_d \sim 10^{-15} \text{ M}$ ), has been demonstrated by appending avidin to liposomes bearing multiple Gd(III) chelates. Biotin binds to a receptor upon the diseased (target) cell, avidin binds to biotin localising the multiple Gd(III) chelates giving a signal, that is discernable from the background noise.<sup>79</sup> One Gd(III) chelate per receptor does not provide enough signal intensity to be seen, as the concentration of receptors are typically small, therefore multiple Gd(III) chelates are needed per receptor.

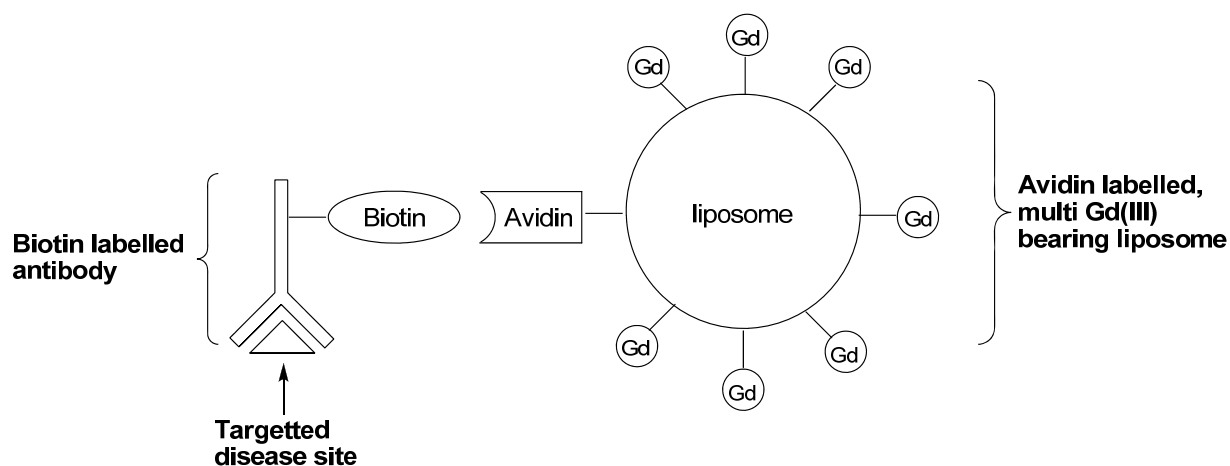
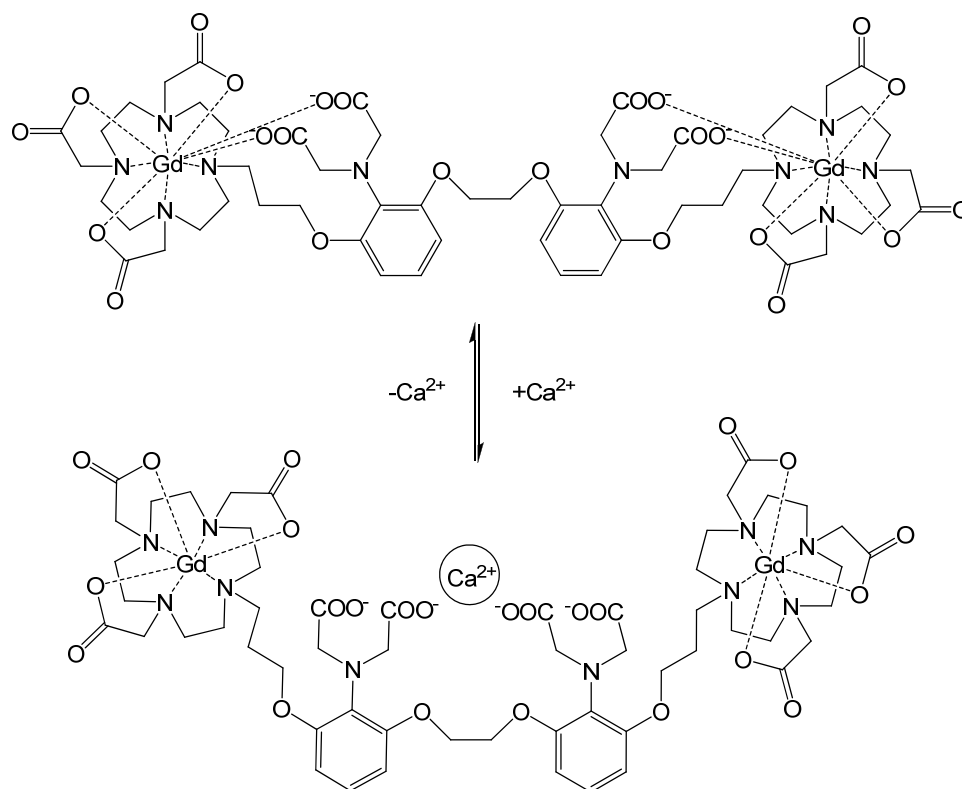


Figure 1.19 Specific disease site targeting of multi-Gd(III)-containing liposome *via* avidin-biotin recognition.

In recent years, one of the most exciting areas in contrast agent development, is in the area of ‘smart’ or responsive contrast agents. The relaxivities of these Gd(III) chelates are modulated by physiological conditions or activity. Functionality incorporated into the Gd(III) chelates respond to biological events, such as variation in pH, metal ion concentration, partial pressure of oxygen or enzyme activity.<sup>7</sup>

Extracellular pH of healthy tissue is 7.4, whereas tumour tissue is more acidic with a pH of 6.8-6.9, therefore contrast agents, which respond to changes in pH, could be used for pH mapping and tumour detection. One approach is the change in hydration state *via* reversible intramolecular anion binding. Sulfonamides have a pH dependent binding to Gd(III), in basic media the sulfonamide is deprotonated and bound to the Gd(III) centre, therefore there are no bound inner-sphere waters ( $q = 0$ ), hence a low relaxivity. In acidic media the sulfonamide is protonated and is not bound to the Gd(III) centre, this results in a di-aqua ( $q = 2$ ) species with a much greater relaxivity.

Contrast agents that respond to different concentrations of metal ions, such as Ca(II), Fe(II)/(III) and Zn(II), are currently being pursued. Meade and co-workers have investigated Ca(II) responsive contrast agents that provide information on physiological signals and biochemical events.<sup>80</sup> The Gd(III) chelate’s relaxivity is dependent on Ca(II) concentration: in the presence of Ca(II), the co-ordination site is unblocked and water is able to bind to the Gd(III) chelate, thus increasing relaxation rates, going from  $q = 0$  at with a low relaxivity of  $3.3 \text{ mM}^{-1} \text{ s}^{-1}$  (500MHz, 25 °C) to  $q = 1.5$  with a 75 % increase in relaxivity, in the presence of Ca(II) (Scheme 1.2).<sup>80</sup>



Scheme 1.2 Meade and co-workers  $\text{Ca}^{2+}$  selective MRI contrast agent.<sup>80</sup>

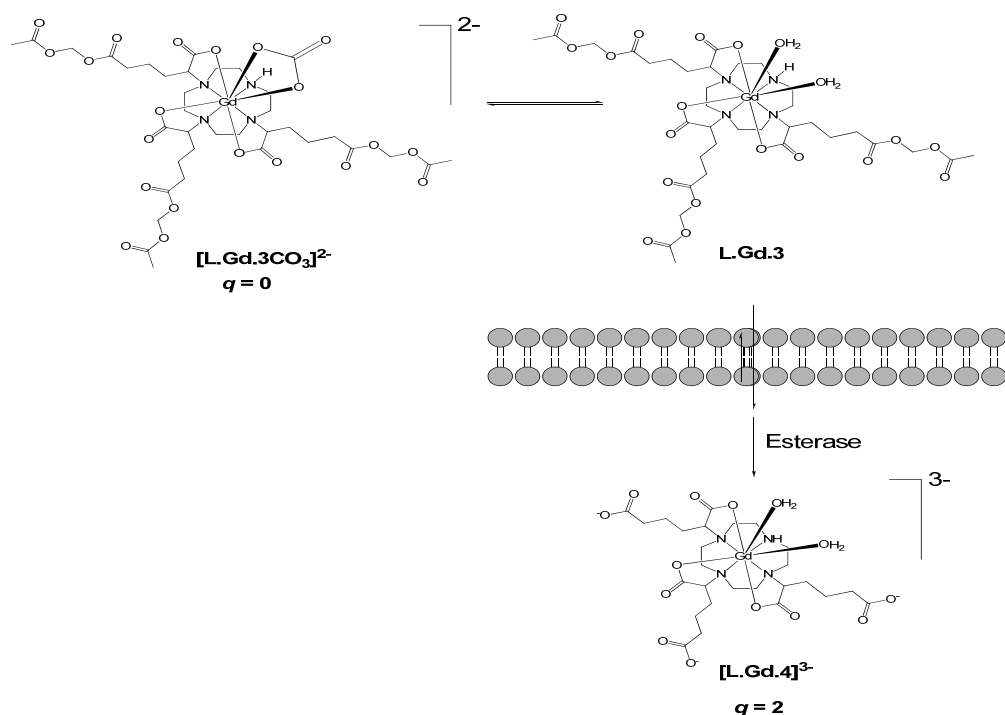
Recently Pope and co-worker have developed a Eu(III)DO3A-based zinc sensor. They have appended a dipicolylaminomethyl-pyridine unit to the DO3A, which binds to the metal centre with a hydration state  $q = 0.2$ , in the presence of Zn(II) the co-ordinated dipicolylaminomethyl-pyridine unit, binds Zn(II), allowing water to bind to Eu(III) with a  $q = 2$ . They have shown that in an aqueous environment at physiological pH, that the complex is selective for Zn(II); it is postulated that a Gd(III) analogue would show significant changes in relaxivity in the presence of Zn(II).<sup>81</sup>

Oxygen-activated contrast agents are being developed with potential for detecting tumours, strokes and ischemic diseases, due to the change in partial pressure of oxygen ( $\text{pO}_2$ ) with these conditions. Merbach and co-workers have developed two macrocycle chelates of Eu(III), these take advantage of the Eu(II)/Eu(III) reduction potential, providing  $\text{pO}_2$ -responsive relaxivity, since the Eu(II) ion has much more significant effect on proton relaxivity than Eu(III), Eu(II) having the same  $[\text{Xe}]4f^7$  configuration as Gd(III).<sup>82</sup>

In recent years there has been much research and development of contrast agents that respond to the presence of an enzyme. Several contrast agents have been designed that incorporate a substrate for a specific enzyme. The concept is: the substrate acts as a “masking” group for the relaxivity properties of the contrast agent, causing a low MR

image intensity. The “masking” group is cleaved in the presence of the enzyme, as a result the relaxivity of the contrast agent is increased and therefore MR image intensity is increased, effectively switching on the contrast agent. An example of this was reported by Meade and co-workers, their  $\beta$ -galactose responsive agent was discussed in Section 1.1.1. McMurry and co-workers developed an agent that binds to HSA, only after interaction with carboxypeptidase B discussed further in Chapter 5.1.<sup>83</sup>

Another approach is the accumulation and activation strategy that involves the contrast agent being able to localise within certain cells and have its relaxivity enhanced following interaction with a specific enzyme. Lowe *and* co-workers,<sup>84</sup> have developed a Gd(III) cyclen-based contrast agent, which interacts with non-specific intracellular esterases, increased levels of this enzyme are associated with such diseases as leukaemia. They hypothesise that the seven-coordinate contrast agent will have a neutral charge *in vivo*; this allows for a high affinity for binding endogenous anions such as  $\text{HCO}_3^-$  (bound as carbonate,  $\text{CO}_3^{2-}$ ), the most abundant in serum (20-30mM). Once in a cell the acetoxymethyl esters are cleaved by intracellular esterase changing the charge to  $-3$ . The change in charge suppresses the affinity for binding carbonate opening up the internal water binding sites on the contrast agent, changing  $q = 0$  to  $q = 2$ . This increase in proton relaxivity, therefore increases signal intensity, switching on the contrast agent. The second effect of the interaction is the localization of the contrast agent within cells as the outflow of the negatively charged complexes will be reduced (Scheme 1.3).<sup>84,7</sup>



Scheme 1.3

## 1.6 Lanthanides

### 1.6.1 Properties of the Lanthanides

The lanthanides are a series of electropositive period 6 metals, which lie between the *s*- and *d*-blocks of the periodic table. The series comprises the elements cerium (atomic number 58) to lutetium (71); the elements feature a xenon core electron configuration, periodically filling the seven  $4f$  orbitals, from  $4f^1$  (Ce) to  $4f^{14}$  (Lu). The  $4f^n$  sub-shell is contracted, shielded from the environment by the  $5s^2$  and  $5p^6$  closed sub-shells, and thus the *f*-orbitals are not available for bonding.<sup>85</sup> The lanthanides are often referred to as the rare earth elements, this is misleading as over 100 minerals contain the metals, such as bastnaesite; a lanthanide fluorocarbonate and monoazite; a phosphate mineral of mixed lanthanides and thorium,  $(Ln,Th(PO)_4)$ . The most abundant lanthanide is cerium (Ce), the first member of the series discovered in 1803, the 26<sup>th</sup> most abundant element on earth, which is present at ~66ppm in the earth's crust. The least abundant lanthanide, thulium (Tm, 1879) is more abundant than iodine. The final member promethium (Pm) was synthesised and characterised in 1947 completing the series.<sup>86, 87</sup>

Chemical properties within the lanthanide series are traversed extremely uniformly, unlike that of the *d*-block elements. The common oxidation state in aqueous solution is +3,

however Eu(II) can be prepared by reduction with zinc, also Yb(II) and Sm(II) can be prepared but all are readily oxidised. Reduction potentials,  $E^0$ , for the  $\text{Ln}^{3+}/\text{Ln}^{2+}$  process are  $E^0 = -0.35$  V,  $-1.05$  V and  $-1.55$  V for Eu(II), Yb(II) and Sm(II) respectively. Cerium can exist in the +4 oxidation state, with the  $\text{Ce}^{4+}/\text{Ce}^{3+}$  reduction potential of  $E^0 = +1.72$  V, and can exist in solution for several weeks.<sup>86</sup> The trivalent state results in sequential loss of the  $5d^1 6s^2$  electrons from the  $[\text{Xe}]5d^1 6s^2 4f^n$  core. The uniform +3 oxidation state is shown by the similar observed  $\text{Ln}^{3+}/\text{Ln}^{0+}$  reduction potentials across the series, measured at around  $E^0 = -2.80$  V in basic media and  $E^0 = -2.30$  V in acidic media for each of the lanthanide metals, with the exception of europium at  $E^0 -2.51$  V (basic) and  $E^0 = -1.51$  V (acidic).<sup>86</sup>

The ionic radii of the lanthanides decrease across the series: however, the observed decrease is greater than expected, with the ionic radii measured as  $1.16\text{\AA}$  (La(III)) and  $0.97\text{\AA}$  (Lu(III)) (C.N. = 8).<sup>88,89</sup> Lanthanide contraction is the result of poor shielding properties of the  $4f$  orbitals. The increasing effective nuclear charge,  $Z_{\text{eff}}$ , along the series is not compensated by the addition of the electrons to the  $4f$  shell, resulting in the large contraction observed in the ionic radii.<sup>90</sup>

### 1.6.2 Coordination Chemistry of the Lanthanides

The lanthanide ions are hard Lewis acids, preferably binding hard bases such as oxygen and nitrogen.<sup>91</sup> The buried  $4f$  orbitals are not available for covalent interactions with coordinating ligands. This shielding by the  $5s$  and  $5p$  core electrons, results in large similarities in the chemical behaviour of each of the Ln(III) ions. Ln(III)-ligand interactions are largely electrostatic, with the coordination geometry of the complexes formed being affected by steric factors due to lanthanide contraction.<sup>91</sup>

The large size of lanthanide ions result in complex formation with coordination numbers of 8 or 9 very common. Ligands are arranged around the Ln(III) ion to minimize repulsion; this is affected by the varying sizes of the lanthanide ions, leading to irregular complex geometries across the series. An example of this is shown by contrasting geometries of the  $\text{acac}^-$  ( $\text{CH}_3\text{COCHCOCH}_3^-$ ) complexes formed with Yb(III) and La(III). The  $[\text{Yb}(\text{acac})_3\text{H}_2\text{O}]$  complex forms a capped trigonal prismatic structure. The monohydrate species is seven coordinate, as a result of the small ionic radius of the metal ion centre. The  $[\text{La}(\text{acac})_3(\text{H}_2\text{O})_2]$  complex is eight coordinate forming a square antiprismatic geometry as a result of a larger ionic radius.

In aqueous solution the Ln(III) aqua ion is formed with C.N. 9 for the larger ions (La(III)-Nd(III)) and 8 for the smaller (Dy(III)-Lu(III)). The Ln(III) ions undergo hydrolysis at pH > 6 resulting in precipitation of Ln(OH)<sub>3</sub>. pH control is important during the preparation of lanthanide complexes in aqueous solution.<sup>86</sup>

As mentioned, the lanthanide ions have a strong hard Lewis acid behaviour causing a preference for coordination with hard Lewis bases such as oxygen donors, with the 4*f* orbitals unaffected by the large electrostatic interactions. With the exception of Lu(III), each of the Ln(III) ions contain 1-7 unpaired 4*f* electrons; they are therefore paramagnetic. This has led to lanthanide complexes being used as shift reagents in NMR spectroscopy. The NMR active nuclei of a Lewis base coordinated to the Ln(III) ion will feel the effect of the unpaired electrons leading to its paramagnetic relaxation, spectral broadening and shift of resonances in its NMR spectrum. Lanthanide induced shift (LIS) methods have been applied to the structural determination of several biological macromolecules, such as proteins and nucleic acids.<sup>92,93</sup>

### 1.6.3 Luminescence Studies

The German physicist Eilhardt Wiedemann coined the word “Luminescence” in 1888, for characterising light emission not accompanied by a rise in temperature; it is the emission of light from an electronically excited state. Molecular luminescence can be split into two processes: fluorescence, processes that occur without a change in spin typically S<sub>1</sub> → S<sub>0</sub> transitions and phosphorescence, transitions implying a change in spin, typically T<sub>1</sub> → S<sub>0</sub> transitions.<sup>94</sup> The first is a fast allowed process and the second a slow forbidden process because of the change in spin.

### 1.6.4 Lanthanide luminescence

Lanthanide ions possess fascinating photophysical properties that have been intensely researched in recent years. This has led to the development of many optical devices; luminescent lights, light emitting diodes, television displays, optical fibres, computer displays and lasers, as well as luminescent sensors for medical diagnosis, cell imaging and biomedical analysis.<sup>87</sup> Most Ln(III) ions are luminescent, with the exception of La(III) and Lu(III) (4*f*<sup>0</sup> and 4*f*<sup>14</sup> respectively) which have no *f-f* transitions and are therefore not luminescent. The trivalent state of the lanthanide ions emit in the visible and

near IR regions of the electromagnetic spectrum; Gd(III) being the exception that requires a high excitation energy, therefore emission occurs in the UV region.<sup>95</sup> Eu(III) and Tb(III) analogues of Gd(III) complexes are used in studies for novel contrast agent design, due to the similar properties of lanthanides across the series (discussed in Sections 1.6.1 and 1.6.2). The use of Eu(III) and Tb(III) analogues offers insights into structural properties and hydration state determination *via* luminescence and <sup>1</sup>H NMR studies, techniques that cannot be used to study Gd(III) analogues.

The emission properties of a Ln(III) ion are governed by the ease in which it can populate its excited state(s) and the non-radioactive deactivation paths.<sup>94</sup> Lanthanides display three types of electronic transitions. The first arises from the Laporte forbidden *f-f* transitions. The *4f* orbitals are buried within the lanthanide ion, and are little affected by ligand-field effects, giving narrow transitions with absorption coefficients smaller than 1 M<sup>-1</sup>cm<sup>-1</sup>. The second is *via* both ligand-to-metal and metal-to-ligand charge transfer, these are allowed but their energies are high and very few are observed, only Eu(III) and Yb(III) LMCT are commonly observed. The final process is *via* promotion of a *4f* electron into the *5d* subshell, this is a broader transition than *f-f* transitions; their energies are dependent largely upon metal environment as the *5d* orbitals are external and interact directly with ligand orbitals.<sup>95</sup>

Inter-electronic repulsion splits the *4f* orbitals into <sup>(2S+1)</sup> Γ terms (S = total spin) angular momentum, which are separated by around 10<sup>4</sup> cm<sup>-1</sup>, where Γ = S, P, D, F etc. representing the total orbital angular momentum quantum number L = 0, 1, 2, 3. Spin orbit coupling then splits these terms into *J* states (*J* = total angular momentum quantum number = L+S → L-S), which are separated by 10<sup>3</sup> cm<sup>-1</sup>.<sup>85</sup> The ease of excitation is governed by the energy gap, Δ*E*, between the ground state and the excited state of the Ln(III) ion.

The largest ground state to excited state energy gap (Δ*E*) is that of Gd(III) ion, at around 32,000 cm<sup>-1</sup> (<sup>8</sup>S<sub>7/2</sub> to <sup>6</sup>P<sub>7/2</sub>), which would require a large energy input to achieve excitation. The maximum emission wavelength, λ<sub>max</sub>, occurs in the UV region, which would overlap with the emission of organic chromophores that may be present in solution.<sup>94</sup> For these reasons Gd(III) cannot be used in luminescence studies. Analogues using Eu(III) or Tb(III) are used, as these elements sit either side of gadolinium in the periodic table, they have much smaller Δ*E*, 12,300cm<sup>-1</sup> and 14,800cm<sup>-1</sup> respectively and due to the similar chemical properties across the lanthanide series, luminescence studies on Eu(III) and Tb(III) complexes allow conclusions drawn that can be attributed to the Gd(III) analogue with considerable confidence.

Transitions between energy levels occur *via* two operators: the electrical dipole operator (ED), and the magnetic dipole operator (MD). ED transitions are forbidden by the Laporte rule, which states that the only allowed transitions, are those that are accompanied by a change of parity.<sup>40</sup> If there is symmetry within a complex with respect to the inversion centre (*g*-symmetry) parity must be inverted, *i.e.* *g*-*u* are allowed whereas *g*-*g* transitions are forbidden (*u*-symmetry is a complex where there is no symmetry with respect to the inversion centre). *d*-*p* or *p*-*f* transitions are allowed whereas *p*-*p* or *f*-*f* transitions are forbidden. This can be overcome, if the centre of symmetry is eliminated by asymmetric vibrations, induced by the ligand field and surrounding solvent oscillations, interconverting electronic states with different *j* values, but with the same S and L, known as *J* mixing.<sup>96</sup> MD transitions are not forbidden by the parity rule, however their oscillator strength is extremely low, within the range  $10^{-9}$  to  $10^{-7}$  cm<sup>-1</sup>. The selection rules are  $\Delta S = 0$ ,  $\Delta L = 0$  and  $\Delta J = 0 \pm 1$  are allowed and  $\Delta J = 0$  to 0 is forbidden.<sup>97</sup>

The Laporte-forbidden electronic transfer between the *4f* energy states result in long lived radiative emission with, small extinction coefficients,  $\epsilon < 1\text{M}^{-1}\text{cm}^{-1}$ ; the resulting narrow emission bands are specific for each lanthanide, making them very recognisable as luminescent probes. Competition for radiationless energy transfer processes occurs through coupling of the emissive states of nearby oscillators, such as O-H and N-H, resulting in the quenching of the observed luminescence.<sup>98</sup> The larger the energy gap,  $\Delta E$ , between the ground state and the excited state, the more difficult it is for vibrational quenching to occur.<sup>95</sup>

### 1.6.5 Sensitised Emission

The intrinsic low extinction coefficients of the lanthanide ions ( $\epsilon < 1\text{M}^{-1}\text{cm}^{-1}$ ) mean direct excitation of the Laporte forbidden *f*-*f* transitions is difficult. The use of laser light, such as tuneable dye lasers and argon lasers, has been implemented to overcome the required high intensity. The most efficient form of lanthanide excitation arises from the incorporation of an organic chromophore into the Ln(III) ligand, energy transfer from which results in the indirect excitation of the Ln(III) ion.<sup>99</sup>

Organic chromophores (often referred to as antennae) with high extinction coefficients,  $\epsilon$ , are attached to the Ln(III) ligand. These absorb light efficiently in the UV

region resulting in population of their singlet excited state. The heavy-atom effect, arising from the presence of the large (Ln(III) ion) strengthens the spin-orbit coupling of the organic chromophore, inducing the increased rate of intersystem crossing (ISC) from the singlet to the triplet excited state. Provided the triplet excited state energy of the chromophore is higher than the Ln(III) excited state, energy transfer can occur to the lanthanide, enhancing the emission intensity of the Ln(III) ion and increasing the effective extinction coefficient of the complex, represented by the Jabłoński diagram in Figure 1.20.<sup>96</sup>

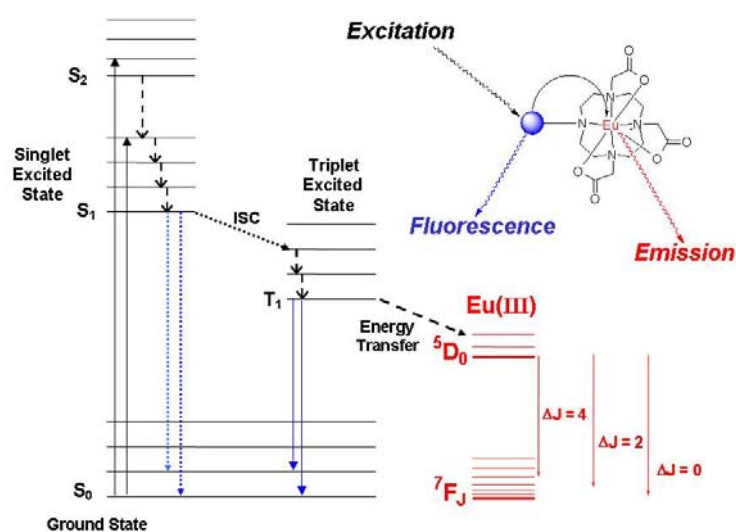


Figure 1.20 Jabłoński diagram demonstrating Eu(III) sensitised emission. The excitation (black, solid arrows) of an organic chromophore to its singlet excited states ( $S_1$  and  $S_2$ ), and short-lived fluorescence (blue dotted arrows). ISC to the chromophore triplet excited state,  $T_1$ , occurs due the heavy-atom effect, caused by the presence of the Ln(III) ion (black dotted arrow), followed by its associated phosphorescence (blue solid arrows). Energy transfer from  $T_1$  to the  $^5D_0$  excited state of Eu(III) occurs as  $T_1$  is higher in energy (black, dashed arrow), resulting in enhanced Eu(III) emission (red, solid arrows).

The efficiency of sensitised emission is indicated by the overall quantum yield,  $\Phi_{overall}$ , which is governed by three factors. Firstly, the quantum yield of formation of the chromophore triplet excited state,  $\Phi_A$ , which is dependent on the efficiency of the ISC process. Secondly, the rate of energy transfer to the Ln(III) excited state,  $\eta_{ET}$ , which is enhanced by reduction of the Ln(III)-antenna distance which in turn reduces the degree of back energy transfer. Finally, the emissive quantum yield of the Ln(III) ion,  $\Phi_{em}$ , which comprises the reduced emissive lifetime,  $\tau$ , caused by vibrational energy transfer to nearby O-H and N-H oscillators, and the natural radiative rate constant,  $k_o$  (*i.e.* the rate of decay of Ln(III) emission in the absence of the induced decay processes, Equations 30-32).<sup>100</sup>

$$\Phi_{overall} = \Phi_A \eta_{ET} \Phi_{em} \quad (30)$$

$$\Phi_{em} = k_o \tau \quad (31)$$

$$\Phi_{overall} = \Phi_A \eta_{ET} k_o \tau \quad (32)$$

Greater efficiency is therefore achieved by the incorporation of organic chromophores within the Ln(III) chelate, minimising the Ln(III)-distance and reducing the degree of interaction with solvent oscillations. The rate of energy transfer is  $1/r^6$  distance dependent, where  $r$  is the distance between the metal and chromophore centre.<sup>100</sup> Quenching of the singlet excited state must also be reduced in order to enhance the efficiency of the ISC process. Quenching may occur by either intermolecular electron transfer, *i.e.* through anionic species present in solution, such as halides, or intermolecular electron transfer, through the central Ln(III) ion (typically Eu(III) and Sm(III), each known to exist in the +2 oxidation state). Equation 33 shows the free energy of the excited state electron transfer process,  $\Delta G_{ET}$ , in which  $E_{ox}$  is the oxidation potential of the donor,  $E_{red}$  is the reduction potential of the acceptor,  $E_s$  is the singlet excited state energy,  $n$  is the number of moles,  $F$  is the Faraday constant ( $9.64853 \times 10^4 \text{ C mol}^{-1}$ ) and  $e^2/\epsilon r$  is related to the formation of a radical ion pair (usually less than 0.2 eV).<sup>100</sup>

$$\Delta G_{ET} = nF([E_{ox} - E_{red}] - E_s - e^2 / \epsilon r) \quad (33)$$

The quenching effects are reduced by modulation of the redox potentials of the chromophores. For example, the addition of electron withdrawing groups to aromatic ring chromophores increases its oxidation potential, resulting in the reduction of electron transfer to Eu(III).<sup>101</sup>

Finally, the energy of the triplet excited state chromophore must be higher than the Ln(III) excited state, with efficient overlap. Several heteroaromatic compounds have been used to achieve this, the parameters of which are shown in Table 1.6.<sup>97</sup>

Chromophore	$E_s$ (eV)	$E_t$ (cm <sup>-1</sup> )	$E_{ox}$ (V)	$E_{red}$ (V)
Phenanthrene	3.57	21,500	1.5	-2.44
Triphenylene	3.65	23,400	1.55	-2.46
1-O-Me-naphthalene	3.88	20,900	1.38	-2.65
O-Me-benzene	4.46	28,200	1.76	> -2.70

Table 1.6 Parameters of several heteroaromatic chromophores.<sup>97</sup>  $E_s$  and  $E_t$  represent the singlet and triplets energies respectively. Redox potentials were measured in DMF and MeCN.

Not only does the incorporation of organic chromophores enhance the effective extinction coefficient of the Ln(III) complex, it does so with almost no background fluorescence. Organic chromophores absorb light and fluoresce in the UV region of the electromagnetic spectrum, with  $\lambda_{ex} \sim 270$ -300 nm for aromatic compounds and  $\lambda_{em} \sim 350$ -400 nm. Lanthanide emission is within the visible light region,  $\lambda_{em} \sim 570$ -720 nm for Eu(III) complexes, resulting in a large Stokes shift observed in the emission spectra. Figure 1.21 show the typical excitation and emission spectra for a Eu(III) complex bearing an organic chromophore, demonstrating the large observed Stokes shift between the organic absorption and the Eu(III) emission.

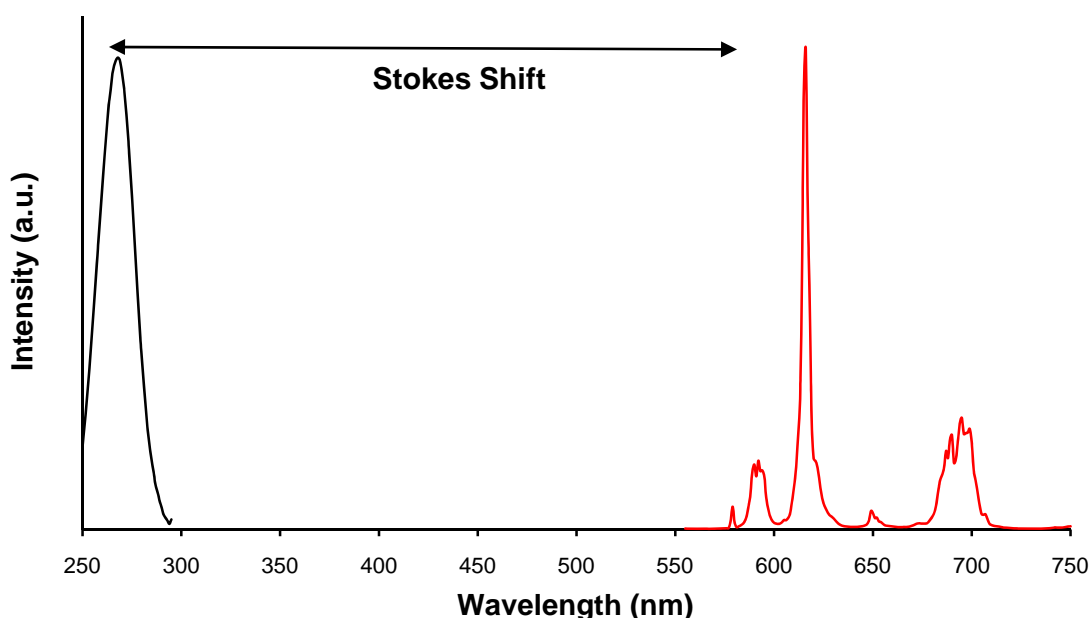


Figure 1.21 Typical Eu(III) emission spectrum (red) of a Eu-DO3A species bearing an organic antenna. Excitation (black) of the organic chromophore occurs at much shorter wavelengths in the UV region, resulting in a large Stokes shift from the Eu(III) emission in the visible light region.

Figure 1.21 shows a typical Eu(III) emission spectrum, in which the narrow bands correspond to the varying  $J$  values between the  $^5D_0$  to  $^7F_J$  transitions, *i.e.*  $\Delta J = 0$  corresponds to the  $^5D_0$ - $^7F_0$  transition,  $\Delta J = 1$  corresponds to the  $^5D_0$ - $^7F_1$  transition *etc.* The inherent low extinction coefficient of the Eu(III) ion arising from the transitions between the deeply buried  $4f$  orbitals, which are not involved in bonding and therefore not affected by ligand field effects result in the appearance of the narrow bands in the emission spectrum with little variation in the emission wavelength. The bands, however, vary in intensity and spectral form depending on the Eu(III) coordination environment, which is summed up in Table 1.7.<sup>97, 85</sup>

$\Delta J$	$\lambda_{em}$ range (nm)	Intensity	Comments
0	577 - 581	Very weak	ED Forbidden transition, gains intensity through $J$ -mixing
1	585 - 600	Strong	MD allowed, intensity independent from environment. Three transitions observed for low symmetry, with two for $C_3$ and $C_4$
2	610 - 625	Strong to very strong	ED hypersensitive, increases intensity as symmetry is lost and donor atom type is changed
3	640 - 655	Very weak	ED forbidden always weak
4	680 - 710	Medium to strong	ED, sensitive to Eu(III) coordination environment
5	740 - 770	Very weak	Forbidden, rarely observed
6	810 - 840	Very weak	Rarely observed

Table 1.7 Factors effecting Eu(III)  $\Delta J$  transitions.<sup>97, 85</sup>

#### 1.6.6 Determination of Hydration state, $q$ : Luminescent Lifetime Studies

Hydration state,  $q$ , is of considerable importance in the development of Gd(III)-based MRI contrast agents. The greater the hydration state the more intense the MR signal.

Hydration state can be determined *via* the X-ray structure, this technique has its limitations: firstly it is often difficult to grow crystals and secondly the structure obtained is in the solid state not of the compound in solution, therefore it is not exact. The luminescence of Eu(III) and Tb(III) offers a convenient method for determination of  $q$ , using the radiationless energy transfer that occurs between the vibrational energy levels of H<sub>2</sub>O and the excited states of Eu(III) and Tb(III). H<sub>2</sub>O quenches their excited states, D<sub>2</sub>O does not.

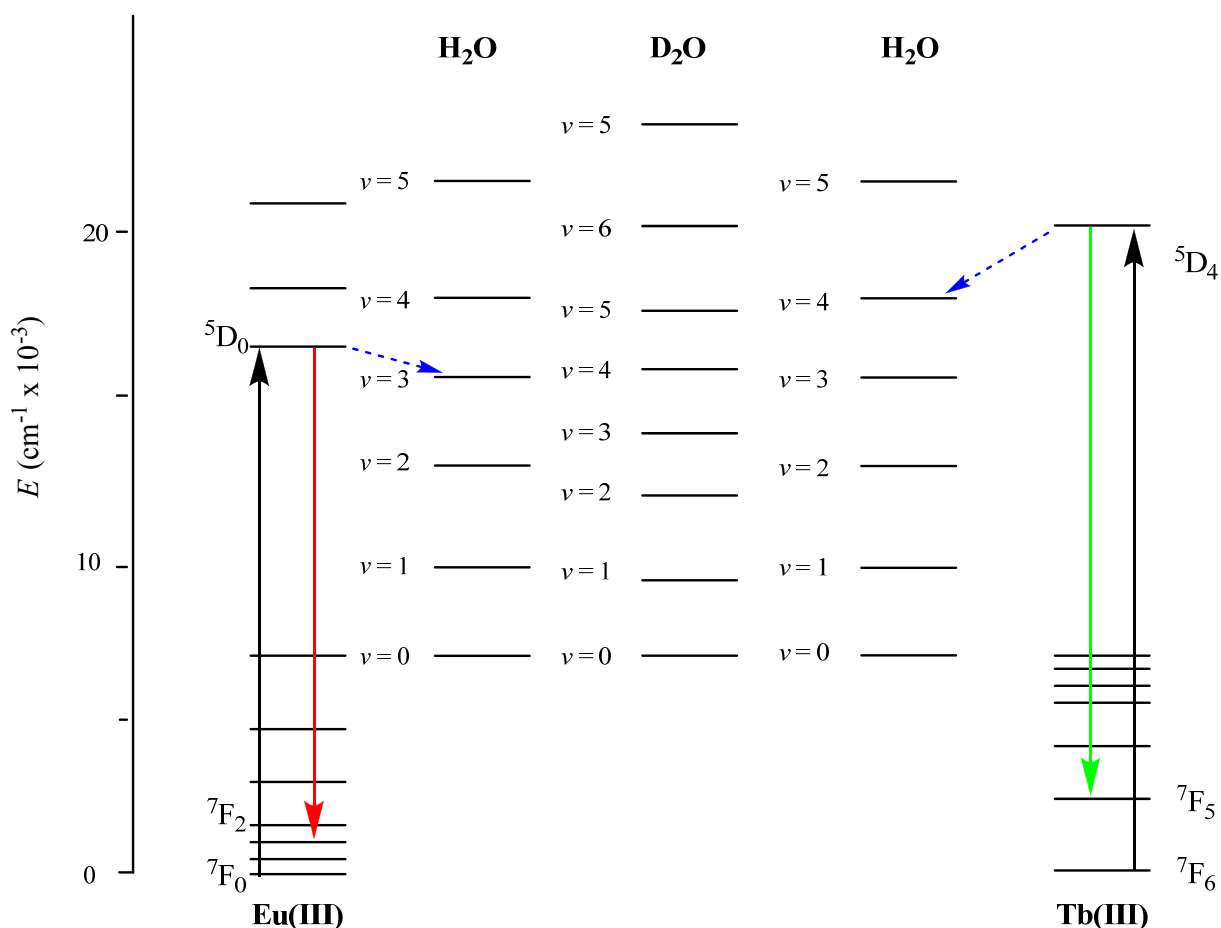


Figure 1.22 Vibrational quenching of Eu(III) and Tb(III) excited states. Excitation (black arrow) occurs from the ground to excited state ( ${}^7F_0$  to  ${}^5D_0$  for Eu(III) and  ${}^7F_6$  to  ${}^5D_4$  for Tb(III)) followed by emission, showing the  $\Delta J = 2$  transition for Eu(III) (red arrow,  ${}^5D_0$  to  ${}^7F_2 \sim 615 \text{ nm}$ ) and  $\Delta J = 1$  for Tb(III) (green arrow,  ${}^5D_4$  to  ${}^7F_5 \sim 545 \text{ nm}$ ). There is greater overlap of the  $v = 3$  vibrational level of H<sub>2</sub>O with the  ${}^5D_0$  excited state of Eu(III) than with the  ${}^5D_4$  excited state of Tb(III) resulting in greater quenching and shorter lifetime of Eu(III) emission *via* radiationless energy transfer (blue dashed arrow). Overlap of the less populated  $v = 4$  and  $v = 5$  vibrational level of D<sub>2</sub>O with the excited states of Eu(III) and Tb(III) respectively results in reduced quenching and longer emission lifetimes in this media.

Figure 1.22 shows the overlap between the excited energy states of the Eu(III) and Tb(III) with the vibrational energy level of H<sub>2</sub>O and D<sub>2</sub>O.  $\Delta\nu_{\text{OH}}$  and  $\Delta\nu_{\text{OD}}$  are  $3,405 \text{ cm}^{-1}$

and  $2,520\text{cm}^{-1}$  respectively, with no anharmonicity assumed in the vibrational ladder.<sup>85</sup> Radiationless energy transfer between  $^5\text{D}_0$  excited state of Eu(III) with the  $\nu = 3$  vibrational energy level of  $\text{H}_2\text{O}$  occurs due to the efficient overlap of the two energy states. In accordance with the Frank-Condon principle, the vibrational state populations decrease dramatically with increasing energy. Energy transfer efficiency is reduced in Tb(III) as the  $^5\text{D}_4$  excited state overlaps the less populated  $\nu = 4$  vibrational energy level of  $\text{H}_2\text{O}$ , resulting in longer emission lifetimes in comparison with Eu(III). Vibrational quenching in the presence on  $\text{D}_2\text{O}$  is lower with respect to  $\text{H}_2\text{O}$  due to the overlap of the  $^5\text{D}_0$  to  $\nu = 4$  energy levels in Eu(III) and the  $^5\text{D}_4$  to  $\nu = 5$  in Tb(III). The rate of decay of emission in  $\text{D}_2\text{O}$  for both Eu(III) and Tb(III) is 200 times slower than in  $\text{H}_2\text{O}$ , due to the lower vibrational frequency of the O-D oscillations. Measuring emission intensity vs. time in both  $\text{D}_2\text{O}$  and  $\text{H}_2\text{O}$  allows the first order decay constants,  $k_{\text{H}_2\text{O}}$  and  $k_{\text{D}_2\text{O}}$  to be calculated. When applied to Equations 34 and 35 the hydration state,  $q$  can be calculated, the correction factors take into account quenching of outer-sphere waters.<sup>98</sup>

$$q_{\text{Eu}} = 1.2[(k_{\text{H}_2\text{O}} - k_{\text{D}_2\text{O}}) - 0.25] \quad (34)$$

$$q_{\text{Tb}} = 5[(k_{\text{H}_2\text{O}} - k_{\text{D}_2\text{O}}) - 0.06] \quad (35)$$

## 1.7 Thesis Outline

The factors affecting the efficiency of MRI Gd(III) contrast agents, such as the hydration state,  $q$ , has been manipulated in order to enhance relaxivity and MR image intensity. Furthermore, the luminescent properties of the chemically similar lanthanide ions have been explored.

Chapter 2 describes the use of ‘click’ chemistry, *via* the Cu(I) catalysed cycloaddition reaction, between substituted alkynes and an organic azide, to link propargyl appended Ln(III) DO3A complexes to target molecules. It outlines the issues of using *in situ* generation of azides with the propargyl appended chelates and a way to overcome these problems. The pH dependent behaviour of the unexpected product of the reaction is also described.

Chapter 3 focuses on the multiple uses of *p*-ethynylbenzyl lanthanide chelates as precursors for the ‘click’ reaction. By using *p*-ethynylbenzyl lanthanide complexes (Eu,

Gd, and Tb), it is possible to generate azides *in situ* and perform cycloaddition reactions without side products. This chapter shows that from the *p*-ethynylbenzyl appended complexes can be used to produce multimeric lanthanide complexes. Chapter 4 covers the use of ‘click’ chemistry with *p*-ethynylbenzyl lanthanide chelates that form self-associating and *d-f* hybrid lanthanide complexes.

The final focus of the thesis is described in Chapter 5 uncovers efforts towards the imaging of gene therapy, using a smart MRI contrast agent that is designed to localise and activate within a cell, after interaction with the enzyme HSV-1 kinase, expressed by the cell undergoing gene therapy. The thesis, on a whole focuses on the design and synthesis of novel ligands for lanthanide metals (Eu, Gd and Tb).

Chapter 6 describes the conclusions of the thesis and suggests future work. Chapter 7 describes all the experimental detail for the thesis.

## 1.8 References

1. M. Doubrovin, I. Serganova, P. Mayer-Kuckuk, V. Ponomarev and R. G. Blasberg, *Bioconj. Chem.*, 2004, **15**, 1376.
2. K. Brindle, *Br. J. Radiol.*, 2003, **76**, S11.
3. R. Huabner, H. J. Wester, W. A. Weber, C. Mang, S. I. Zeigler, S. L. Goodman, R. Senekowitsch-Schmidtke, H. Kessler and M. Schwaiger, *Cancer Res.*, 2001, **61**, 1781.
4. A. Y. Louie, M. M. Hüber, E.T. Ahrens, U. Rothbacher, R. Moats, R. E. Jacobs, S. E. Fraser and T. J. Meade, *Nat. Biotechnol.*, 2000, **18**, 321.
5. G. D. Demetri, M. von Mehren, C. D. Blanke, A. D. Van den Abbeele, B. Eisenberg, P. J. Roberts, C. M. Heinrich, A. D. Tuveson, S. Singer, M. Janicek, J. A. Fletcher, S. G. Silverman, S. L. Silberman, R. Capdeville, B. Kiese, B. Peng, S. Dimitrijevic, B. J. Druker, C. Corless, C. D. M. Fletcher and H. Joensuu, *N. Engl. J. Med.*, 2002, **347**, 472.
6. A. D. Van den Abbeele, *Proc. Am. Soc. Clin. Oncol.*, 2001, **20**, 362a.
7. M. P. Lowe, *Aust. J. Chem.*, 2002, **55**, 551.
8. P. C. Lauterbur, *Biosci. Rep.*, 2004, **24**, 165.
9. P. Mansfield, *Angew. Chem. Int. Ed.*, 2004, **43**, 5456.
10. J. P. Hornak, ‘The Basics of MRI’ 1996.
11. P. W. Atkins, 'Physical Chemistry, 6<sup>th</sup> Edition', Oxford University Press, 1998.

12. S. Mansson and A. Bjornerud, 'The Chemistry of Contrast Agents in Magnetic Resonance Imaging; Physical Principles of Medicinal Imaging by Nuclear Magnetic Resonance', ed. A. E. Merbach and E. Toth, Wiley, 2001.
13. V. Jacques and J. F. Desreux, 'Topics in Current Chemistry; New Classes of MRI Contrast Agents', ed. W. Krause, Springer, 2002.
14. R. B. Lauffer, *Chem. Rev.*, 1987, **87**, 901.
15. N. Kaltsoyannis and P. Scott, 'The f Elements', ed. J. Evans, Oxford University Press, 1999.
16. R. M. Weisskoff and P. Caravan, MR Contrast Agent Basics in *Cardiovascular Magnetic Resonance*, A. Lardo, Z. A. Fayed, N. A. F. Chronos and V. Fuster, eds., Martin Dunitz, London, 2003, 17.
17. P. Caravan, *Chem. Soc. Rev.*, 2006, **35**, 512.
18. R. D. Shannon and C. T. Prewitt, *Acta Cryst.*, 1969, **B25**, 925.
19. R. D. Shannon, *Acta Cryst.*, 1976, **A32**, 751.
20. F.C. Stevens, *Can. J. Biochem. Cell Biol.*, 1983, **61**, 906.
21. S. P. Fricker, *Chem. Soc. Rev.*, 2006, **35**, 524.
22. H.-J. Weinmann, R. C. Brasch, W.-R. Press and G. E. Wesbey, *Am. J. Roentgenol.*, 1984, **142**, 619.
23. R. C. Brasch, *Western J. Med.*, 1985, **142**, 847.
24. J.-C. Bousquet, S. Saini, D. D. Stark, P. F. Hahn, M. Nigam, J. Wittenberg and J. T. Ferucci, *Radiology*, 1988, **166**, 693.
25. T. Frenzel, P. Lengsfeld, H. Schirmer, J. Hütter and H. J. Weinmann, *Invest. Radiol.*, 2008, **43**, 817.
26. K. Kumar, T. Jin, X. Wang, J. F. Desreux and M. F. Tweedle, *Inorg. Chem.*, 1994, **33**, 3823.
27. K. Kumar, C. A. Chang, L. C. Francesconi, D. D. Dischino, M. F. Malley, J. Z. Gougoutas and M. F. Tweedle, *Inorg. Chem.*, 1994, **33**, 3567.
28. K. Kumar and M. F. Tweedle, *Inorg. Chem.*, 1993, **32**, 4193.
29. D. H. White, L. A. Delearie, D. A. Moore, R. A. Wallace, T. J. Dunn, W. P. Cacheris, H. Imura and G. R. Choppin, *Invest. Radiol.*, 1991, **26**, S226.
30. A. E. Martell and R. M. Smith, 'Critical Stability Constants', Plenum, 1974.
31. R. M. Smith, R. J. Motekaitis and A. E. Martell, National Institute of Standards and Technology, 1997.

32. P. Caravan, J. J. Ellison, T. J. McMurry and R. B. Lauffer, *Chem. Rev.*, 1999, **99**, 2293.
33. W. P. Cacheris, S. C. Quay and S. M. Rocklage, *Magn. Reson. Imaging*, 1990, **8**, 467.
34. V. M. Runge, D. Y. Gelblum and S. Jacobson, *Magn. Reson. Imaging*, 1991, **9**, 79.
35. K. Kumar, M. F. Tweedle, M. F. Malley and J. Z. Gougoutas, *Inorg. Chem.*, 1995, **34**, 6472.
36. D. Meyer, M. Schaefer and D. Doucet, *Invest. Radiol.*, 1990, **25**, S53.
37. M. Giardiello, PhD Thesis, University of Leicester, 2007.
38. V. C. Pierre, M. Botta, S. Aime and K. N. Raymond, *Inorg. Chem.*, 2006, **45**, 8355.
39. D. M. J. Doble, M. Botta, J. Wang, S. Aime, A. Barge and K. N. Raymond, *J. Am. Chem. Soc.*, 2001, **123**, 10758.
40. B. O'Sullivan, D. M. J. Doble, M. K. Thompson, C. Siering, J. Xu, M. Botta, S. Aime and K. N. Raymond, *Inorg. Chem.*, 2003, **42**, 2577.
41. P. Caravan, A. V. Astashkin and A. M. Raitsimring, *Inorg. Chem.*, 2003, **42**, 3972.
42. A. M. Raitsimring, A. V. Astashkin, D. Baunte, D. Goldfarb and P. Caravan, *J. Phys. Chem. A.*, 2004, **108**, 7318.
43. E. Toth, D. Pubanz, S. Vauthey, L. Helm and A. E. Merbach, *Chem. Eur. J.*, 1996, **2**, 1607.
44. S. Aime, M. Botta, S. G. Crich, G. Giovenzana, R. Pagliarin, M. Sisti and E. Terreno, *Magn. Reson. Chem.*, 1998, **36**, S200.
45. M. Botta, *Eur. J. Inorg. Chem.*, 2000, 399.
46. J. H. Freed, *J. Chem. Phys.*, 1978, **68**, 4034.
47. S. Aime, M. Botta, M. Fasano and E. Terreno, *Acc. Chem. Res.*, 1999, **32**, 941.
48. T. J. Swift and R. E. J. Connick, *J. Chem. Phys.*, 1962, **37**, 307.
49. S. Aime, M. Botta, M. Fasano, S. G. Crich and E. Terreno, *Coord. Chem. Rev.*, 1999, **321**, 185.
50. S. Aime, M. Botta, S. G. Crich, G. Giovenzana, R. Pagliarin, M. Sisti and E. Terreno, *Magn. Reson. Chem.*, 1998, **36**, S200.
51. E. Toth, I. van Uffelen, L. Helm, A. E. Merbach, D. Ladd, K. Briley-Saebo and K. E. Kellar, *Magn. Reson. Chem.*, 1998, **36**, S125.
52. S. Aime, M. Botta, M. Fasano and E. Terreno, *Chem. Soc. Rev.*, 1998, **27**, 19.
53. D. H. Powell, O. M. N. Dhubhghaill, D. Pubanz, L. Helm, Y. S. Lebedev, W. Schlaepfer and A. E. Merbach, *J. Am. Chem. Soc.*, 1996, **118**, 9333.

54. R. Ruloff, E. Toth, R. Seopelliti, R. Tripier, H. Handel and A. E. Merbach, *Chem. Commun.*, 2002, 2630.
55. S. Laus, R. Ruloff, E. Toth and A. E. Merbach, *Chem. Eur. J.*, 2003, **9**, 3555.
56. M. Woods, M. Botta, S. Avedano, J. Wang and A. D. Sherry, *Dalton Trans.*, 2005, 3829.
57. F. Yerly, A. Borel, L. Helm and A. E. Merbach, *Chem. Eur. J.*, 2003, **9**, 5468.
58. M. Woods, S. Aime, M. Botta, J. A. K. Howard, J. M. Moloney, M. Navet, D. Parker, M. Port and O. Rousseaux, *J. Am. Chem. Soc.*, 2000, **122**, 9781.
59. S. Aime, M. Botta and G. Ermondi, *Inorg. Chem.*, 1992, **31**, 4291.
60. V. Jaques and J. F. Desreux, *Inorg. Chem.*, 1994, **33**, 4048.
61. S. Aime, A. Barge, M. Botta, A. S. de Sousa and D. Parker, *Angew. Chem. Int. Ed.*, 1998, **37**, 2673.
62. S. Aime, A. Barge, J. I. Bruce, M. Botta, J. A. K. Howard, J. M. Moloney, D. Parker, A. S. de Sousa and M. Woods, *J. Am. Chem. Soc.*, 1999, **121**, 5762.
63. J. A. K. Howard, A. M. Kenwright, J. M. Moloney, D. Parker, M. Port, M. Navet, O. Rousseau and M. Woods, *Chem. Commun.*, 1998, 1381.
64. D. M. Corsi, L. Vander Elst, R. N. Muller, H. van Bekkum and J. A. Peters, *Chem. Eur. J.*, 2001, **7**, 1383.
65. D. Messeri, M. P. Lowe, D. Parker and M. Botta, *Chem. Commun.*, 2001, 2742.
66. M. Botta, *Eur. J. Inorg. Chem.*, 2000, 399.
67. V. C. Pierre, M. Botta and K. N. Raymond, *J. Am. Chem. Soc.*, 2005, **127**, 504.
68. C. Sudan, P. Ceroni, V. Vicinelli, M. Maestri, V. Balzani, M. Gorka, S.-K. Lee, J. van Heyst and F. Vogtle, *Dalton Trans.*, 2004, 1597.
69. H. Kobayashi and M. W. Brechbiel, *Curr. Pharm. Biotechnol.*, 2004, **5**, 539.
70. H. Kobayashi and M. Brechbiel, *Mol. Imaging*, 2003, **2**, 1.
71. R. Esfand and D. A. Tomalia, *Drug Discov. Today*, 2001, **6**, 427.
72. L. Henry Bryant Jr., M. W. Brechbiel, C. Wu, J. W. M. Butle, V. Herynek and J. A. Frank, *J. Magn. Reson. Imaging*, 1999, **9**, 348.
73. J. P. Cross, M. Lauz, P. D. Badger and S. Petoud, *J. Am. Chem. Soc.*, 2004, **126**, 16278.
74. J. Rudovsky, P. Hermann, M. Botta, S. Aime and I. Lukes, *Chem. Commun.*, 2005, 2390.
75. J. Rudovsky, M. Botta, P. Hermann, K. I. Hardcastle, I. Lukeš and S. Aime, *Bioconjugate Chem.*, 2006, **17**, 975.

76. R. B. Lauffer, *Magn. Reson. Med.*, 1991, **22**, 339.
77. P. Caravan, *Acc. Chem. Res.*, 2009, **42**, 851.
78. T. N. Parac-Vogt, K. Kimpe, S. Laurent, C. Pierart, L. Vander Elst, R. N. Muller and K. Binnemans, *Eur. Biophys. J.*, 2006, **35**, 136.
79. S. Aime, C. Cabella, S. Colombatto, S. G. Crich, E. Gianolio and F. Maggioni, *J. Magn. Res. Imaging*, 2002, **16**, 394.
80. W. Li, S. E. Fraser and T. J. Meade, *J. Am. Chem. Soc.*, 1999, **121**, 1413.
81. S. J. A. Pope and R. H. Layeb, *Dalton Trans.*, 2006, 3108.
82. L. Burai, E. Toth, G. Moreau, A. Sour, R. Scopelliti and A. E. Merbach, *Chem. Eur. J.*, 2003, **9**, 1394.
83. A. L. Nivorozhkin, A. F. Kolodziej, P. Caravan, M. T. Greenfield, R. B. Lauffer and T. J. McMurry, *Angew. Chem. Int. Ed.*, 2001, **40**, 2903.
84. M. Gardiello, M. P. Lowe and M. Botta, *Chem. Commun.*, 2007, **39**, 4044.
85. J. I. Bruce, M. P. Lowe and D. Parker, Chapter 11 in *The Chemistry of Contrast Agents in Medical Magnetic Resonance Imaging*, eds., A. E. Merbach and E. Tóth, John Wiley and Sons, 2001, 437.
86. G. R. Choppin, 'Lanthanide Probes in Life, Chemical and Earth Sciences, Theory and Practice; Chemical Properties of the Rare Earth Elements', ed. J.-C. G. Bunzli and G. R. Choppin, Elsevier, 1989.
87. H. C. Aspinall, 'Chemistry of the F-Block Elements', CRC Press, 2001.
88. D. Parker, *Chem. Brit.*, 1994, 818.
89. J. Leveille, G. Demonceau, M. de Roo, P. Rigo, R. Taillefer, R. A. Morgan, D. Kupranick and R. C. Walovitch, *J. Nucl. Med.*, 1989, **30**, 1902.
90. D. F. Shriver, P. W. Atkins and C. H. Langford, 'Inorganic Chemistry, Second Edition', Oxford University Press, 1994.
91. A. D. Sherry and C. F. G. C. Geraldes, 'Lanthanide Probes in Life, Chemical and Earth Sciences, Theory and Practice; Shift Reagents in NMR Spectroscopy', ed. J.-C. G. Bunzli and G. R. Choppin, Elsevier, 1989.
92. C. F. G. C. Geraldes and C. Luchinat, *Met. Ions Biol. Syst.*, 2003, **40**, 513.
93. J.-C. G. Bunzli and C. Piguet, *Chem. Soc. Rev.*, 2005, **34**, 1048.
94. J.-C. G. Bunzli, *Acc. Chem. Res.*, 2006, **39**, 53.
95. P. W. Atkins, 'Physical Chemistry, 6<sup>th</sup> Edition', Oxford University Press, 1998.
96. D. Parker, *Coord. Chem. Rev.*, 2000, **205**, 109.

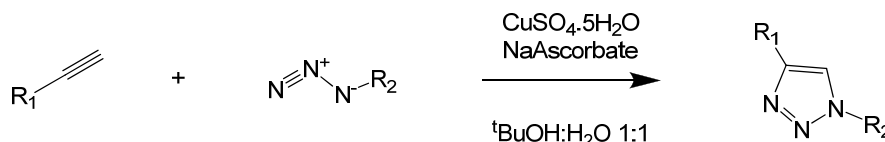
97. J.-C. G. Bunzli, 'Lanthanide Probes in Life, Chemical and Earth Sciences, Theory and Practice; Luminescent Probes', ed. J.-C. G. Bunzli and G. R. Choppin, Elsevier, 1989.
98. A. Beeby, I. M. Clarkson, R. S. Dickins, S. Faulkner, D. Parker, L. Royle, A. S. de Sousa, J. A. G. Williams and M. Woods, *J. Chem. Soc., Perkin Trans. 2*, 1999, 493.
99. D. Parker, R. S. Dickins, H. Puschmann, C. Crossland and J. A. K. Howard, *Chem. Rev.*, 2002, **102**, 1977.
100. A. Dossing, *Eur. J. Inorg. Chem.*, 2005, 1425.
101. K. Matsumoto and Z. Yuan, *Met. Ions Biol. Syst.*, 2003, **40**.

## Chapter 2

### 'Click' Chemistry with Lanthanide Chelates

#### 2.1 Introduction

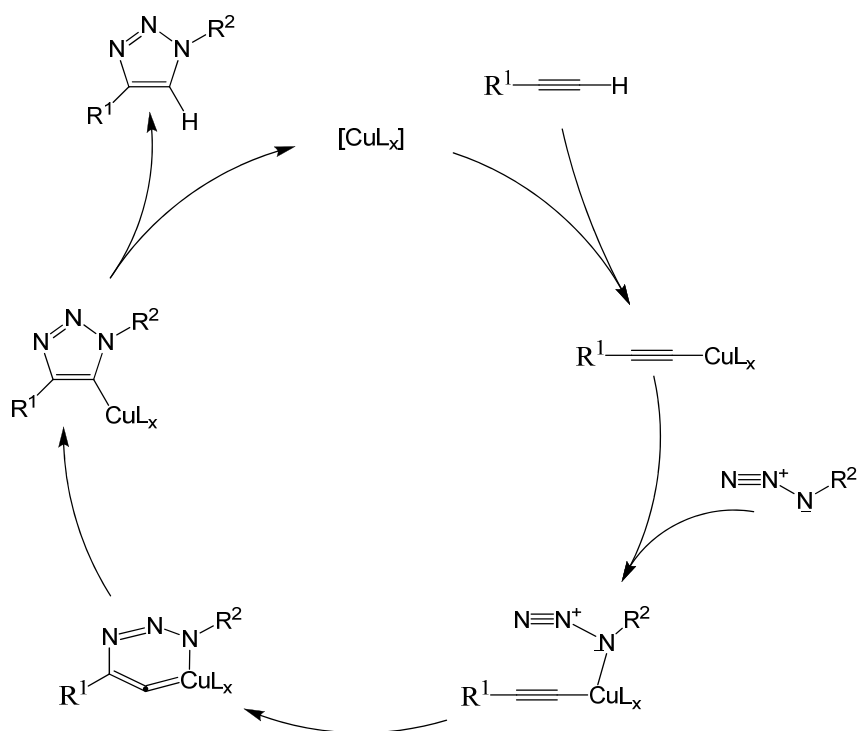
The term "click chemistry" was coined by Sharpless and co-workers in 2001.<sup>1</sup> The phrase has become synonymous with the atom efficient Huisgen, Cu(I) azide, alkyne cycloaddition, to form 1,2,3-triazole.



Scheme 2.1 Copper(I)-catalyzed triazole formation

The technique has proven very effective at linking two organic molecules stereoselectively with near quantitative yields shown in many recent publications by Sharpless and co-workers.<sup>1,2</sup> They have developed ideal and facile conditions to produce 1,2,3-triazoles, with 5 mol% copper sulphate as catalyst, 10 mol% sodium ascorbate as a reducing agent to convert Cu(II) to the reactive catalytic Cu(I). The reaction mixture is heated at 60°C for 18 hours producing the desired product, under non-Cu(I) catalysed conditions the desired triazole may be formed, although this is at elevated temperatures and usually results in a mixture of the 1,4 and 1,5 regioisomers.<sup>1</sup>

Catalytic studies and DFT calculations by Himo *et al.*, have predicted the catalytic cycle shown in Scheme 2.2.<sup>2</sup> Insertion of the copper into the terminal alkyne, forming an activated copper (I) acetylide complex, is followed by coordination of the organic azide. The copper directs the azide to an orientation, which allows the distal nitrogen of the azide to attack the C-2 of the acetylide, forming the unusual six membered metallacycle. From this metallocycle, ring contraction is favoured as the energy barrier is very low, driving the formation of the five membered ring. Proteolysis of the five membered ring releases the triazole and regenerates the Cu(I) species, starting the catalytic cycle again.<sup>2</sup>



Scheme 2.2 Proposed mechanism for Cu(I) catalysed 1,2,3-triazole formation.<sup>2</sup>

### 2.1.1 *In situ* generation of azides

Organic azides are potential explosives, cutting-edge explosives research suggests that materials with very high nitrogen content maximise heat of formation and gas output. As a general rule of thumb: if  $(N_C + N_O) / N_N < 3$  the compound is considered a potential explosive hazard.<sup>3</sup> To avoid isolation of potential explosive organic azides, methods have been developed to produce azides for use in the cycloaddition reaction, *via* the *in situ* generation of azides from the corresponding alkyl halide and  $\text{NaN}_3$ .<sup>4,5</sup> Fokin and co-workers discuss this as a one-pot synthesis that makes the “already powerful click process even-more user-friendly and safe”.<sup>6</sup> *In situ* generation of azides is the reaction between an alkyl halide and sodium azide to create an alkyl azide, this reaction occurs in the same pot, prior to the Cu(I) catalysed cycloaddition. This *in situ* generation of azides makes the reaction more facile and is recommended as an undergraduate laboratory experiment by Wu *et al.*<sup>7</sup> An excess of azide reportedly does not interfere with the cycloaddition reaction, *i.e.* there is no side reaction with  $\text{NaN}_3$  forming unsubstituted triazoles. The synthesis of unsubstituted triazoles has been reported, although these tend to be formed at elevated temperatures, with hazardous reagents such as hydroazidoic acid, not under ambient conditions.<sup>8,9</sup>

### 2.1.2 'Click' Chemistry and Biological Molecules

The Cu(I) catalysed technique has been used with great effect to make many compounds of biological interest. Such is the ease of click chemistry, it can be used to make libraries of compounds that are employed in drug discovery,<sup>10,11,12</sup> a recent review by Kolb *et al.* documents recent advances in this field.<sup>13</sup> The 1,2,3-triazole has been used to mimic the amide bond in peptides; this provides a structural mimic, preventing cleavage of the peptide bond. Used in this manner, it has been put to use in the development of HIV protease inhibitors, (Figure 2.1a) by Brik *et al.*<sup>14</sup> Wang and co-workers have been investigating triazole linked glycoconjugates, (Figure 2.1b) which exert important effects on many complex biological events: standard protocol for regio- and stereo-control in glycoside bond formation often leads to laborious synthetic transformations and protecting group manipulations; however, using click chemistry, Wang and co-workers have developed a one pot glycolation method for the synthesis of 1,2,3-triazole bridged glycoconjugates.<sup>15</sup>

Potential antifungals have also been developed to incorporate the 1,2,3- triazole, by Abrams and co-workers.<sup>16</sup> They have been looking at the antifungal activity of  $\beta$ -methoxyacrylate analogues (Figure 2.1c), and have produced small libraries of compounds using the 'click' reaction, identifying four possible candidates for antifungals.<sup>16</sup>

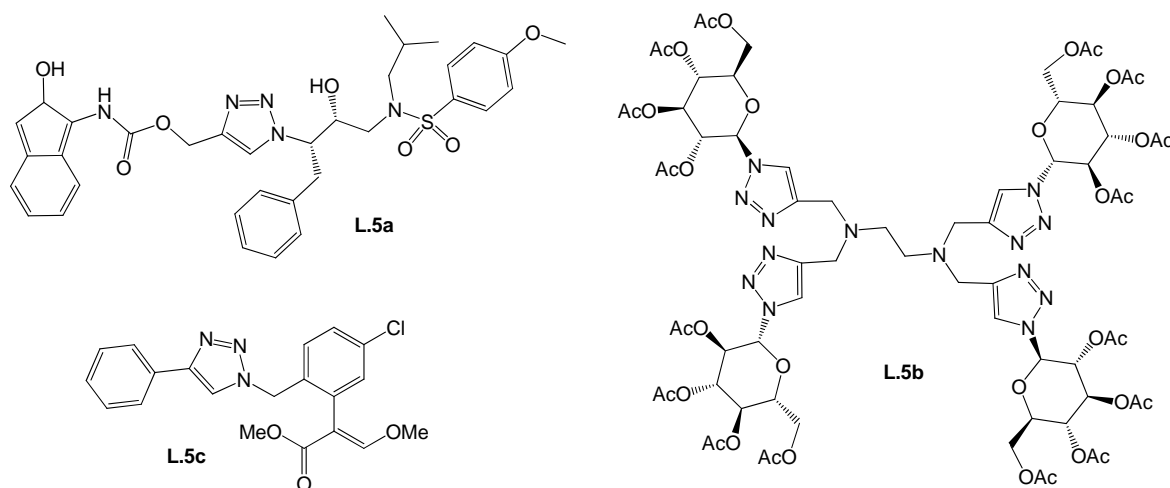


Figure 2.1 Click chemistry and drug design: a) HIV protease inhibitor,<sup>14</sup> b) Glycoconjugate,<sup>15</sup> c)  $\beta$ -methoxyacrylate analogue.<sup>16</sup>

### 2.1.3 'Click' Chemistry on Metal Chelates

It is not just drug design and discovery that has reaped the benefits of 'click' chemistry, it is also the field of imaging agents. The use of 1,2,3-triazoles to link imaging agents to biological molecules, is a fast growing area of current research (for *e.g.*: luminescent probes, PET, SPECT and MR imaging agents).

Two groups have recently reported adding  $^{18}\text{F}$ -labelled alkynes to azide appended peptides, *via* 'click' chemistry, these are specific targeting molecules for integrins, for use as PET imaging agents. Integrins are vital peptides located on the surface of the cell, that allow movement of the cell *i.e.* metastasis, also they allow cells to communicate with each other. Imaging these peptides could be vital in spotting cancerous cells within the body. Chen and co-workers used the  $\alpha_v\beta_3$  integrin expression, based on the RGD protein, which interact with the integrin using primary amines. They attached an  $^{18}\text{F}$ -PEG alkyne and 'clicked' with the azide appended RGD protein, giving the  $^{18}\text{F}$ -PEG-triazole-RGD<sub>2</sub> (Figure 2.2a). Chen and co workers have shown integrin  $\alpha_v\beta_3$ -specific tumour imaging.<sup>17</sup>

Sutcliffe and co-workers have also shown that  $^{18}\text{F}$ -alkynes can be attached to azide appended peptides, in this case specific for the  $\alpha_v\beta_6$  integrin (Figure 2.2b). They have also shown that this peptide will specifically image the integrin, the only drawback is that the prosthetic groups of the agent show a noticeable effect on pharmacokinetics, *i.e.* the vast majority is localised within the kidney of the animal.<sup>18</sup>

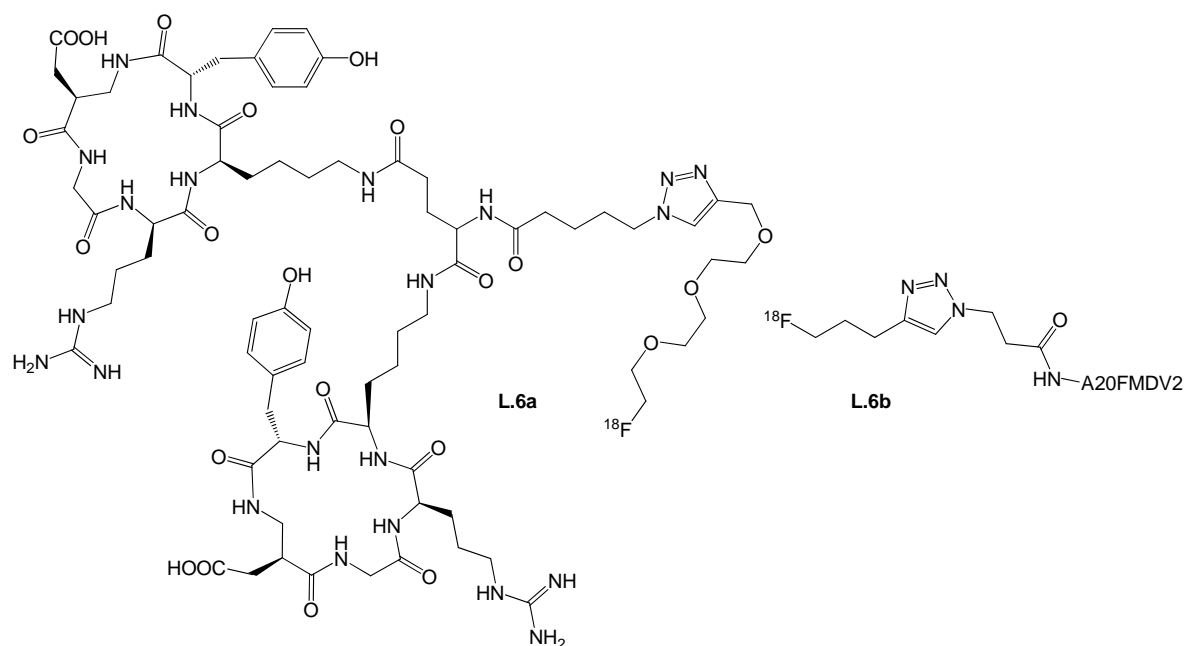


Figure 2.2  $^{18}\text{F}$  labelled peptides for integrin PET-imaging.<sup>17,18</sup>

Schibli and co-workers have developed a novel approach to attaching metal chelates to biologically active molecules, *via* ‘click’ chemistry, using a propargyl glycine and an biological molecule of interest bearing an azide, either a peptide, DNA base or glucose. In the case of the azido sugar it forms a 1,2,3-triazole with a glycine residue from the 4 position, creating a chelating agent (Figure 2.3) which can be used to ligate metals such as Re and  $^{99m}\text{Tc}$ , giving a biologically active SPECT Imaging agent, as Schibli coins the phrase ‘Click to Chelate’.<sup>19</sup> Using the N(3) of the 1,2,3-triazole to coordinate the metal, means there is no need to use a separate chelating agent. Schibli’s use of ‘click’ chemistry opens up a very facile synthetic route to an otherwise laborious synthesis of specific imaging probes.

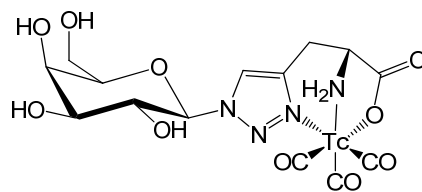


Figure 2.3  $^{99m}\text{Tc}$  ‘Click to Chelate’ glucose based imaging agent.<sup>19</sup>

Attaching lanthanide chelates to biologically active molecules has been developed by many groups, this usually involves long and difficult synthesis. Using click chemistry to attach bio-molecules to lanthanide opens up a facile solution to this problem, one of the first reported examples was detailed by Hulme and co-workers in 2006 (Figure 2.4).<sup>20</sup>

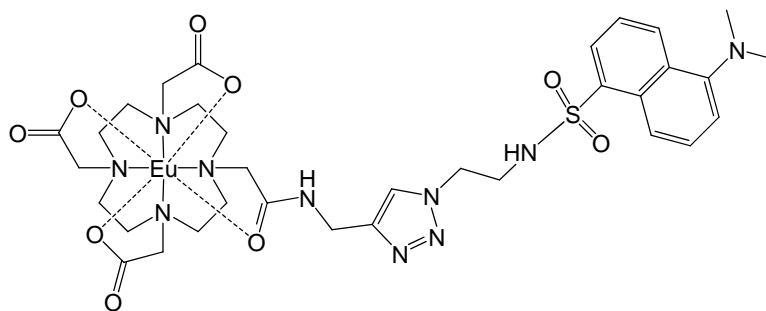


Figure 2.4 Dansyl appended Eu(III) complex generated by click chemistry.<sup>20</sup>

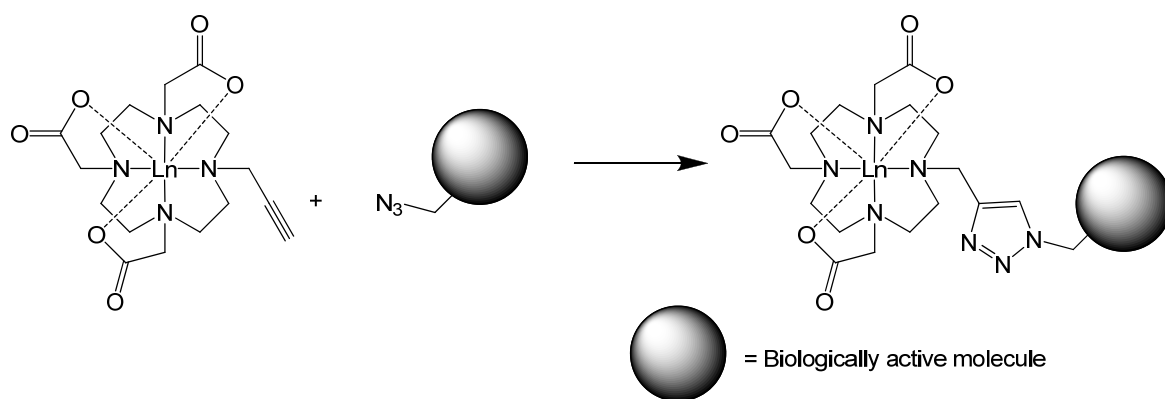
The approach taken by Hulme involved synthesis of a Eu(III) DO3A-based chelate with an appended propargyl amide on position 10 of the ring. This stable eight-coordinate chelate for europium, was ‘clicked’ with a dansyl azide giving the desired product. The N-(2-propynyl)acetamide appended complex is a very weak luminescent emitter; however, attaching the dansyl group increases the intensity of the europium emission ten fold, *via*

energy transfer (sensitised emission) from the dansyl group.<sup>20</sup> Dansyl amide appended europium complexes, usually quench the europium emission above pH 5.7,<sup>21</sup> but the triazole spacer affects the pH dependence of Eu(III) emission. The triazole spacer prevents dansyl coordination to the europium and emission intensity is at a maximum between pH 5 to 9 (this range is known to protonate the dansyl fluorophore).<sup>20</sup> This work showed that complex biologically active luminescent sensors can be synthesised using click chemistry.

#### 2.1.4 1,2,3-Triazole Appended Lanthanide Complexes

The major interest in the area of ‘click’ chemistry and lanthanide chelates, is to link biologically active molecules, to DO3A based complexes *via* an amide 1,2,3-triazole linker.<sup>20</sup> This approach is not ideal for the synthesis of an efficient MRI contrast agent, as amides are known to slow water exchange rates, decreasing the signal intensity<sup>22</sup> (as discussed in Chapter 1.3.3). To overcome this limitation, our approach was to prepare Ln.DO3A bearing a pendant propargyl moiety. As a Ln(III) complex, facile conversion to the corresponding triazole was envisaged *via* the Cu(I) catalyzed click reaction with a variety of biologically active molecules (nucleoside, amino acid or a sugar) bearing an appended azide (Scheme 2.3). This approach takes the idea that biologically active molecules that can ‘click’ to lanthanide chelates,<sup>20</sup> without having amide groups as direct linkers to Ln.DO3A. Using this approach for MR contrast agents, there are many questions to answer:

- Is the click chemistry reaction facile and high yielding?
- Does the triazole bind to the lanthanide?
- How many inner-sphere waters will be present on the Ln(III) complex?
- Will it be a suitable linker molecule for MRI contrast agents?
- Will the triazole affect lanthanide luminescence, will the 1,2,3-triazole sensitise Ln luminescence?
- Will the triazole affect water exchange rates on Gd(III) complexes?

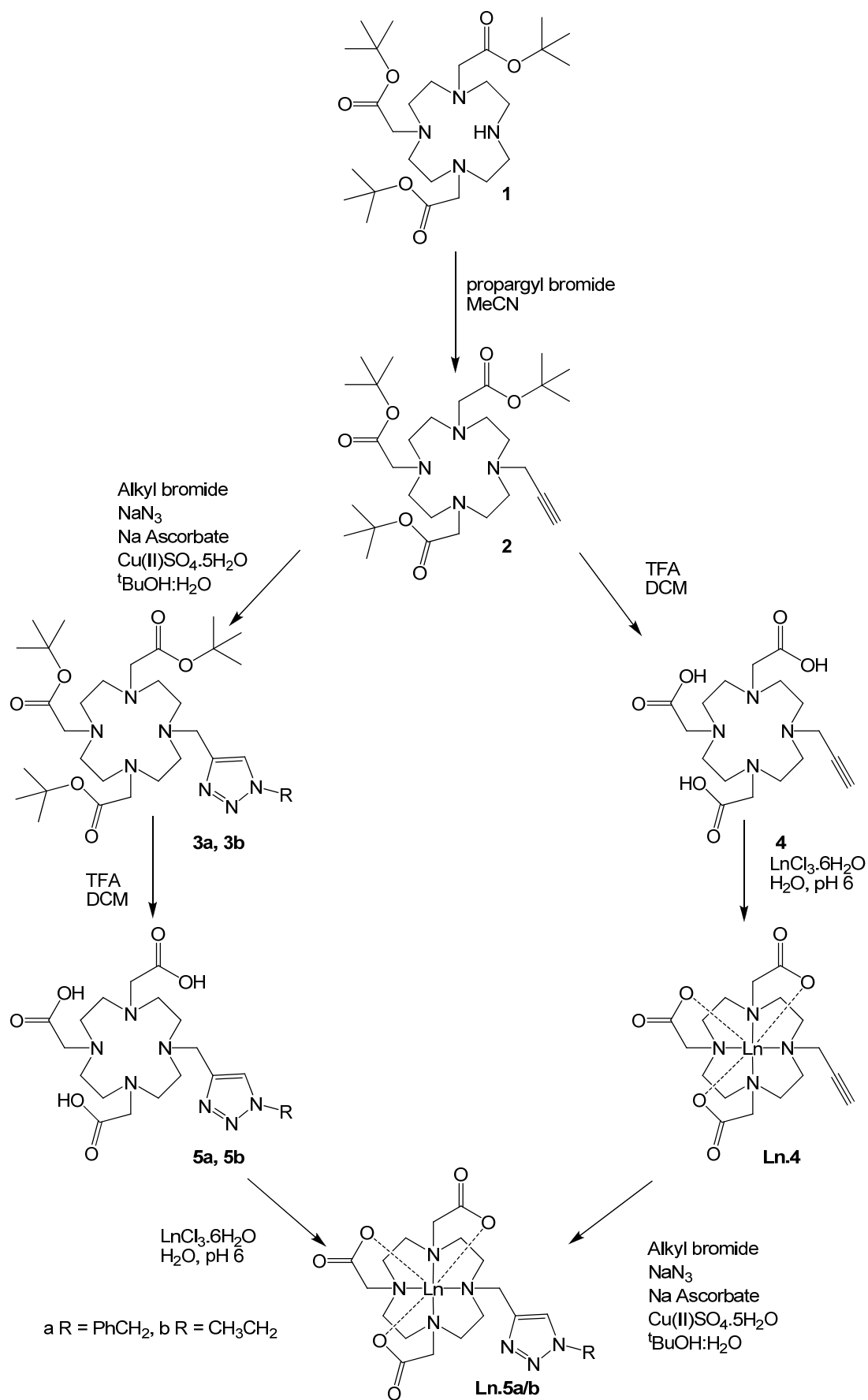


Scheme 2.3 Proposed approach to 'click' chemistry with lanthanide chelates and biological active molecules.

Before embarking on this research effort, the isolation of the potentially explosive azide precursors was of concern. Conventional wisdom suggests that reaction of alkynes with *in situ* generated azides (*via* alkyl halides in the presence of  $\text{NaN}_3$ ) is a clean, facile reaction and residual  $\text{NaN}_3$  does not interfere with the cycloaddition reaction.<sup>66</sup> We believed that this attractive synthetic trick would allay these safety concerns, circumventing the need to isolate compounds containing azides.

### 2.1.5 Target Lanthanide compounds

To test the 1,2,3-triazole as a viable and stable linker for attaching bio-molecules to lanthanide chelates, simple alkyl 1,2,3-triazole appended lanthanide chelates were synthesised. The first target compound was a Ln.D03A chelate bearing a pendant 1,2,3-triazole with a benzyl or ethyl in N3 position (**Ln.5a/b**). It was envisioned that the benzyl group would act as an antenna for sensitised emission in lanthanide luminescence, making it facile to characterise, and a good target compound *i.e.* to test the synthetic hypothesis. The synthesis of **Ln.5** was achieved *via* two synthetic routes (Scheme 2.4). One route carries out the click reaction with the benzyl/ethyl bromide on the preformed complex, **Ln.4**, the other generates the proligand *via* click chemistry before lanthanide complexation.

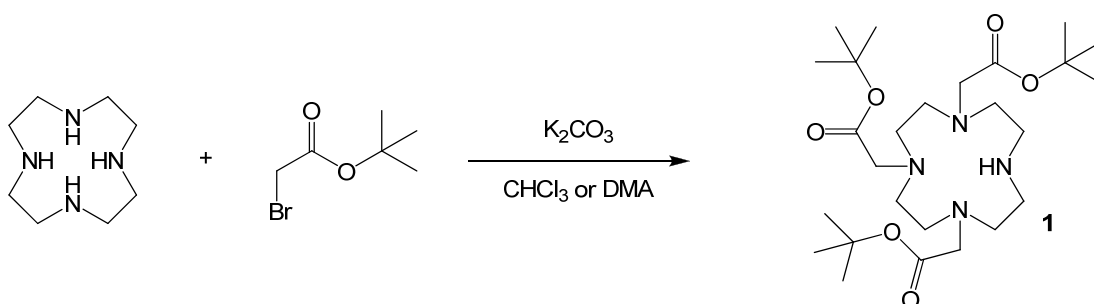


Scheme 2.4

## 2.2 Macrocycle Synthesis

### 2.2.1 Formation of 1,4,7-tris(tert-butoxycarbonylmethyl)-10-(prop-2-ynyl)-1,4,7,10-tetraazacyclododecane. (2)

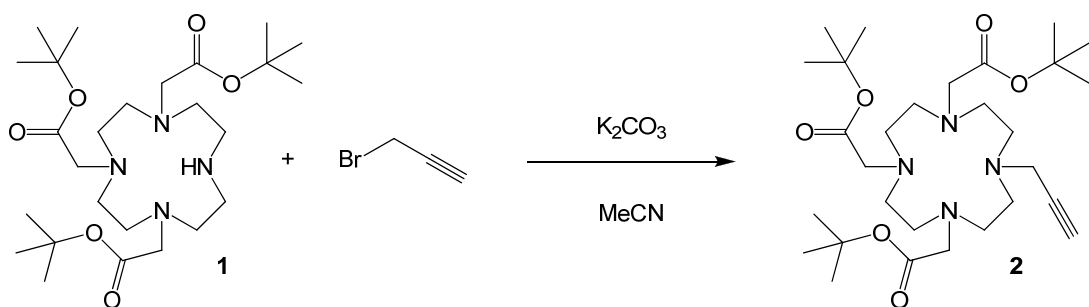
The precursor to the synthesis of **2** was 1,4,7-tris(tert-butoxycarbonylmethyl)-1,4,7,10-tetraazacyclododecane, was **1** (<sup>t</sup>BuDO3A), this was synthesised *via* two methods: from 1,4,7,10-tetraazacyclododecane (cyclen) and <sup>t</sup>butyl bromoacetate, either stirred for 3 days in CHCl<sub>3</sub> or 19 days in DMA, the latter just needing to be filtered and washed with diethyl ether to separate from the tetra substituted product, giving the hydrobromide salt. Giving a yield of 53% and 61% respectively.<sup>23,24</sup>



Scheme 2.5

**1** is the building block for the vast majority of lanthanide chelates used in imaging, it helps form a seven-coordinate chelate that can be modified in the N10 position, to perform a specific task. In this case, a pendant propargyl group was added for use as a reagent in the ‘click’ reaction.

The initial attempts to prepare **2**, were to react **1** with propargyl bromide in the presence of  $K_2CO_3$ , the mixture was stirred under nitrogen for 2 hours. The crude product was purified on silica using a DCM: Methanol (92:8) solvent system giving a yellow oil, 93% yield.

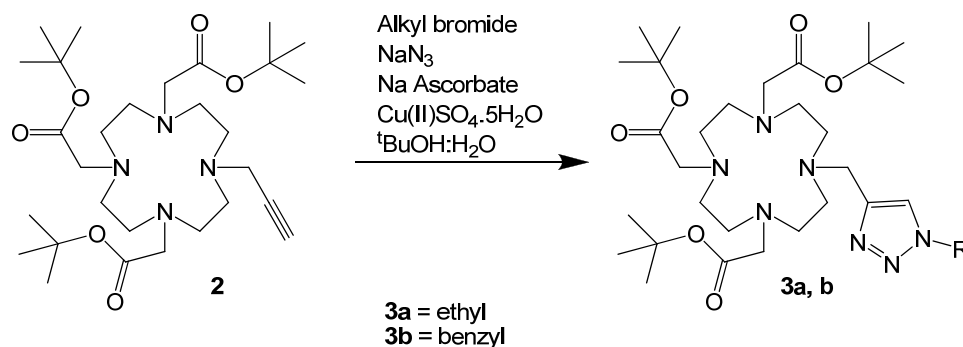


Scheme 2.6

The ESMS<sup>+</sup> showed a peak at  $m/z$  553 [M+H]<sup>+</sup> indicating the formation of the desired product; in the <sup>1</sup>H NMR spectrum a broad singlet at 2.1 ppm integrating to 1H is indicative of the alkyne proton. There are issues with the reaction when carried out in DMF, if the reaction mixture is heated (to remove DMF), reduction of the alkyne to an alkene, this was observed both in the ESMS<sup>+</sup> where a peak was observed at  $m/z$  555 [M+H]<sup>+</sup> and the <sup>1</sup>H NMR spectrum. The two compounds have very similar R<sub>f</sub> values and are difficult to separate *via* column chromatography. Subsequent attempts to synthesis **2** were carried out in MeCN which was much easier to remove along with the excess propargyl bromide under reduced pressure, giving a yellow oil (86%), that was used without further purification. Although the yield was lower, there was no side reaction and no formation of alkene.

From compound **2** there are two possible routes to **Ln.5**, one route is *via* **Ln.4**, in which **2** is deprotected using TFA to form **4**, then complexed with LnCl<sub>3</sub>.6H<sub>2</sub>O and finally ‘clicked’ to produce **Ln.5** (discussed in Section 2.5). The alternative route is *via* **3**, whereby **2** undergoes the ‘click’ reaction before deprotection and finally complexation with a lanthanide, forming **Ln.5**.

### 2.2.2 1,2,3-Triazole Formation Before Ln(III) Coordination

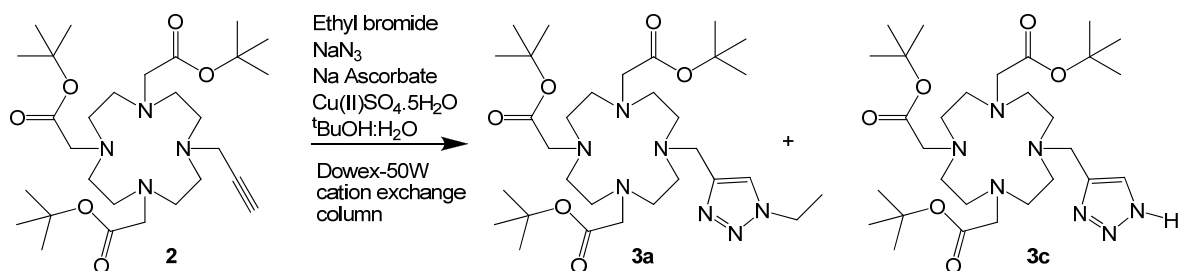


Scheme 2.7

The 1,2,3-triazoles **3a** and **3b** were formed *via* the Cu(I) catalyzed cycloaddition reaction of the alkyne **2** and an azide. **2** and sodium azide were dissolved in <sup>t</sup>BuOH:H<sub>2</sub>O, to this the alkyl halide was added (benzyl bromide or bromoethane), this formed the alkyl-azide *in situ*, ready for the ‘click’ reaction. To the mixture, sodium ascorbate and CuSO<sub>4</sub>.5H<sub>2</sub>O were added sequentially, followed by stirring for 18 hours at room temperature. This procedure was adapted from Sharpless *et al.*,<sup>1</sup> the Cu(II) is reduced *in situ*

to Cu(I) to perform the reaction. The reactions were followed by ESMS<sup>+</sup>, it was found that catalytic amounts of copper were insufficient to cause reaction, so 1.2 equivalents of CuSO<sub>4</sub>·5H<sub>2</sub>O were added along with 1.2 equivalents of sodium ascorbate. The reason that catalytic amounts had no effect, was presumably due to **2** acting as a ligand, chelating the copper; this does not enable it to catalyse the cycloaddition reaction. Only after one equivalent of CuSO<sub>4</sub>·5H<sub>2</sub>O was added, did the triazole form. The ESMS<sup>+</sup> spectrum exhibited a peak at *m/z* 827 corresponding to [M+Cu+Br]<sup>+</sup> for the benzyl triazole; the isotope pattern was correct for the copper complex. The ethyl triazole ESMS spectrum showed interesting peaks at *m/z* 765, corresponding to the [M+Cu+Br]<sup>+</sup>, and *m/z* 737 corresponding to an unsubstituted N-H 1,2,3-triazole (no ethyl group), chelating a copper with an associated bromide (Scheme 2.8). The formation of the N-H 1,2,3-triazole with a proton on the N3 nitrogen of the triazole directly from the Cu(I) catalysed reaction has not been reported in literature. Unsubstituted triazoles have appeared, but these tend to be formed at elevated temperatures, not under ambient conditions.<sup>8,9</sup> This was also observed in the formation of benzyl triazole.

The reaction was repeated in the absence of alkyl halide, *i.e.* just in the presence of sodium azide, again peaks were observed in the ESMS at 737 [M+Cu+Br]<sup>+</sup> as before indicating the formation of the 1,2,3-triazole.



Scheme 2.8

To remove the copper from the reaction, the aqueous solution was passed down a strong acid cation exchange column (Dowex-50W), the aqueous solution was lyophilised giving a white solid. Mixtures of the ethyl and benzyl triazole compounds with the H-triazole were observed, also trace amounts of copper were still found in the ESMS<sup>+</sup> spectra. The likely problem with the cation exchange column is that, the compounds ‘physically’ stick to the column while it was acidic, due to their insolubility in water. This process did

remove the copper from the chelate. Once the copper was washed from the column, it was washed with a 12% ammonium solution to elute the ligand.

### 2.2.3 Formation of 1,4,7-tris(*tert*-butoxycarbonylmethyl)-10-((1*H*-1,2,3-triazol-4-yl)methyl)-1,4,7,10-tetraazacyclododecane. (**3c**)

The initial attempt at making the N-H 1,2,3-triazole using sodium azide as a reagent gave a promising result, on purification the ESMS<sup>+</sup> spectra showed a peak at *m/z* 596 [M+H]<sup>+</sup> and the <sup>1</sup>H NMR spectrum showed a 1H broad singlet at 8.4 ppm corresponding to the CH on the triazole ring, also the absence of a 1H singlet at 2.1 ppm indicated that the alkyne had been consumed in the reaction.

In the absence of an N-substituted azide, according to conventional wisdom, the click reaction should not work, in the presence of only sodium azide no reaction should occur. This is the reason that *in situ* generation of the azide can be used, *i.e.* NaN<sub>3</sub> does not compete with the click reaction. The macrocycle compound **1** can chelate copper(II), this copper is not expected to bind to the alkyne, but will still likely bind to azide (N<sub>3</sub><sup>-</sup>), this may orientate the azide into the correct position with respect to the activated copper (I) acetylide complex (Scheme 2.2) allowing the cycloaddition reacts to occur with N<sub>3</sub><sup>-</sup>.

It is unlikely that the macrocycle-bound copper participates in the catalytic cycle, no evidence for reaction is observed until > 1 equivalent of copper is used, *i.e.* only the ‘free’ copper in solution can catalyse the click reaction. The yield of the compound was much lower than expected for an atom efficient process as described by Sharpless *et al.*<sup>7</sup> This could be due to the work up process rather than the reaction procedure.

Figure 2.5 is a representation of the crystal structure of **3c**, it clearly shows the N-H 1,2,3-triazole was formed, the structure is typical for the twelve membered aza ring. The crystal was grown by slow evaporation from H<sub>2</sub>O, the representation omits solvent molecules for clarity, which show intermolecular hydrogen bonding to **3c**.

N(5)-N(6)	1.340(3)	N(6)-N(5)-C(28)	107.6(2)
N(5)-C(28)	1.344(4)	N(7)-N(6)-N(5)	109.7(2)
N(6)-N(7)	1.327(4)	N(6)-N(7)-C(29)	107.8(2)
N(7)-C(29)	1.329(4)	N(6)-N(7)-H(7)	126.1
N(7)-H(7)	0.88	C(29)-N(7)-H(7)	126.1

Table 2.1 Selected bond lengths [Å] and angles [°] for **3c**

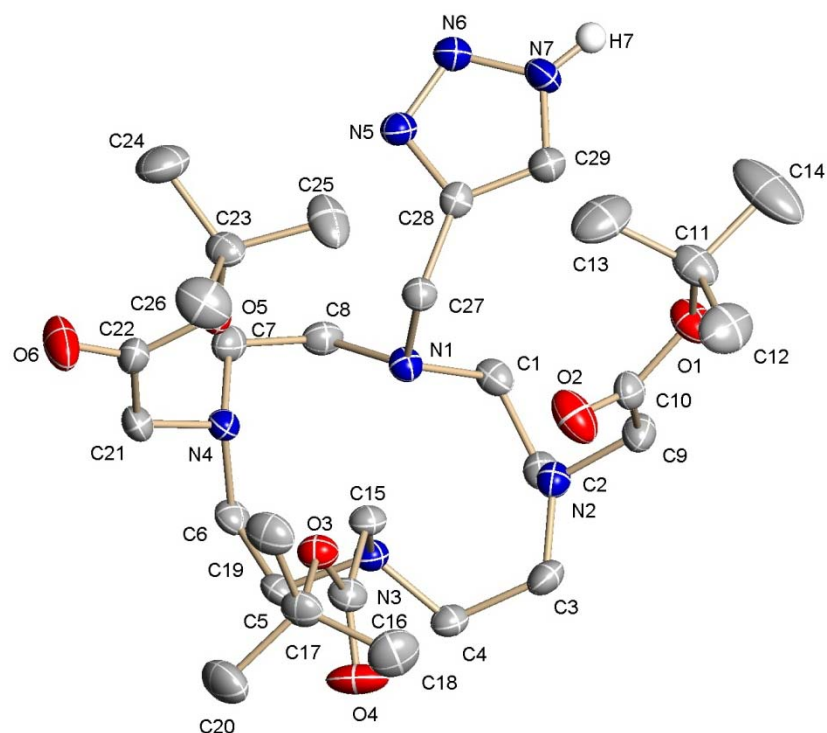
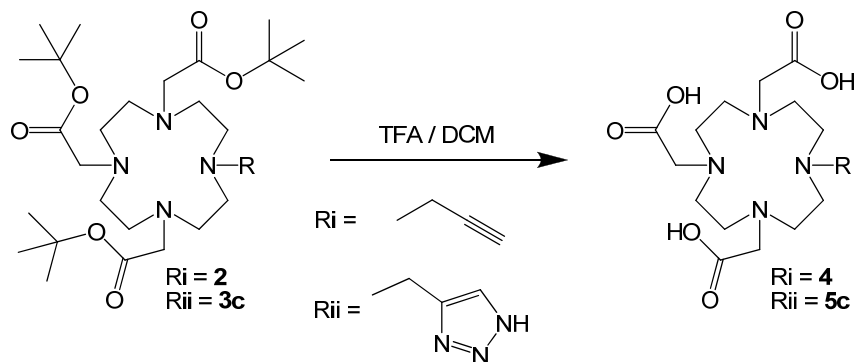


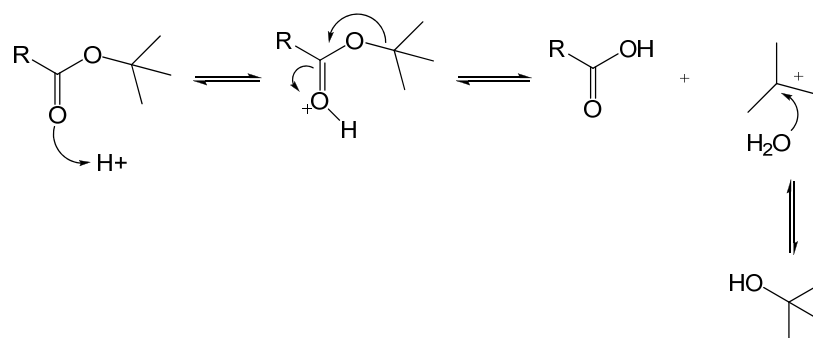
Figure 2.5 Representation of the X-ray crystal structure of **3c**

#### 2.2.4 Cleavage of *tert*-butyl Esters



Scheme 2.9

The *tert*-butyl esters were hydrolysed with trifluoroacetic acid in DCM to give a DO3A-R appended pro-ligands which are afforded in near quantitative yield. The hydrolysis requires adventitious water, thus the reaction was carried out in an open vessel. During the reaction, *tert*-butyl cations are formed, which are then converted to, *tert*-butanol as seen in Scheme 2.10.



Scheme 2.10 Mechanism for acid catalysed hydrolysis.

#### 2.2.5 Formation of 1,4,7-tris(carbonylmethyl)-10-(prop-2-ynl)-1,4,7,10-tetraazacyclododecane. (4)

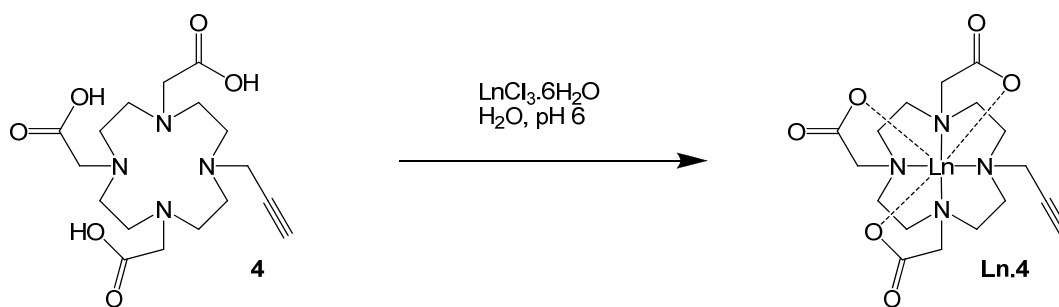
The *t*-butyl ester cleavage was as described above in TFA/DCM, the work up is facile as the only side product is <sup>t</sup>BuOH, which along with the TFA can be removed under reduced pressure, to remove the TFA completely two portions of DCM are added and reduced under pressure sequentially followed by two amounts of diethyl ether. This process works very well and yields a white hygroscopic solid (96%).

Analysis by <sup>1</sup>H NMR spectroscopy showed an absence of the C(CH<sub>3</sub>) peaks at 1.38 ppm, indicating cleavage of the *tert*-butyl esters, the ESMS<sup>+</sup> gave a peak at *m/z* 385 [M + H]<sup>+</sup>

**5c** was synthesised in the same manner giving a white solid of (93%). Analysis by <sup>1</sup>H NMR spectroscopy showed an absence of the C(CH<sub>3</sub>) peaks at 1.45 ppm, indicating cleavage of the *tert*-butyl esters, the ESMS<sup>+</sup> gave a peak at *m/z* 427 [M + H]<sup>+</sup>.

### 2.3 Lanthanide Complex Preparation

All lanthanide compounds synthesised *via* the same manner, using **4** or **5c** with LnCl<sub>3</sub>.6H<sub>2</sub>O in H<sub>2</sub>O at pH 6. The reaction is carried out above pH 4, to ensure the complexation of the metal. At pH above 7 the lanthanide starts to precipitate as hydroxide, therefore control of pH is vital to the reaction, (the ideal pH range is between 5-7). The reactions were monitored by ESMS for the specific mass and lanthanide isotope pattern for the complex and the depletion of starting material.



Scheme 2.11

Any unreacted lanthanide salts were removed using DOWEX MAC-3<sup>®</sup> weak acid cation exchange resin (Chapter 7.1.2). The solutions were tested for the presence of uncomplexed lanthanide ions using urotropine buffered solutions of xylenol orange at pH 5. If the solutions remained orange no free lanthanide ions were left in the solution.<sup>25</sup>

## 2.4 Luminescence Studies of Pendant Alkyne Complexes Ln.4

### 2.4.1 Characterisation of **Eu.4**

**Eu.4** was synthesised from **4** and  $\text{EuCl}_3 \cdot 6\text{H}_2\text{O}$ , giving a white solid (86%). **Eu.4** is a seven coordinate complex, the  $^1\text{H}$  NMR spectrum is consistent with those observed for unsymmetrically substituted cyclen derivatives,<sup>26</sup> in which all protons are non-equivalent. The resonances are only observed at low temperature ( $\sim 278\text{K}$ ), these signals are broad even at this temperature, implying a relatively low barrier to arm rotation in the complex that would allow exchange between diastereoisomers. This behaviour is to be expected given that the alkyne moiety cannot coordinate to the metal centre.<sup>27</sup> The hydration state  $q$ , of the complex was determined and its luminescent properties investigated.

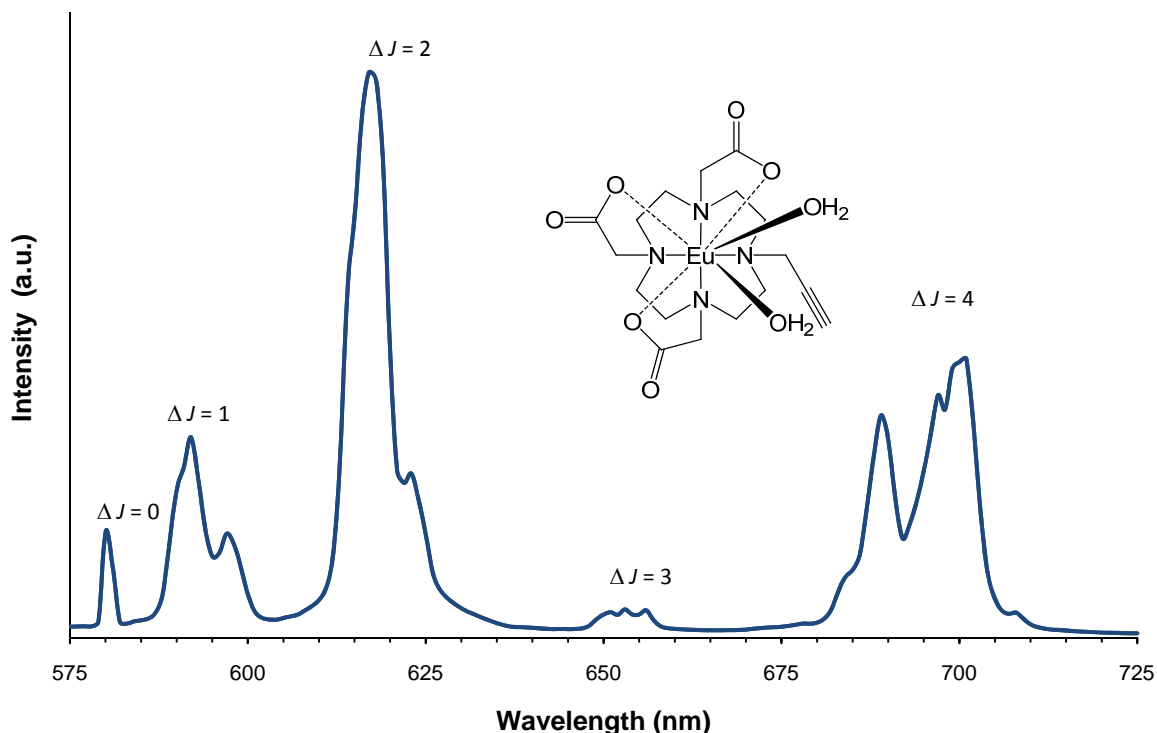


Figure 2.6 Luminescent emission spectrum of **Eu.4**, ( $\lambda_{\text{ex}} = 395 \text{ nm}$ ,  $\text{H}_2\text{O}$ , 298K,  $\text{pH} = 6$ ).

The complex was excited directly at  $\lambda = 395 \text{ nm}$  to give an emission spectrum as shown in Figure 2.6. This spectrum is typical for Eu(III) emission, showing the various  $^5\text{D}_0$  to  $^7\text{F}_J$  transitions, with an intense hypersensitive  $\Delta J = 2$  transition ( $^5\text{D}_0$  to  $^7\text{F}_5$ ), *c.f.* that of the  $\Delta J = 1$  transition. This is typical of a seven-coordinate complex with  $q = 2$ . This complex, as with  $q = 2$  complexes based on DO3A, will bind bi-dentate anions such as carbonate; this would also result in an increased  $\Delta J = 2$  transition; however as the pH of the solution is  $\sim 6$  the binding of carbonate is ruled out. Excited state lifetime measurements (Figure 2.7) confirm that two inner-sphere waters are present in **Eu.4**.

The excitation spectrum (monitoring the emission at  $\lambda = 618 \text{ nm}$ ,  $\Delta J = 2$  transition), showed weak peaks at  $\lambda = 317 \text{ nm}$  and  $\lambda = 395 \text{ nm}$ . The peak observed at  $\lambda = 395 \text{ nm}$  represents direct excitation of the Eu(III) ion, the less intense peak at  $\lambda = 317 \text{ nm}$ , could be weak sensitisation from the alkyne to the Eu(III) ion, but is more likely the weak sensitisation *via* the weak LMCT absorption. The  $\Delta J = 2$  transition, at  $618 \text{ nm}$  is the wavelength that is monitored during lifetime studies in  $\text{H}_2\text{O}/\text{D}_2\text{O}$  to determine  $k_{\text{H}_2\text{O}}$  and  $k_{\text{D}_2\text{O}}$  in order to calculate  $q$  (Equation 34). The Lifetime studies are shown in Figure 2.7.

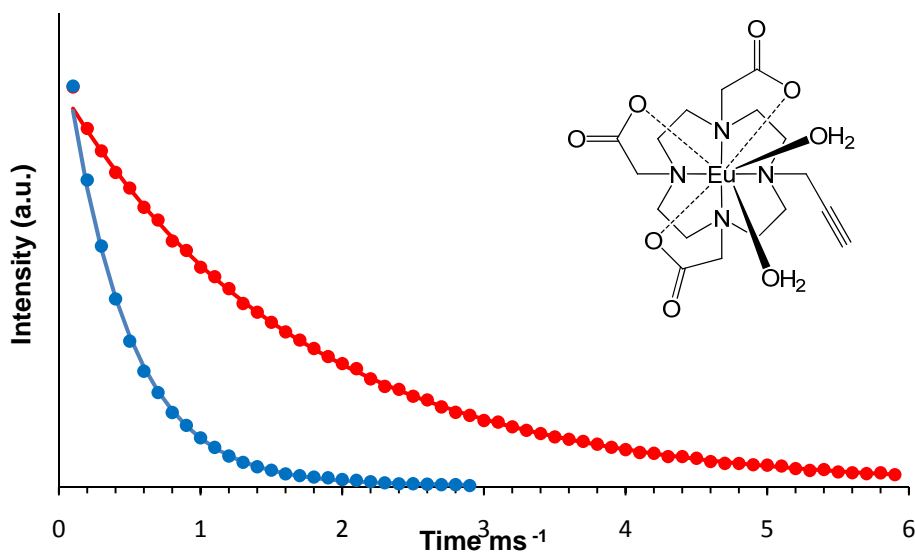


Figure 2.7 Excited state life time studies for **Eu.4** at 298K, pH 6,  $\lambda_{\text{ex}} = 395$  nm,  $\lambda_{\text{em}} = 618$  nm. Blue = H<sub>2</sub>O, Red = D<sub>2</sub>O.

The rate of decay is faster in H<sub>2</sub>O than in D<sub>2</sub>O, this is due to the O-H oscillators quenching the excited state of the Eu(III) ion far more efficiently than the O-D oscillators of D<sub>2</sub>O. From the lifetime studies, it was found that as expected, (**Eu.4**) is  $q = 1.7$  (Table 2.2); as expected. It shows that **Eu.4** is seven-coordinate, with respect to the ligand, with two inner-sphere water molecules, giving a coordination number of 9.

Complex	$\lambda_{\text{em}} / \text{nm}$	$\lambda_{\text{ex}} / \text{nm}$	$k_{\text{H}_2\text{O}} (\text{ms}^{-1})$	$k_{\text{D}_2\text{O}} (\text{ms}^{-1})$	$q (\pm 0.2)$
<b>Eu.4</b>	395	618	2.3	0.59	1.7
<b>Tb.4</b>	260 / 355	546	0.95	0.69	1

Table 2.2 Rate constants,  $k$ , for depopulation of the excited state and derived hydration states,  $q$ , for the decay of **Eu.4** and **Tb.4**

#### 2.4.2 Characterisation of **Tb.4**

**Tb.4** was synthesised as above from **4** and TbCl<sub>3</sub>.6H<sub>2</sub>O, the reaction gave a white solid (97%). The ESMS of the compound gave the peak,  $m/z$  541 [M + H]<sup>+</sup>. In collaboration with Faulkner the <sup>1</sup>H NMR spectrum for **Tb.4**,<sup>27</sup> was reported, this is similar to that of **Eu.4**, though the form is reversed and implies that there are two waters bound at the metal centre, as would be expected for a heptadentate ligand. The hydration state  $q$ , of the complex was determined and its luminescent properties investigated.

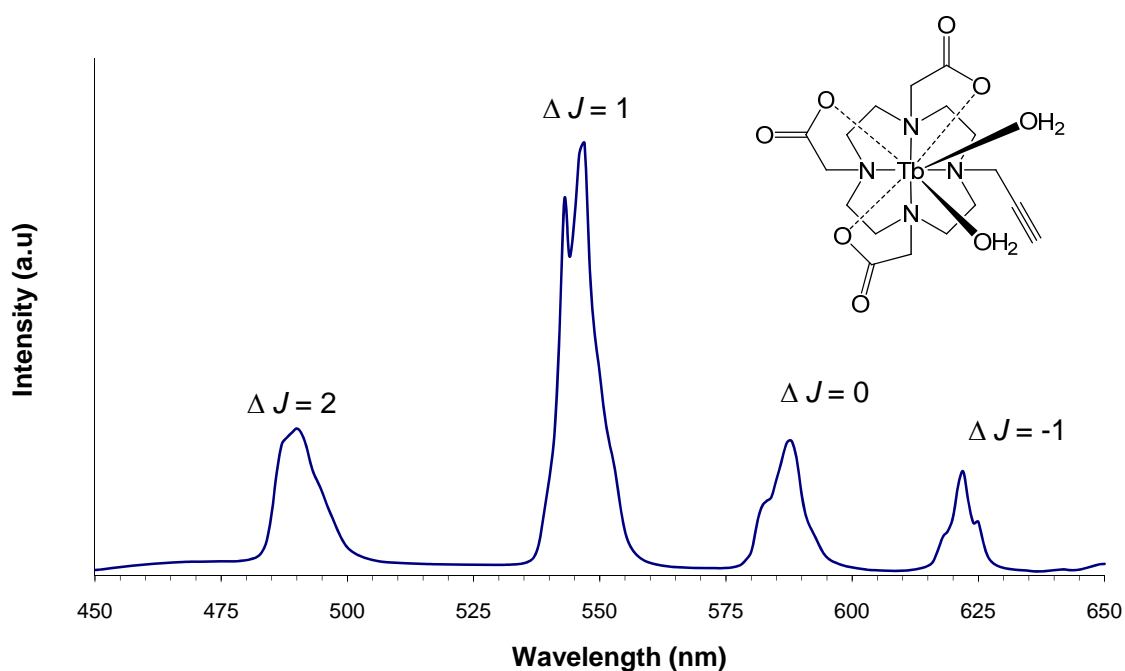


Figure 2.8 Emission spectrum of **Tb.4**, ( $\lambda_{\text{ex}} = 260$  nm,  $\text{H}_2\text{O}$ , 298K, pH 6).

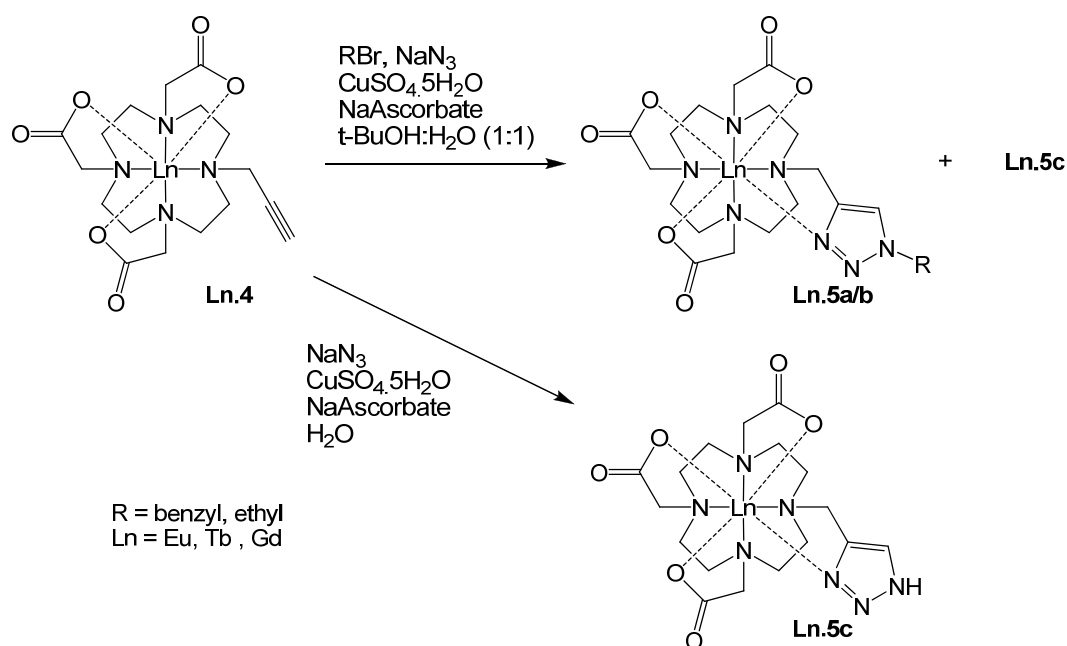
The emission spectrum in Figure 2.8 was recorded following excitation at  $\lambda_{\text{ex}} = 260$  nm, this spectrum is typical for Tb(III) emission showing the various  $^5\text{D}_4$  to  $^7\text{F}_J$  transitions. The form of a terbium (III) emission spectrum is not as sensitive to water coordination environment as europium (III), as the excited state of terbium (III) is of higher energy and therefore, less effected by quenching from the O-H oscillators. The excitation spectrum monitors the emission at  $\lambda = 546$  nm,  $\Delta J = 1$  ( $^5\text{D}_4 - ^7\text{F}_5$ ) transition. This shows strong peaks at  $\lambda = 260$  nm and weaker peaks at  $\lambda = 355$  nm. The peak observed at  $\lambda = 355$  nm represents direct excitation of the Tb(III) ion, the more intense peak at  $\lambda = 260$  nm, could be sensitisation from the alkyne to the Tb (III) ion. The Tb(III) excitation does not completely correlate with the Eu(III), this is due to the Tb(III) being more amenable to sensitisation at  $\lambda = 260$  nm, as Tb (III) excited state is higher than that of Eu(III) and therefore closer in energy to the ligand excited state at  $\lambda = 260$  nm.

The  $\Delta J = 1$  transition, at 546 nm is the wavelength that is monitored during lifetime studies. The lifetimes for **Tb.4** are considerably longer (Table 2.1) than that of **Eu.4**, as there is less efficient quenching from O-H oscillators as overlaps occur *via* the less populated  $\nu = 5$  vibrational levels of water with the  $^5\text{D}_4$  excited state of Tb(III).<sup>28</sup> The results from the lifetime studies confirm the NMR data, that **Tb.4** is heptadentate chelate and will bind one water, this is not unusual when the fourth nitrogen is substituted by a

non-coordinating group for smaller Tb(III) complexes. This corresponds with the results from **Eu.4**, that **4** can be complexed to form a seven-coordinate lanthanide chelate.

## 2.5 Triazole-appended Lanthanide Complexes

Conversion of **Ln.4** to the corresponding triazole *via* the Cu(I) catalyzed click reaction with organic azides,<sup>27</sup> will be discussed later in the chapter. It has been shown that the reaction of alkynes with *in situ* generated azides (*via* alkyl halides in the presence of NaN<sub>3</sub>) is a facile reaction and residual NaN<sub>3</sub> does not interfere with the cycloaddition reaction.<sup>4</sup> It is believed that this attractive synthetic trick would allay safety concerns, circumventing the need to isolate compounds containing azides. The unexpected reactivity of **Ln.4** with NaN<sub>3</sub>, to yield a Ln(III) complex containing an unsubstituted NH-triazole **Ln.5c** is reported.

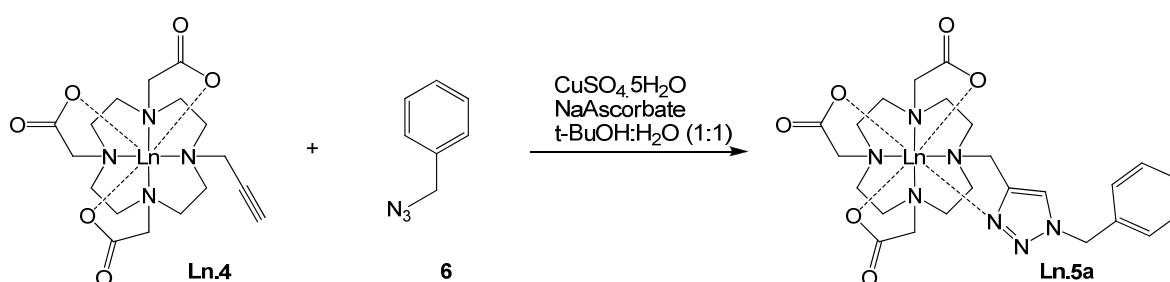


Scheme 2.12

Due to the unexpected reaction of **Ln.4** with NaN<sub>3</sub> to form the side product **Ln.5c**, isolation of the organic azides needed to form **Ln.5a/b** is necessary if **Ln.4** is to be a viable starting material for triazole appended contrast agents. To test the conversion of **Ln.4** to **Ln.5a**, benzyl azide was isolated (this is known to be safe to handle).

### 2.5.1 1,2,3-Triazole-3-benzyl appended lanthanide complexes (**Ln.5a**)

The Cu(I) catalyzed click reaction with **Ln.4** and benzyl azide (**6**) (Scheme 2.13), was achieved using standard click reaction conditions. Having filled the macrocycle cavity with the Ln(III) metal, it is now possible to undergo the ‘click’ reaction using 5 mol% copper and 10 mol % sodium ascorbate. **6** was synthesised from benzyl bromide and NaN<sub>3</sub> in MeCN as an orange oil at 96%, it was important to remove all NaN<sub>3</sub>, so the sample was taken up in diethyl ether and washed multiple times with water, thus removing all the NaN<sub>3</sub> from the sample of **6**.



Scheme 2.13

## 2.6 Characterisation and luminescence studies of **Ln.5a**

### 2.6.1 Characterisation of **Eu.5a**

**Eu.5a** was synthesised from **Eu.4** and **6** via the Cu(I) cycloaddition reaction, in 53% yield. As the complex is soluble in water, the copper was removed using a protein desalting resin, Amberlite XAD-16 (as described in Chapter 7.1.2), this gives a white hygroscopic solid **Eu.5a**. The ligand is potentially octadentate, binding through one of the triazole nitrogen atoms as well as through seven donor atoms of the DO3A core. The <sup>1</sup>H NMR shows four resonances shifted to highest frequency corresponding to four axial ring hydrogens of the square antiprismatic (SAP) geometry ( $\Delta(\lambda\lambda\lambda\lambda)/\Lambda(\delta\delta\delta\delta)$ ),  $\delta$  29.7, 27.3, 26.9, 26.3 ppm, along with the resonances corresponding to four axial ring hydrogens of the twisted square antiprismatic (TSAP) geometry ( $\Delta(\lambda\lambda\lambda\lambda)/\Lambda(\delta\delta\delta\delta)$ ),  $\delta$  13.1, 11.3, 11.1, 10.2 ppm.<sup>27</sup> This suggests that a triazole nitrogen binds to the metal centre, predominantly in the square antiprismatic geometry (10:1(SAP:TSAP)), the <sup>1</sup>H NMR spectrum suggests

that **Eu.5a** 1,2,3-triazole binds to the metal centre, in a ‘pyridinic’ coordination fashion, confirmed by luminescence studies.

ESMS of the compound gave the peak,  $[M+H]^+$  667 ( $^{151}\text{Eu}$ ), showing the correct isotope splitting pattern for a europium (III) complex. The hydration state  $q$ , of the complex was determined and its luminescent properties investigated.

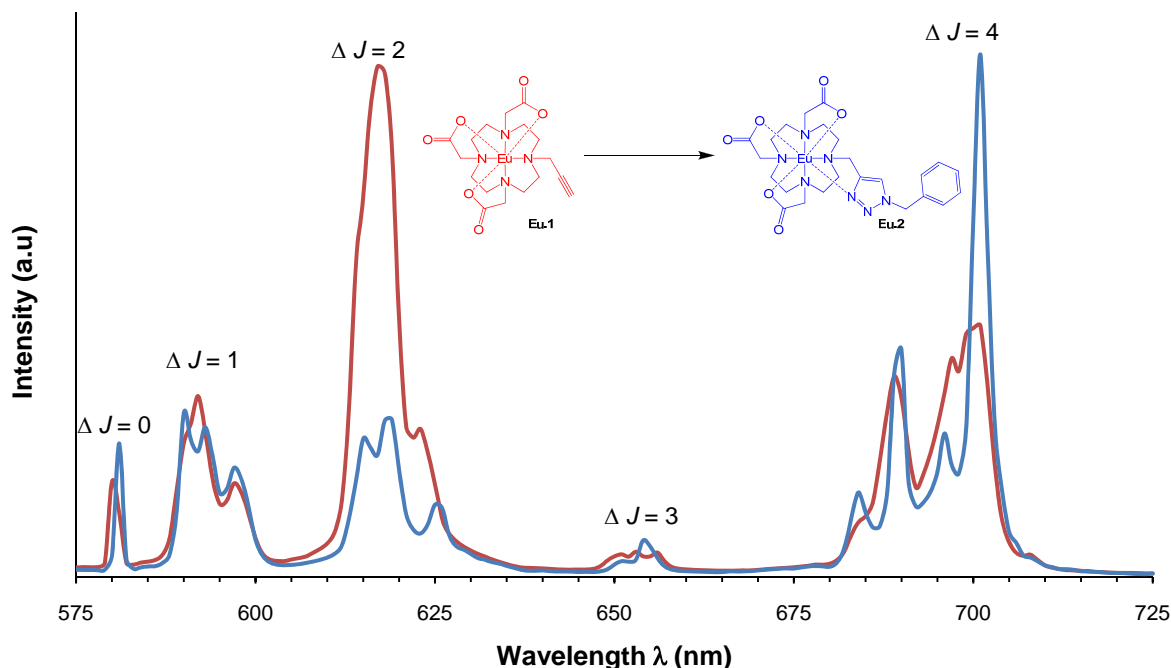


Figure 2.9 Luminescent emission spectra of **Eu.4** (red), and **Eu.5a** (blue) ( $\lambda_{\text{ex}} = 395 \text{ nm}$ ,  $\text{H}_2\text{O}$ , 298K, pH 5.5).

The Eu(III) emission spectra in Figure 2.9 show the various  $^5\text{D}_0$  to  $^7\text{F}_J$  transitions of the pre-‘click’ **Eu.4** (red) compared to post ‘click’ **Eu.5a** (blue) complex. The spectra show a decrease in intensity of the hypersensitive  $\Delta J = 2$  transition, relative to the  $\Delta J = 1$  transition, on moving from **Eu.4** to **Eu.5a**, this corresponds to a change in local coordination environment. The form of the **Eu.5a** spectrum is more like that of Eu.DOTA,<sup>29</sup> with both the  $\Delta J = 1$  and  $\Delta J = 2$  transition being of similar intensity; is typical of an eight-coordinate DOTA-based Eu(III) complex. At pH 5.5 the form of the spectrum is reminiscent of DOTA-based Eu(III) complexes bearing pendant coordinated pyridyls.<sup>30</sup> This suggests along with the NMR data that in **Eu.5a** the ligand is eight-coordinate.

The  $^5\text{D}_0$  excited state of Eu(III) lies at  $E = 17,277 \text{ cm}^{-1}$ ,<sup>28</sup> provided the triplet state energy of the benzyl moiety is greater than that of the Eu(III), energy transfer can occur, which should increase the intensity of the Eu(III) emission (Chapter 1, Section 1.6.5). The triplet excited states of phenyl groups usually lie between  $E \sim 20,000\text{-}30,000 \text{ cm}^{-1}$  and

therefore it was hypothesised that sensitised emission should occur.<sup>31</sup> The excitation spectrum monitors the emission at  $\lambda = 618$  nm, ( $\Delta J = 2$ ), and shows peaks at  $\lambda = 237$  nm and  $\lambda = 260$  nm, with weaker peak at  $\lambda = 395$  nm. The peak observed at  $\lambda = 395$  nm corresponds to direct excitation of the Eu(III) ion, the more intense peak at  $\lambda = 260$  nm, represents the benzyl chromophore, whereby energy transfer from the triplet excited state of the benzyl can transfer to the Eu(III) ion, giving an increased emission. The benzyl chromophore is not a great sensitizer, as can be seen in Figure 2.10 there is little difference between direct and sensitised Eu(III) emission.

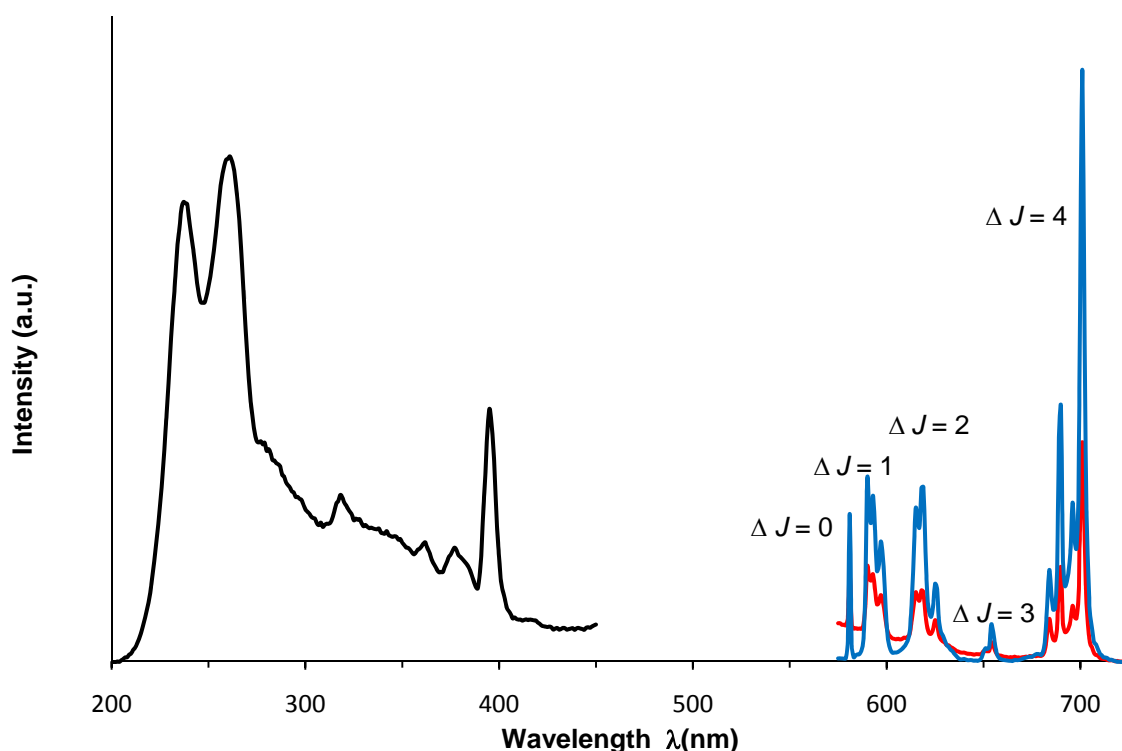


Figure 2.10 Eu(III) emission spectra for **Eu.5a** following direct excitation (red,  $\lambda_{ex} = 395$  nm) and sensitised excitation (blue,  $\lambda_{ex} = 260$  nm). The excitation spectrum for **Eu.5a** (black,  $\lambda_{em} = 618$  nm), ( $H_2O$ , 298K, pH 5.5).

### 2.6.2 *Eu(III) Emission Intensity vs. pH for Eu.5a*

Eu(III) emission was found to increase in intensity as the pH of the solution was raised. This could arise from two possible mechanisms: either the triazole subunit protonates and dissociates from the metal centre allowing coordination of a second water molecule, or the deprotonation of coordinated water in more basic media, resulting in the ligation of a single hydroxide ion to the Eu(III) centre. The latter is more likely as

protonation of substituted triazoles at the N1 or N2 position occurs at pH  $\sim 1$ .<sup>32</sup> At pH 5.5 the form of the spectrum is reminiscent of DOTA-based Eu(III) complexes bearing pendant coordinated pyridyls.<sup>30</sup> The  $^1\text{H}$  NMR spectrum shows no change with respect to pH (Figure 2.11); however, the hydration state changes, where at low pH  $q = 1$  and at pH 10  $q = 0.5$  (Table 2.3).

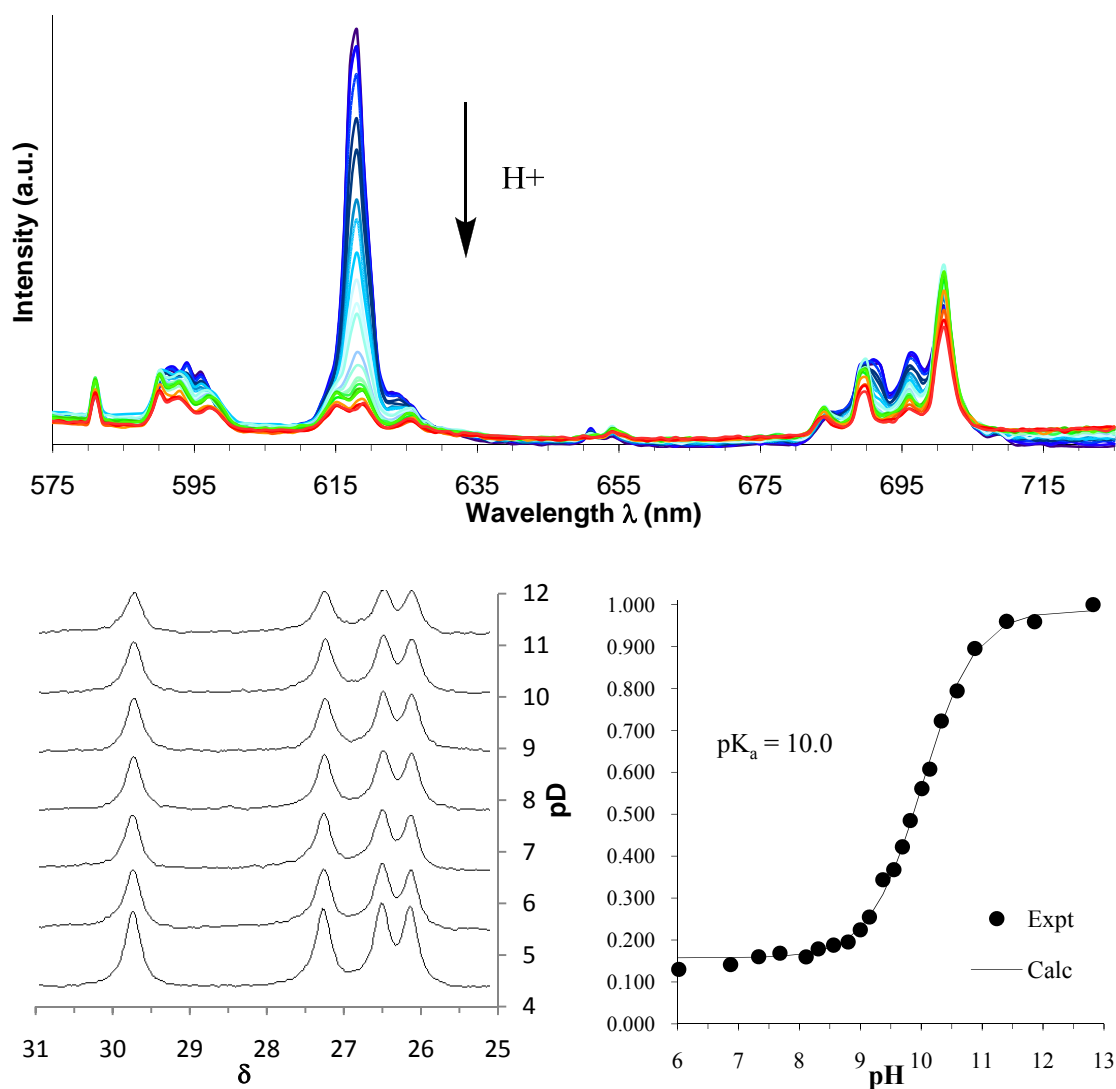


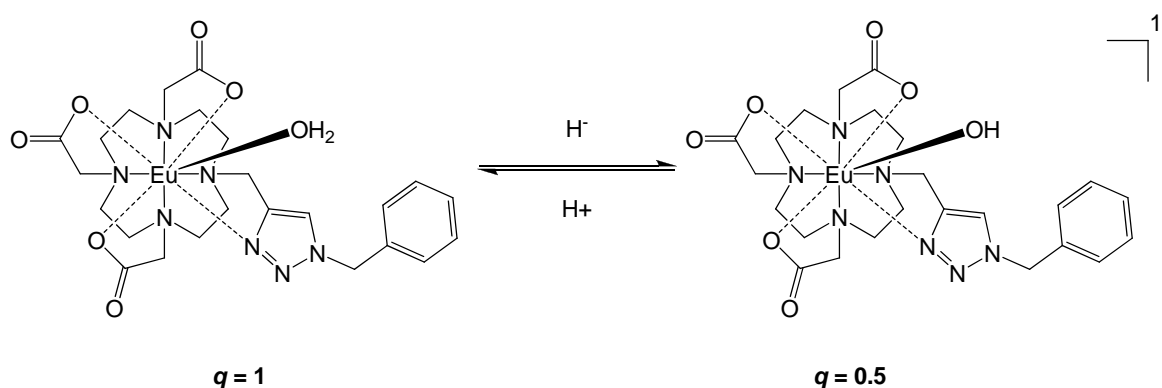
Figure 2.11 Top: Eu(III) luminescence emission spectra vs. pH for **Eu.5a**. Bottom Left:  $^1\text{H}$  NMR spectra vs. pD for **Eu.5a**. Bottom Right: Eu(III) emission intensity  $I/I_0$  ( $\Delta J = 2$ ) vs. pH for **Eu.5a**.

The only possible protonation event occurring with respect to pH, is deprotonation of the bound water (Scheme 2.14). This event has a  $\text{pK}_a = 10$  for **Eu.5a** (calculated from the luminescence data). The data shows that **Eu.5a** must be an eight-coordinate with respect to ligand **5a**, with seven-donating ligands from the DO3A core and one from the triazole nitrogen. The triazole subunit is stable with respect to pH and remains bound to the metal centre at high pH. The deprotonation of bound water does not affect the form of the

$^1\text{H}$  NMR spectra (as expected), as there is no structural change in the coordination geometry of **Eu.5a**, but deprotonation of the water changes the form of the Eu(III) luminescence emission, having a dramatic affect on the form and intensity of the hypersensitive  $\Delta J = 2$  transition.

Complex	pH	$k_{\text{H}_2\text{O}}$ ms $^{-1}$	$k_{\text{D}_2\text{O}}$ ms $^{-1}$	$q$ ( $\pm 0.2$ )
<b>Eu.5a</b>	4	3.05	1.47	1.6
<b>Eu.5a</b>	7	2.14	0.89	1.2
<b>Eu.5a</b>	11	1.59	0.61	0.8

Table 2.3 Rate constants,  $k$ , for depopulation of the excited state and derived hydration states,  $q$ , for the decay of **Eu.5a** vs. pH ( $\lambda_{\text{ex}} = 395$  nm,  $\lambda_{\text{em}} = 618$  nm)



Scheme 2.14

### 2.6.3 Characterisation of **Tb.5a**

**Tb.5a** was synthesised in the same manner as **Eu.5a**, and was obtained in 66% yield. ESMS of the compound gave the peak, 674  $[\text{M}+\text{H}]^+$ . Our collaborators have shown the  $^1\text{H}$  NMR spectrum for **Tb.5a**<sup>27</sup>, which is similar to that of **Eu.5a**, though the form is reversed and implies that there is one water molecule bound at the metal centre, as would be expected for an octadentate ligand. Non-green coloured samples are found to be pure Ln(III) complexes, leaving some residual Ln(III) compounds in green coloured samples, containing copper.

**Tb.5a** is an eight-coordinate metal complex with respect to ligand **5a**, as like **Eu.5a**, it has seven donor atoms from the DO3A core and one from the appended triazole (N2).

The hydration state  $q$ , of the complex was determined and its luminescent properties investigated.

Complex	$\lambda_{em} / \text{nm}$	$\lambda_{ex} / \text{nm}$	$k_{\text{H}_2\text{O}} \text{ms}^{-1}$	$k_{\text{D}_2\text{O}} \text{ms}^{-1}$	$q (\pm 0.2)$
<b>Eu.5a</b>	395	618	2.14	0.89	1.2
<b>Tb.5a</b>	355	546	0.89	0.7	0.6
<b>Tb.5a</b>	264	546	0.79	0.61	0.6

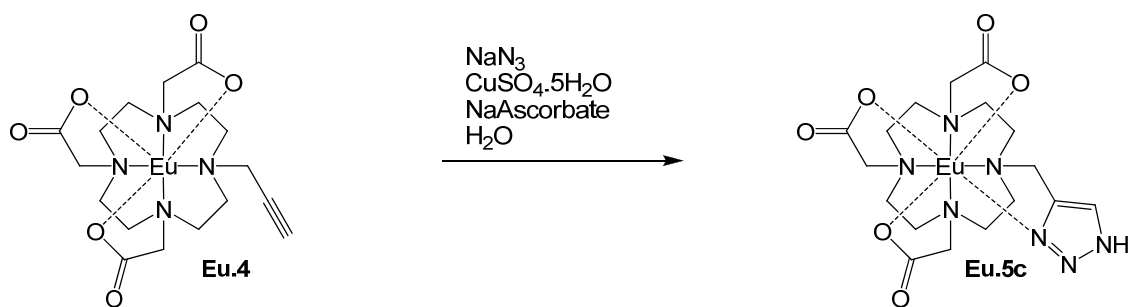
Table 2.4 Rate constants,  $k$ , for depopulation of the excited state and derived hydration states,  $q$ , for the decay of **Eu.5a** and **Tb.5a**

The luminescent studies confirm that the excited state of the benzyl chromophore is at  $\lambda = 260 \text{ nm}$ , that **Tb.5a** is  $q = 0.6$ , from both sensitised and direct excitation (Table 2.4). This confirms the data from **Eu.5a** that the 1,2,3-triazole-3-appended Ln(III) complexes are octadentate, therefore bind only one water molecule. The data shows that the 1,2,3-triazole can be used as a stable linker and a viable synthetic route to linking molecules to Ln(III) chelates.

The sensitised emission from the excited triplet state of the benzyl chromophore at  $\lambda = 260 \text{ nm}$  is no more efficient than the direct sensitisation of the Tb(III) ion at  $\lambda = 355 \text{ nm}$ . This is partly due to the higher excited energy state  $^5\text{D}_4$  of Tb(III), being less accessible sensitisation.

## 2.7 Unsubstituted 1,2,3-triazole appended lanthanide complexes

There is currently much interest in the generation of unsubstituted 1,2,3-triazoles due to their topological and electronic similarities to amides; their biological activity is being explored as peptide bond mimics.<sup>13</sup> Synthesis of NH-triazoles usually requires the use of a ‘protected’ organic azide, such as azidomethyl pivalates and carbamates that can be easily removed once the triazole is formed.<sup>33</sup> The alternative is the highly undesirable reaction with hydrazoic acid at high temperature.<sup>34</sup> Unsubstituted triazoles have been reported, these tend to be formed at elevated temperatures, not under ambient conditions.<sup>8,9</sup>



Scheme 2.15

Due to the unexpected reactivity of **Ln.4** with  $\text{NaN}_3$ , the click reaction of **Ln.4** was attempted in water in the presence of  $\text{CuSO}_4$ , sodium ascorbate and  $\text{NaN}_3$  (Scheme 2.15). Under these conditions complete conversion to **Ln.5c** was seen after stirring at room temperature for 12 hours. It is evident that Ln(III) complexes based on proligand **4** are unsuitable for use in click reactions where the azide is generated *in situ*, due to their propensity to react with  $\text{NaN}_3$ . This effect has been observed with a variety of lanthanides (*e.g.* Sm-Dy) and it is possibly linked to the close proximity of the alkyne to the Ln(III) ion. There are numerous postulated intermediates in the proposed mechanism of the Cu(I) catalyzed 1,3 Huisgen cycloaddition reaction, in all cases an organic azide is deemed essential for the reaction to proceed.<sup>4</sup> One mechanism suggests the Cu-acetylide that is initially formed, and the azide, are bound to different copper atoms in a doubly bridged assembly (Figure 2.12).<sup>35</sup> This may offer some clues to the unusual reactivity observed in **Ln.4** as the copper acetylide must be in close proximity to the central Ln(III) ion. It is likely that the  $\text{N}_3^-$  ligand bound to Ln(III) is amenable to cycloaddition to the activated alkyne (Section 2.9).

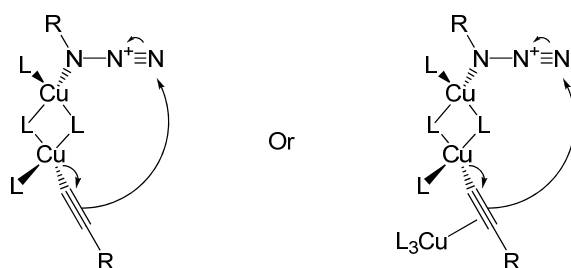


Figure 2.12 Copper azide alkyne doubly bridged assembly<sup>35</sup>

Figure 2.12 shows the di-copper doubly bridged assembly suggested by Walker and co-workers,<sup>35</sup> this could explain the unusual reactivity of **Ln.4** with  $\text{N}_3^-$ . They suggest that  $\pi$ -activation of the copper acetylide unit by coordination of a second copper atom (Figure

2.12) greatly enhances the reactivity of the copper acetylide, accelerating formation of the metallacycle.<sup>35</sup> This suggests  $N_3^-$  may bind to the lanthanide and the alkyne binds to a Cu(I) metal in the terminal position, acting as an enhancement to the ‘click’ mechanism, aiding the formation of the metallocycle.

### 2.7.1 Characterisation of **Eu.5c**

**Eu.5c** was isolated as a white hygroscopic solid in 68% yield, this is lower than expected as yields described in the literature for the Cu(I) catalyzed 1,3 Huisgen cycloaddition reaction are near quantitative.<sup>1</sup> Due to the purification technique and the solubility of **Eu.5c** in water, separation of the salts from the Ln(III) complex results in some loss of yield (ESMS of the crude suggests 100% conversion). It would be expected that the unsubstituted 1,2,3-triazole would behave like the pyridinic appended Ln(III) complex reported by Aime *et al.*<sup>30</sup> in which the pyridine nitrogen remains bound to the Ln(III) metal throughout pH range 2.5-12.5, this would also match the pH vs. <sup>1</sup>H NMR data obtained for **Eu.5a**. The behaviour of the unsubstituted 1,2,3-triazole is also expected to be similar to that of the unsubstituted tetrazole described by Aime *et al.*<sup>36</sup>, the unsubstituted Gd(III) tetrazole complex shows no change in relaxivity with respect to pH, suggesting that the tetrazole remains bound to the metal centre over a wide pH range, with a relaxivity of  $r_1 = 4.8 \text{ mM}^{-1}\text{s}^{-1}$  (pH 7.4, 298 K, 0.47 T), suggesting an octadentate ligand.<sup>36</sup>

### 2.7.2 pH responsive behaviour of **Eu.5c**

**Eu.5c** was characterized by <sup>1</sup>H NMR and luminescence spectroscopy and displays interesting pH-responsive behaviour in the physiological pH range. The <sup>1</sup>H NMR spectrum (400 MHz, pD 9.0, 278K) is typical of a rigid eight-coordinate unsymmetrical Eu(III) complex exhibiting a broad range of resonances from -18 to 33.5 ppm. This is indicative of triazole coordination to Eu(III). The restricted arm rotation in eight-coordinate (*cf.* 7-coordinate) complexes slows the exchange between the various stereoisomers, resulting in resolution of the axial and equatorial cyclen ring hydrogens. The four axial resonances shifted to high frequency are typical of a square antiprismatic coordination geometry, ( $\Delta(\lambda\lambda\lambda\lambda)/\Lambda(\delta\delta\delta\delta)$ ). The presence of the minor twisted square antiprismatic isomer is also

demonstrated by four resonances at slightly lower frequency ( $(\Delta(\lambda\lambda\lambda\lambda)/\Lambda(\delta\delta\delta\delta))$ , 9.9 to 13.6 ppm).

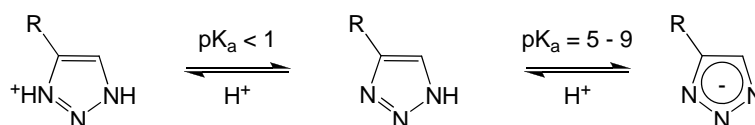
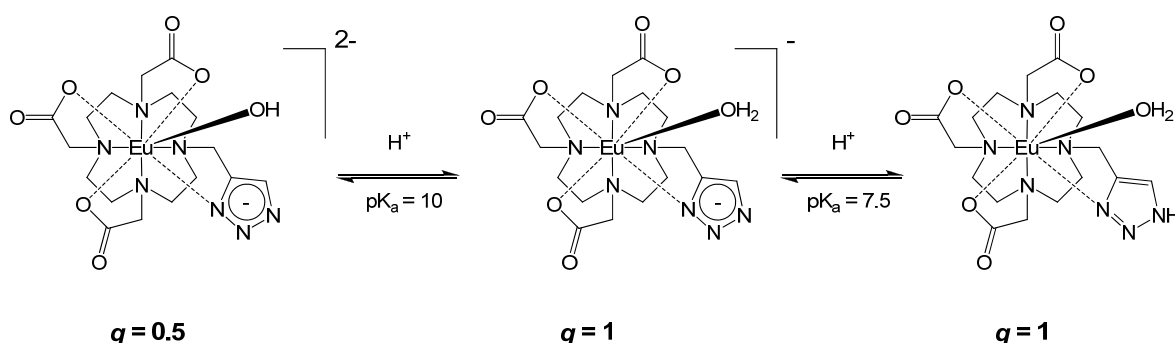


Figure 2.13 Protonation scheme of an unsubstituted 1,2,3 triazole

At basic pH, the triazole is bound to Eu(III) as a monoanionic donor *i.e.* as the 1,2,3-triazolide (Scheme 2.16), further evidence for coordination of 1,2,3-triazolide is offered by the negative ESMS,  $[M-H]^-$   $m/z = 574.1060$  ( $^{151}\text{Eu}$ ) (Figure 2.13, shows the protonation sequence for NH triazoles, at  $\text{pH} > 9$  the negatively charged triazolide is expected to be present) if the pH of the solution is greater than 9 then the complex will be negatively charged and can be observed in the negative ESMS $^-$ . NH-triazoles are acidic; their  $\text{pK}_a$ s typically  $\sim 5-9$ .<sup>32</sup> This anionic coordination mode is different to the coordination behaviour of N-substituted triazoles that coordinate *via* a ‘pyridinic’ nitrogen atom<sup>27</sup> (the  $\text{pK}_a$  of this nitrogen is typically  $< 1$ ). The  $^1\text{H}$  NMR spectrum of **Eu.5c** exhibits pH-dependent behaviour (Figure 2.14). On titrating from base to acid, three of the four most shifted axial resonances (33.4, 33.1 and 32.6 ppm) broaden, moving to lower frequency, the fourth (31.1 ppm) moves to higher frequency. On moving to acidic media, the resonances are once more resolved. The resonance that shifts to higher frequency now appears at 32.1 ppm; the three resonances that shift to lower frequency now appear at 29.8, 29.2 and 28.6 ppm. This is a clear indication of a protonation event, *i.e.* of one of the triazolide nitrogens.



Scheme 2.16

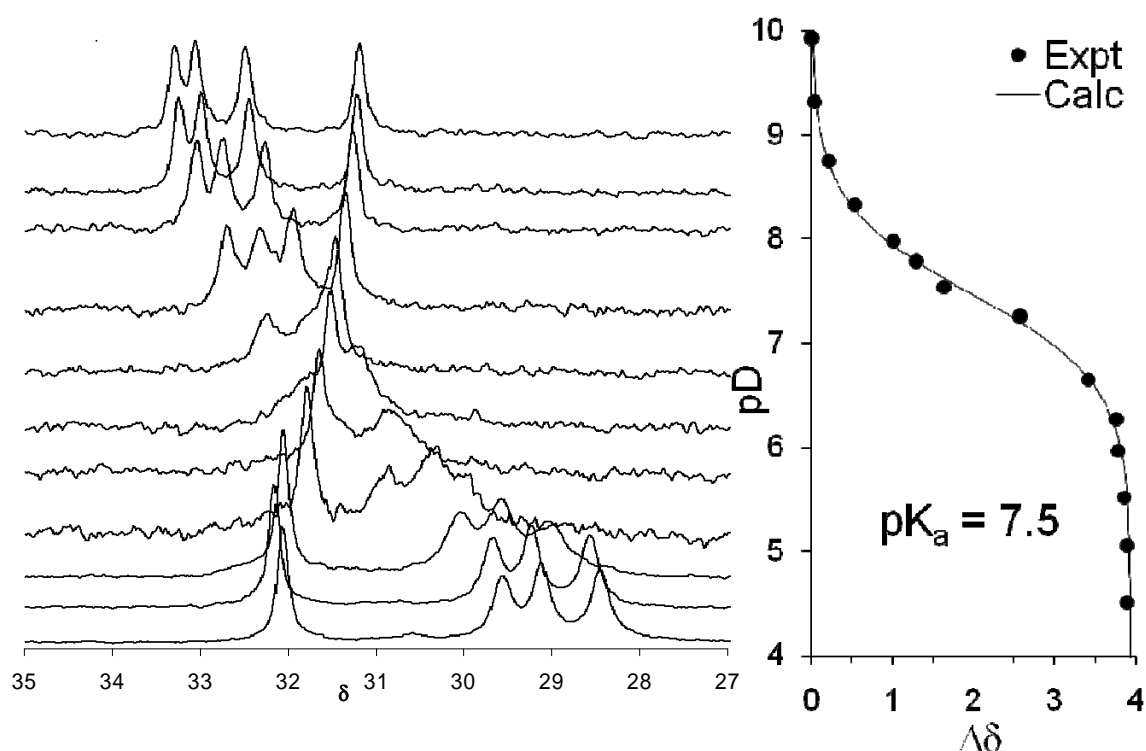


Figure 2.14 Left:  $^1\text{H}$  NMR vs. pD for **Eu.5c** (400 MHz, 278K), Right:  $^1\text{H}$   $\Delta\delta$  vs. pH for **Eu.5c**

The subtle change from effectively  $\text{N}^-$  coordination to pyridinic N-coordination results in a marked change in spectral form. Similar movements can be traced for other resonances in the spectrum for both the square and the twisted square antiprismatic isomers. The change in chemical shift of these resonances  $\Delta\delta$  enable the determination of a protonation constant ( $\log K_{\text{MLH}}$  or  $\text{p}K_{\text{a}}$ ) of  $7.5 \pm 0.1$  *i.e.* **Eu.5c** exhibits pH-responsive behaviour in the physiological pH range. Given the apparent rigidity demonstrated in the  $^1\text{H}$  NMR spectrum after protonation, the triazole remains coordinated to Eu(III) after protonation, but *via* the pyridinic nitrogen, indeed the form of the spectrum in acid media is very similar to related coordinated N-substituted triazoles.<sup>27</sup>

### 2.7.3 *Eu(III) Emission Intensity vs. pH for Eu.5c*

The luminescent emission spectrum of **Eu.5c** is typical of an eight-coordinate DOTA-based Eu(III) complex. At pH 5.5 the form of the spectrum is reminiscent of DOTA-based Eu(III) complexes bearing pendant coordinated pyridyls<sup>30</sup> (and indeed of the

N-substituted triazoles)<sup>17</sup> as are the relative intensities of the  $\Delta J = 1$  ( $^5D_0 \rightarrow ^7F_1$ ) and  $\Delta J = 2$  ( $^5D_0 \rightarrow ^7F_2$ ) transitions.

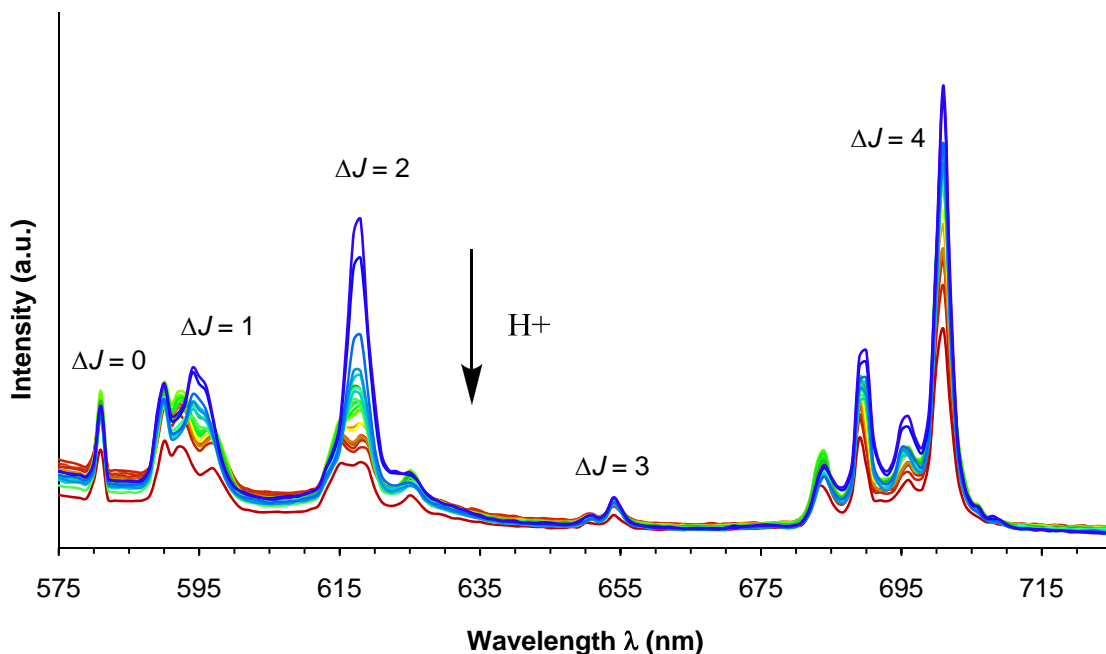


Figure 2.15 Luminescent Eu(III) emission spectra vs. pH for **Eu.5c**, ( $\lambda_{\text{ex}} = 395$  nm, 0.1 M NaCl, 25°C)

On raising the pH of the solution, one of the transitions in the  $\Delta J = 1$  manifold shifts from 592 to 597 nm, Figure 2.16 shows the change in spectral form of the  $\Delta J = 1$  between pH 5 - 8. The ratio of intensities of these peaks enables a protonation constant of  $6.9 (\pm 0.1)$  to be extracted from the data (an excited-state  $pK_a$  recorded at 298K), *i.e.* ratiometric concentration independent pH response. This is consistent with the changes observed in the  $^1\text{H}$  NMR spectrum ( $pK_a = 7.5$ , a ground-state  $pK_a$  recorded at 278K). This behaviour supports the idea of a subtle change in coordination mode of the triazole from neutral ‘pyridyl’ to anionic triazolide. The titration is complicated by a second deprotonation event occurring at  $\text{pH} > 8$  (hence the absence of data points at  $\text{pH} > 8$  in Figure 2.16). This is deprotonation of the bound water molecule in the ninth coordination site of **Eu.5c** and is characteristic of such complexes: there is a change in spectral form of  $\Delta J = 1$  and an increase in intensity of the hypersensitive  $\Delta J = 2$  transition. This transition is particularly sensitive to the polarisability of the axial donor atom<sup>37</sup> and moving from bound  $\text{H}_2\text{O}$  to bound  $\text{OH}^-$  invokes this change. The  $pK_a$  of the bound water, extracted from the luminescence data, is  $9.9 \pm 0.1$ , similar to that obtained for **Eu.5a** (section 2.6.2).

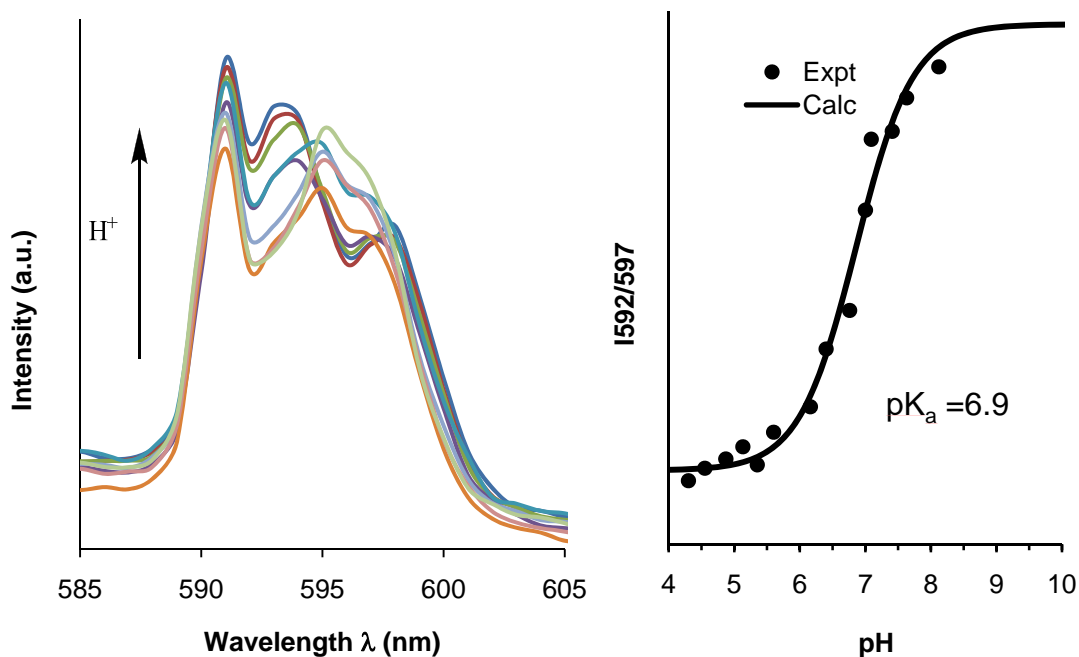


Figure 2.16 Left: Luminescent Eu(III) emission spectra vs. pH for **Eu.5c**,  $\Delta J = 1$  between pH 5-8. Right: Eu(III) emission intensity  $I_{592}/I_{597}$  ( $\Delta J = 1$ ) vs. pH for **Eu.5c**

Luminescent lifetime measurements confirm these conclusions. The lifetime of the Eu(III) excited state is susceptible to quenching from O-H oscillators. Luminescent lifetime measurements on **Eu.5c** in  $H_2O$  and  $D_2O$  Shown in Table 2.4 (The lifetimes monitored the  $\Delta J = 2$  peak at  $\lambda_{em} = 618$  nm with a  $\lambda_{ex} = 395$  nm). At pH 10.0  $q = 0.4$  consistent with deprotonation of the bound water molecule, *i.e.*  $OH^-$  is bound. At pH 8.5, before hydrolysis of the bound water, when the triazole is bound in an anionic manner,  $q = 1.1$ . At pH 5.5 when bound in a pyridinic manner, the apparent hydration state is slightly higher than unity  $q = 1.4$ , the modified Horrock's equation used to calculate  $q$ , does not correct for quenching by the triazole NH, it is likely that this quenching N-H oscillator is in close proximity to the Eu(III) contributes to the decrease of lifetime in  $H_2O$ , hence the slightly higher calculated  $q$  value.

Complex	pH	$k_{\text{H}_2\text{O}}$ ms <sup>-1</sup>	$k_{\text{D}_2\text{O}}$ ms <sup>-1</sup>	$q$ ( $\pm 0.2$ )
<b>Eu.5c</b>	5.5	2.51	1.06	1.4
<b>Eu.5c</b>	8.5	2.27	1.11	1.1
<b>Eu.5c</b>	10	1.81	1.2	0.4

Table 2.5 Rate constants depopulation of the Eu(III) excited state and calculated hydration state of **Eu.5c** at different pH values ( $\lambda_{\text{ex}} = 395$  nm,  $\lambda_{\text{em}} = 618$  nm).

The formation of **Eu.5c** has demonstrated that a seemingly small structural alteration, substituting an N-(2-propynyl)acetamide for propargyl as a means of coupling lanthanide chelates *via* click chemistry is only suitable if the organic azide involved in the click reaction is pre-formed and the solution is free of NaN<sub>3</sub>. The unexpected product of this click reaction **Eu.5c** showed interesting protonation behaviour, switching from triazole bound to Eu(III) in an N-deprotonated anionic form in basic media, to an N–H protonated pyridyl form in acidic media. This pH-dependent switch, demonstrated by both <sup>1</sup>H NMR and luminescence studies, occurs in the physiological pH range.

## 2.8 Characterisation of **Tb.5c**

**Tb.5c** was synthesised to determine whether the same pH response is observed across the lanthanide series. **Tb.5c** was isolated as a white hydroscopic solid at 59% yield.

### 2.8.1 *Tb(III) Emission Intensity vs. pH for **Tb.5c***

The emission spectra in Figure 2.17 were recorded following excitation at  $\lambda_{\text{ex}} = 280$  nm, this spectrum is typical for Tb(III) emission showing the various <sup>5</sup>D<sub>4</sub> to <sup>7</sup>F<sub>J</sub> transitions. On raising the pH of the solution, all of the transitions increase in intensity. The emission spectra show a protonation event. The ratio of intensities of peaks  $\lambda = 488$  nm,  $\Delta J = 2$  (<sup>5</sup>D<sub>4</sub> to <sup>7</sup>F<sub>6</sub>) and  $\lambda = 546$  nm,  $\Delta J = 1$  (<sup>5</sup>D<sub>4</sub> to <sup>7</sup>F<sub>5</sub>) enables a protonation constant of 6.4 ( $\pm 0.07$ ) to be extracted from the data (an excited-state pK<sub>a</sub> recorded at 298K), *i.e.* ratiometric concentration independent pH response. This is consistent with the changes observed in the Eu (III) spectrum for **Eu.5c** (pK<sub>a</sub> = 6.9, an excited-state pK<sub>a</sub> recorded at 298K). This behaviour supports the idea of a subtle change in coordination mode of the triazole from

neutral 'pyridyl' to anionic triazolide. Presumably the more charge dense metal within the chelate, alters the  $pK_a$  from 6.9 to 6.4, for Eu(III) (1.07 Å) as Tb(III) (1.04 Å).

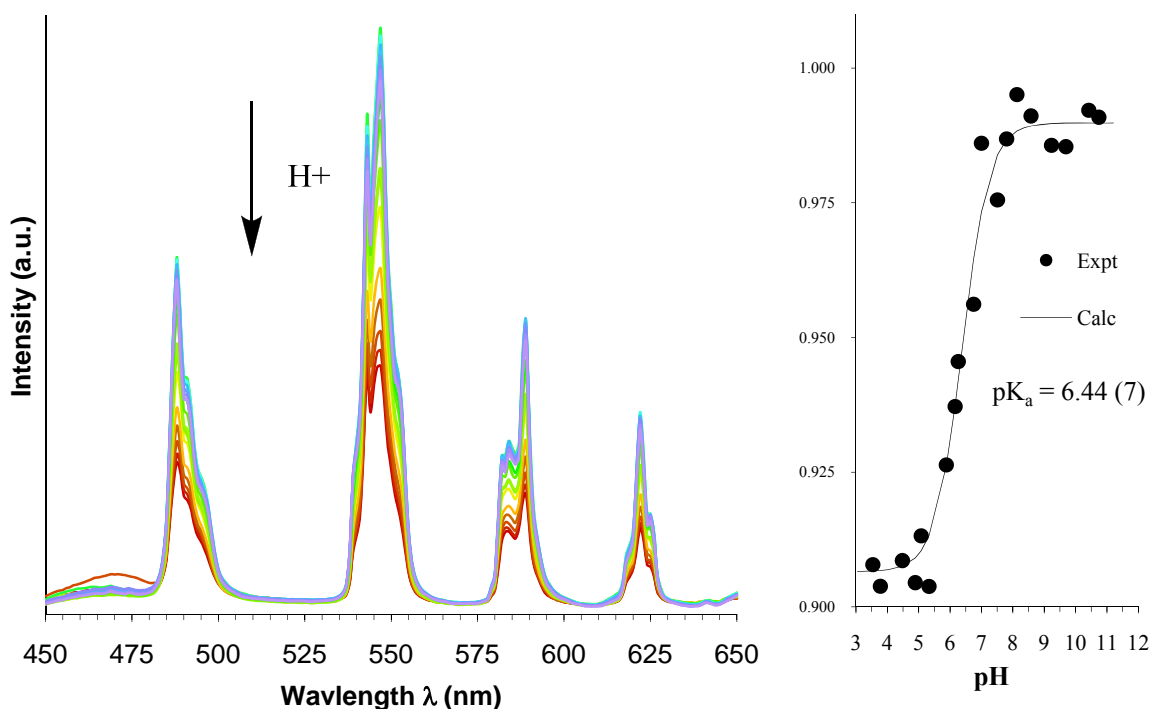


Figure 2.17 Left: Tb (III) emission vs. pH for **Tb.5c**  $\lambda_{ex} = 280$  nm. Right: Tb(III) emission intensity  $I_{488}/I_{546}$  ( $\Delta J = 2/\Delta J = 1$ ) vs. pH for **Tb.5c**.

The emission spectra in Figure 2.17, were recorded with a  $\lambda_{ex} = 280$  nm in  $H_2O$ , which is not direct sensitisation of Tb(III) ( $\lambda = 355$  nm) it is sensitised emission from the triazole subunit ( $\lambda = 280$  nm). Figure 2.18 shows the excitation spectra of **Tb.5c** with respect to pH monitoring  $\lambda_{em} = 546$  nm ( $\Delta J = 1$ ), the intensity of the excitation spectrum increases with pH, this shows that the triazolide coordination mode of **Tb.5c** is more efficient at transferring energy to the Tb(III) ion than the pyridinic bound form of **Tb.5c**. A shift in wavelength from  $\lambda = 272$  nm to  $\lambda = 286$  nm, also indicates a protonation event, the change in coordination mode from pyridinic to anionic triazolide bound changing the absorption maximum. For both emission (Figure 2.17) and excitation (Figure 2.18) spectra, an increase in intensity can be seen with an increase in pH. This protonation event represents the formation of the negatively charged triazolide, the excited state of the triazolide must be closer in energy to the excited state the  $^5D_4$  of the Tb(III) ion, than the N-H 1,2,3-triazole excited state, as the increase in intensity suggests more efficient energy transfer from the triazolide to the Tb(III) ion.

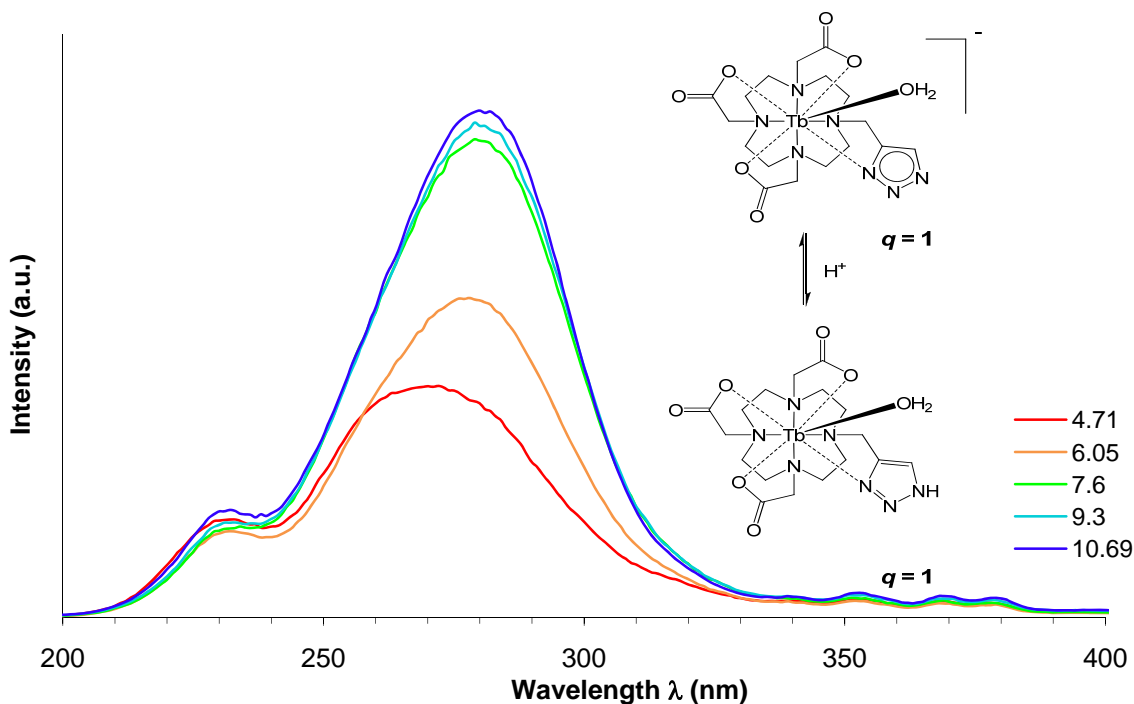


Figure 2.18 Tb(III) excitation spectra vs. pH of **Tb.5c** ( $\lambda_{em} = 546$  nm)

The excited state of the triazolide must be closer in energy to the Tb(III) excited state ( $^5D_4$ ) than the pyridinic form of triazole coordination. Therefore more accessible for energy transfer to the Tb(III), as seen by the increase in intensity (Figure 2.18). **Eu.5c** does not show sensitised emission from the triazole unlike **Tb.5c**, this is likely due to the excited state energy levels of the triazole being too high for efficient energy transfer to the Eu(III) excited state  $^5D_0$ . The energy gap is too great to allow for efficient transfer of energy and sensitised emission of Eu(III), with Tb(III) the triazole excited state must be closer in energy to the  $^5D_4$  of Tb(III) and therefore efficient energy transfer can occur.

Complex	pH	$k_{H_2O}$ ms $^{-1}$	$k_{D_2O}$ ms $^{-1}$	$q$ ( $\pm 0.2$ )
<b>Tb.5c</b>	4	1.1	0.84	1
<b>Tb.5c</b>	7	0.78	0.59	0.7
<b>Tb.5c</b>	10	0.75	0.56	0.5

Table 2.6 Rate constants depopulation of the Tb(III) excited state and calculated hydration state of **Tb.5c** at different pH values ( $\lambda_{ex} = 280$  nm and  $\lambda_{ex} = 355$  nm,  $\lambda_{em} = 546$  nm)

Luminescent lifetime measurements confirm these conclusions. The lifetime of **Tb.5c** is longer than that of **Eu.5c** at comparable pH value, this is due to Tb(III) being less

susceptible to O-H oscillators than Eu(III). Luminescent lifetime measurements on **Tb.5c** in H<sub>2</sub>O and D<sub>2</sub>O enable the determination of the hydration state ( $q$ ) of the complex, the lifetimes monitored the  $\Delta J = 1$  peak at  $\lambda_{em} = 546$  nm with a  $\lambda_{ex} = 355$  nm and  $\lambda_{ex} = 280$  nm. At pH 10.0  $q = 0.5$  consistent with deprotonation of the bound water molecule, *i.e.* OH<sup>-</sup> is bound, although a smaller effect from this is exerted on the Tb(III) ion than the Eu(III) ion. Due to the O-H oscillator being closer in energy to the excited state <sup>5</sup>D<sub>0</sub> of the Eu(III) ion than the excited state <sup>5</sup>D<sub>4</sub> of Tb(III), therefore less quenching can occur, as there is less efficient energy transfer from the excited state of the Eu(III) ion.<sup>28</sup> At pH 7, before hydrolysis of the bound water, when the triazole is bound in an anionic manner,  $q = 0.7$ . At pH 4 when bound in a pyridinic manner,  $q = 1$ . Unlike **Eu.5c**, **Tb.5c** is little affected as much from quenching of the N-H of the triazole. In general both **Eu.5c** and **Tb.5c** show shorter lifetimes than expected at all pH values, this could be due to the bound 1,2,3-triazole, exerting some quenching effect (*e.g.* photo-induced electron transfer for Eu(III), back energy transfer for Tb(III)).

These results confirm that, **Tb.5c** is eight-coordinate with the triazole binding through a pyridinic nitrogen<sup>27</sup> at low pH and through an anionic triazolide<sup>38</sup> at higher pH, this change in coordination mode is just inside the physiological range, and maybe could be put to use as a ratio metric luminescent sensor of cancer cells which have a pH  $\sim 6$ .<sup>39</sup> The lifetime measurements of **Tb.5c** also confirm that it is not reversible binding of the triazole but a subtle change in coordination mode as hydration state remains at one water molecule bound with respect to pH.

## 2.9 N<sub>3</sub><sup>-</sup> binding studies upon Eu.4

For the formation of **Ln.5c**, from **Ln.4** it is likely that N<sub>3</sub><sup>-</sup> must be bound to the Ln(III) metal centre, so that the N<sub>3</sub><sup>-</sup> is amenable to cycloaddition to the activated alkyne. As discussed earlier, one mechanism suggests the Cu-acetylide that is initially formed, and the azide, are bound to different copper atoms in a doubly bridged assembly. This may offer some clues to the unusual reactivity observed in **Ln.4** as the copper acetylide must be in close proximity to the central Ln(III) ion. Luminescence studies of **Eu.4** emission intensity *vs.* [N<sub>3</sub><sup>-</sup>], suggest that N<sub>3</sub><sup>-</sup> can displace the bound H<sub>2</sub>O, the decrease in signal intensity of the spectra as [N<sub>3</sub><sup>-</sup>] is increased, suggests that N<sub>3</sub><sup>-</sup> exerts a greater quenching effect than the O-H oscillators of H<sub>2</sub>O. The titration data shows that N<sub>3</sub><sup>-</sup> has a very low binding constant,  $K =$

2.3  $M^{-1}$  (Figure 2.19 using emission intensity at  $\lambda = 701$  nm). This suggests that under ‘click conditions, that 1%  $N_3^-$  is bound to **Eu.4**. This percentage appears very low, although in terms of the Cu(I) cycloaddition, it may be sufficient to allow the formation of **Eu.5c**.

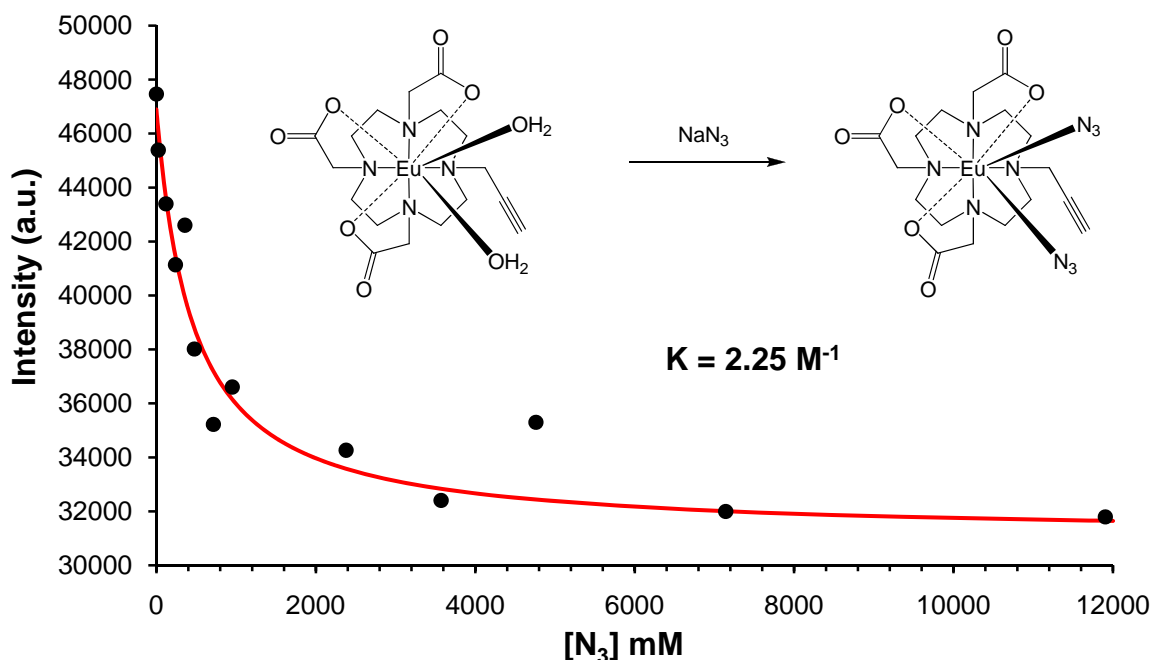


Figure 2.19 Eu(III) emission intensity  $I_{701}$  vs.  $[N_3^-]$  for **Eu.4** (1mM),  $\lambda_{ex} = 395$  nm,  $H_2O$ , 298K, pH 5.

**Eu.4** was excited directly at  $\lambda_{ex} = 395$  nm, and the titration was carried out at pH 5, the pH at which the ‘click’ reaction takes place, it is also low enough to prevent competitive binding of carbonate (from dissolved  $CO_2$ ), which would show an adverse effect on Eu(III) emission altering the spectral form giving false results. The  $\Delta J = 4$  peak ( $\lambda = 701$  nm) was used to determine the binding constant, as there was less noise / scattered light in this part of the spectra, giving the most accurate result. The equilibrium (Equation 36) was assumed for **Eu.4**, where Ln represents the Ln(III) ligand complex. The concentration of bound lanthanide complex,  $[LnN_3]$ , is determined by expansion of Equation 45, where  $[N_3^-]_T$  and  $[Ln]_T$  are the total concentrations of  $N_3^-$  and the Ln(III) complex (Ln = Eu(III)), (Equation 37).<sup>40</sup> The Ln(III) concentrations can be substituted for of Eu(III) emission intensity as shown in Equation 38, where  $I_{calc}$  is the theoretical Eu(III) emission intensity (to be compared with the experimentally observed Eu(III) emission intensity),  $I_{Eu}$  is the intensity of the Eu(III) complex when no  $N_3^-$  is bound (*i.e.* at the start of the titration) and  $I_{EuN_3}$  is the intensity of the Eu(III) complex when  $N_3^-$  is entirely bound (*i.e.* at the end of the titration).



$$[\text{LnN}_3] = \frac{([\text{N}_3]_T + [\text{Ln}]_T + 1/K) - \sqrt{([\text{N}_3]_T + [\text{Ln}]_T + 1/K)^2 - 4[\text{N}_3]_T[\text{Ln}]_T}}{2} \quad (37)$$

$$I_{calc} = \frac{1}{[\text{Eu}]_T} ([\text{Eu}]_T I_{Eu} + (I_{Eu\text{N}_3} - I_{Eu}) [\text{EuN}_3]) \quad (38)$$

## 2.10 Relaxometric Investigation of Gd(III) Triazole Complexes

As MRI contrast agents, it is expected that the triazole appended Gd(III) complexes will behave like Gd(III) DOTA as an 8-coordinate ligand, allowing one coordinated inner-sphere water molecule. Relaxivity studies upon **Gd.4**, **Gd.5a** and **Gd.5c**, show how stable the triazole is with respect to pH, to confirm the formation of the N-H 1,2,3-triazole, to verify the switch in coordination mode of the triazole and to confirm hydration state, as relaxivity is greatly affected by hydration states (Equation 21, Chapter 1), as well as anion binding studies to determine hydration state.

### 2.10.1 Relaxivity vs. [carbonate] studies of **Gd.4**

**Gd.4** is a seven-coordinate chelate (with respect to the ligand) and shows a clear difference in hydration state in presence of carbonate. Carbonate is a bidentate anion that has a high affinity for binding Ln(III) chelates with a hydration state of two. Carbonate is the most abundant bidentate anion in human serum, with concentrations around 20-30 mM. It is also abundant inside cells at around 10 mM.<sup>39</sup> Carbonate has a binding constant  $K = 1451 \text{ M}^{-1}$  for **Gd.4** (Figure 2.20), this means that at in a cell ~93% of **Gd.4** would be bound to carbonate.

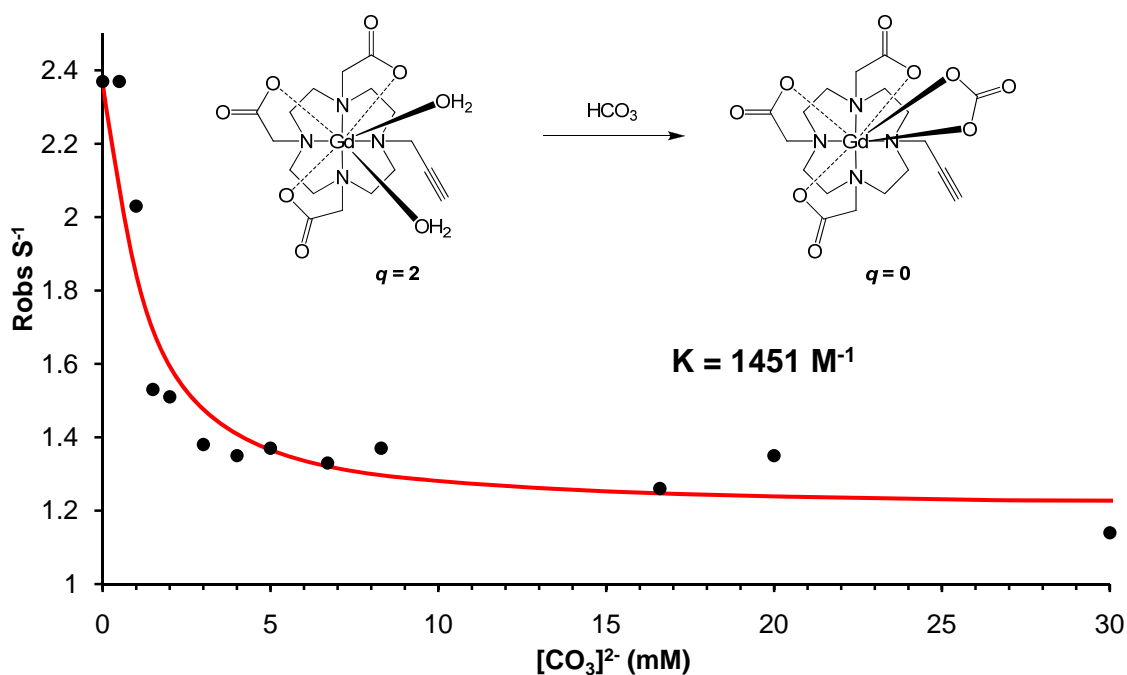
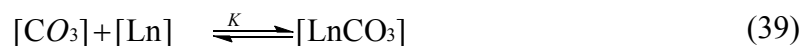


Figure 2.20 Relaxation rate (observed) vs.  $[\text{CO}_3]^{2-}$  for **Gd.4**,  $\text{H}_2\text{O}$ , 298K, pH 7.4

The concentration of bound lanthanide complex,  $[\text{LnCO}_3]$ , was determined by expansion of Equation 39, where  $[\text{CO}_3]_T$  and  $[\text{Ln}]_T$  are the total concentrations of  $\text{CO}_3$  and the Ln(III) complex (Ln = Gd(III)), (Equation 40).<sup>40</sup> The Ln(III) concentrations can be substituted for of Gd(III) relaxation rate as shown in Equation 541, where  $R_{calc}$  is the theoretical Gd(III) relaxation rate (to be compared with the experimentally observed Gd(III) relaxation rate),  $R_{Gd}$  is the relaxation rate of the Gd(III) complex when no carbonate is bound (*i.e.* at the start of the titration) and  $R_{Gd\text{CO}_3}$  is the relaxivity of the Gd(III) complex when carbonate is entirely bound (*i.e.* at the end of the titration).



$$[\text{LnCO}_3] = \frac{([\text{CO}_3]_T + [\text{Ln}]_T + 1/K) - \sqrt{([\text{CO}_3]_T + [\text{Ln}]_T + 1/K)^2 - 4[\text{CO}_3]_T [\text{Ln}]_T}}{2} \quad (40)$$

$$I_{calc} = \frac{1}{[\text{Gd}]_T} ([\text{Gd}]_T I_{Gd} + (I_{Gd\text{CO}_3} - I_{Gd}) [\text{GdCO}_3]) \quad (41)$$

Carbonate tends to bind to DO3A based contrast agents with  $q = 2$ , therefore **Gd.4**, which has reasonably high affinity with carbonate, infers a hydration state,  $q = 2$ , at least confirms there is enough space for carbonate to bind, as shown in Figure 2.20, the dramatic reduction in relaxivity of **Gd.4** in the presence of carbonate. As **Gd.4** is only seven coordinate with respect to the ligand, it would be expected that as a contrast agent **Gd.4** would not be as stable as Gd-DOTA within a body.<sup>41</sup> Binding carbonate would also make it a very ineffective contrast agent, this suggests that **Gd.4** will bind two solvent molecules, with a  $q = 2$ .

### 2.10.2 Relaxivity vs. pH for **Gd.5a**

**Gd.5a** is eight-coordinate with respect to **5a**, showing no change in relaxation with pH (Figure 2.21). This lack of response to pH, shows that the triazole remains bound throughout the pH range, with a hydration state  $q = 1$ , this supports the conclusions from the luminescence studies for **Eu.5a** and **Tb.5a**. *i.e.* the benzyl substitute 1,2,3-triazole remains bound in a ‘pyridinic’ manner to the Gd(III) metal centre throughout the pH range.

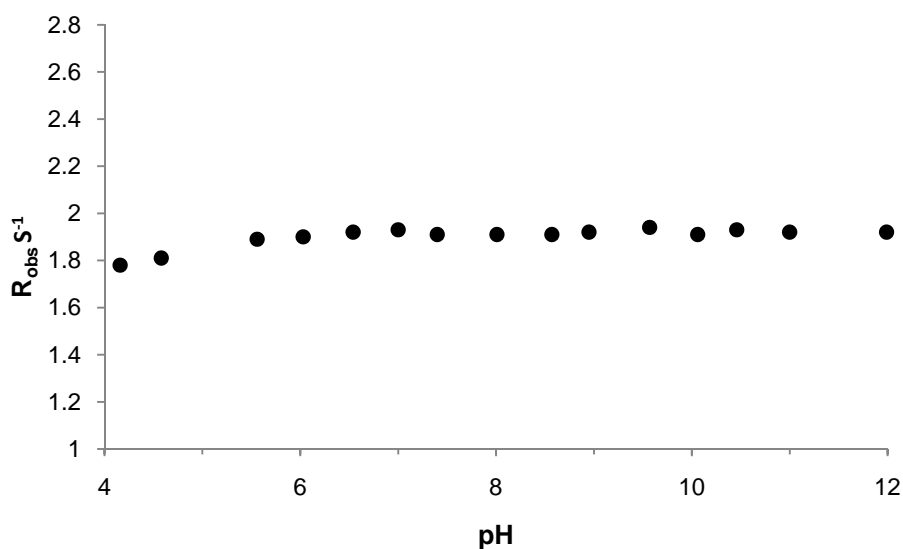


Figure 2.21 Relaxation rate (observed) vs. pH for **Gd.5a**, 298K, H<sub>2</sub>O.

Carbonate was also added to a solution of **Gd.5a**, no change in relaxation was observed, indicating that the bidentate anion had no affinity for **Gd.5a**. These studies support the conclusion that the triazole binds to Gd(III) metal centre through a ‘pyridinic’ nitrogen,<sup>27</sup> and **Gd.5a** remains unchanged by pH in the range 4 - 12, showing the 1,2,3-

triazole to be a suitable linker, for bio-molecule of interest to a stable eight-coordinate MRI contrast agent.

### 2.10.3 Relaxivity vs. pH for **Gd.5c**

Studies of **Eu.5c** and **Tb.5c**, have shown that coordination mode of the unsubstituted 1,2,3-triazole changes with respect to pH from the pyridinic nitrogen bound at low pH to anionically bound through the triazolide at higher pH. The change of coordination mode occurs within the physiological pH range. In **Gd.5c** it would be expected that the change in charge of complex from neutral to negative, would attract a larger outersphere contribution and show an increase in relaxivity.

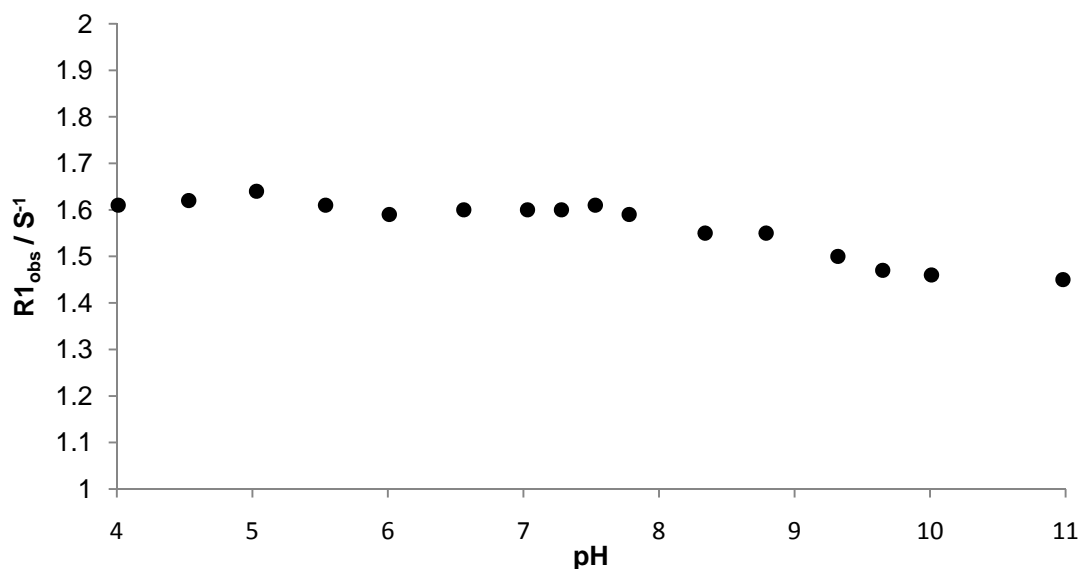


Figure 2.22 Relaxation rate (observed) vs. pH for **Gd.5c**, 298K

Figure 2.22 shows relaxivity vs. pH for **Gd.5c**, recorded at 298K, this shows little response to pH, there is no change in hydration state, we can determine that as with **Eu.5c** and **Tb.5c** that **Gd.5c** has a hydration state,  $q = 1$ . The opposite to what is expected happens from pH 8 – 11, the triazolide anionically bound coordination mode, shows a decrease in relaxivity. This effect could be due to a second sphere ordering, in acidic media from the N-H 1,2,3-triazole, which can hydrogen bond to  $\text{H}_2\text{O}$ , in basic media this effect would not be observed as the triazolide cannot hydrogen bond, therefore less order to the second-sphere water, appearing as a decrease in observed relaxation rate, although these changes are very small  $\sim 5\%$  decrease in  $R_{1\text{obs}}$ . Furthermore, the observed relaxivity values

are more typical of a  $q = 1$  complex. The coordination of a single, non-exchanging hydroxide molecule would result in the observed relaxivity based entirely on outer sphere water contributions, which would be expected to be at around  $r_1 \sim 2 \text{ mM}^{-1}\text{s}^{-1}$ .<sup>42</sup> The observed  $r_1$  values for **Gd.5c**, are somewhat lower than the measured relaxivities of the  $q = 1$  commercially available contrast agents *e.g.*  $[\text{Gd-DOTA}]^-$   $r_1 = 4.2 \text{ mM}^{-1}\text{s}^{-1}$  (20 MHz at 25°C)<sup>43</sup> while the  $q = 2$  compound Gd-DO3A  $r_1 = 5.7 \text{ mM}^{-1}\text{s}^{-1}$  (20 MHz, 25°C),<sup>42</sup> concentrations determination needs to be confirmed to calculate  $r_1$ .

#### 2.10.4 NMRD: Rotational correlation time, $\tau_R$ , for **Gd.4** – **5d**

Nuclear magnetic resonance dispersion (NMRD) profiles are measured in order to calculate the rotational correlation time ( $\tau_R$ ) of a Gd(III) complex. These values are extremely important in determining the relaxivity of a contrast agent; the slower a complex tumbles, the higher the relaxivity at clinical MRI magnetic field frequencies (Chapter 1, Section 1.3.6). NMRD profiles of **Gd.4**, **Gd.5a**, **Gd.5c** and **Gd.5d** were measured and are shown in Figure 2.23 and 2.24.

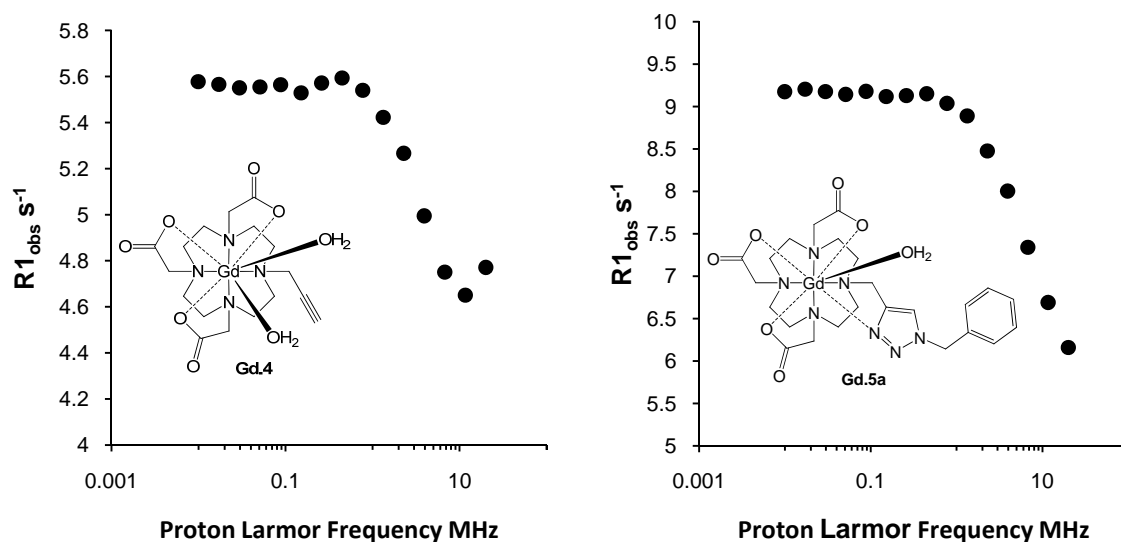


Figure 2.23 NMRD profile of **Gd.4** (left) and **Gd.5a** (right), 1.0 mM **Gd.4** or **Gd.5a** 0.1 M NaCl, pH 7.4, 25°C.

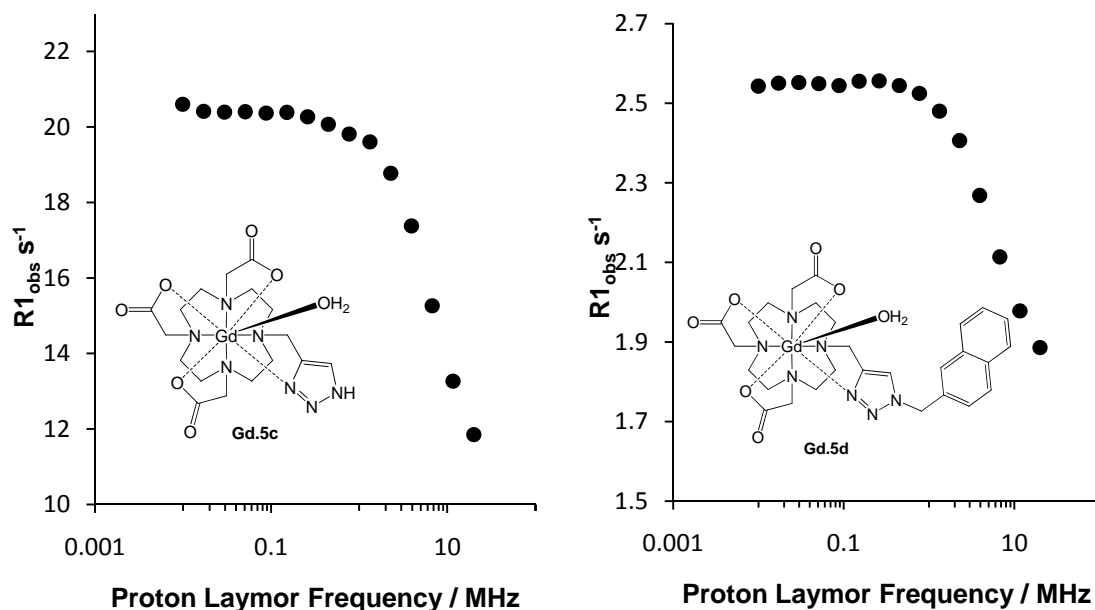


Figure 2.24 NMRD profile of **Gd.5c** (left) and **Gd.5d** (right), 1.0 mM **Gd.5c** or **Gd.5d** 0.1 M NaCl, pH 7.4, 25°C.

The similar size and shape of **Gd.4** to **Gd.5d** accounts for the similarity of the plots (Figure 2.23 and 2.24). The form of the plots are similar to that of Gd(III)DOTA for **Gd.5a/c/d**, inferring a  $q = 1$  complex of a similar shape and size. This is not surprising, however, as the molecular weight for **Gd.5a**, **Gd.5c** and **Gd.5d** (672 Da, 580Da and 722Da) is similar to that of Gd-DOTA (557 Da), resulting in similar tumbling in solution.

#### 2.10.5 $^{17}O$ variable temperature of **Gd.5c**

Variable temperature  $^{17}O$  NMR studies were carried out in order to determine the water exchange lifetime ( $\tau_m$ ) as discussed in Chapter 1, Section 1.3.9. The variable temperature  $^{17}O$  NMR profile for **Gd.5c**, Figure 2.25, was recorded at pH 7.4.

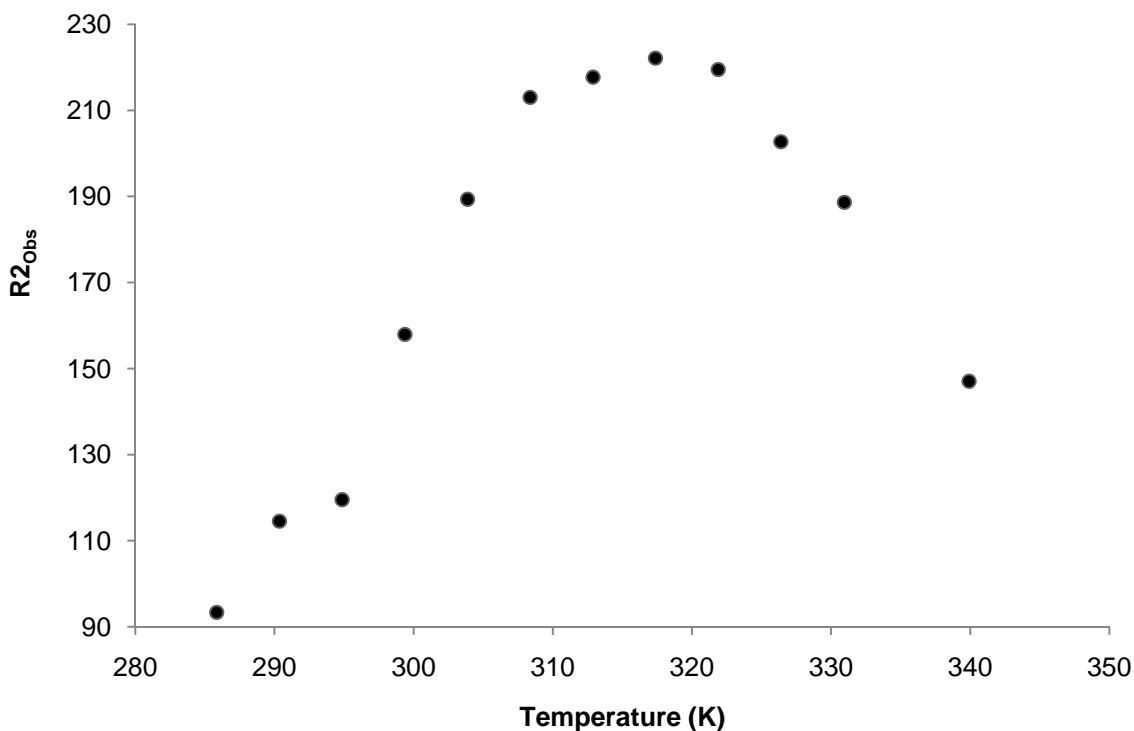


Figure 2.25 Variation of  $^{17}\text{O}$  transverse relaxation rate,  $R_{2p}$ , with temperature for **Gd.5c**, 2.1 T, pH 7.4.

The water exchange was observed and is shown by the bell-shaped curve in Figure 2.25, which demonstrates a short, slow exchange period, very similar in form to Gd-DOTA measurements.<sup>43</sup> The exchange is similar to the analogous Gd-DOTA complex ( $\tau_m = 244$  ns), providing an explanation for the similar observed relaxivity with respect to Gd-DOTA;  $r_1 = 4.2 \text{ mM}^{-1}\text{s}^{-1}$  (20 MHz, 25°C).<sup>45</sup> The coordination geometry about the Gd(III) ion influence the short  $\tau_m$ .  $^1\text{H}$  NMR spectroscopy studies of the Eu(III) analogues showed resonances at  $\delta = 28.6, 29.8, 29.2$  and  $32.1$  ppm (**Eu.5c**) (400 MHz,  $\text{D}_2\text{O}$ , pD 5, 4°C), which is typical of the square antiprismatic geometry (SAP) about the Eu(III) centre.<sup>46</sup> As mentioned in Chapter 1, Section 1.4.1, the twisted square antiprismatic (TSAP) geometry has increased steric crowding about the metal centre and facilitates the release of the coordinated water molecules, enhancing the exchange rate in comparison to the SAP isomer,<sup>47,48</sup> this could explain the slow exchange rates as the major geometry around the Gd(III) must be square antiprismatic.

## 2.11 Summary and conclusions

It has been demonstrated that 1,2,3-triazole appended Ln(III) complexes can be formed *via* the ‘Huisgen’ Cu(I) catalysed cycloaddition reaction between an azide and an alkyne. The desired product can be formed *via* two routes: chelating the alkyne complex with a Ln(III) metal ion and ‘clicking’, or ‘clicking’ first and then chelating with a Ln(III) metal ion. The former route is the more desirable as it requires a catalytic amount of Cu (I) for the ‘click’ reaction to occur. The latter needs more than one equivalent of Cu(I) as no reaction occurs until the macrocycle is filled. The removal of the copper from the macrocycle is not facile, and lowers yields for the Cu(I) cycloaddition reaction.

**Ln.4** has a hydration state  $q = 2$ , this is a precursor for the 1,2,3-triazole.  $N_3$  binds to **Ln.4** with a  $K = 2.3 M^{-1}$ , this is weak binding, with only 1% of azide bound under ‘click’ chemistry conditions; however the ‘click’ reaction, is still sufficient enough to allow the formation of the 1,2,3-triazole.

The 1,2,3-triazole in the case of **Ln.5a**, is a stable linker, which remains coordinated to the lanthanide in the pH range 4- 12, this is unsurprising and is observed for in pyridyl and tetrazole appended lanthanide complexes.<sup>30,36</sup> **Ln.5a** has a hydration state  $q = 1$ . The change in local coordination environment from the performed complex **Ln.4**, demonstrated by the change in form of luminescence and  $^1H$  NMR spectra, shows that the Cu(I) cycloaddition reaction to form 1,2,3-triazoles is a very efficient way of linking molecules of interest to lanthanide chelates, forming a stable linker that bonds to the metal centre, as well as to switch on the luminescence from the metal centre.

The formation of **Ln.5c** demonstrated that a seemingly small alteration, substituting an N-(2-propynyl)acetamide for propargyl as a means of coupling lanthanide chelates *via* click chemistry is only suitable if the organic azide involved in the click reaction is pre-formed and the solution is free of  $NaN_3$ . The unexpected product of this click reaction **Ln.5c** showed interesting protonation behaviour, switching from triazole bound to Ln(III) in an N-deprotonated anionic form in basic media, to an N–H protonated pyridyl form in acidic media, this change of coordination mode does not change the hydration state with  $q = 1$ . This pH-dependent switch, demonstrated by both  $^1H$  NMR and luminescence studies occurs in the physiological pH range.

Studies on various lanthanide DO3A-based complexes (Eu, Tb and Gd) confirm that the 1,2,3-triazole could provide a kinetically stable coordinating linker to biomolecules of interest.

## 2.12 References

1. V. V. Rostovtsev, L. G. Green, V. V. Fokin and B. Sharpless, *Angew. Chem. Int. Ed.*, 2002, **41**, 2597.
2. F. Himo, T. Lovell, R. Hilggraf, V. V. Rostovtsev, L. Noodleman, K. B. Sharpless and V. V. Fokin, *J. Am. Chem. Soc.*, 2005, **127**, 210.
3. E. E Gilbert, W. E. Voreck, *Propellants, Explos., Pyrotech.*, 1989, **14**, 19.
4. P. Wu and V. V. Fokin, *Aldrichimica Acta*, 2007, **40**, 7.
5. K. Kacprzak, *Synlett.*, 2005, **6**, 0943.
6. P. Appukkuttan, W. Dehaen, V. V. Fokin and E. Van der Eycken, *Org. Lett.*, 2004, **6**, 4223.
7. W. D. Sharpless, P. Wu, T. V. Hansen and J. G. Lindberg, *J. Chem. Edu.*, 2005, **82**, 1833.
8. J. Andersen, S. Bolvig and X. F. Liang, *Synlett*, 2005, 2941.
9. A. K. Feldman, B. Colasson and V. V. Fokin, *Org. Lett.*, 2004, **6**, 3897.
10. J. E. Moses and A. D. Moorhouse, *Chem. Soc. Rev.*, 2007, **36**, 1249.
11. M. V. Gil, M. J. Ar'evalo and O'. Lo'pez, *Synthesis*, 2007, 1589.
12. V. D. Bock, H. Hiemstra and J. H. van Maarseveen, *Eur. J. Org. Chem.*, 2006, 51.
13. H. C. Kolb and K. B. Sharpless, *Drug Discovery Today*, 2003, **8**, 24, 1128.
14. A. Brik, J. Alexandratos, Y. C. Lin, J. H. Elder, A. J. Olson, A. Wlodawer, D. S. Goodsell and C. H. Wonget, *Chem. Bio. Chem.*, 2005, **6**, 7, 1167.
15. S. Chittaboina, F. Xie and Q. Wang, *Tetrahedron Letters*, 2005, **46**, 2331.
16. H. Chen, J. L. Taylor and S. R. Abrams, *Bioorganic & Medicinal Chemistry Letters*, 2007, **17**, 1979.
17. Z. Li, Z. Wu, K. Chen, F. T. Chin and X. Chen, *Bioconjugate Chem.*, 2007, **18**, 1987.
18. S. H. Hausner, J. Marik, M. Karen, J. Gagnon and J. L. Sutcliffe, *J. Med. Chem.*, 2008, **51**, 5901.
19. T. L. Mindt, H. Struthers, L. Brans, T. Anguelov, C. Schweinsberg, V. Maes, D. Tourwe and R. Schibli, *J. Am. Chem. Soc.*, 2006, **128**, 15096.
20. F. H. Romain and A. N. Hulme, *J. Am. Chem. Soc.*, 2006, **128**, 11370.
21. M. P. Lowe and D. Parker, *Inorg. Chim. Acta.*, 2001, **317**, 163.

22. A. L. Thompson, D. Parker, D. A. Fulton, J. A. K. Howard, S. U. Pandya, H. Puschmann, K. Senanayake, P. A. Stenson, A. Badari, M. Botta, S. Avedano and S. Aime, *Dalton Trans.*, 2006, 5603.
23. A. Beeby, L. M. Bushby, D. Maffeo and J. A. G. Williams, *J. Chem. Soc., Dalton Trans.*, 2002, 48.
24. L. M. Shultze, A. R. Bulls, *U. S. patent* 5,631,368, 1997; *Chem. Abstr.*, 1996, **125**, 315328.
25. G. Brunisholz and M. Randin, *Helv. Chim. Acta*, 1959, **42**, 1927.
26. J. P. Andre, C. F. G. C. Geraldés, J.A. Martins, A.E. Merbach, M. I. M. Prata, A. C. Santos, J. J. P. De Lima and E. Toth, *Chem. Eur. J.*, 2004, **10**, 5804.
27. M. Jauregui, W. S. Perry, C. Allain, L. R. Vidler, M. C. Willis, A. M. Kenwright, J. S. Snaith, G. J. Stasiuk, M. P. Lowe and S. Faulkner, *Dalton Trans.*, 2009, 6283.
28. J. I. Bruce, M. P. Lowe and D. Parker, 'The Chemistry of Contrast Agents in Magnetic Resonance Imaging; Phototypical Aspects of Lanthanide(III) Complexes', ed. A. E. Merbach and E. Toth, Wiley, 2001.
29. S. Aime, A. Barge, M. Botta, A. S. de Sousa and D. Parker, *Angew. Chem. Int. Ed.*, 1998, **37**, 2673.
30. S. Aime, A. S. Batsanov, M. Botta, J. A. K. Howard, M. P. Lowe and D. Parker, *New J. Chem.*, 1999, **23**, 669.
31. S. L. Murov, I. Carmichael and G. L. Hug, 'Handbook of Photochemistry, Second Edition', Marcel Dekker, 1993.
32. Y. Tanaka, S. R. Velen and S. I. Miller, *Tetrahedron*, 1973, **29**, 3271.
33. J. C. Loren, A. Krasinski, V. V. Fokin and K. B. Sharpless, *Synlett*, 2005, 2847.
34. T. Jin, S. Kamijo and Y. Yamamoto, *Eur. J. Org. Chem.*, 2004, 3789.
35. V. Aucagne, J. Berna', J. D. Crowley, S. M. Goldup, K. D. Hanni, D. A. Leigh, P. J. Lusby, V. E. Ronaldson, A. M. Z. Slawin, A. Viterisi and D. B. Walker, *J. Am. Chem. Soc.*, 2007, **129**, 11950.
36. S. Aime, G. Cravotto, S. G. Crich, G. B. Giovenzana, M. Ferrari, G. Palmisano and M. Sisti, *Tetrahedron Let.*, 2002, **43**, 783.
37. R. S. Dickins, D. Parker, J. I. Bruce and D. J. Tozer, *Dalton Trans.*, 2003, 1264.
38. G.J. Stasiuk and M.P. Lowe, *Dalton Trans.*, 2009, 9725.
39. G. M. Cooper and E. E. Hausman, 'The Cell; A Molecular Approach 4<sup>th</sup> Edition', ASM Press, 2004.

40. S. Aime, M. Botta, M. Fasano and E. Terreno, 'The Chemistry of Contrast Agents in Magnetic Resonance Imaging; Protein Bound Metal Chelates', ed. A. E. Merbach and E. Toth, Wiley, 2001.
41. K. Kumar, C. A. Chang, L. C. Francesconi, D. D. Dischino, M. F. Malley, J. Z. Gougoutas and M. F. Tweedle, *Inorg. Chem.*, 1994, **33**, 3567.
42. S. Aime, M. Botta, S. G. Crich, G. Giovenzana, R. Pagliarin, M. Sisti and E. Terreno, *Magn. Reson. Chem.*, 1998, **36**, S200.
43. V. C. Pierre, M. Botta, S. Aime and K. N. Raymond, *Inorg. Chem.*, 2006, **45**, 8355.
44. D. H. Powell, O. M. N. Dhubhghaill, D. Pubanz, L. Helm, Y. S. Lebedev, W. Schlaepfer and A. E. Merbach, *J. Am. Chem. Soc.*, 1996, **118**, 9333.
45. D. M. J. Doble, M. Botta, J. Wang, S. Aime, A. Barge and K. N. Raymond, *J. Am. Chem. Soc.*, 2001, **123**, 10758.
46. M. Woods, S. Aime, M. Botta, J. A. K. Howard, J. M. Moloney, M. Navet, D. Parker, M. Port and O. Rousseaux, *J. Am. Chem. Soc.*, 2000, **122**, 9781.
47. S. Aime, A. Barge, M. Botta, A. S. de Sousa and D. Parker, *Angew. Chem. Int. Ed.*, 1998, **37**, 2673.
48. S. Aime, A. Barge, J. I. Bruce, M. Botta, J. A. K. Howard, J. M. Moloney, D. Parker, A. S. de Sousa and M. Woods, *J. Am. Chem. Soc.*, 1999, **121**, 5762.

## Chapter 3

### 'Click' Chemistry as a Route to Multimeric MRI Contrast Agents

#### 3.1 Introduction

Magnetic Resonance (MR) imaging compared with other imaging modalities, has excellent anatomical resolution; however, it suffers at the molecular scale due to its intrinsic low sensitivity. To produce a detectable change in water signal intensity, a relatively high concentration of contrast agent (0.01 - 0.1 mM) is required.<sup>1</sup> This creates problems when imaging at the molecular level, as the most interesting targets are present at much lower concentrations, typically in the nano- or picomolar range. In order to overcome the inherent sensitivity problem of the NMR phenomenon,<sup>2</sup> recent studies have been geared towards developing Gd(III) complexes as contrast agents that respond to physiological changes such as enzyme activity to amplify the signal.<sup>3</sup> Other approaches to improve the sensitivity of MR contrast agents focusing on 'increasing the payload', *i.e.* by delivering multiple Gd(III) chelates. Multimeric contrast agents have recently been developed by research groups, by attaching anything from two to several hundred chelates, in an attempt to amplify the local signal to overcome the inherent sensitivity problem.

Boswell *et al.* have developed a dual modal multimeric contrast agent that targets the  $\alpha_v\beta_3$  integrin,<sup>4</sup> which are integral for the movement of cells and can be an indicator of angiogenesis. They attached multiple modified Gd(III)-DTPA chelates to a polyamidoamine (PAMAM) dendrimer that is conjugated to RGD-cyclopeptides that target the  $\alpha_v\beta_3$  integrin along with a fluorescent probe Alexa Fluor 594 (Figure 3.1). They overcame the inherent insensitivity of the technique by loading multiple Gd(III) agents and targeting to a molecule of interest (on the surface of cells) that is found in picomolar concentrations. Not only is  $\tau_r$  lengthened due to the increased mass of the compound, the fluorescent probe provides a second imaging modality that can be overlapped onto the MR image giving a more accurate image of local concentrations of the  $\alpha_v\beta_3$  integrin. This is not the first time multiple Gd(III) chelates have been attached to the PAMAM dendrimer, it has been used for the synthesis of MRI contrast agents which feature a high molar relaxivity and superb image enhancement, as shown by Weiner *et al.*<sup>5</sup>

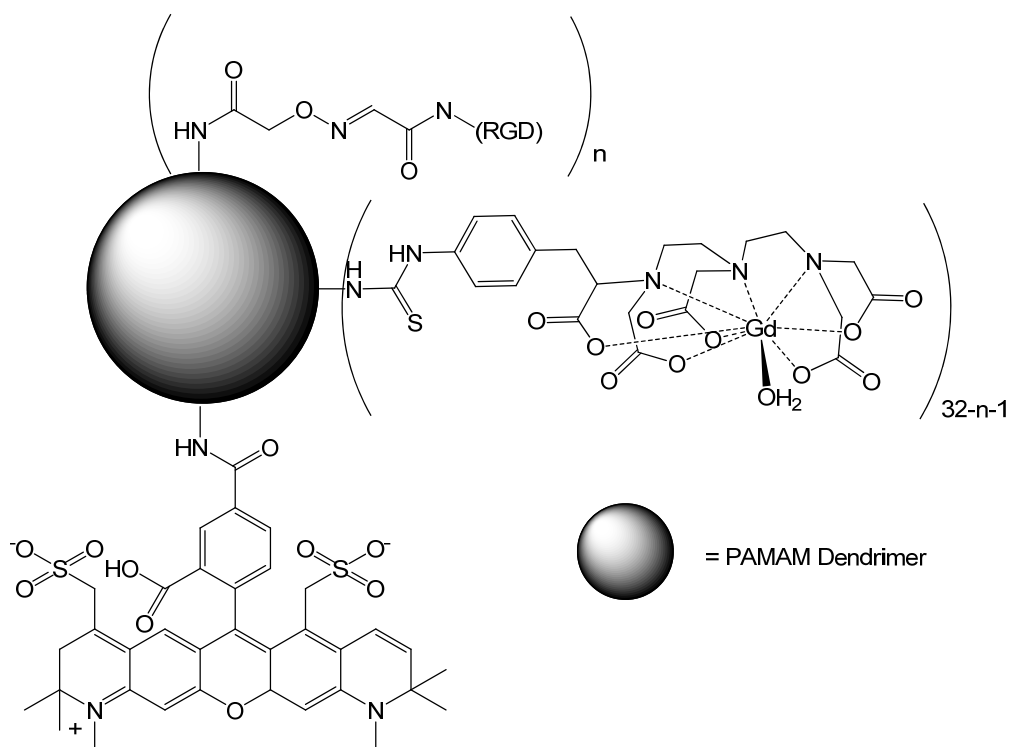


Figure 3.1 PAMAM dendrimer appended with multiple Gd (III) DTPA chelates, incorporating a cyclic RGD peptide and conjugated Alexa Fluor 594 dye.

Boswell *et al.* have shown that the PAMAM dendrimer can be successfully functionalised to create an effective and specific imaging agent. Many groups have looked at other ways of increasing the Gd(III) payload, Aime and co-workers have developed several cyclodextrin (CD) based multimeric contrast agents.<sup>6,7,8</sup> Their first example using CD, was a self-assembling contrast agent<sup>6</sup> consisting of three parts: a  $\beta$ -cyclodextrin bearing a covalently bound Gd(III)-DTPA-Lys complex; a polypeptide containing a high percentage of tyrosine residues (PLT); a second  $\beta$ -CD derivative bearing a peptide vector (CCK8) that can recognize specific cell membranes. They showed that relaxation rates increase with concentration of PLT, indicating that these compounds can self assemble, giving a high mass, therefore increasing  $\tau_r$ , forming a large multimeric compound (Figure 3.2).<sup>6</sup> Aime and co-workers have used a poly  $\beta$ -CD-<sup>19</sup>F-Gd(III) adduct to validate a new pH mapping MRI method.<sup>8</sup> Using poly  $\beta$ -CD they bind alternatively a pH responsive Gd(III) DOTA based agent, or a <sup>19</sup>F reporter molecule, the latter enables determination of local concentration of agent, the former can show slight changes in pH. The supramolecule has  $q = 2$  at acidic pH and  $q = 0$  at basic pH, this change in relaxivity can be very useful in locating cancer cells which have a pH as low as 6.<sup>9</sup> They have also shown how CD can be

used to increase payload, and be modified to target specific cells, overcoming the inherent insensitivity of MR Imaging as a technique.

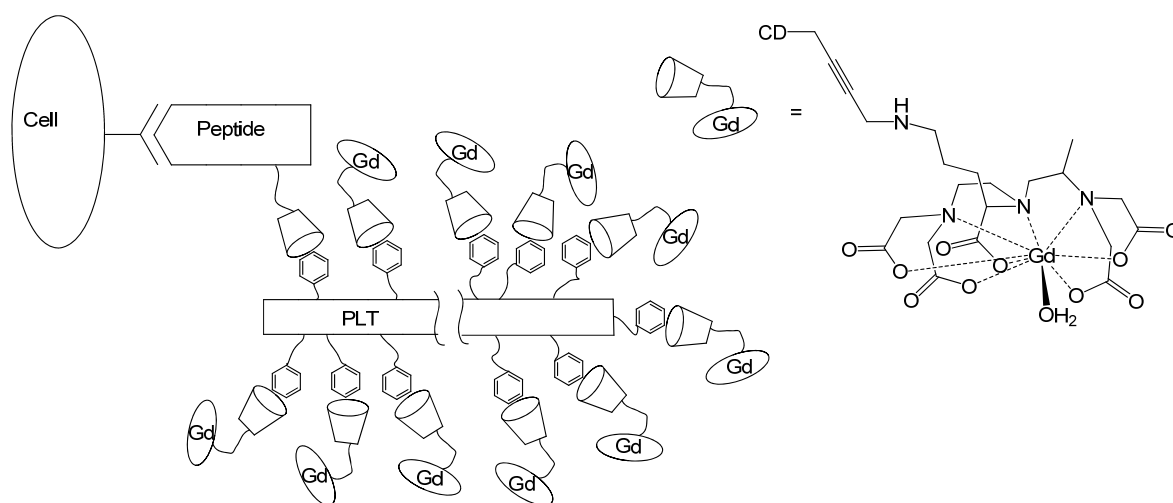


Figure 3.2 Aime and co-workers Cyclodextrin (CD) based multimeric self assembling MR contrast agent

### 3.1.1 Using 'Click' Chemistry to Generate Multimeric Contrast Agents

The 'Huisgen' Cu(I) catalysed cycloaddition reaction between an organic azide and a substitute alkyne offers an apparent facile method in order to append multiple lanthanide chelates to a central 'hub'. Faulkner and co-workers synthesised a dimer based on **Ln.4** (Chapter 2.4), attaching two Ln(III) DOTA based chelates to a central *p*-xylyl-benzyl hub (Figure 3.3) using the propargyl appended Ln(III) chelate and 1,4-diazidomethylbenzene as precursors for the 'click' reaction.<sup>10</sup> **L.Eu.7** uses the 1,2,3-triazole to form a stable eight coordinate chelate, this shows that 'click' chemistry can be used to form at least dimeric MRI contrast agents.

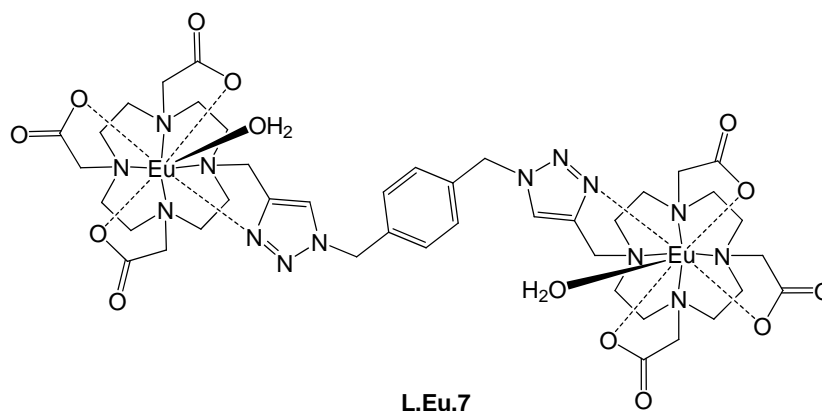


Figure 3.3 Faulkner and co-workers dimeric Ln(III) chelate using 'click' chemistry

Cyclodextrin has been utilised as a hub to generate multimeric contrast agents using click chemistry, by two groups: Bryson *et al.* attached seven Gd(III) DTTA analogues to CD;<sup>11</sup> while Meade and co-workers used a Gd(III)DO3A in a similar fashion,<sup>12</sup> (Figure 3.4).

CD as a hub can accommodate seven Gd(III) chelates; it increases the total mass of the contrast agent significantly over small aromatic hubs, helping lengthen  $\tau_R$  and increase relaxivity. Organic azides are potentially unstable with respect to explosive decomposition, especially compounds containing multiple azides. As a rule of thumb compounds or azide containing compounds are considered explosive if  $N_C + N_O / N_N$  equal less than 3.  $\beta$ -CD containing six azides gives a value of 3.33 and would probably not be considered explosive. This suggests that 6N<sub>3</sub>-CD can be safely isolated, making the ‘click’ procedure safer, compared with the isolation of a smaller azido-hub which could be potentially explosive and much harder to handle. CD also exhibits excellent properties that makes it a host scaffold for functionalisation *via* non-covalent assembly with receptor specific targeting moieties for biomolecular imaging shown by Aime and co-workers.<sup>6,8</sup>

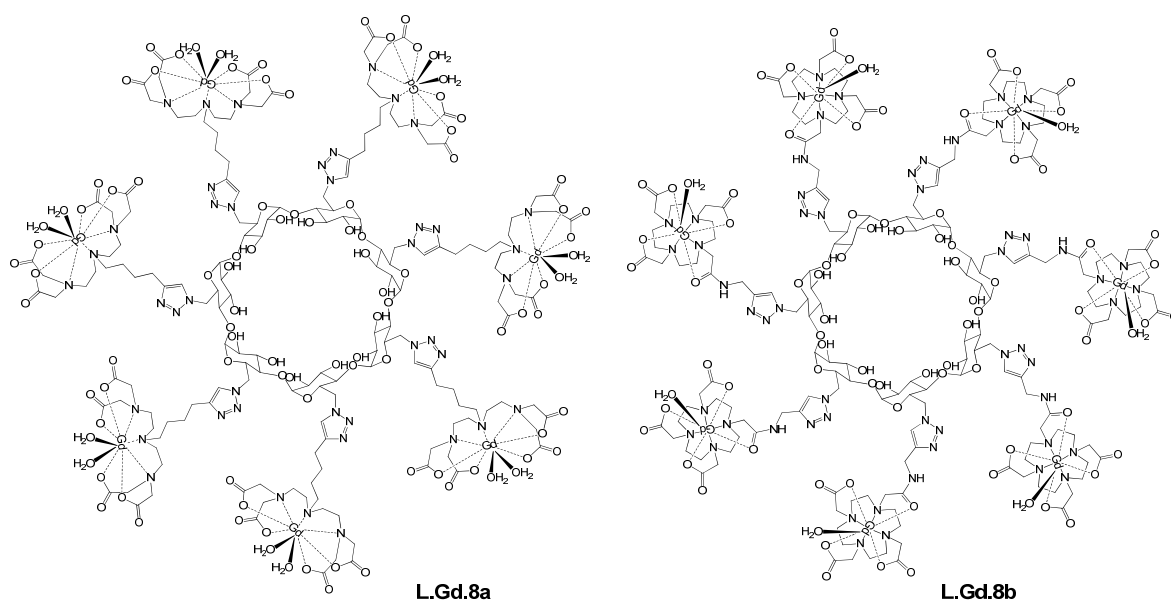


Figure 3.4 Cyclodextrin based multimeric Gd contrast agents using click chemistry.

**L.Gd.8a** developed by Bryson *et al.* incorporates seven  $q = 2$  Gd(III) chelates, this allows for an exceptionally high relaxivity  $r_1 = 43.4 \text{ mM}^{-1} \text{ s}^{-1}$  (9.4 T, 400 MHz, 37°C), this averages as  $6.2 \text{ mM}^{-1} \text{ s}^{-1}$  per Gd (III) chelate, compared to commercially available Magnevist (Gd-DTPA<sup>2-</sup>) at the same field, is  $3.2 \text{ mM}^{-1} \text{ s}^{-1}$ . **L.Gd.8a** has significantly higher

relaxivity, a 94% increase in relaxivity compared with Magnevist, although within the body it would be expected that **L.Gd.8a** would bind endogenous anions such as carbonates, displacing the two waters bound to the metal centre. The increase in relaxivity can be attributed to a higher molecular weight of **L.Gd.8a** increasing  $\tau_R$ , the increased negative charge at  $\tau_7$ , added to the greater innersphere contribution, account for the exceptionally high relaxivity compared with Magnevist. Another issue with **L.Gd.8a**, is that of stability of the Gd(III) chelate, it has been suggested that in certain cases the Gd-DTPA based commercially available OptiMARK agent can release the Gd(III) metal in the kidneys.<sup>13</sup> **L.Gd.8a** being based on DTPA with one less chelating arm, would make it less stable than Gd-DTPA, with respect to Gd(III) loss, also with the high negative charge of **L.Gd.8a**, the bio-distribution of the agent would be mainly to the kidneys, this would cause severe health issues to a patient if the Gd(III) metal was released, this agent would be unsafe to use in the human body.

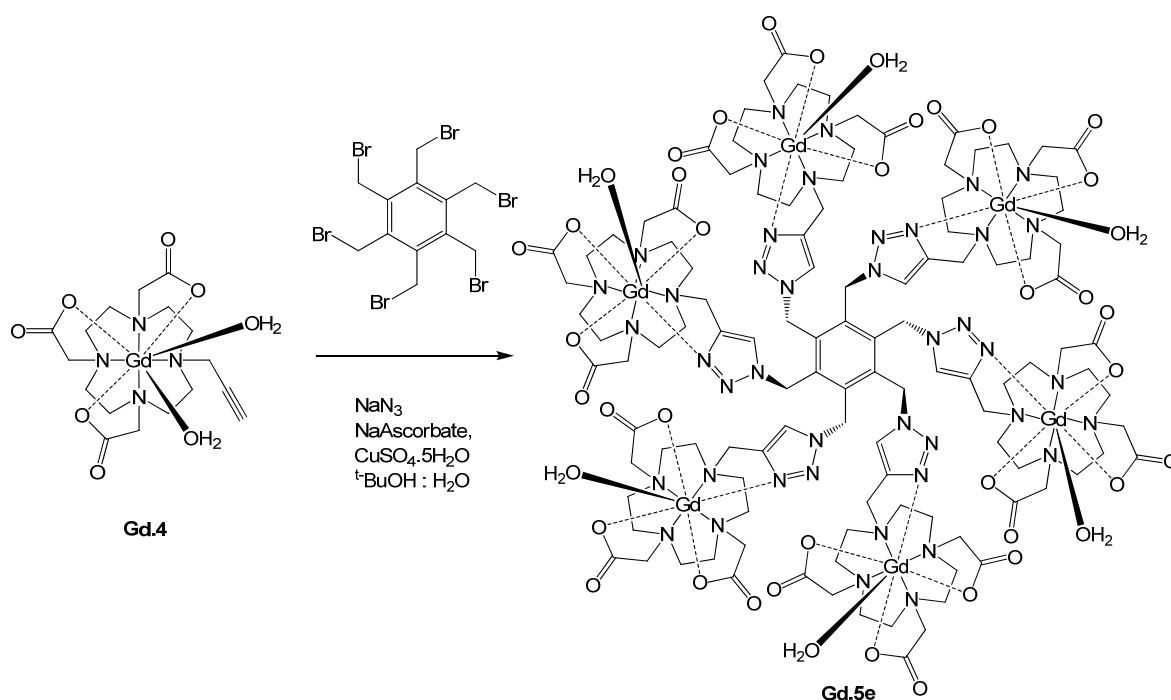
Meade and co-workers developed **L.Gd.8b**, the multimeric CD Gd(III) contrast agent, based on Gd-DO3A with an appended propargyl amide. This precursor for the 'click' reaction, was developed by Hulme and co-worker,<sup>14</sup> and is an eight coordinating chelate with a hydration state  $q = 1$ , (discussed in chapter 2.2), thus it will be a more stable contrast agent, therefore less likely to release the Gd(III) metal in the body. **L.Gd.8b** has a relaxivity  $r_1 = 85.4 \text{ mM}^{-1}\text{s}^{-1}$  (60 MHz, 37 °C), this averages as  $12.2 \text{ mM}^{-1}\text{s}^{-1}$  per Gd(III) chelate, compared with the commercially available Gd-DOTA (Dotarem), which is 2.7-3.1  $\text{mM}^{-1}\text{s}^{-1}$  (60 MHz, 37 °C).<sup>15</sup> This again shows the benefit of a significant increase in relaxivity by increasing the payload of an agent, although no reports of *in vivo* uses of these agents have been published, this is a step in the right direction to get around the problem with the inherent insensitivity of MR Imaging.

Aime *et al.* have also used 'click' chemistry to develop a multimeric contrast agent by linking two  $\beta$ -CD together, forming a dimer, which binds non covalently the Gd-DTPA-di/tri-benzyl appended complex. This can form multiple dimer or trimer complexes that show an increasing relaxivity upon increasing the number of Gd(III) chelates.<sup>7</sup>

### 3.2 Target Multimeric MRI Contrast Agent

The aim of the research in this chapter was to attach six **Gd.4** chelates to hexakis(bromomethyl)benzene hub, *via* 'click' chemistry, as it offers a facile synthesis to a

multimeric MRI contrast agent (Scheme 3.1). Isolating the hexakis(azidomethyl)benzene was considered too risky because of the explosive potential ( $N_C + N_O / N_N = 0.66$ ). Handling such a compound with a high number of azides was not recommended, it was thought likely to explode when isolated.<sup>16</sup> It is understood that reaction of alkynes with *in situ* generated azides (*via* alkyl halides in the presence of  $\text{NaN}_3$ ) is a clean, facile reaction and residual  $\text{NaN}_3$  does not interfere with the cycloaddition reaction.<sup>17</sup> It was thought that this attractive synthetic trick would allay these safety concerns, circumventing the need to isolate compounds containing multiple azides.



Scheme 3.1

As discussed in Chapter 2.2.2, the reaction between **Gd.4**, sodium azide and an alkyl bromide gives a side product **Gd.5c**, *i.e.* the unsubstituted N-H 1,2,3-triazole, this makes the proposed reaction in Scheme 3.1 unviable. Another Gd-DOTA based alkyne needed to be developed to create the proposed multimeric contrast agent, one that does not undergo the ‘click’ reaction with sodium azide. Meade and co-workers were developing their multimeric contrast agent based on hexakis-azido benzene,<sup>12</sup> (Figure 3.5). **L.Gd.9** has a relaxivity of  $65.8 \text{ mM}^{-1}\text{s}^{-1}$  (60 MHz, 37 °C) which equates to  $10.97 \text{ mM}^{-1}\text{s}^{-1}$  per Gd(III) chelate, compared to Gd-DOTA ( $2.7\text{-}3.1 \text{ mM}^{-1}\text{s}^{-1}$  (60 MHz, 37 °C)), this is still a significant increase in relaxivity, showing that this is still an attractive procedure for the synthesis of multimeric contrast agents. Despite the impressive relaxivity data, Meade’s system does not

achieve the relaxivity that it might, **L.Gd.9** incorporates an amide linker between the 1,2,3-triazole and the chelate, amides are known to slow down water exchange rates, therefore decreasing relaxivity. Given this handicap, an observed relaxivity of  $\sim 11 \text{ mM}^{-1}\text{s}^{-1}$  per Gd(III) is all the more impressive. Meade's alkyne complex is that originally published by Hulme and Romain.<sup>14</sup> Working independently of Meade this route to a multimeric contrast agent was considered, but discounted due to the disadvantages of an amide linker. A Gd(III) alkyne complex was synthesised that did not contain amides that slow water exchange rates, and not having the alkyne in the vicinity of the metal centre, so as not to form an unsubstituted 1,2,3-triazole, in the presence of sodium azide.

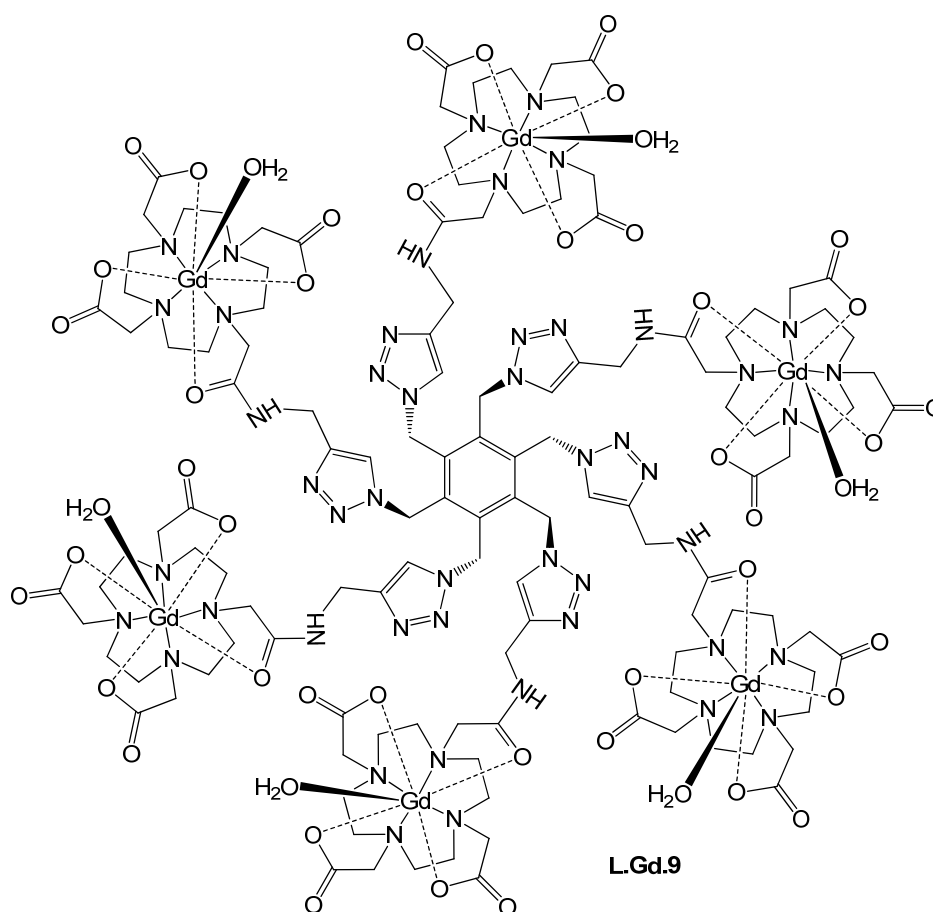
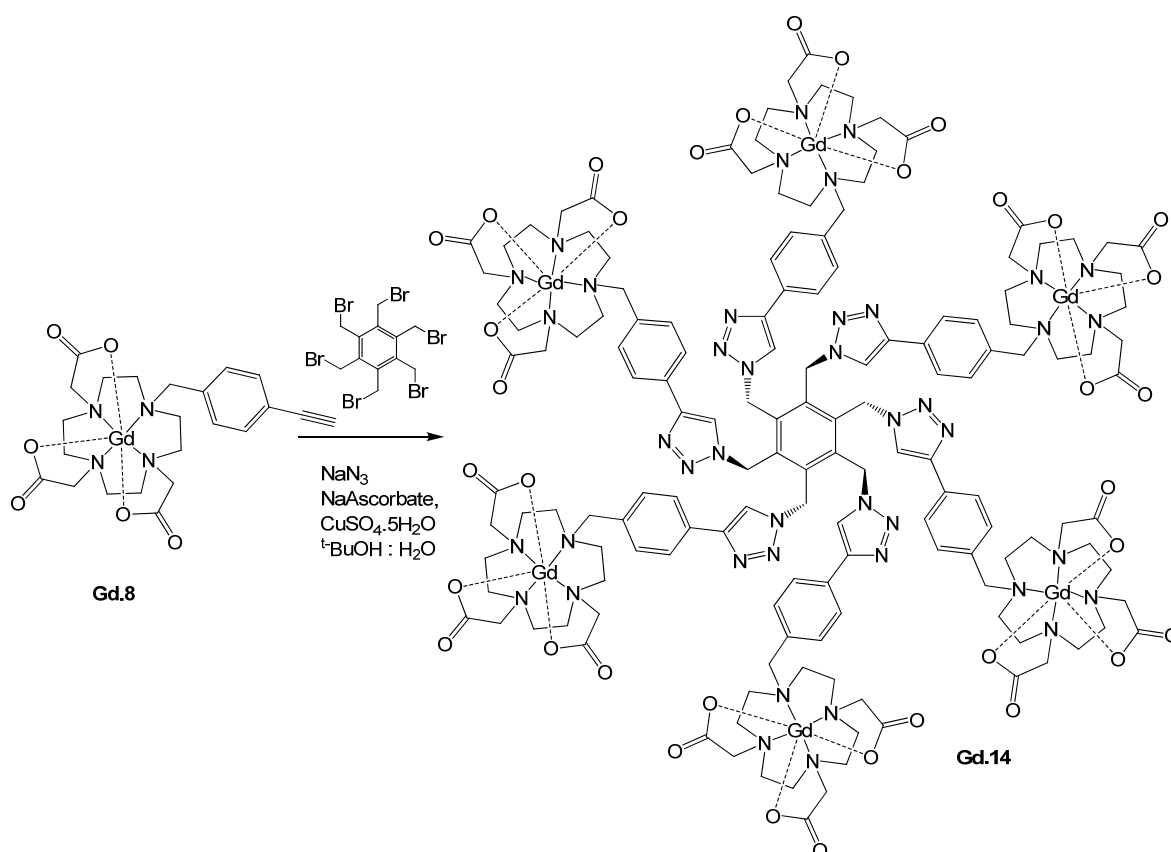


Figure 3.5 Meade's multimeric contrast agent.<sup>12</sup>

A DOTA-based chelate appended with a *p*-ethynylbenzyl moiety (Scheme 3.2), was proposed. The *p*-ethynylbenzyl has four functions: it attaches the alkyne to the chelate without using amides which slow down water exchange rates; it moves the alkyne away from the metal centre, preventing reactions with  $\text{NaN}_3$ ; it acts as an antenna to sensitise lanthanide luminescence in Eu and Tb complexes; it generates  $q = 2$  Ln complexes. The new alkyne appended Gd complex was intended to make synthesis of multimeric

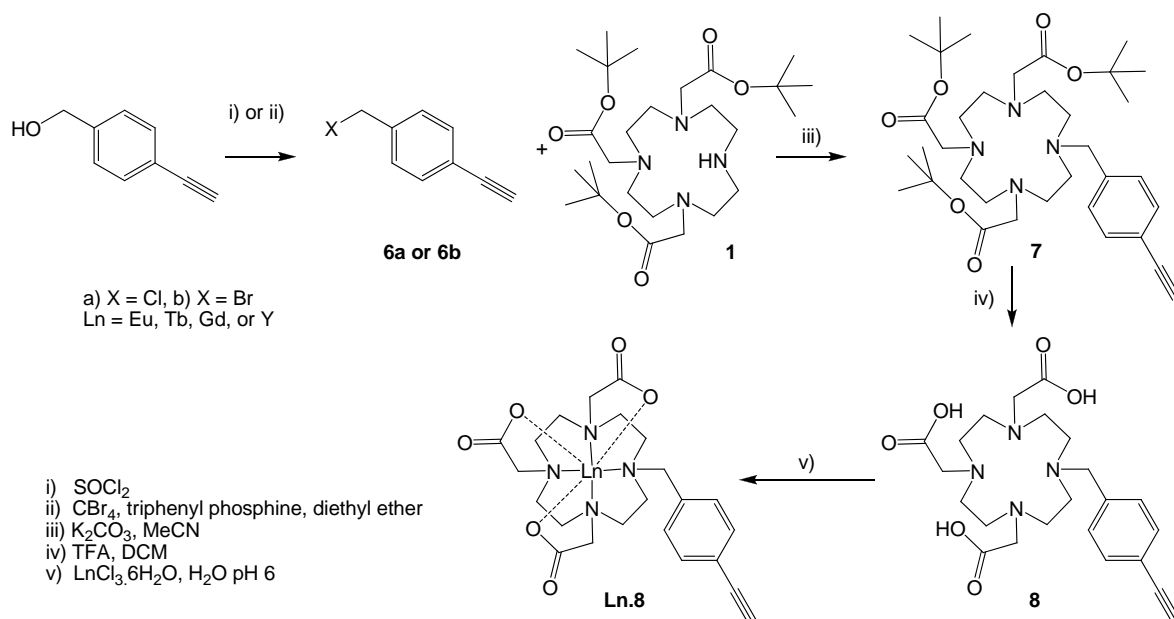
compounds facile, undergoing the ‘Huisgen’ Cu(I) catalysed cycloaddition reaction, to form 1,2,3-triazoles.

Hereby, Eu, Tb, Y and Gd(III) complexes of **Ln.8** were synthesised, their ease of use in the Cu(I) catalysed cycloaddition reaction to make monomeric and multimeric compounds will be discussed, as well as their luminescence, NMR and UV-vis studies.



Scheme 3.2

### 3.3 Synthesis of Ln.8



Scheme 3.3

Halogenation of 4-ethynylbenzyl alcohol, was achieved by either treatment with thionyl chloride to generate the chloride **6a** (98% yield) (Scheme 3.3),<sup>18</sup> or the bromide by reaction with carbon tetrabromide, to give **6b** (22% yield).<sup>19</sup> Chlorination of 4-ethynylbenzyl alcohol gives the higher yield and was used for the subsequent synthesis of **7**. Chlorination was more facile than bromination; it did not require separation on silica, *cf.* the bromination method. **6a** showed a peak in the ESMS at 151 [M + H]<sup>+</sup> with the correct isotope pattern for chloride and **6b** showed a peak at 195 [M + H]<sup>+</sup>, with the correct isotope splitting pattern for bromine.

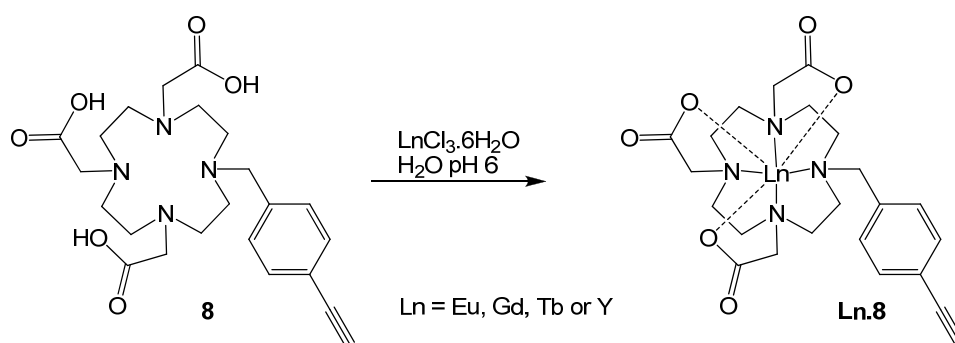
Reaction of 4-ethynylbenzyl chloride or bromide (**6a** or **6b**) with <sup>t</sup>BuDO<sub>3</sub>A (**1**) yielded **7** in good yield. In the reaction with **6a**, the chloride gives **7** at 70%, while reaction with **6b** the bromide gives **7** at 56% yield after purification on silica.

The ES<sup>+</sup> mass spectrum showed a peak at *m/z* 628 [M+H]<sup>+</sup> indicating the formation of the product; the <sup>1</sup>H NMR spectra a broad singlet at 2.14 ppm is indicative of the alkyne CH and in the aromatic region two 2H doublets at 7.2 ppm and 7.3 ppm, this is typical of the para-substituted benzyl of **7**. Care is needed to be taken too avoid heating as conversion of the alkyne to an alkene, has been noted for these systems and are noted in the ES<sup>+</sup> mass spectrum where a peak is observed at *m/z* 630 [M+H]<sup>+</sup>, *i.e.* two mass higher than for the

alkyne, these compounds have very similar  $R_f$  values and are difficult to separate via column chromatography.

Deprotection of the carboxylic acid using TFA gave, **8** in a 98% yield, as a yellow oil. The absence of C(CH<sub>3</sub>) peaks at 1.38 ppm in the <sup>1</sup>H NMR, indicated hydrolysis of the *tert*-butyl esters, the ES<sup>+</sup> mass spectrum gave a peak at  $m/z$  461 [M + H]<sup>+</sup>.

**Ln.8** compounds were synthesised, from **8** and the appropriate lanthanide chloride (LnCl<sub>3</sub>.6H<sub>2</sub>O) in H<sub>2</sub>O at pH 6 at room temperature.



Scheme 3.4

### 3.4 Luminescence Studies of Lanthanide Complexes Bearing a Pendant *p*-Ethynylbenzyl Ln.8

#### 3.4.1 Characterisation of **Eu.8**

**Eu.8** was isolated as a white hygroscopic solid in 83% yield. **Eu.8** is expected to be seven-coordinate with respect to the ligand **8**; <sup>1</sup>H NMR studies suggest this is the case, as broad featureless resonances were observed. This indicates a seven coordinate DO<sub>3</sub>A based complex, which lack the rigidity of their eight-coordinate analogues. Due to ring inversion and side arm rotation, an intermediate exchange process is observed at this frequency (400MHz).<sup>20</sup> This conclusion is supported by hydration state  $q$ , determination.

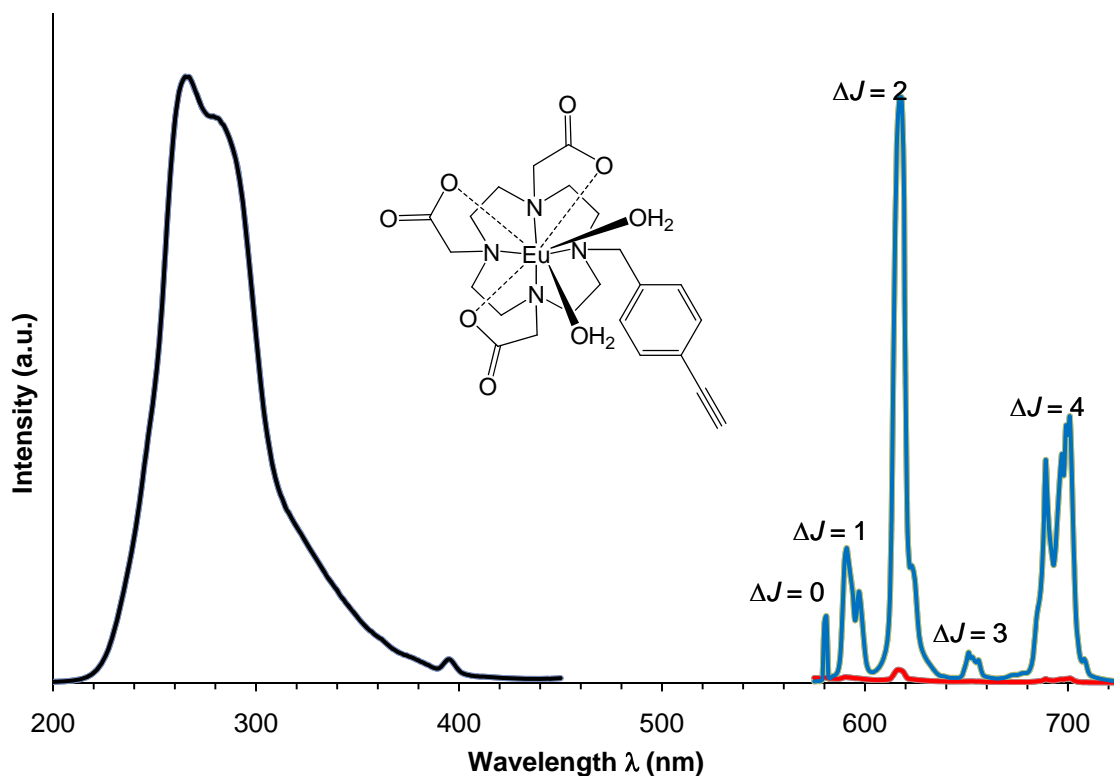


Figure 3.6 Luminescent emission spectra following direct excitation (red,  $\lambda_{ex} = 395$  nm) and sensitised excitation (blue,  $\lambda_{ex} = 260$  nm), and excitation spectra of **Eu.8** (black,  $\lambda_{em} = 618$  nm) ( $\text{H}_2\text{O}$ , 298K, pH 6).

The  $^5\text{D}_0$  excited state energy =  $17,277 \text{ cm}^{-1}$ .<sup>21</sup> In order to achieve indirect excitation of Eu(III), the sensitising moiety must be of higher than that of the Eu(III), for energy transfer to occur, this increases the intensity of the Eu(III) emission (Chapter 1, Section 1.6.5). The triplet excited state of phenyl groups usually lie between  $E \sim 20,000 - 30,000 \text{ cm}^{-1}$  and therefore sensitised emission was anticipated for **Eu.8**.<sup>22</sup> The excitation spectrum monitoring Eu(III) emission at  $\lambda = 618$  nm, ( $\Delta J = 2$  transition), shows more intense indirect sensitisation at  $\lambda = 260$  nm, and a weaker peak at  $\lambda = 395$  nm, corresponding to direct excitation of the Eu(III) ion. The more intense peak at  $\lambda = 260$  nm, corresponds to the ethynylbenzyl chromophore. The ethynylbenzyl chromophore offers reasonable sensitisation (Figure 3.6), there is a large difference between intensity of emission observed from direct excitation (red) and sensitised excitation (blue) under the same experimental conditions. This spectrum is typical of Eu(III) complexes of this type, displaying the various  $^5\text{D}_0$  to  $^7\text{F}_J$  ( $J = 0-4$ ) transitions; the hypersensitive  $\Delta J = 2$  transition is particularly intense, compared to that of the  $\Delta J = 1$  transition. This is typical of a seven-coordinate complex with  $q = 2$ . Such a  $q = 2$  complex is expected to bind bi-dentate anions such as carbonate, this would show an intense  $\Delta J = 2$  transition; however as the pH of the solution

is 6 the binding of carbonate is ruled out, luminescent lifetime measurements confirm that a  $q = 2$  species exists in solution.

The hydration state was calculated from the luminescence lifetimes measured in H<sub>2</sub>O and D<sub>2</sub>O, the luminescence lifetime were recorded using both direct and sensitised excitation ( $\lambda = 395$  nm and  $\lambda = 260$  nm respectively), the wavelength monitored was the  $\Delta J = 2$  transition at  $\lambda = 618$  nm, giving  $k_{\text{H}_2\text{O}} = 2.4 \text{ ms}^{-1}$  and  $k_{\text{D}_2\text{O}} = 0.65 \text{ ms}^{-1}$ , which corresponds to a hydration state,  $q = 1.8$ .

#### 3.4.2 Characterisation of **Tb.8**

**Tb.8** was isolated as a white hygroscopic solid in 80% yield, from **8** and TbCl<sub>3</sub>.6H<sub>2</sub>O. **Tb.8** is also seven-coordinate with respect to ligand **8**, *cf.* **Eu.8**. The hydration state  $q$ , of the complex was determined and its luminescent properties investigated.

The emission spectrum in Figure 3.7 was recorded following excitation at  $\lambda_{\text{ex}} = 260$  nm, this spectrum is typical for Tb(III) emission showing the various <sup>5</sup>D<sub>4</sub> to <sup>7</sup>F<sub>J</sub> ( $J = 6-2$ ) transitions. The form of terbium (III) emission is not as sensitive to the changes in coordination environment as europium (III) emission.<sup>21</sup> The excitation spectrum was obtained by monitoring the emission at  $\lambda = 546$  nm, ( $\Delta J = -1$  (<sup>5</sup>D<sub>4</sub> – <sup>7</sup>F<sub>5</sub>) transition). This shows a maximum at  $\lambda = 260$  nm and a weaker peak at  $\lambda = 355$  nm. The peak observed at  $\lambda = 355$  nm represents direct excitation of the Tb(III) ion, the more intense peak at  $\lambda = 260$  nm, represents the sensitised emission from the appended ethynylbenzyl group.

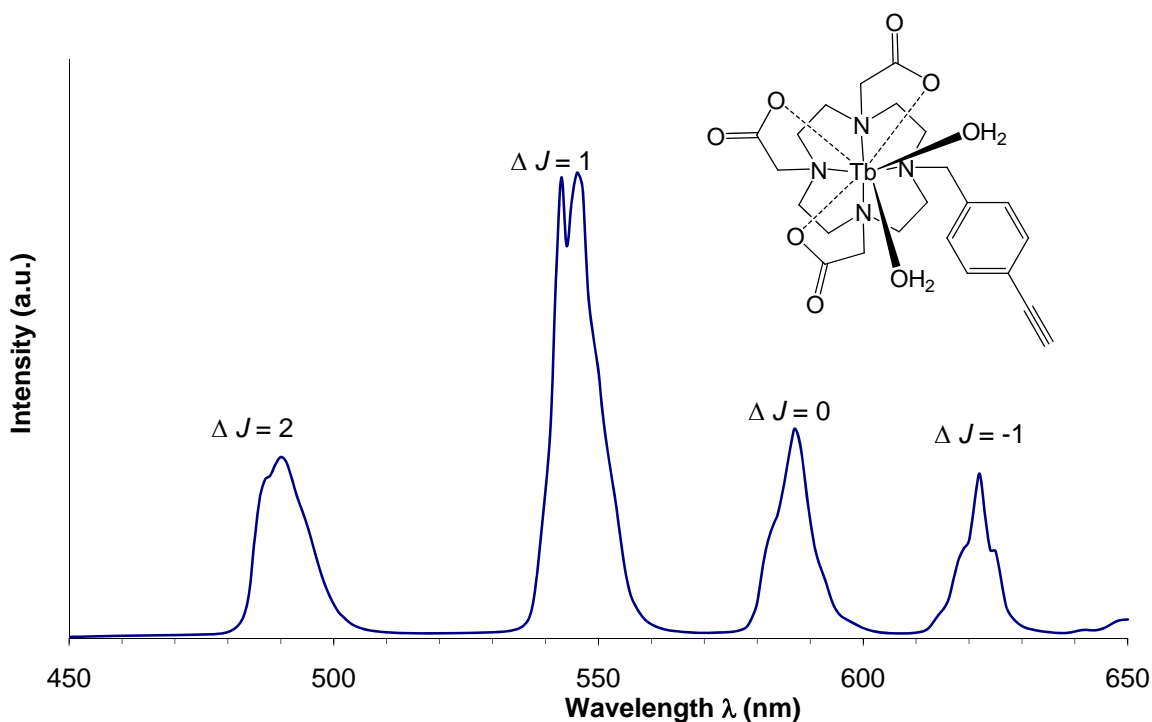


Figure 3.7 Emission spectrum of **Tb.8**, ( $\lambda_{\text{ex}} = 260$  nm,  $\text{H}_2\text{O}$ , 298K, pH 7).

The Tb(III) excitation spectrum is similar to that of the Eu(III), both Tb(III) and Eu(III) being sensitised by the chromophore, with maximum sensitisation achieved at  $\lambda = 260$  nm. The  $\Delta J = 1$  transition, at  $\lambda = 546$  nm was monitored during luminescence lifetime studies, in order to calculate  $q$  (Table 3.1). The rate constants for **Tb.8** are considerable longer than that of **Eu.8**, because of less efficient quenching from O-H oscillators as overlap occurs *via* the less populated  $\nu = 5$  vibrational levels of water with the  $^5\text{D}_4$  excited state of Tb(III).<sup>21</sup> The results from the lifetime studies show that **Tb.8** also comprises a heptadentate coordinating ligand with a hydration state  $q = 1.4$ , this suggests a mixture of  $q = 1$  and  $q = 2$  species. This corresponds with the results from **Eu.8**, that **8** can be used to form a seven-coordinate ligand for these lanthanide ions.

Complex	$\lambda_{\text{em}} / \text{nm}$	$\lambda_{\text{ex}} / \text{nm}$	$k_{\text{H}_2\text{O}}$	$k_{\text{D}_2\text{O}}$	$q$
<b>Eu.8</b>	260 / 395	618	2.39	0.65	1.8
<b>Tb.8</b>	260 / 355	546	0.83	0.49	1.4

Table 3.1 Rate constants,  $k$ , for depopulation of the excited state and derived hydration states,  $q$ , for the decay of **Eu.8** and **Tb.8**

### 3.4.3 Characterisation of **Y.8**

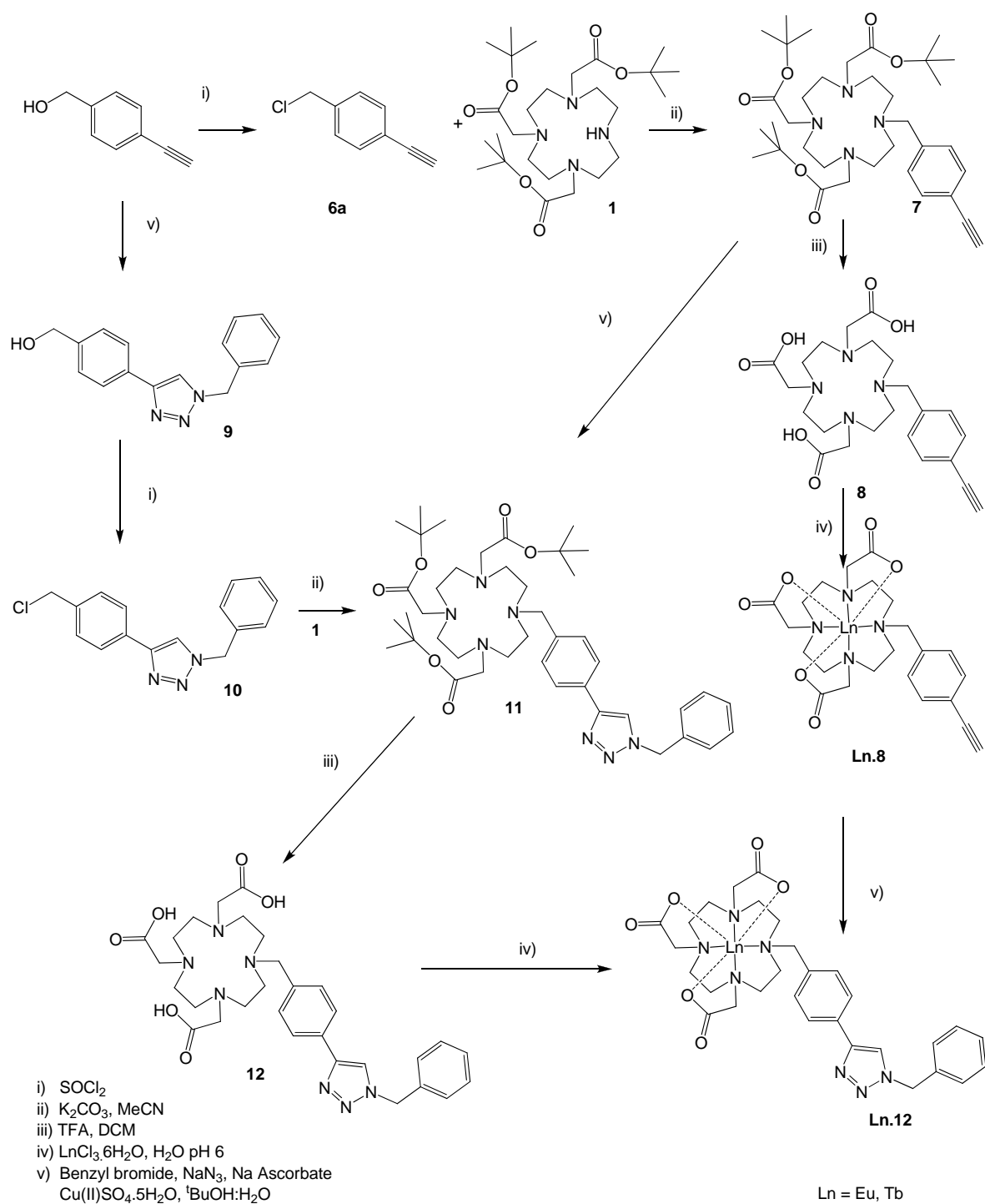
**Y.8** was isolated as a white hygroscopic solid in 80% yield, from **8** and  $\text{YCl}_3 \cdot 6\text{H}_2\text{O}$ . **Y.8** was expected to be a seven-coordinate complex with respect to ligand **8** (as **Eu.8** and **Tb.8**), Yttrium is non-paramagnetic, and therefore  $^1\text{H}$  NMR spectra can sometimes be more easily studied as chemical shift values fall in narrow range and line widths are not subjected to the broadening that is observed for the paramagnetic analogues. The ionic radius of Y(III) is similar to Ho(III) at  $r = 1.02 \text{ \AA}$ ; it is the most similar sized non-paramagnetic ion to Gd(III) ( $r = 1.05 \text{ \AA}$ ). La(III) and Lu(III) ions are also non-paramagnetic but possess ionic radii too dissimilar to Gd(III) at  $r = 1.16 \text{ \AA}$  and  $r = 0.97 \text{ \AA}$  respectively.<sup>23, 24</sup>

The  $^1\text{H}$  NMR spectrum of **Y.8** shows two 2H broadened doublets at 7.10-7.65 ppm and 8.4 ppm this is typical of the aromatic para substituted benzene ring, the resonances are broadened due to the fluxional nature of the Y(III) complex. The UV – vis spectrum shows absorption at  $\lambda = 251\text{nm}$ , the peak at  $\lambda = 251 \text{ nm}$  correlates to the  $\pi\text{-}\pi^*$  transition of the benzene ring, this is consistent with the UV- vis and excitation spectra of **Eu.8** and **Tb.8**.

The luminescence, NMR and UV–vis studies of **Ln.8** suggests that the ligand **8** is seven-coordinate, allowing two waters to bind to the metal centre to give a coordination number of 9. This suggests that **Ln.8** will be a useful precursor for the synthesis of multimeric MRI contrast agents, *via* the ‘click’ cycloaddition reaction.

### 3.5 Synthesis of **Ln.12**

To investigate the potential applications of **Ln.8**, a test ‘click’ reaction was performed. **Ln.8** was reacted with benzyl bromide to form **Ln.12**. Three possible routes to **Ln.12** (shown in Scheme 3.5) were attempted. The first involves carrying out the ‘click’ reaction on a Ln(III) complex (**Ln.8**), in the second route the ‘click’ reaction is performed to yield proligand **12** before complexation. **11** can in turn be synthesised by two routes, by carrying out the ‘click’ reaction on **7**, or performing the triazole **10**. There are five steps in each route, and the Cu(I) catalysed reaction with benzyl bromide is performed at different steps for each route to synthesise **Ln.12**, the merits of each route will be described.



Scheme 3.5

### 3.5.1 Synthesis of precursors for Ln.12

The phenyl triazole **9** was synthesised *via* the Cu(I) catalysed reaction between 4-ethynyl-1-(hydroxymethyl)-benzene and benzyl bromide *via in situ* generation of the benzyl azide using sodium azide (Scheme 3.5).<sup>17</sup> **9** was isolated on silica in 32% yield, the <sup>1</sup>H NMR spectrum showed the loss of the alkyne, a 1H singlet at 2.1 ppm and the

observation of a new <sup>1</sup>H singlet at 7.57 ppm indicating the CH on the 1,2,3-triazole ring, the ES<sup>+</sup> mass spectrum showed a peak at *m/z* 266 [M + H]<sup>+</sup> indicating product formation.

Conversion to the benzyl chloride **10** was achieved by chlorinating **9** in the presence of thionyl chloride (Scheme 3.5). **10** was isolated as a hydrochloride salt in good yield.<sup>25</sup> This is indicated in the <sup>1</sup>H NMR spectrum with a broadening of spectral form and the shift of the <sup>1</sup>H singlet, the CH of the 1,2,3-triazole ring (from 7.57 ppm to 8.87 ppm), indicating protonation of the triazole ring. Conversion to the basic form was achieved by washing with sodium hydrogen carbonate; the form of the <sup>1</sup>H NMR spectrum sharpened and the <sup>1</sup>H singlet of the CH of the 1,2,3-triazole ring shifted back to 7.6 ppm.

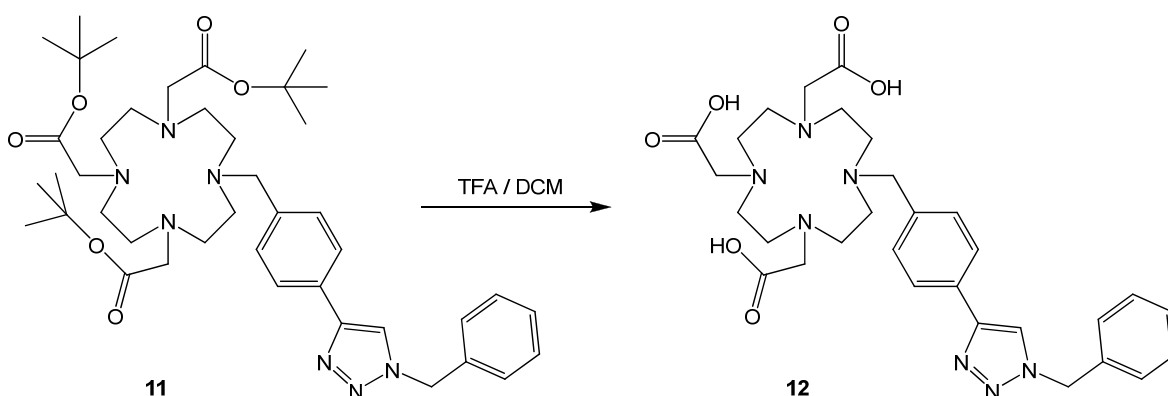
**11** can be formed *via* two procedures, either from reaction of the preformed phenyl triazole **10** with t-BuDO<sub>3</sub>A **1** or the Cu(I) catalysed reaction between **7** and benzyl bromide in the presence of sodium azide (Scheme 3.5). The reaction between **1** and **10** using K<sub>2</sub>CO<sub>3</sub> as a base gave **11** in good yield. Purification on silica is not facile and required several attempts to purify completely; however, this is still the more favourable method of synthesising **11**, as the Cu(I) catalysed reaction between **7** and benzyl bromide in the presence of sodium azide gives **11** in only moderate yield. There are multiple reasons for the distinctly low yield for the Cu(I) catalysed reaction forming **11**, firstly the macrocycle chelates the copper, therefore more than one equivalent of copper is required. This presents the second problem with the reaction, which is the removal of the copper from the macrocycle and separation of excess reagents.

The removal of copper from the macrocycle was achieved by passing the reaction mixture down a strong acid cation exchange resin, DOWEX-50W. To give a copper free sample of **11**, the product is very insoluble in aqueous media, therefore, it is likely that a proportion of **11** remains precipitated on the resin, lowering the yield. There are no side reactions with this alkyne in the presence of sodium azide, unlike the propargyl appended macrocycle (**2**) as described in Chapter 2.2.2; moving the alkyne further away from the macrocycle (as in **11**) prevents formation of unsubstituted 1,2,3-triazoles, allowing for *in situ* generation of azides.

To reduce the reaction time of *in situ* generation of azides and increase the overall yield of the product of the ‘click’ reaction (**11**), two methods were tried: firstly pre-forming the azide by reacting the benzyl bromide with sodium azide for two hours at 60°C before adding the subsequent reagents for the formation of the 1,2,3-triazole, secondly carrying out the reaction at 60°C, both of these show increased yields. The best method to form **11** is

to prepare **10** and react with **1**, as there is no need to use copper which will chelate to the macrocycle and require removal, which lowers the overall yield.

Deprotection of the carboxylic acid by TFA, **12** was indicated by the absence of the C(CH<sub>3</sub>)<sub>3</sub> peaks at 1.38 ppm in the <sup>1</sup>H NMR spectrum, indicating cleavage of the *t*-butyl esters, the ES<sup>+</sup> mass spectrum gave a peak at *m/z* 595 [M + H]<sup>+</sup>. The removal of the *t*-butyl ester markedly increasing solubility in aqueous media, allowing for a facile complexation of lanthanides.

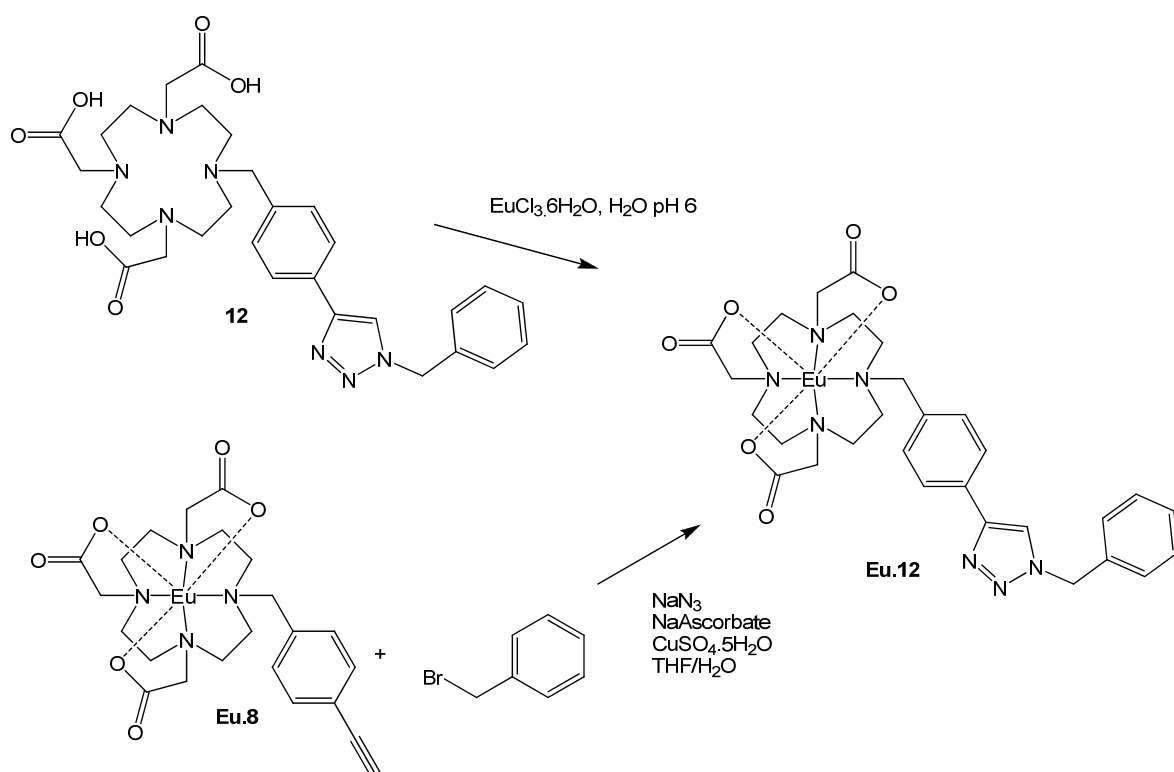


Scheme 3.6

### 3.5.2 Formation of **Eu.12**

**Eu.12** was synthesised *via* two routes either from **12** and EuCl<sub>3</sub>·6H<sub>2</sub>O, or from the Cu(I) catalysed reaction of **Eu.8** with benzyl bromide in the presence of sodium azide (Scheme 3.7). **Eu.12** compounds were synthesised using EuCl<sub>3</sub>·6H<sub>2</sub>O in H<sub>2</sub>O at pH 6, the ES<sup>+</sup> mass spectrum gave a peak at *m/z* 781 [M+K]<sup>+</sup>, with the correct Eu(III) isotope pattern.

The formation of **Eu.12** *via* the Cu(I) catalysed cycloaddition reaction from **Eu.8** and benzyl bromide in the presence of sodium azide, for the *in situ* generation of benzyl azide, gave **Eu.12** in good yield. As the complex is soluble in water the salts (CuSO<sub>4</sub>, NaN<sub>3</sub>, NaAscorbate) were removed using a protein desalting resin, Amberlite XAD-16, yielding a white hygroscopic solid **Eu.12**. The use of excess sodium azide does not interfere with the cycloaddition reaction, unlike the problems encountered in chapter 2. Therefore by using a different appended alkyne, the *p*-benzyl alkyne of **Eu.8**, the remoteness from the Ln(III) centre, prevents the side reactions that are observed with the propargyl appended complex **Eu.4**.



Scheme 3.7

### 3.5.3 Characterisation of **Eu.12**

The ligand of **Eu.12** is potentially heptadentate, binding through the seven donor atoms of the DO3A core. The hydration state  $q$ , of the complex was determined and its luminescent properties investigated. The Eu (III) emission spectra in Figure 3.8 show the various  $^5\text{D}_0$  to  $^7\text{F}_J$  transitions of pre-‘click’ **Eu.8** (red) compared to post ‘click’ reaction **Eu.12** (blue). The spectra shows very little change in relative intensity of the hypersensitive  $\Delta J = 2$  transition, with a slight shift in emission maximum, this is expected as there is no change in local coordination environment, as the modifications are remote from the Eu(III) centre. There are small changes in the form of the spectra of **Eu.12** compared with that of **Eu.8**, the  $\Delta J = 1$  and  $\Delta J = 4$  transitions show a slightly decreased intensity, and a subtle change in the appearance of peaks at  $\lambda = 594 \text{ nm}$  and  $\lambda = 693 \text{ nm}$  respectively. These small changes indicate the ‘click’ reaction has occurred (mass spectral evidence also confirms this), the slight change in appearance of the peaks as a result of the change in ligand structure; however, as there is no coordination of the triazole to the metal centre and no change in local coordination, such subtle changes are expected. It was seen in Chapter 2 when converting **Eu.4** to **Eu.5** that a noticeable change in spectral form is observed

indication of binding of the 1,2,3-triazole to the metal centre, *i.e.* a change in coordination environment.<sup>10</sup> The form of the **Eu.12** spectrum is more like that of Eu.DO3A,<sup>26</sup> with a large  $\Delta J = 2$  transition compared with that of the  $\Delta J = 1$ . The luminescent emission spectrum is typical of a seven-coordinate DO3A-based Eu(III) complex.<sup>26</sup>

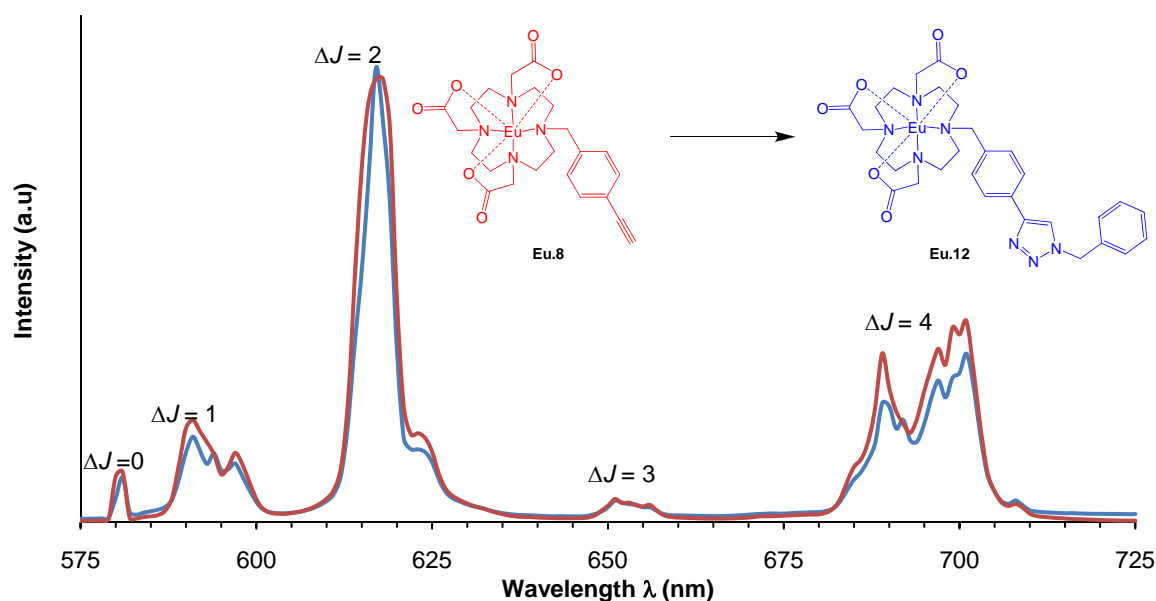


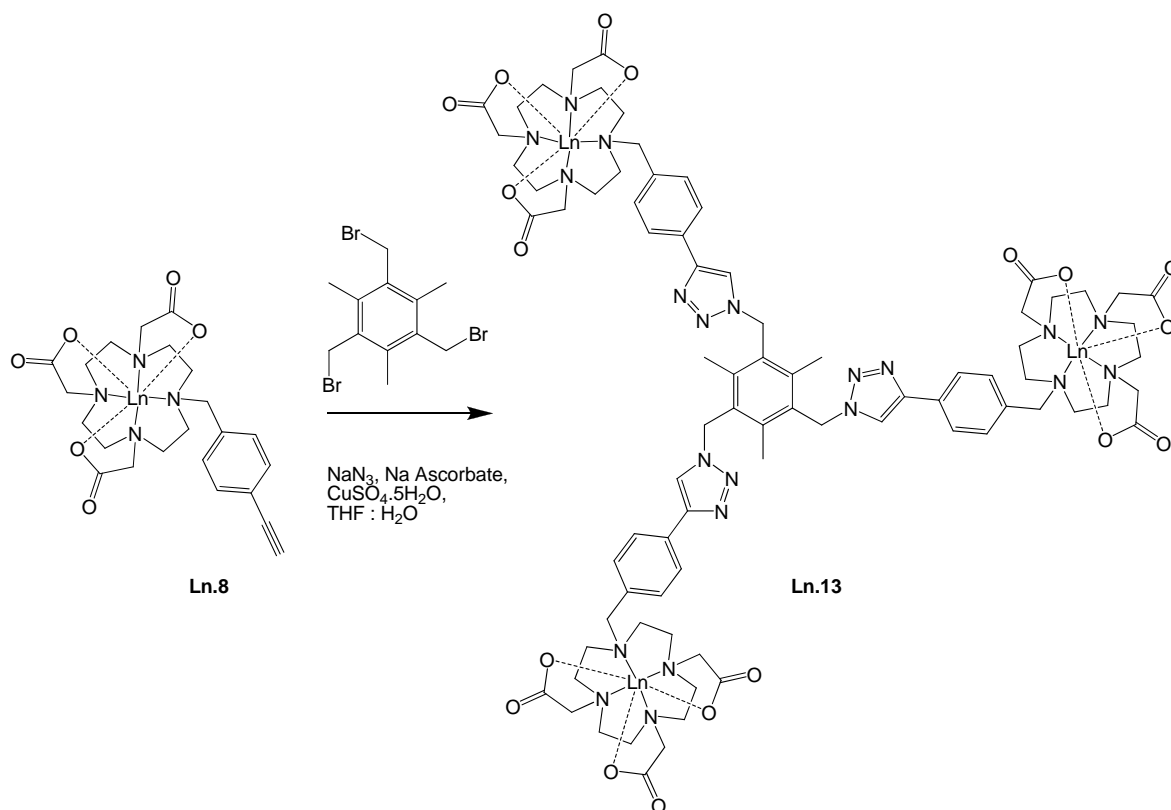
Figure 3.8 Luminescence emission spectra of **Eu.8** (red), ( $\lambda_{\text{ex}} = 260$  nm, H<sub>2</sub>O, 298K, pH 7) and **Eu.12** (blue), and showing the change in form of the  $^5\text{D}_0\text{-}^7\text{F}_1$  transition ( $\Delta J = 1$ ).

The excitation spectrum monitored the emission at  $\lambda = 618$  nm,  $\Delta J = 2$  transition. This shows intense maximum at  $\lambda = 260$  nm and  $\lambda = 283$  nm, and a weaker peak at  $\lambda = 395$  nm (direct excitation of the Eu(III) ion). The intense maximum at  $\lambda = 260$  nm, is expected to be the  $\pi\text{-}\pi^*$  transition of the p-benzyl. The maximum at  $\lambda = 283$  nm is absent in the precursor **Eu.8** and is likely to represent the 1,2,3-triazole chromophore.

The  $\Delta J = 2$  transition, ( $\lambda = 618$  nm) was monitored during luminescence lifetime studies showing the hydration state  $q = 2$ , showing that **Eu.12** is a seven-coordinate chelate.

The formation of **Eu.12** shows that it is possible to use **Eu.8** as a precursor for the ‘click’ reaction, the data suggests that complexes formed *via* the ‘click’ reaction from **Ln.8** will provide a seven-coordinate ligand with space to bind two solvent molecules. This suggests that the 1,2,3- triazole does not bind to the metal centre, also an excess of sodium azide will not interfere with the cycloaddition reaction. The model reaction to form **Eu.12** suggests that **Eu.8** can be used for the formation of multimetric contrast agents *via* the click reaction with *in situ* generation of the azide.

### 3.6 Synthesis of Trimeric Lanthanide Complexes Ln.13



Scheme 3.8

Multimeric lanthanide chelates were synthesised *via* the Cu(I) catalysed cycloaddition reaction between **Ln.8** and a hub, in the presence of sodium azide. 2,4,6-tris(bromomethyl)mesitylene was used a central hub for the synthesis of **Ln.13**, the azide was generated *in situ* before the addition of **Ln.8**, sodium ascorbate and copper sulphate. It was found that THF / H<sub>2</sub>O as reaction solvent gave better yields.<sup>12</sup> The trimeric compounds were purified *via* HPLC using 25% methanol in water over 20 minutes then gradient up to 100% methanol over 35 minutes.

#### 3.6.1 Characterisation of **Eu.13**

**Eu.13** was synthesised as above from **Eu.8**, and was purified on HPLC with an elution time 21.4 minutes, obtained as a white powder in 19% yield. This is a significantly low yield for the Cu(I) catalysed cycloaddition reaction. The solubility of the compound in aqueous media decreases as further Eu(III) chelates are added to the hub, therefore the concentrations of THF: H<sub>2</sub>O are important to push the reaction to the trimeric compound,

multiple different compounds can be formed during this reaction, with various numbers of azides or Eu(III) chelates appended to the hub. This is seen in the HPLC trace of the reaction mixture, as multiple peaks with differing elution times.

**Eu.13** contains three Eu(III) chelates appended to the mesitylene hub. The hydration state  $q$ , of the complex was determined and its luminescent properties investigated.

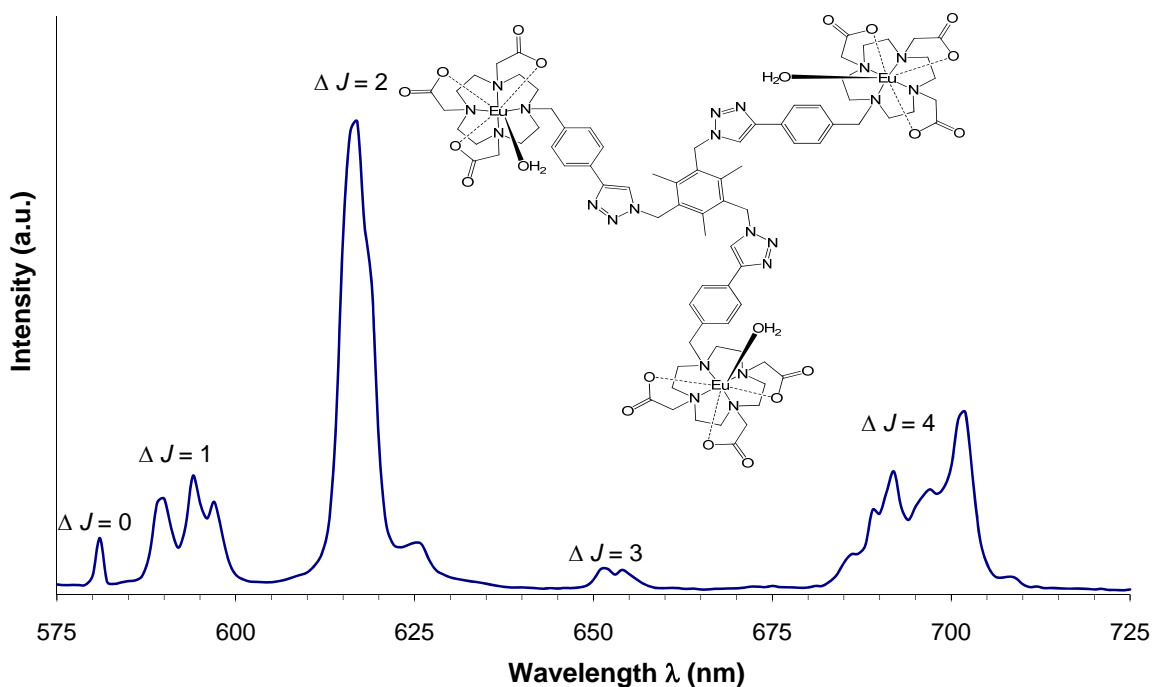


Figure 3.9 Luminescence emission spectrum of **Eu.13**, ( $\lambda_{\text{ex}} = 256$  nm,  $\text{H}_2\text{O}$ , 298K, pH 7).

The emission spectrum of **Eu.13** in Figure 3.9 was recorded following excitation at  $\lambda_{\text{ex}} = 256$  nm, this spectrum is typical for Eu(III) emission showing the various  $^5\text{D}_0$  to  $^7\text{F}_J$  transitions. The hypersensitive  $^5\text{D}_0$ - $^7\text{F}_2$  transition or  $\Delta J = 2$  transition ( $\lambda = 618$  nm), is of greater intensity to that of the  $^5\text{D}_0$ - $^7\text{F}_1$  transition or  $\Delta J = 1$  transition ( $\lambda = 594$  nm), this is typical of a compound containing seven-coordinating chelates such as EuDO3A,<sup>26</sup> which is similar to that of the ‘click’ model compound, allowing for two waters to coordinate. There is a change in spectral form compared with that of **Eu.8** (Figure 3.8), the  $\Delta J = 1$  transition ( $\lambda = 594$  nm) there is an appearance of a third peak showing a change in ligand structure. There is very little change in the  $\Delta J = 2$  transition ( $\lambda = 618$  nm), showing that this change does not affect the local coordination of the chelate; therefore the triazole has been formed, and does not bind to the metal centre.

The excitation spectrum in (Figure 3.10) was recorded monitoring the emission at  $\lambda_{em} = 618$  nm, the  $\Delta J = 2$  transition. This shows moderate maximum at  $\lambda = 256$  nm,  $\lambda = 291$  nm,  $\lambda = 321$  nm and a weaker peak at  $\lambda = 395$  nm (direct excitation of the Eu(III) ion). The most intense maximum at  $\lambda = 256$  nm, is expected to be the  $\pi-\pi^*$  transition of the *p*-benzyl. The maximum at  $\lambda = 291$  nm is absent in the precursor **Eu.8** and is likely to represent the 1,2,3-triazole chromophore. The final peak at  $\lambda = 321$  nm could represent the mesitylene hub chromophore, or the ligand to metal charge transfer band, emission spectra obtained by exciting at all these wavelengths are identical showing that this is a pure trimeric compound **Eu.13**, the most efficient chromophore for sensitisation is the *p*-benzyl subunit appended to the Eu(III) chelate.

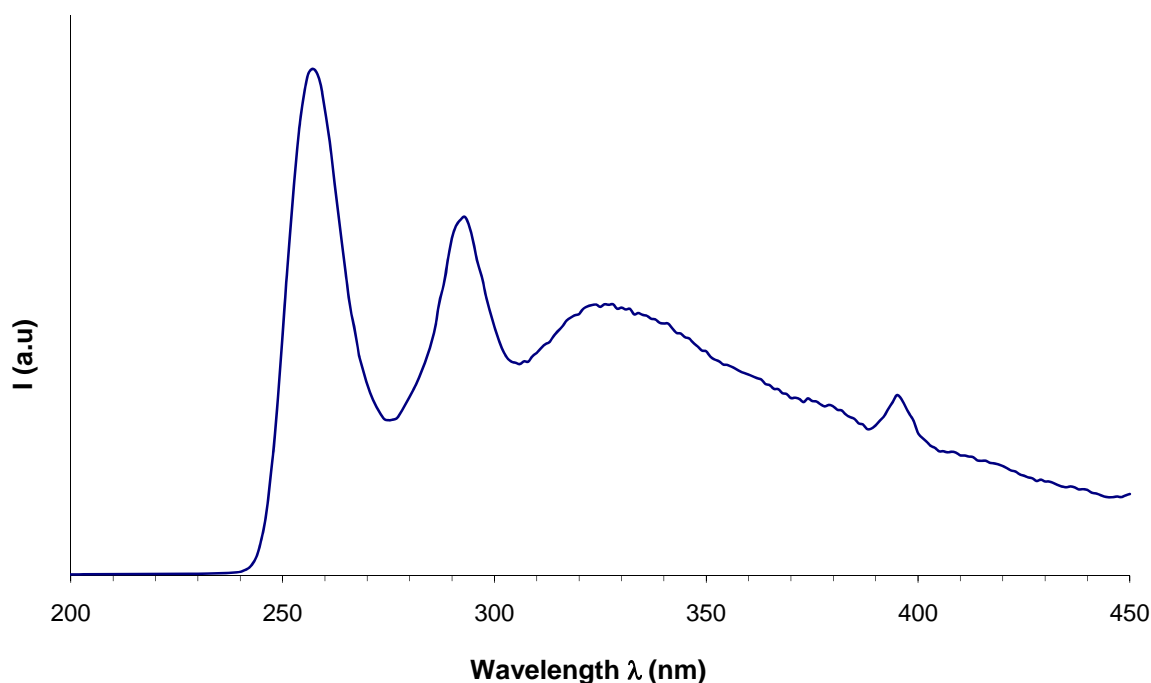


Figure 3.10 Excitation spectrum for **Eu.13**,  $\lambda_{em} = 618$  nm ( $H_2O$ , 298K, pH 7)

The UV-visible spectrum shows absorbencies at,  $\lambda = 213$  nm,  $\lambda = 249$  nm and  $\lambda = 297$  nm, these correspond to the excitation wavelengths for the appended *p*-benzyl subunit at  $\lambda = 256$  nm in the excitation and the 1,2,3-triazole subunit at  $\lambda = 291$  nm. There is no peak around  $\lambda \sim 290$  nm in the UV-visible spectra of **Eu.8**, the change in spectral form indicates the formation of the 1,2,3-triazole. This verifies that the click reaction has occurred and that **Eu.13**, has been synthesised.

The  $\Delta J = 2$  transition, at 618 nm was monitored during luminescence lifetime studies to determine  $q$ . All four excitation wavelengths were tested and the hydration state  $q$

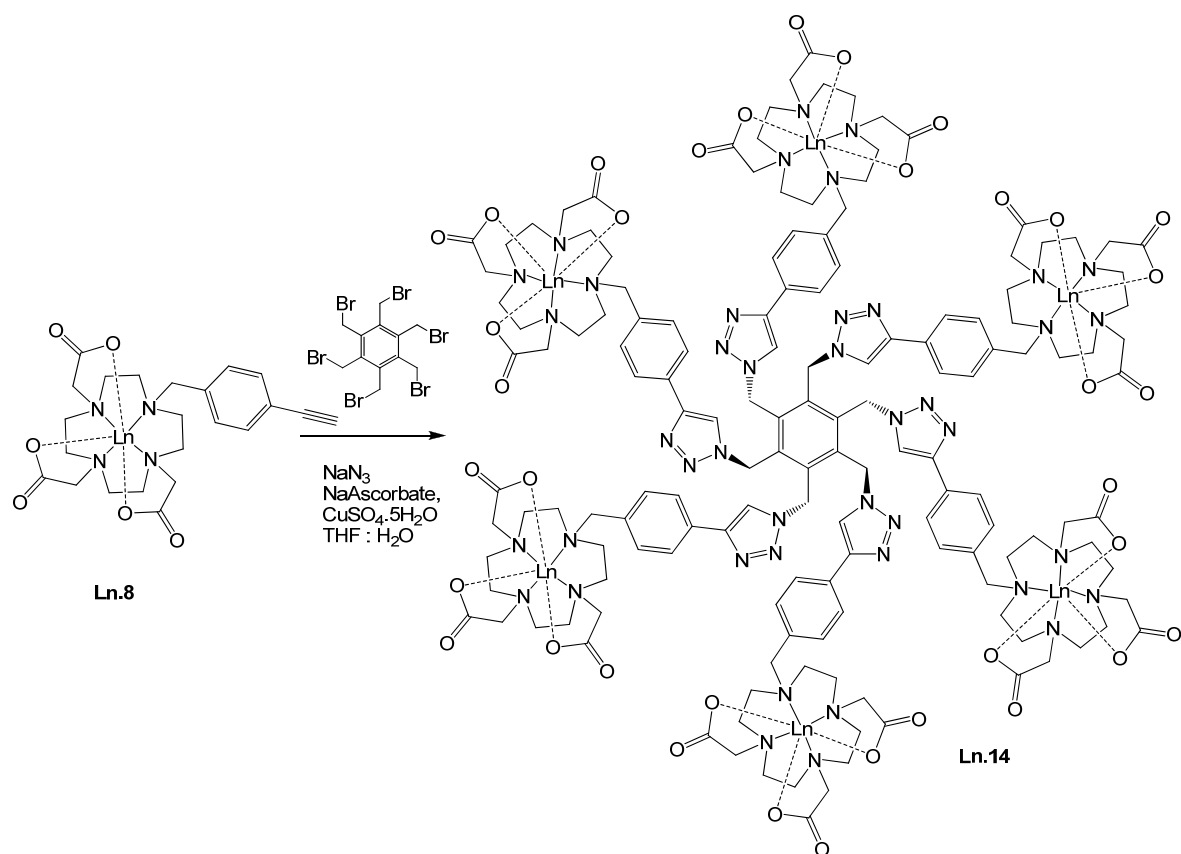
= 1 (Table 3.2). The luminescence data suggests that **Eu.13** contains seven-coordinate chelates, the lifetime data shows that either a small proportion of the bidentate anion carbonate is bound (Ln(III) compounds have a high affinity for this anion at pH 7.5), or that there is not enough space around the Eu(III) centre to allow two waters to bind, due to the bulky trimeric compound formed after the Cu(I) cycloaddition reaction. The hydrophobic nature of the compound means it could possibly be aggregating or ‘bundling’ up, only allowing coordination of one water. **Eu.13** is seven-coordinate with respect to ligand. The luminescence data, UV–visible data and HPLC data suggests that **Eu.13** has been synthesised and purified.

Complex	$\lambda_{em} / \text{nm}$	$\lambda_{ex} / \text{nm}$	$k_{\text{H}_2\text{O}} (\text{ms}^{-1})$	$k_{\text{D}_2\text{O}} (\text{ms}^{-1})$	$q$
<b>Eu.13</b>	395	618	2.57	1.38	1
<b>Eu.13</b>	256	618	2.45	1.47	0.9
<b>Eu.13</b>	291	618	2.44	1.47	0.9

Table 3.2 Rate constants,  $k$ , for depopulation of the excited state and derived hydration states,  $q$ , for the decay of **Eu.13**

### 3.7 Synthesis of Hexameric Compounds Using ‘Click’ Chemistry Ln.14

Hexakis(bromomethyl)benzene has been used as a central hub for the synthesis of **Ln.14**. The azide was formed *in situ* before the addition of **Ln.8**, sodium ascorbate and copper sulphate, the compounds were purified on HPLC. The multimeric compounds were purified *via* HPLC using 20% methanol in water over 25 minutes then gradient up to 100% methanol over 45 minutes.



Scheme 3.9

### 3.7.1 Characterisation of **Eu.14**

**Eu.14** was synthesised from **Eu.8**, and was purified on HPLC with an elution time 26.35 mins, obtained as a white powder in 6% yield. This is a significantly low yield for the Cu(I) catalysed cycloaddition reaction, due to the low rate of formation for the hexakis-(azidomethyl)-benzene hub. It is postulated that the solubility of the compound in aqueous media decreases as further Eu(III) chelates are added to the hub, therefore the concentrations of THF:H<sub>2</sub>O are important to push the reaction to the multimeric compound. Multiple different compounds can be formed during this reaction, with various numbers of azides or Eu(III) chelates attached to the hub. This gives multiple variations of complexes that can be formed over a 24 hour period, such as the product **Eu.14**. This is seen in the HPLC trace of the reaction mixture, as multiple peaks with differing elution times.

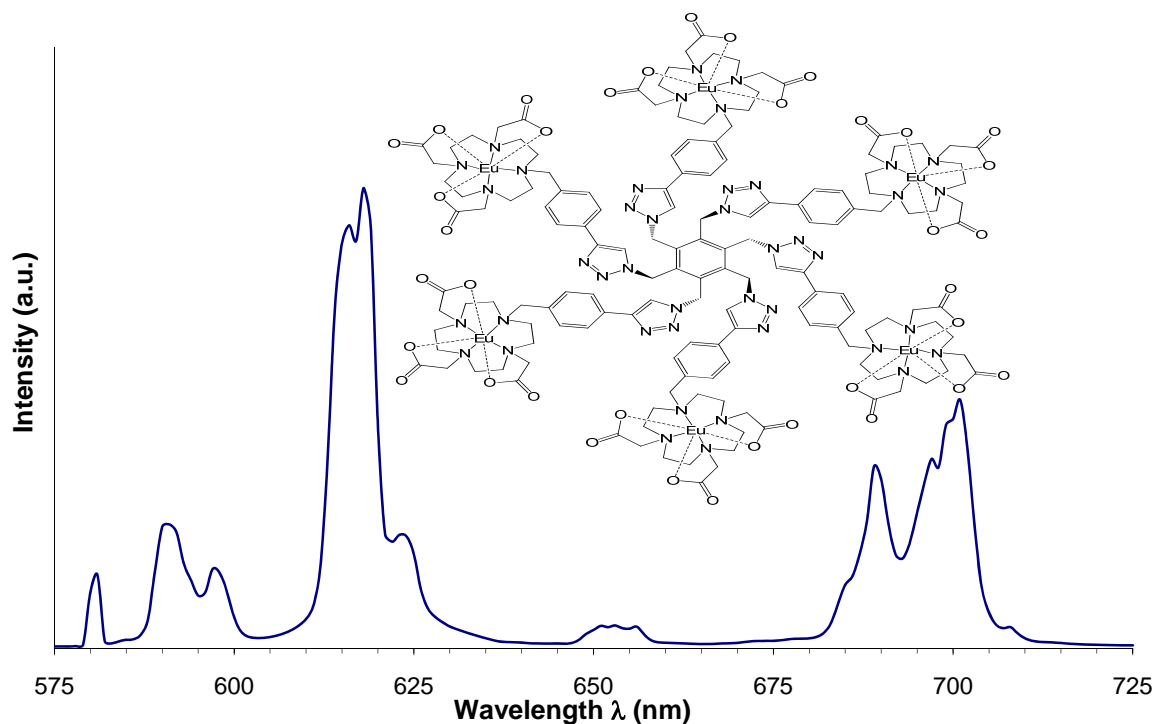


Figure 3.11 Luminescence emission spectra of **Eu.14** ( $\lambda_{\text{ex}} = 259 \text{ nm}$ ,  $\text{H}_2\text{O}$ , 298K, pH 7).

The emission spectrum in Figure 3.11 was recorded following excitation at  $\lambda_{\text{ex}} = 259 \text{ nm}$ , this spectrum is typical for Eu(III) emission showing the various  $^5\text{D}_0$  to  $^7\text{F}_1$  transitions. The hypersensitive  $^5\text{D}_0$ - $^7\text{F}_2$  transition or  $\Delta J = 2$  transition ( $\lambda = 618 \text{ nm}$ ), is of greater intensity to that of the  $^5\text{D}_0$ - $^7\text{F}_1$  transition or  $\Delta J = 1$  transition ( $\lambda = 594 \text{ nm}$ ), this is typical of a seven-coordinating chelate such as  $\text{EuDO3A}$ .<sup>26</sup> Which is similar to that of the ‘click’ model compound **Eu.12** and that of the trimeric compound **Eu.13**, potentially allowing 2 waters to coordinate. There is very little change in the  $\Delta J = 2$  transition ( $\lambda = 618 \text{ nm}$ ), compared with that of **Eu.8** (Figure 3.8) showing that this change does not affect the local coordination of the chelate; therefore the triazole has been formed, and does not bind to the metal centre.

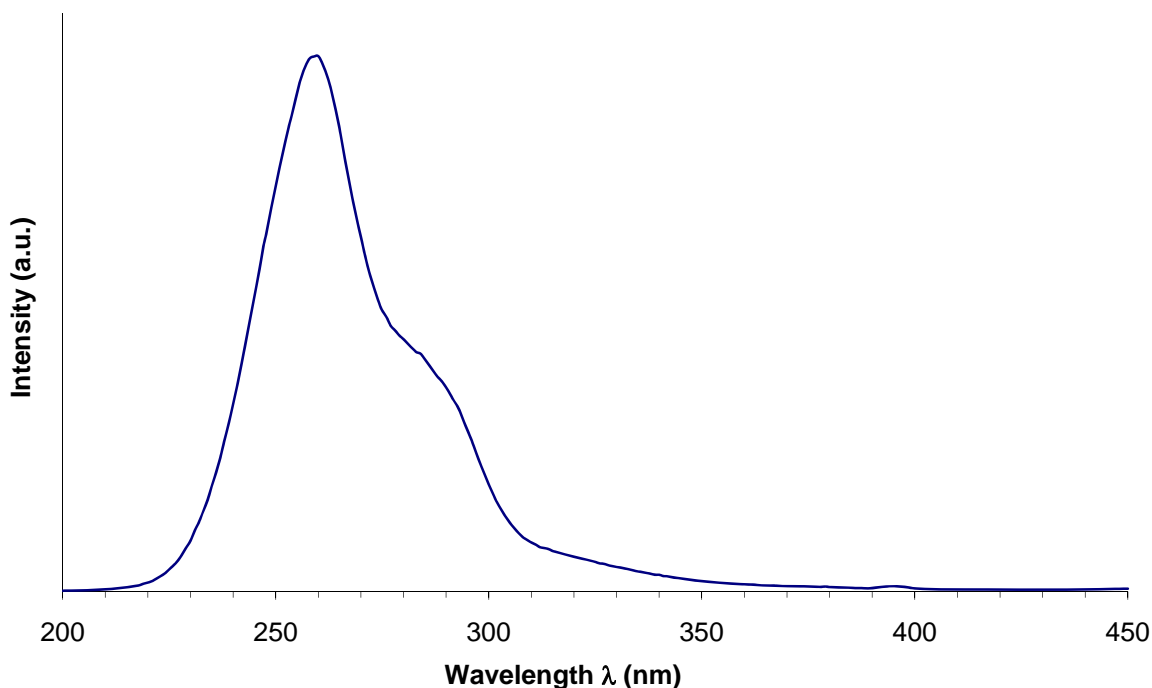


Figure 3.12 Excitation spectra for **Eu.14**,  $\lambda_{em} = 616$  nm (H<sub>2</sub>O, 298K, pH 7)

The excitation spectrum in figure 3.12 was recorded monitoring the emission at  $\lambda_{em} = 616$  nm, the  $\Delta J = 2$  transition. This shows intense maximum at  $\lambda = 259$  nm,  $\lambda = 283$  nm and a significantly weaker peak at  $\lambda = 395$  nm (direct excitation of the Eu(III) ion). The most intense maximum at  $\lambda = 259$  nm, is expected to be the  $\pi$ - $\pi^*$  transition of the *p*-benzyl. The maximum at  $\lambda = 283$  nm is absent in the precursor **Eu.8** and is likely to represent the 1,2,3-triazole chromophore. All emission spectra are identical showing that this is a pure compound, the most efficient chromophore for sensitisation is the *p*-benzyl subunit appended to the Eu(III) chelate.

Complex	$\lambda_{em} / \text{nm}$	$\lambda_{ex} / \text{nm}$	$k_{\text{H}_2\text{O}} (\text{ms}^{-1})$	$k_{\text{D}_2\text{O}} (\text{ms}^{-1})$	$q$
<b>Eu.14</b>	395	616	1.46	0.64	0.7
<b>Eu.14</b>	292	616	1.46	0.74	0.6
<b>Eu.14</b>	262	616	1.44	0.73	0.6

Table 3.3 Rate constants,  $k$ , for depopulation of the excited state and derived hydration states,  $q$ , for the decay of **Eu.14**

The UV-visible spectra shows absorbance maxima at,  $\lambda = 194$  nm,  $\lambda = 251$  nm and  $\lambda = 299$  nm, these correspond to the excitation wavelengths for the appended *p*-benzyl subunit at  $\lambda = 251$  nm in the excitation and the 1,2,3-triazole subunit at  $\lambda = 299$  nm. This verifies that the click reaction has occurred and that **Eu.14**, may have been synthesised.

The  $\Delta J = 2$  transition, at  $\lambda = 616$  nm is the wavelength that is monitored during luminescence lifetime studies to determine  $q$ . All three excitation wavelengths were tested and the hydration state  $q = 1$  (Table 3.3). The luminescence data suggests that **Eu.14** contains seven-coordinate chelates, the lifetime data suggests that there is not enough space around the Eu(III) centre to allow two waters to bind, this could be due to the bulky multimeric compound either aggregating or the hydrophobic nature of the compound folds preventing coordination of more than one solvent molecule. The luminescence lifetime data suggests the formation of a ‘click’ compound, however, it cannot confirm that **Eu.14** has been formed, it does suggest that a pure compound based on a hexa-substituted phenyl hub has been synthesised, but how many seven-coordinate chelates have been appended is unclear.

The luminescence data, UV-visible data and HPLC suggest that **Eu.14** may have been synthesised and purified, it definitely confirms that a pure ‘click’ compound has been formed. In the absence of mass spectrometry data, how many bromomethyl groups underwent the ‘click’ reaction is still unknown.

The Gd(III) analogue of **Ln.14** was not made due to the problems with characterisation encountered with the synthesis of **Eu.14**. It has been shown that **Ln.14**, can be synthesised and that pure compounds can be obtained from **Ln.8**, *via* the Cu(I) catalysed cycloaddition reaction. Further work on techniques to characterise **Ln.14** is required to develop **Gd.14**.

### 3.8 Summary and Conclusions

It has been demonstrated that *p*-ethynylbenzyl appended Ln(III) complexes (**Ln.8**) can be used to form multimeric lanthanide complexes, *via* the ‘Huisgen’ Cu(I) catalysed cycloaddition reaction. The desired products **Ln.13** and possibly **Ln.14** were synthesised *via in situ* generation of azides from the relevant central bromide phenyl hub starting material and sodium azide, avoiding isolation of compounds, bearing multiple azides, without side products as seen in **Ln.4**.

Luminescent lifetime studies indicate that **Ln.8** has a hydration state  $q = 2$ , this is the precursor for the synthesis of 1,2,3-triazole substituted complexes **Ln.12**, **Ln.13** and **Ln.14**. **Ln.12** has a hydration state  $q = 2$ , there are three routes to **Ln.12**, firstly by the ‘click’ reaction with **Ln.8** and benzyl bromide, which is the desired route. Secondly by undergoing the ‘click’ reaction with 4-ethynyl(hydroxymethyl)benzyl, followed by chlorination and reaction with **1**, giving the t-butyl macrocycle ligand **11**, the precursor for **Ln.12**. The third route is to undergo the Cu(I) cycloaddition reaction with **7** to form **11**, this requires an excess of copper and removal from the macrocycle, which is not facile, and the least desirable route to **Ln.12**. The use of ‘click’ chemistry *via in situ* generation of azides enables safe preparation of 1,2,3-triazole complexes.

The trimeric complex based on a mesitylene hub, **Ln.13** has a hydration state  $q = 1$ . This shows that the Cu(I) cycloaddition reaction to form 1,2,3-triazoles is an efficient way of linking multiple lanthanide chelates together, forming a viable linker. **Ln.13** has  $q = 1$ , presumably due to sterics around the metal centre, caused by aggregation or folding due to the hydrophobic nature of the complex, allowing only one water to bind.

The possible formation of **Ln.14** or the isolation of a pure complex that has ‘clicked’ based upon the hexakis(azidomethyl)benzene hub, has demonstrated that multimeric lanthanide complexes, can be formed *via* the Cu(I) catalysed cycloaddition reaction. **Ln.14** has a hydration state  $q = 1$ . Purification of a **Ln.14** based pure complex was not facile and requires HPLC, the complex itself is not detectable using mass spectrometric techniques. **Gd.14** was not synthesised due to the constraints in characterisation. It is postulated that **Gd.14** would have a higher relaxivity than Meade’s **L.Gd.9**.<sup>12</sup> Further work is required to developing techniques to characterise these multimeric complexes and optimise their synthesis.

Test reactions on various lanthanides Eu(III) and Tb(III), show that it is possible to make various multimeric compounds *via* the Cu (I) catalysed cycloaddition reaction. The *in situ* generation of the azide allows for safe preparation of highly explosive multi azide benzyl hubs without isolation. Despite this, there are many limitations to this technique, *i.e.* characterisation and isolation of pure products, this method as it stands, is not ideal for the synthesis of multimeric lanthanide compounds.

### 3.9 References

1. P. J. Endres, K. W. MacRenaris, S. Vogt, and T. J. Meade, *Biocon. Chem.* 2008, **19**, 2049.
2. P. Caravan, *Chem. Soc. Rev.*, 2006, **35**, 512.
3. M. Giardiello, M. P. Lowe and M. Botta, *Chem. Commun.*, 2007, 4044.
4. C. A. Boswell, P. K. Eck, C. A. S. Regino, M. Bernardo, K. J. Wong, D. E. Milenic, P. L. Choyke and M. W. Brechbiel, *Molecular Pharmaceutics*, 2008, **5**, 527.
5. E. Wiener, M. W. Brechbiel, H. Brothers, R. L. Magin, O. A. Gansow, D. A. Tomalia and P. C. Lauterbur, *Magn. Reson. Med.*, 1994, 1.
6. A. Barge, G. Cravotto, B. Robaldo, E. Gianolio and S. Aime, *J. Incl. Phenom. Macrocycl. Chem.*, 2007, 489.
7. S. Aime, E. Gianolio, F. Arena, A. Barge, K. Martina, G. Herepoulos and G. Cravotto, *Org. Biomol. Chem.*, 2009, 370.
8. E. Gianolio, R. Napolitano, F. Fedeli, F. Arena and S. Aime, *Chem. Commun.*, 2009, 6044.
9. G. M. Cooper and E. E. Hausman, 'The Cell; A Molecular Approach 4<sup>th</sup> Edition', ASM Press, 2004.
10. M. Jauregui, W. S. Perry, C. Allain, L. R. Vidler, M. C. Willis, A. M. Kenwright, J. S. Snaith, G. J. Stasiuk, M. P. Lowe and S. Faulkner, *Dalton Trans.*, 2009, 6283.
11. J. M. Bryson, W. J. Chu, J. H. Lee and T. M. Reineke, *Biocon. Chem.*, 2008, **19**, 1505.
12. Y. Song, E. K. Kohlmeier and T. J. Meade, *J. Am. Chem. Soc.*, 2008, **130**, 6662.
13. T. Frenzel, P. Lengsfeld, H. Schirmer, J. Hutter and H. Weinmann, *Invest. Radiol.*, **43**, 2008, 817.
14. F. H. Romain and A. N. Hulme, *J. Am. Chem. Soc.*, 2006, **128**, 11370.
15. M. Rohrer, H. Bauer, J. Mintorovitch, M. Requardt, H.-J. Weinmann, *Invest. Radiol.* 2005, **40**, 715.
16. Private communication. Dr C. Murray, Atomic Weapons Establishment, March 2007.
17. P. Wu and V. V. Fokin, *Aldrichimica Acta*, 2007, **40**, 7.
18. L.-Y. Wu, Z.-Y. Yan, Y.-X. Xie, Y.-N. Niu and Y.-M. Liang, *Tetrahedron Asymmetry.*, 2007, **18**, 2086.

19. V. Aucagne, J. Berna, J. D. Crowley, S. M. Goldup, K. D. Hanni, D. A. Leigh, P. J. Lusby, V. E. Ronaldson, A. M. Z. Slawin, A. Viterisi and D. B. Walker, *J. Am. Chem. Soc.*, 2007, **129**, 11950.
20. S. Aime, A. Barge, M. Botta, A. S. de Sousa and D. Parker, *Angew. Chem. Int. Ed.*, 1998, **37**, 2673.
21. J. I. Bruce, M. P. Lowe and D. Parker, 'The Chemistry of Contrast Agents in Magnetic Resonance Imaging; Phototypical Aspects of Lanthanide(III) Complexes', ed. A. E. Merbach and E. Toth, Wiley, 2001.
22. S. L. Murov, I. Carmichael and G. L. Hug, 'Handbook of Photochemistry, Second Edition', Marcel Dekker, 1993.
23. R. D. Shannon and C. T. Prewitt, *Acta Cryst.*, 1969, **B25**, 925.
24. R. D. Shannon, *Acta Cryst.*, 1976, **A32**, 751.
25. K. E. Krakowiak, J. S. Bradshaw, *Organic Syntheses, Coll.*, 1998, **75**, 89.
26. J. I. Bruce, R. S. Dickins, L. J. Govenlock, T. Gunnlaugsson, S. Lopinski, M. P. Lowe, D. Parker, R. D. Peacock, J. J. B. Perry, S. Aime and M. Botta, *J. Am. Chem. Soc.*, 2000, **122**, 9674.

## Chapter 4

### 'Click' Chemistry as a Route to Dual Modal Contrast Agents

#### 4.1 Introduction

Magnetic Resonance (MR) imaging compared with other imaging modalities, has excellent anatomical resolution; however, it suffers at the molecular scale due to its intrinsic low sensitivity. An area of research that has started to grow; is the attachment of a secondary imaging agent for *e.g.* PET, SPECT or fluorescence imaging to an MRI contrast agent. The goal is to overlay images from different techniques, giving better image resolution and co-validation of the accumulation of targeted MR contrast agents at a specific site. MRI has superb resolution but very low sensitivity, whereas PET has very high sensitivity but relatively poor resolution, and optical fluorescence is difficult to quantify in tissues more than a few millimetres thick. Combining two of these techniques is seen as advantageous for molecular imaging purposes. The vast majority of dual modal agents reported to date have focused on attaching optical probes to MRI, PET or SPECT agents; a recent review by Long has discussed the merits of recent developments in the area over the last five years.<sup>1</sup>

##### 4.1.1 MR/Optical Imaging Agents

There are multiple approaches to generate dual modal contrast agents, Mishra *et al.* have attached an organic fluorescein *via* a ethylthioureido linker to a Gd(III) DO3A complex, **L.Gd.10a** (Figure 4.1).<sup>2</sup> Meade and co-workers have covalently attached another fluorescent dye, tetramethylrhodamine-5-isothiocyanate (TRITC) directly to the Gd(III) DOTA backbone; however, despite showing promise in *in vitro* studies, when applied to living embryos, the hydrophobic nature of the probe meant it was localised in the fatty tissue and no MR signal was observed.<sup>3</sup> A more viable agent used TRITC and Gd(III) DTPA appended to a dextrin polymer, which remained in the aqueous phase, **L.Gd.10b** (Figure 4.1).<sup>3</sup>

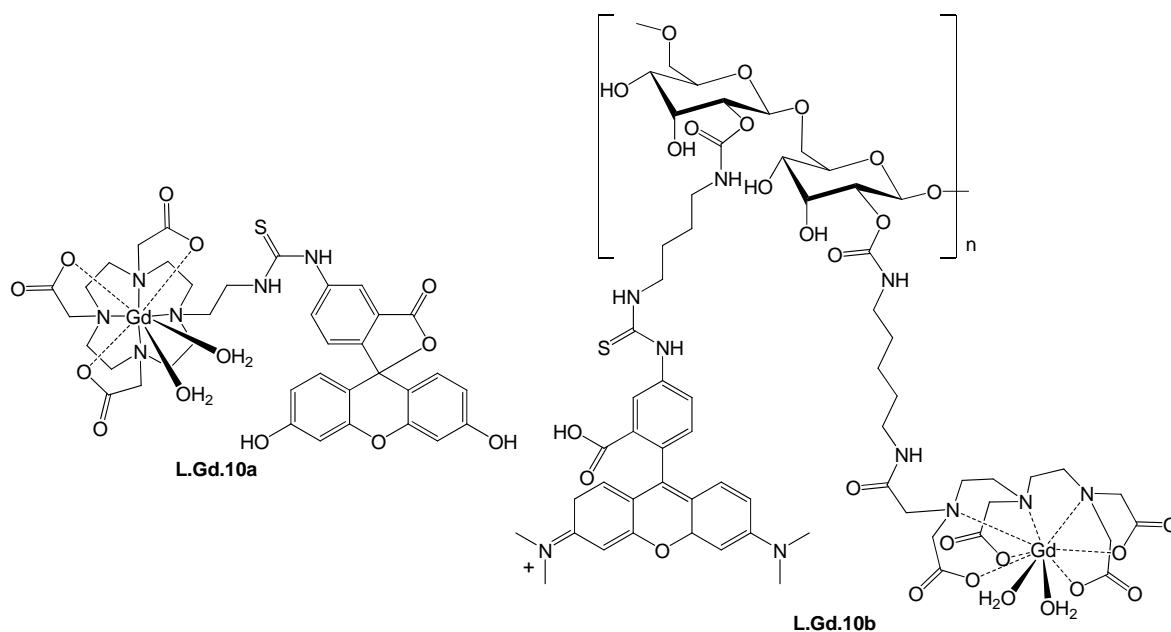


Figure 4.1 Gd (III) chelates appended with fluorescent dyes, Gd(III) DO3A appended with fluorescein (left),<sup>2</sup> and Gd(III) DTPA- tetramethyl-rhodamine-aminedextran (right).<sup>3</sup>

Other groups have taken a different approach to dual MRI/optical imaging agents, Faulkner and co-workers have developed a heterobimetallic rhenium-gadolinium complex.<sup>4</sup> They have synthesised a Gd(III)DO3A appended with a pyridine, this was coordinated to a *fac*-Re(CO)<sub>3</sub>-bipy complex (**L.Gd.11a**). Lanthanide luminescence studies indicate that it has hydration state  $q = 1$ , showing that the bulky and lipophilic pyridyl substituent hinders close approach of the solvent to the metal centre. In the case of the Yb(III) version the lanthanide quenches the MLCT of the Re, in the form of sensitised emission of the Yb(III). The measured relaxivity when coordinated to Re(CO)<sub>3</sub>bipy was,  $r_1 = 8.6 \text{ mM}^{-1}\text{s}^{-1}$  (500 MHz), *Cf.*,  $r_1 = 4.5 \text{ mM}^{-1}\text{s}^{-1}$  (500 MHz); in the absence of the Re complex, the *d-f* hybrid tumbles more slowly than the precursor, as it has a larger molecular mass.<sup>4</sup> Moriggi *et al.* have developed a self-assembling metallostar based on a modified [Ru(bpy)<sub>3</sub>]<sup>2+</sup> bearing multiple Gd(III)DTTA complexes **L.Gd.11b** (Figure 4.2), a *d-f* heptametallic hybrid. [Ru(bpy)<sub>3</sub>]<sup>2+</sup> being low-spin  $d^6$  octahedral is known for its kinetic stability, this compound has good photophysical properties, the MLCT state is in the visible region of the spectrum.<sup>5</sup> The relaxivity of Ru[Gd<sub>2</sub>bpy-DTTA<sub>2</sub>(H<sub>2</sub>O)<sub>2</sub>]<sub>3</sub> was reported at  $r_1 = 30.6 \text{ mM}^{-1}\text{s}^{-1}$  (20 MHz, 25°C) which is higher than Gd(III)DOTA which has a relaxivity of  $r_1 = 4.2 \text{ mM}^{-1}\text{s}^{-1}$  (20 MHz, 25°C)<sup>6</sup> due to the increased mass and slower tumbling.<sup>7</sup> The observed relaxivity is much lower than expected for a  $q = 2$  Gd chelate, the relaxivity averages out at  $5.1 \text{ mM}^{-1}\text{s}^{-1}$  per Gd chelate, which is lower than that of Gd(III)DO3A  $r_1 = 5.7 \text{ mM}^{-1}\text{s}^{-1}$  (20 MHz,

25°C),<sup>8</sup> it would be expected to show a greater relaxivity due to the increased mass and slower tumbling. When the lanthanide is changed from Gd(III) to Eu(III), the sensitised Eu emission is masked by the broad and much stronger [Ru(bpy)<sub>3</sub>]<sup>2+</sup> MLCT emission, therefore there is no energy transfer observed to the Eu(III) metal.<sup>7</sup>

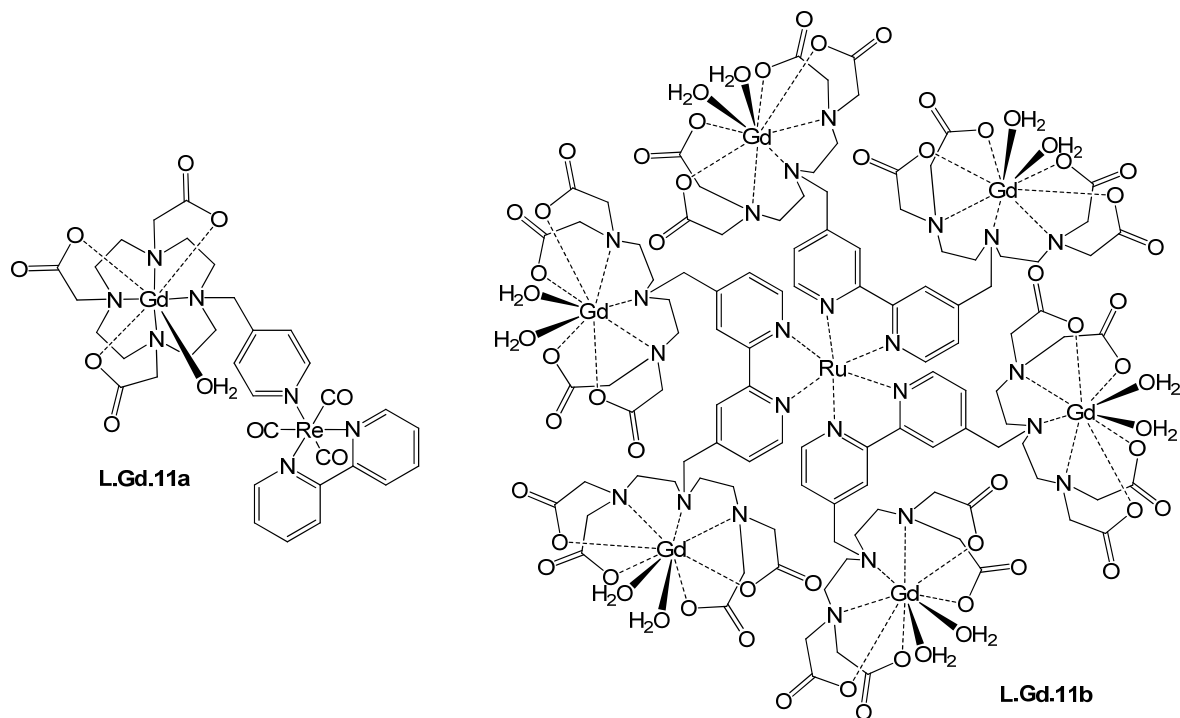


Figure 4.2 Heterometallic *d-f* hybrid MRI / optical imaging agents

#### 4.1.2 PET/Optical Imaging Agents

The fusion of radionuclear and optical methods has potential for molecular imaging, tackling the disadvantages and enhancing the strengths of both techniques, while the research is in its infancy, it has focused on the metal-based radioisotopes, which can be bound in a similar way to that of Gd MR/optical contrast agents. Chen and co-workers have been developing PET/NIRF imaging agent, by attaching DOTA ligand to a CdTe quantum dot (QD) with amine functionalised surface modified with VEGF protein, which can target tumours. The CdTe QD is the NIRF optical probe and the PET agent is <sup>64</sup>Cu, which can be chelated to the appended DOTA ligand (Figure 4.3).<sup>9</sup> Although *in vivo* studies of the PET/QD dual modal agents have been qualitative, this probe has shown specifically target tumour vascular VEGFR-2 and quantitatively evaluate the targeting efficacy for the first time.

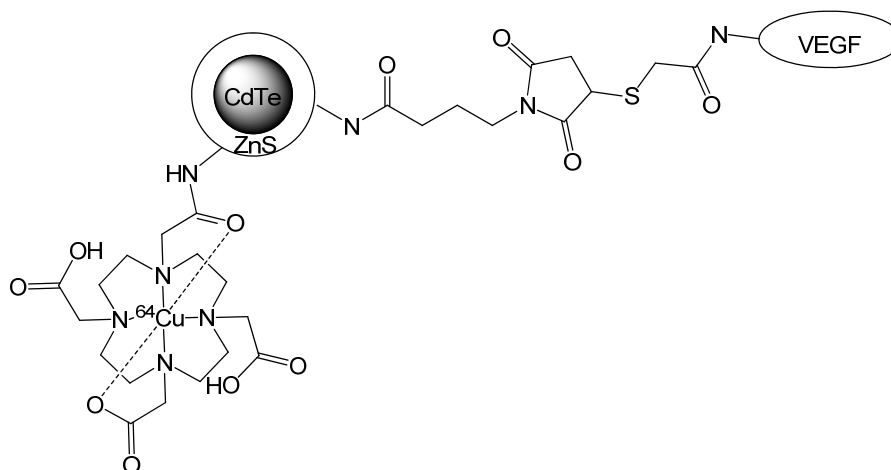


Figure 4.3 Chen and co-workers PET/NIRF DOTA-QD-VEGF conjugate.<sup>9</sup>

Other groups have investigated the detection of reporter gene expression, by combining bioluminescence probes with the PET radionuclide  $^{18}\text{F}$ . Ray *et al.* have fused together two different reporter genes (HSV1-TK and sr39 renilla luciferase) for the study of roles of genes in cancer development.<sup>10</sup> The HSV1-sr39-TK contained a radio labelled tag, 9-(4-[ $^{18}\text{F}$ ]-fluro-3-hydroxymethylbutyl)guanine and the renilla luciferase contained the bioluminescent tag.<sup>10</sup> Bioluminescence has a higher signal to background ratio which is an advantage compared to other fluorescence techniques.

The combination of two different imaging modalities provides advantages to overcome the problems of the individual modalities. Combining two techniques provides a better image of the targeted area. Although all these examples are in the early stages of development, they are providing a method for better image resolution and increasing the sensitivity of the image for molecular imaging.

#### 4.1.3 Rhenium as an Optical Probe

Rhenium is a third row transition metal in group seven of the periodic table, it is naturally occurring with molybdenite ( $\text{MoS}_2$ ) and some copper ores, as two isotopes  $^{185}\text{Re}$  (37.4%) and  $^{187}\text{Re}$  (62.6%). Re is isolated as  $\text{ReO}_4^-$ , the perrhenate ion, the first detection of Re was in 1925 via its X-ray spectrum.<sup>11</sup> Re has nine oxidation states; -1 to +7, due to this Re has diverse applications, from *e.g.* catalysis to imaging probes. The most useful oxidation state of Re for the purposes of optical imaging, is the kinetically stable, octahedral Re(I), complexes of which are low-spin  $d^6$  and highly luminescent. The Re(I) bipyridine complex by Wrighton and co-workers (Figure 4.4), is a very stable and

luminescent complex that has been used as a base for multiple targeted Re(I) optical probes.<sup>12</sup> These probes have a luminescence emission maximum around  $\lambda \sim 550 - 600$  nm in the visible spectrum this is due emission from the <sup>3</sup>MLCT band, which can be tuned by altering the substituents on the coordinated bipy.<sup>12</sup> Re(I) can also be cyclometallated using a phenyl pyridine to form a kinetically stable, luminescent complex with an emission maximum in the visible region at  $\lambda \sim 500$  nm. As a result of the emission from the triplet MLCT state the lifetimes are considerably longer lived than that of the organic chromophores, typically of the ns -  $\mu$ s time scale. All these properties of Re(I) octahedral complexes makes them ideal for use as the optical probe in a dual modal MR/optical imaging contrast agent.

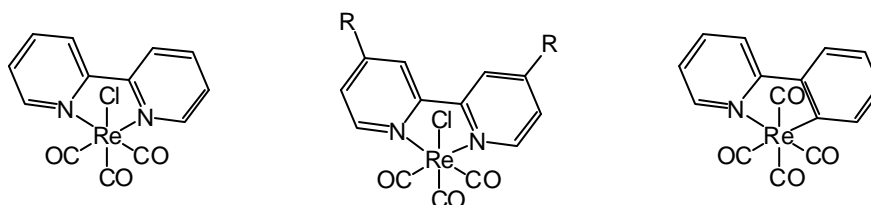
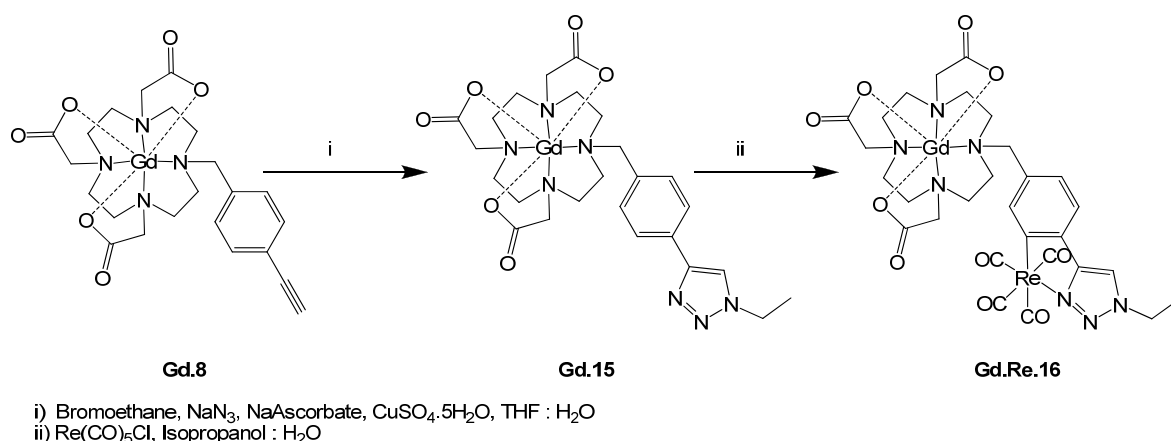


Figure 4.4 Re(I) octahedral complexes

#### 4.1.4 Synthesis of a Potential Dual Mode MR/Optical Imaging Agent

The aim of this chapter was to utilise the *p*-ethynylbenzyl appended chelates developed in Chapter 3 and investigate their potential use as precursors for dual modal contrast agents. To these ends, attempts were made to synthesise a Gd(III) chelate linked to a Re(I) complex. The Gd(III) chelate was based on DO3A with an appended *p*-ethynylbenzyl (**Ln.8**) to be used in the Cu(I) catalysed cycloaddition or ‘click’ reaction, to form a substituted 1,2,3-triazole. This triazole was designed to coordinate Re(I) *via* cyclometallation of the phenyltriazole. The resulting complex (Scheme 4.1) was designed to provide both MR (Gd) and optical (Re) signal, *i.e.* to be a dual mode optical/MR imaging agent.

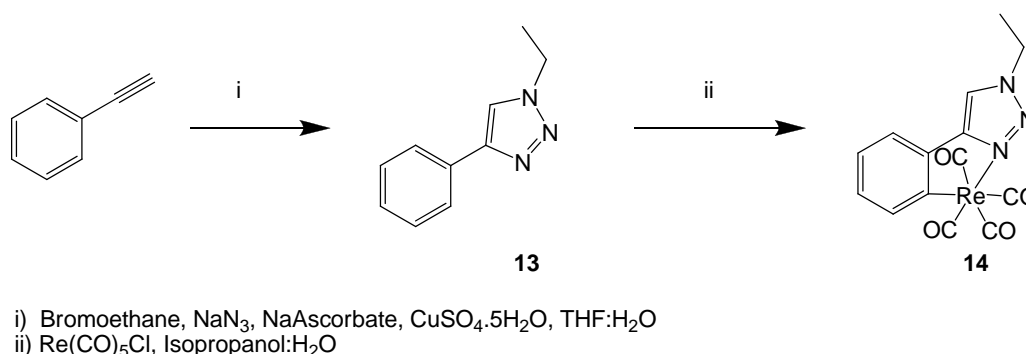


Scheme 4.1

Octahedral Re(I) was used due to the inherent kinetic stability of its low-spin  $d^6$  complexes and their luminescent properties.<sup>12</sup> The SPECT agent developed by Schibli and described in Chapter 2<sup>13</sup> uses <sup>99m</sup>Tc which lies directly above Re in the periodic table has been shown to be kinetically stable as it is low spin  $d^6$ , this suggests that Re would be stable for use in an imaging agent.

A phenyltriazole, **Gd.15** was to be synthesised from **Gd.8**, using ‘click’ chemistry with bromoethane (*via in situ* azide generation). It offers a facile synthesis to a dual modal contrast agent (Scheme 4.1). An ethyl substituted 1,2,3-triazole was proposed, mainly as an ethyl in the N1 position was not expected to interfere sterically with coordination of Re, and secondly would not prove to be lipophilic a substituent.

To test the feasibility of rhenium coordination *via* cyclometallation, the synthesis of a model phenyl-1,2,3-triazole (**13**) was attempted (Scheme 4.2). The experimental conditions were optimised before the attempted synthesis of **Ln.Re.16**.



Scheme 4.2

## 4.2 Attempted Synthesis of 14

The proligand **13** was synthesised *via* the Cu(I) catalysed reaction between phenylacetylene and bromoethane *via in situ* generation of the ethyl azide with sodium azide (Scheme 4.2).<sup>14</sup> **13** was isolated *via* silica column chromatography in moderate yield. The <sup>1</sup>H NMR spectrum clearly shows the loss of a 1H singlet at 2.1 ppm (the CH of the terminal alkyne) and the appearance of a 1H singlet at 7.70 ppm indicating the CH on the 1,2,3-triazole ring, the ES<sup>+</sup> mass spectrum showed a peak at *m/z* 173 [M + H]<sup>+</sup> indicating product formation.

The coordination of Re(CO)<sub>5</sub>Cl to **13**, is based upon Wrighton and co-worker Re(I) coordination to 2-phenylpyridine **L.12** (Figure 4.5).<sup>12</sup> More recently Obata *et al.* have used ‘click’ chemistry to synthesise 4-(2-pyridyl)-1,2,3-triazole rhenium (I) complexes. They have shown that the formation of the 1,2,3-triazole can be used as a novel ligand system coordinating the Re(I) through the pyridine and the nitrogen of the 1,2,3-triazole **L.13** (Figure 4.5).<sup>15</sup> This Re(I) complex exhibits good luminescent properties showing a blue shift in the emission and extended lifetimes  $\tau = 8.90 \mu\text{s}$ , compared with the bipyridyl Re(I) complex with  $\tau = 3.17 \mu\text{s}$ .

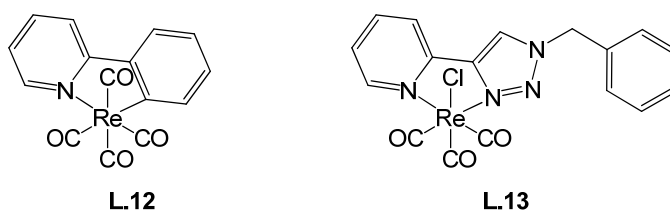


Figure 4.5 Phenyl pyridine rhenium (I) complex (left) and 4-(2-pyridyl)-1,2,3-triazole rhenium (I) complex (right).

Two methods were used to react Re(CO)<sub>5</sub>Cl with **13**; first by conventional heating in mixture of isopropanol and water or *via* microwave radiation for 30 minutes at 90 °C. Three different Re(I) complexes were formed under these condition, evidence from the <sup>1</sup>H NMR and ES<sup>+</sup> mass spectra suggest the compounds in Figure 4.6, were formed.

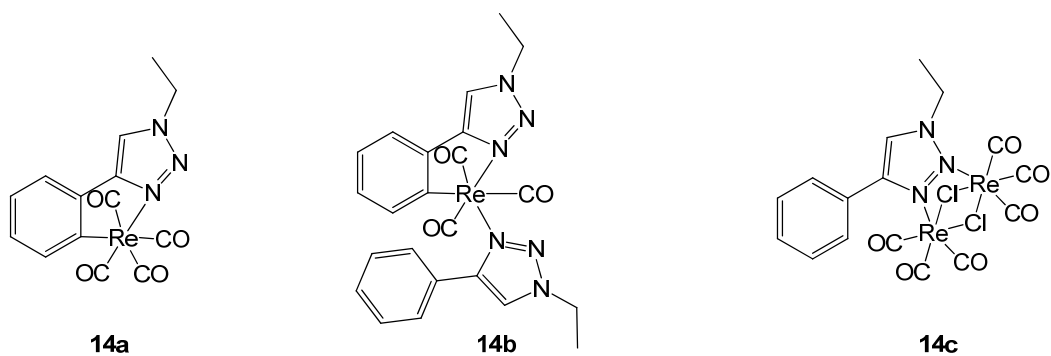


Figure 4.6

The  $^1\text{H}$  NMR spectra in Figure 4.7 show the mixture of products from the reaction (**14a**, **14b** and **14c**), the resonances in the range 4.2 to 5 ppm are representative of the  $\text{CH}_2$  of the ethyl group. In the top spectrum there are four 2H quartets, the peak at 4.3 ppm is the  $\text{CH}_2$  of **14c**, this can be assigned as **14c** has been crystallised to yield the second spectra. The resonances at 4.5 and 4.95 ppm are the two  $\text{CH}_2$  of **14b**; one from a ligand cyclometallated and a second from monodentate N coordination from a second triazole. The resonance at 4.5 ppm could be two overlapping quartets, this could suggest that there is a non-cyclometallated, or monodentate triazole bound to the Re as well as **14b**. The final peak at 4.4 ppm is representative of the methyl of **13**, which is the only species in the bottom spectrum *i.e.* starting material **13**.

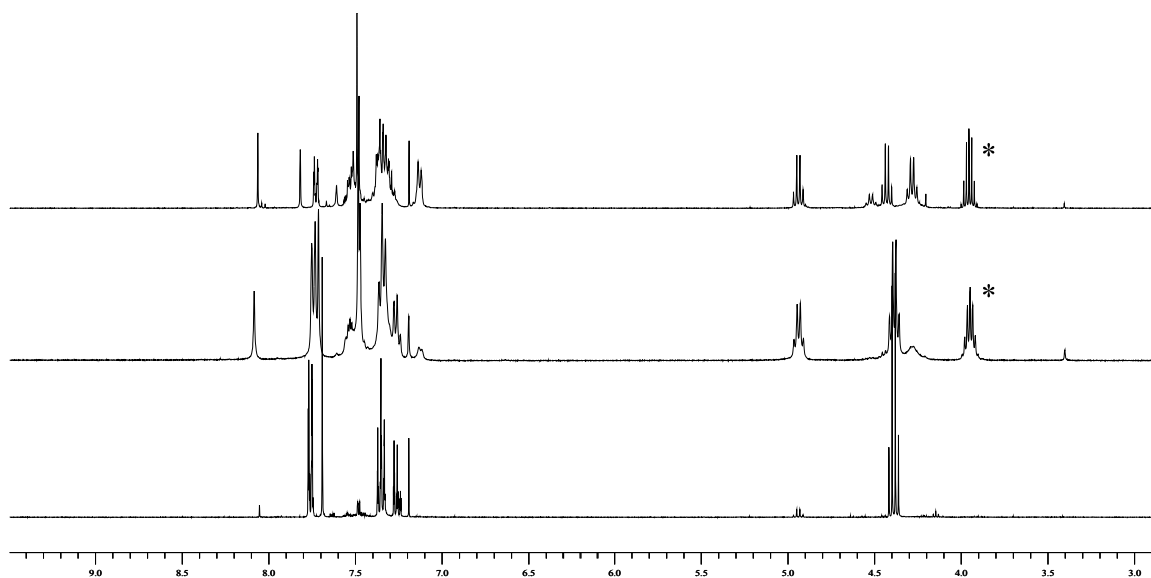


Figure 4.7  $^1\text{H}$  NMR spectrum of the mixture of **14a**, **14b** and **14c** (top), **14a** and **14b** (middle) and **13**(bottom),( $\text{CDCl}_3$ , 400MHz)(\* = isopropanol ethyl resonance).

The peaks in the aromatic region show the shifts for the phenyl ring and the CH of the 1,2,3-triazole. The peak at 8.1 ppm represents the CH of the 1,2,3-triazole that is bound

to the Re centre just through the triazole nitrogens, in **14b** or **14c**. The peak at 7.7 ppm, is the CH of the 1,2,3-triazole in the starting material **13**. **14c** was isolated *via* crystallisation from chloroform, it is observed in the ES<sup>+</sup> mass spectrum 785 [M + H]<sup>+</sup>. A representation of the crystal structure is shown in Figure 4.6, showing the Re bridged by two chlorides, to the 1,2,3-triazole, Table 4.1 show selected bond lengths and bond angles for **14c**, showing tighter bond angles inside the N to Re to Cl ring.

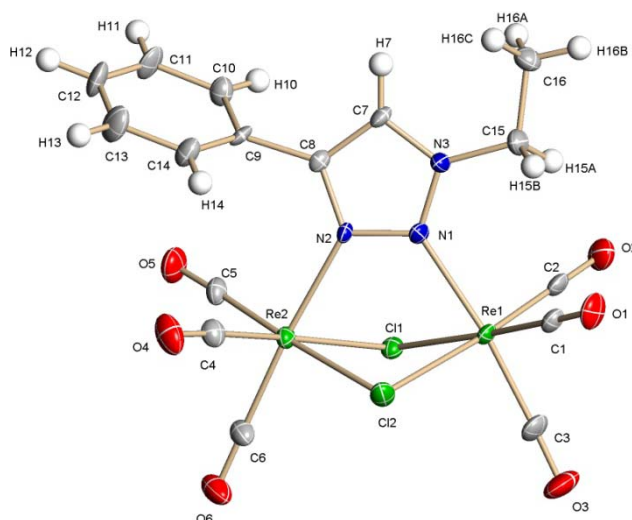


Figure 4.8 X-ray structure of **14c**, showing the triazole bridged Re complex.

Re(1)-C(3)	1.922(7)	C(2)-Re(1)-N(1)	95.1(2)
Re(1)-N(1)	2.205(5)	C(3)-Re(1)-N(1)	173.7(3)
Re(1)-Cl(2)	2.4924(19)	C(1)-Re(1)-Cl(2)	96.6(2)
Re(1)-Cl(1)	2.5092(19)	N(1)-Re(1)-Cl(2)	81.72(14)
Re(2)-C(6)	1.929(7)	C(2)-Re(1)-Cl(1)	93.5(2)
Re(2)-N(2)	2.200(5)	N(2)-Re(2)-Cl(2)	83.74(14)
Re(2)-Cl(2)	2.499(2)	N(2)-Re(2)-Cl(1)	80.53(14)
Re(2)-Cl(1)	2.5084(17)	Cl(2)-Re(2)-Cl(1)	80.47(5)

Table 4.1 Selected bond lengths [Å] and angles [°] for **14c**.

The formation of **14c** the Re(I) dimer, at a one to one ratio of Re:Ligand, leaves a larger amount of ligand than Re(I) under the microwave reaction condition driving the formation of **14b**, the 2:1 L:M complex. In the Cambridge structural database there are only 22 examples of Cl bridged ((CO)<sub>3</sub>ReCl)<sub>2</sub> complexes. Banerjee and co-workers<sup>16</sup> have shown a novel sulphur donor ligand coordinating two Re metal ions bridged by two chloride atoms, Lorenz and co-workers have also shown a similar di-bridged Re(I) complex to a nitrosobenzene bound through the nitrogen and the oxygen of the nitrosobenzene<sup>17</sup> and Donghi *et al.*<sup>18</sup> have shown that a di-bridged Re(I) complex can form on a pyridazine

coordinating in a similar manner to that of **14c** through the N1 and N2 (Figure 4.9). These examples are similar to **14c** in that bridged Re complex is formed when using a 1:1 ratio of ligand to metal.

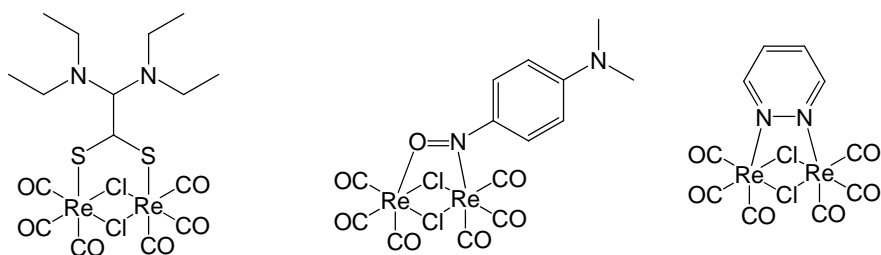
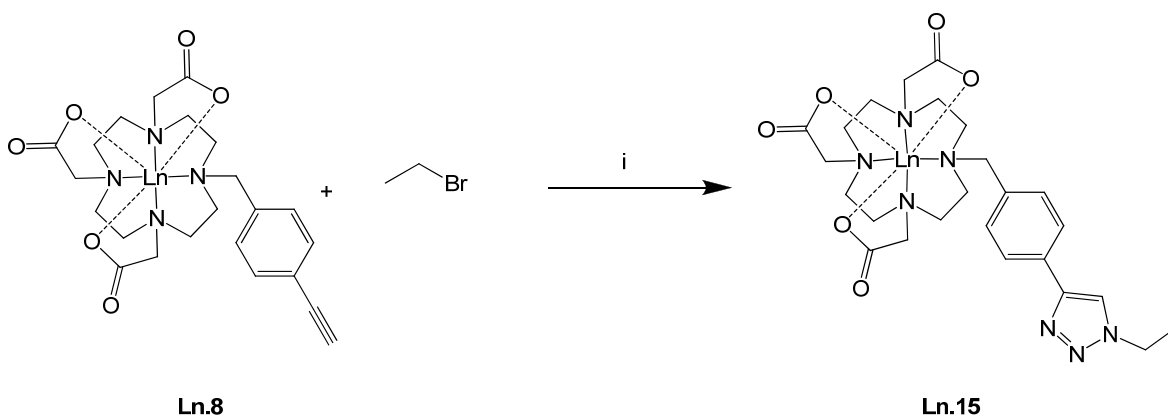


Figure 4.9 Re bridged complexes<sup>16,17,18</sup>

This is a rare example of the 2 and 3 positions of the triazole coordinating in a bridging manner. The only other example is of a bridged Cu(I) complex reported by Williams and co-workers.<sup>19</sup> These results showed that **13** will coordinate Re(I) and therefore **Ln.15** was also expected to cyclometalate Re(I). It has also been shown that Re can coordinate methyl triazole in three different manners, either by cyclometallation such as **14a**, or having a second ligand bound in a pyridinic manner such as **14b** and finally bridged by 1,2,3-triazole and two chlorides, such as **14c**.

### 4.3 Synthesis of Ln.15

**Ln.15** chelates were synthesised *via* the Cu(I) catalysed cycloaddition reaction between **Ln.8** and a bromoethane, in the presence of sodium azide (Scheme 4.3).



i)  $\text{NaN}_3$ , NaAscorbate,  $\text{CuSO}_4 \cdot 5\text{H}_2\text{O}$ ,  $\text{EtOH}:\text{H}_2\text{O}$

Scheme 4.3

### 4.3.1 Luminescence studies of **Eu.15**

**Eu.15** was synthesised from **Eu.8** and bromoethane under ‘click’ conditions, to give a white solid, 86% yield. **Eu.15** is a seven-coordinate complex; it was expected that it would have two coordinated solvent molecules.

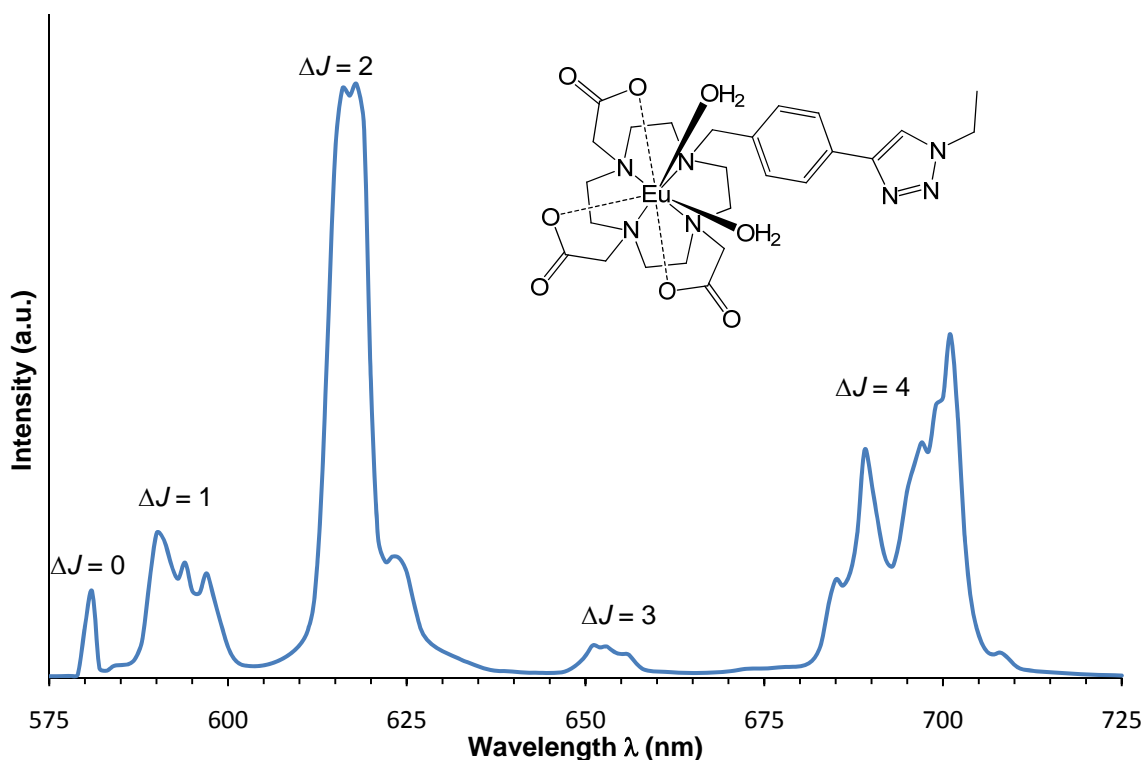


Figure 4.10 Luminescent emission spectrum of **Eu.15**, ( $\lambda_{ex} = 260$  nm,  $H_2O$ , 298K, pH 5)

The spectrum in Figure 4.10 is typical of Eu(III) complexes of this type displaying the various  $^5D_0$  to  $^7F_J$  ( $J = 0-4$ ) transitions; the hypersensitive  $\Delta J = 2$  transition is particularly intense, compared to that of the  $\Delta J = 1$  transition. This is typical of a seven-coordinate complex with  $q = 2$ . Initial lifetime measurements suggest **Eu.15** had a hydration state,  $q = 0$ . It was thought that **Eu.15** was binding carbonate (from dissolved  $CO_2$ ), adjustment of pH to  $\sim 5$ , gave the same reading, a pH at which there is little or no dissolved carbonate.

It was unlikely that the triazole would coordinate to the metal to reduce the  $q$  to zero, or that the pendant phenyl triazole was sterically bulky enough to prevent water coordination, so another reason was sought. One possible explanation for this apparent zero hydration state would be if **Eu.15** self associates, binding a nitrogen of the 1,2,3-triazole of an adjacent **Eu.15**, this would be favoured at higher concentration,  $\pi - \pi$  stacking of the

phenyl rings would facilitate this, relieving entropically unfavourable solvation of the hydrophobic phenyl triazole group. Faulkner and co-worker have shown a self associating lanthanide complex that is pH responsive, **L.Ln.14** in Figure 4.11.<sup>20</sup> The structure of this complex, is not dissimilar to **Eu.15**, the carboxylate group in Faulkners example being replaced by the ethyltriazole in **Eu.15**.

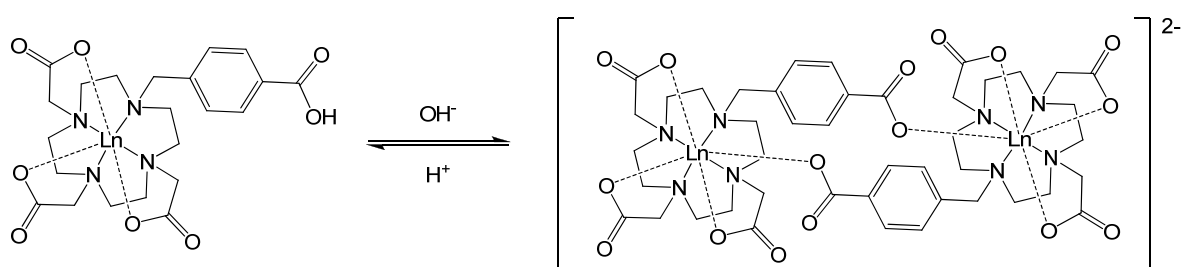


Figure 4.11 Faulkner and co-worker's pH responsive self associating Ln(III) complex

Faulkner and co-worker showed that Tb(III) and Eu(III) analogues, have a hydration state  $q = 2$ , at pH 2 and are monomeric, at pH 8 the complex has a hydration state  $q = 1$ , suggesting a self-associating dimer. It is postulated that at high pH the carboxylate group is deprotonated, allowing binding to an adjacent metal centre.<sup>20</sup>

The luminescent behaviour of **Eu.15** is not pH responsive, but it is concentration dependent. Figure 4.12 shows, the excitation spectra of **Eu.15** at various concentrations, (the intensity per milligram of complex is plotted). Monitoring the emission at  $\lambda = 618$  nm,  $\Delta J = 2$  transition, this shows intense maxima at  $\lambda = 260$  nm and  $\lambda = 285$  nm, (a weaker peak at  $\lambda = 395$  nm corresponds to direct excitation of the Eu(III) ion). The intense maximum at  $\lambda = 260$  nm, is expected corresponds to the  $\pi-\pi^*$  transition of the *p*-benzyl. The maximum at  $\lambda = 283$  nm is absent in the precursor **Eu.8** and is likely to arise from the 1,2,3-triazole chromophore. The highest concentration examined, gives the lowest intensity per unit concentration of complex, whereas the least concentrated sample, gives the highest intensity per unit concentration. This suggests that at higher concentrations, when presumably a dimer is formed, despite the decrease in hydration state, the relative intensity of the compound decreases. Whilst quenching waters are displaced, they are replaced by coordination of the triazole from an adjacent molecule. This assembled dimer has a much shorter lifetime than the monomeric form, *i.e.* there is more quenching of the Eu(III) excited state, either through photoinduced electron transfer involving the triazole or *via* an efficient energy transfer mechanism.

This decrease of intensity per unit concentration of **[Eu.15]** is increased, suggests that **Eu.15** can self-associate and that this process is concentration dependent, Faulkner and co-worker's suggest  $\pi - \pi$  stack of the phenyl rings contribute to the self-associating lanthanide complex that they report.

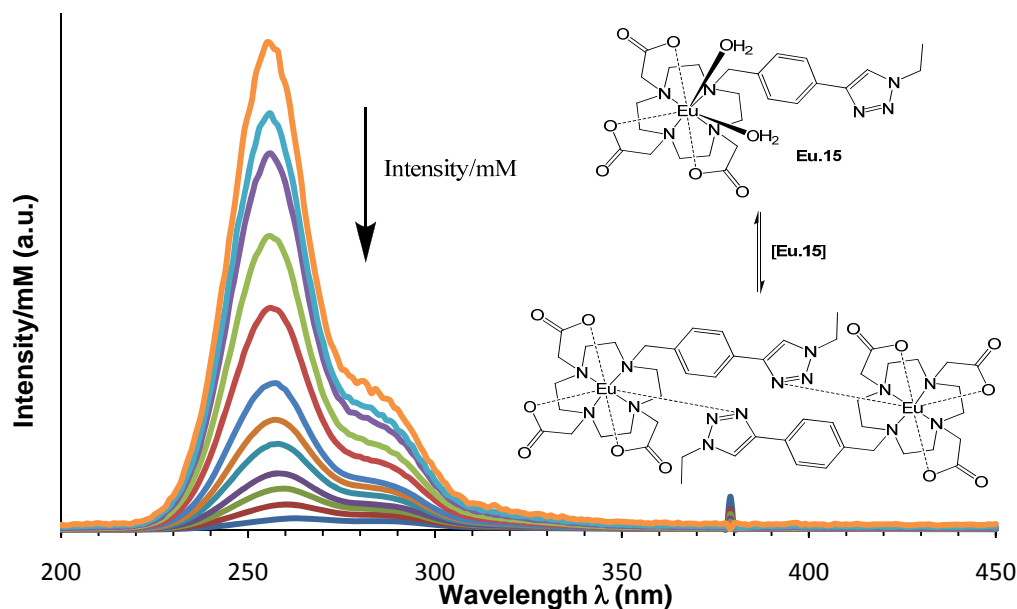


Figure 4.12 Variation in the excitation spectrum of **Eu.15**, as **[Eu.15]** is varied,  $\lambda_{em} = 618$  nm, H<sub>2</sub>O, 298K, pH 6.

The  $\Delta J = 2$  transition, at  $\lambda = 616$  nm was monitored in lifetime studies. All the excitation wavelengths,  $\lambda = 262$  nm,  $\lambda = 285$  nm and  $\lambda = 395$  nm were used each giving the same rate of decay. At low concentrations,  $< 7.35$  mM of **Eu.15** the hydration state is observed at  $q = 2$ ; for high concentrations, 15 – 40 mM of **Eu.15** the hydration state is observed at  $q = 0$ , (Table 4.2).

Concentration (mM)	$\lambda_{em} / \text{nm}$	$\lambda_{ex} / \text{nm}$	$k_{\text{H}_2\text{O}} (\text{ms}^{-1})$	$k_{\text{D}_2\text{O}} (\text{ms}^{-1})$	$q$
14.7	395 / 262 / 285	616	5.1	4.81	0
7.35	395 / 262 / 285	616	3.93	2.43	1.5
3.67	395 / 262 / 285	616	3.46	1.79	1.7
1.83	395 / 262 / 285	616	3	1.4	1.6
1.47	395 / 262 / 285	616	3.15	1.27	1.9
0.73	395 / 262 / 285	616	2.79	1.02	1.8
0.36	395 / 262 / 285	616	2.66	0.86	1.9
0.18	395 / 262 / 285	616	2.65	0.79	1.9

Table 4.2 Rate constants,  $k$ , and derived hydration states,  $q$ , for the decay of **Eu.15**

At higher concentrations the hydration state is zero, although the life times are shorter, compared to that of the lower concentrations, this suggests that the assembly of the dimer results in greater quenching of the excited state. The lifetimes are much shorter when the triazole is bound to the metal centre, much like **Eu.5a** from Chapter 2, and when the triazole is not bound at low concentrations, lifetimes are longer, much like **Eu.8** from Chapter 3 which has no triazole to bind to the metal centre.

The dimer of **Eu.15** can be observed in the  $^1\text{H}$  NMR spectrum (400 MHz, pD 7.0, 278K) at high concentrations, the spectrum resembles that of a rigid eight-coordinate unsymmetrical Eu(III) complex exhibiting a broad range of resonances from -18 to 33.5 ppm. Four resonances shifted to highest frequency correspond to four axial ring hydrogens of the square antiprismatic geometry ( $\Delta(\lambda\lambda\lambda\lambda)/\Lambda(\delta\delta\delta\delta)$ ),  $\delta$  35.1, 34.3, 32.4, 30.2 ppm. This suggests triazole coordination to Eu(III), as seen in **Eu.5a** and **Eu.5c** (Chapter 2)<sup>21,22</sup> unlike **Eu.5a** and **Eu.5c**, which exhibit intramolecular triazole coordination, this must be from second **Eu.15**, as the appended *p*-benzyl-1,2,3-triazole is far too rigid and remote to bind to the metal centre, in an intramolecular manner. Therefore, the likely explanation is intermolecular triazole coordination. There are also broad resonances observed at 2 ppm and 4 ppm corresponding to the ethyl group. Attempts to dilute the NMR solution to generate the monomer resulted in a broadening of the resonances as the speciation changes to favour the broad featureless spectrum of the monomeric seven-coordinate complex. The electronic absorption spectrum shows absorptions at  $\lambda = 242$  nm, corresponding to the benzyl group and a less intense peak at  $\lambda = 297$  nm, of the 1,2,3-triazole subunit.

The luminescence and  $^1\text{H}$  NMR data provide compelling evidence for the formation of the self associating dimer **Eu.15**.

#### 4.3.2 Luminescence studies of **Tb.15**

**Tb.15** was synthesised from **Tb.8** and bromoethane under ‘click’ conditions, to give a white solid, 42% yield. **Tb.15** is a seven-coordinate complex; it was expected to bind two solvent molecules. **Tb.15** shows concentration dependent self-association as seen in Figure 4.11 (*cf.* **Eu.15**). The excitation spectra of **Tb.15** (Figure 4.11) at various concentrations, (the intensity per unit concentration of complex is plotted). Monitoring the emission at  $\lambda = 564$  nm,  $\Delta J = 1$  transition, this shows intense maximum at  $\lambda = 254$  nm and  $\lambda = 285$  nm, similar to that of **Eu.15**. The most concentrated solution has the lowest intensity per unit

concentration of complex and the least concentrated sample has the highest intensity per unit concentration. This again suggests (*cf.* **Eu.15**) that at higher concentrations a dimer is formed, and despite the decrease in hydration state, the relative intensity of the compound decreases, for similar reasons to that of **Eu.15**, the data suggests self-association.

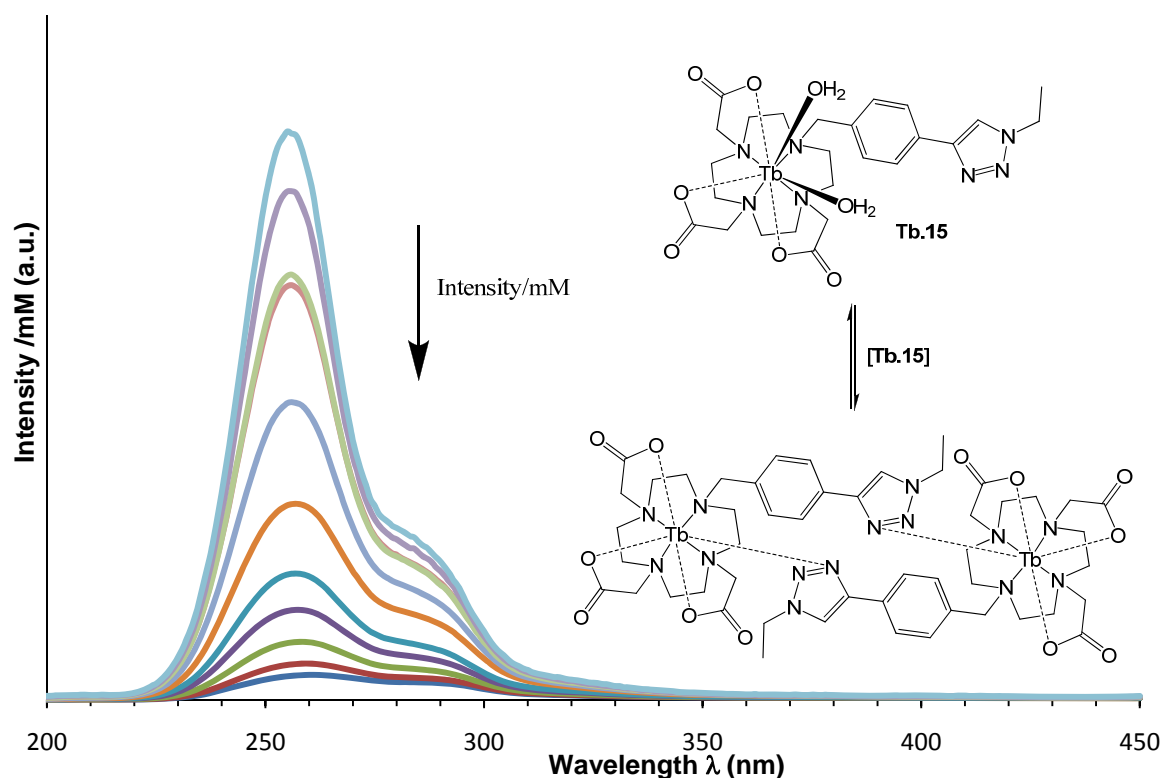


Figure 4.13 Variation in the excitation spectrum of **Tb.15**, as  $[\text{Tb.15}]$  is varied,  $\lambda_{em} = 546 \text{ nm}$ ,  $\text{H}_2\text{O}$ , 298K, pH 6.

The form of the excitation spectrum of **Tb.15** in Figure 4.13 is very similar to that of the excitation spectrum of **Eu.15** in Figure 4.12, this suggests that self-association is occurring at similar concentrations. The decrease in intensity per unit concentration of  $[\text{Tb.15}]$  is increased, suggests that **Tb.15** also self-associates and that  $\pi - \pi$  stacking between phenyl rings aid this self-association. There is also a shift in observed maximum sensitisation in increasing of concentration from 254 nm to 262 nm, this also supports a dimerisation event.

The  $\Delta J = 1$  transition, at  $\lambda = 546 \text{ nm}$  was monitored during luminescence lifetime studies to determine  $q$ . Lifetimes were recorded at three excitation wavelengths,  $\lambda = 260 \text{ nm}$ ,  $\lambda = 285 \text{ nm}$  and  $\lambda = 355 \text{ nm}$ , and as expected the same rates of decay were found for all wavelengths. At lower concentrations, ( $< 7 \text{ mM}$ ) of **Tb.15** the hydration state is calculated as  $q = 2$ , for higher concentrations, (30 – 40 mM) of **Tb.15** the hydration state is

calculated at  $q = 0$ , (Table 4.3). This is a similar result to that obtained for **Eu.15**, *i.e.* this suggests dimerisation occurs at lower concentrations for **Tb.15** than **Eu.15**; this can be explained by the change in ionic radius moving from with Eu(III) (1.07 Å) to Tb(III) (1.04 Å), which may well affect the tightness of binding of the triazole, and thus the concentrations at which self association occurs.

Concentration (mM)	$\lambda_{em} / \text{nm}$	$\lambda_{ex} / \text{nm}$	$k_{H_2O} (\text{ms}^{-1})$	$k_{D_2O} (\text{ms}^{-1})$	$q$
40.7	355 / 260 / 285	546	2.51	2.39	0.3
29.1	355 / 260 / 285	546	2.21	2.05	0.5
20.3	355 / 260 / 285	546	1.94	1.69	0.9
14.5	355 / 260 / 285	546	1.73	1.42	1.3
10.1	355 / 260 / 285	546	1.5	1.19	1.2
7.27	355 / 260 / 285	546	1.31	1.04	1
3.63	355 / 260 / 285	546	1.11	0.83	1
1.81	355 / 260 / 285	546	0.96	0.65	1.2
1.45	355 / 260 / 285	546	0.93	0.62	1.2
0.72	355 / 260 / 285	546	0.84	0.52	1.3
0.36	355 / 260 / 285	546	0.89	0.46	1.8

Table 4.3 Rate constants,  $k$ , and derived hydration states,  $q$ , for the decay of **Tb.15** at various concentrations.

At higher concentrations the hydration state is zero, although the lifetimes are shorter, compared to that of the lower concentrations, this suggests that the assembly of the dimer results in quenching from the excited state, presumably through an energy transfer mechanism involving the triazole a photoinduced electron transfer mechanism is unlikely for **Tb.15** *cf.* **Eu.15**.

#### 4.3.3 Characterisation of **Y.15**

**Y.15** was isolated as a white hygroscopic solid at 36% yield, from **Y.8** and bromoethane under ‘click’ conditions. **Y.15** is a seven-coordinate complex like **Eu.15** and **Tb.15**, Yttrium is non-paramagnetic, and therefore is more amenable to  $^1\text{H}$  NMR spectroscopy as chemical shift values and line widths are not affected as they are for paramagnetic analogues; these display increased spectral line broadening due to the inherent paramagnetism. The  $^1\text{H}$  NMR spectrum (Figure 4.12) shows four  $^1\text{H}$  broadened

overlapping doublets at 8.10-8.60 ppm this is attributed to the aromatic para-substituted benzene ring; these resonances have become inequivalent and broad due to dimerisation. The weak shifted doublet at 8.3 ppm could possibly be monomer, the spectrum also shows a broad 1H singlet at 8.75 ppm representing the CH of the 1,2,3-triazole. The metal free proligand would look very different in the aromatic region with two 2H doublets representing the para-substituted ring *cf.* **10** (Chapter 3). The electronic absorption spectrum shows absorptions at  $\lambda = 255$  nm and  $\lambda = 297$  nm, the peak at  $\lambda = 255$  nm correlates to the  $\pi$ - $\pi^*$  transition of the benzyl ring and the peak at  $\lambda = 297$ . This is similar to the electronic absorption and excitation spectra of **Eu.15** and **Tb.15**.

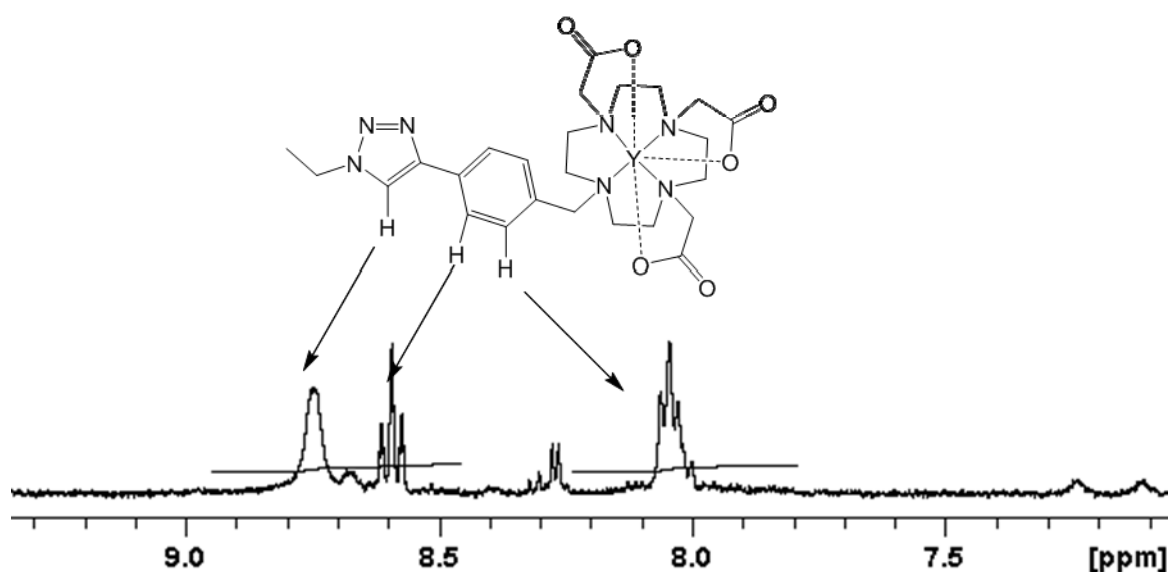


Figure 4.14 Expansion of the  $^1\text{H}$  NMR spectrum of **Y.15** (400 MHz, 278K).

The luminescence, NMR and electronic absorption studies of **Eu.15**, **Tb.15** and **Y.15**, suggest that at higher concentrations these complexes can form dimers, through intermolecular binding of the triazole to an adjacent Ln centre. All the data suggests that **Gd.15** will also form a dimer at higher concentration, with a hydration state  $q = 0$  and at lower concentrations **Gd.15** will be a monomer with a hydration state  $q = 2$ .

#### 4.4 Bimetallic complexes Containing Lanthanides and Rhenium

Given the relative ease of synthesis of Ln complexes appended with phenyl triazoles, it became apparent that these potential could be used for more than a means of linking Ln-chelates to other molecules, *i.e.* as dual modal contrast agents. The model

compounds (Section 4.2) show that the phenyltriazole can act as a cyclometallating ligand for transition metal ions such as Re(I), given this synthesis of a bimetallic *d-f* hybrid contrast agent might be possible. A Gd(III)DO3A based chelate appended *p*-benzyl-1,2,3-triazole unit for Re(I) cyclometallation, could in theory act as a dual modal MR-fluorescent probe (Figure 4.15).

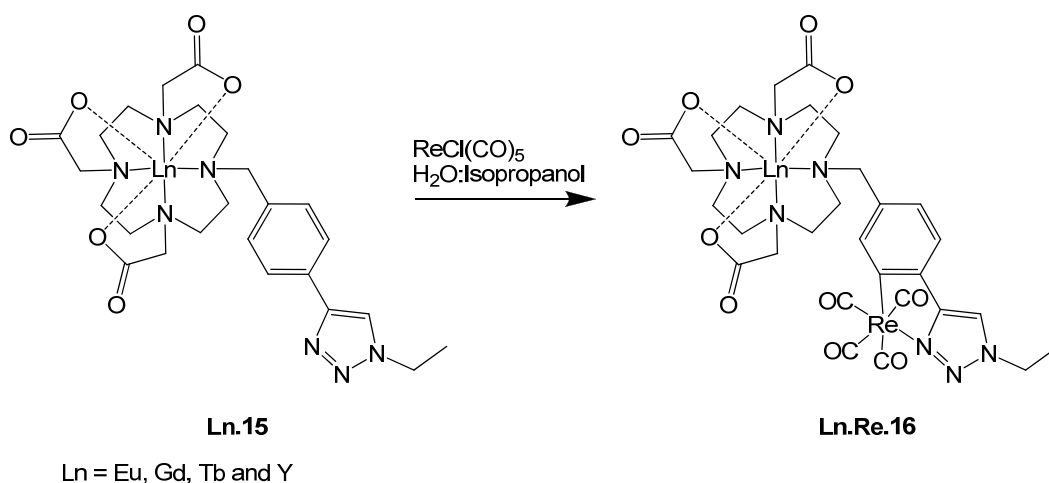


Figure 4.15 *d-f* hybrid bimetallic contrast agent **L.Re.16**

**Ln.15** was synthesised to coordinate Re(I) and generate a luminescent complex. Re(I) phenylpyridine complexes can show long luminescent lifetimes  $\sim 1 \times 10^{-6}$  s,<sup>12</sup> and the Re(I) phenyl-1,2,3-triazoles are expected to show similar luminescent properties. Re(CO)<sub>5</sub>Cl and **Ln.15** were heated by microwave irradiation for 30 minutes in isopropanol / water mixture (3:1) to synthesise **Ln.Re.16**.

#### 4.4.1 Luminescence studies of **Eu. Re.16**

**Eu.Re.16** was synthesised from **Eu.15** and Re(CO)<sub>5</sub>Cl, in a 53% yield. The electronic absorption spectrum shows absorptions at  $\lambda = 263$  nm, the peak at  $\lambda = 263$  nm corresponds to benzyltriazole chromophore. The absence of an absorption around  $\lambda = 280$  nm suggests coordination of Re(I) to the 1,2,3-triazole. The emission spectrum shown in Figure 4.16, shows only luminescent emission from the Re(I) complex, no characteristic Eu(III) emission is observed when a range of excitation wavelengths were used (*e.g.* direct at  $\lambda = 395$  nm, indirectly to the benzyl chromophore at  $\lambda = 262$  nm and  $\lambda = 370$  nm, the <sup>1</sup>MLCT of the bound Re(I) complex).

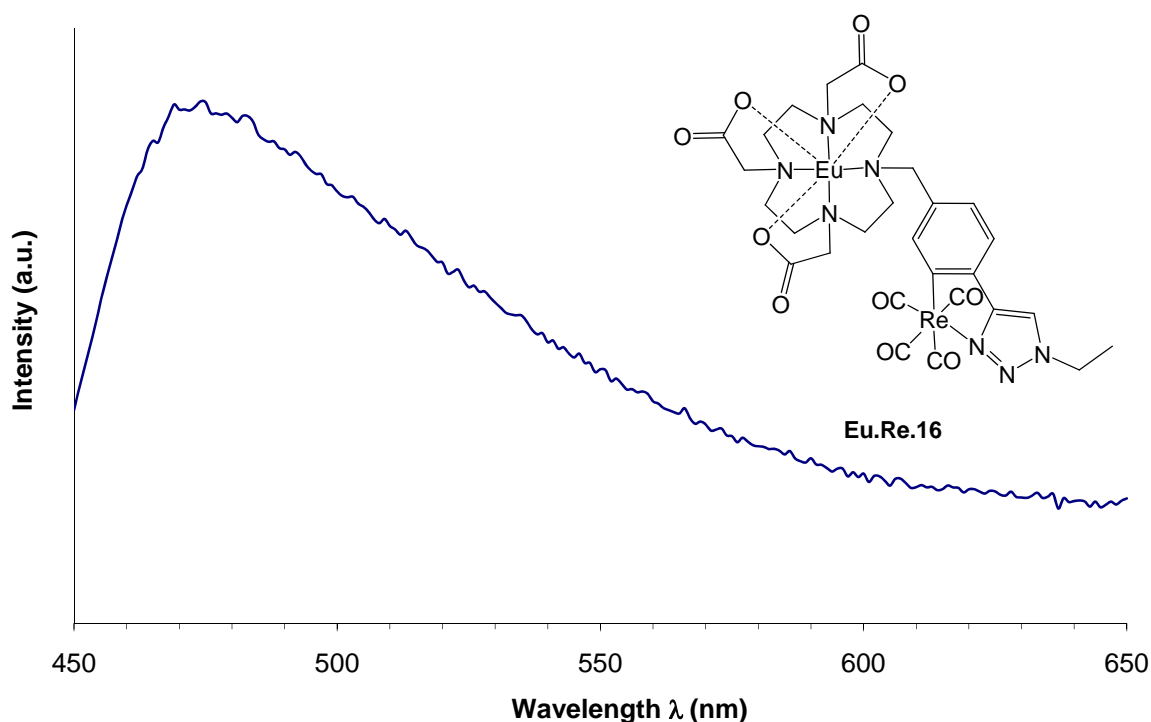


Figure 4.16 Luminescence Emission spectrum for **Eu.Re.16**, ( $\lambda_{ex} = 370$  nm,  $H_2O$ , pH = 7).

There is no evidence of Eu(III) emission, only luminescence is observed with an emission maximum at  $\lambda = 472$  nm, (when excited *via* the  $^1MLCT$  band at  $\lambda = 370$  nm). This resembles the emission profile of the model compound **14**. The absence of Eu(III) luminescence suggests the phenyltriazole chromophore acted as a moderate sensitizer for Eu emission in **Eu.15**; however this moiety is coordinated to Re(I) *via* cyclometallation. The photophysical properties of the chromophore are now changed and emission now occurs from the Re complex or irradiation from the phenyltriazole to Eu(III).

#### 4.4.2 Characterisation of **Tb.Re.16**

**Tb.Re.16** was synthesised from **Tb.15** and  $Re(CO)_5Cl$ , in a 42% yield. The UV-visible spectra shows absorbance at  $\lambda = 262$  nm, the peak at  $\lambda = 262$  nm corresponds to the benzyltriazole chromophore. The absence of an absorption around  $\lambda = 280$  nm suggests coordination of Re(I) to the 1,2,3-triazole. The emission spectrum shown in Figure 4.17, shows only luminescent emission from the Re(I) complex, no characteristic Tb(III) emission is observed when a range of excitation wavelengths were used (*e.g.* direct at  $\lambda =$

355 nm, indirectly to the benzyl chromophore at  $\lambda = 262$  nm and  $\lambda = 370$  nm, the  $^1\text{MLCT}$  of the bound  $\text{Re(I)}$  complex)

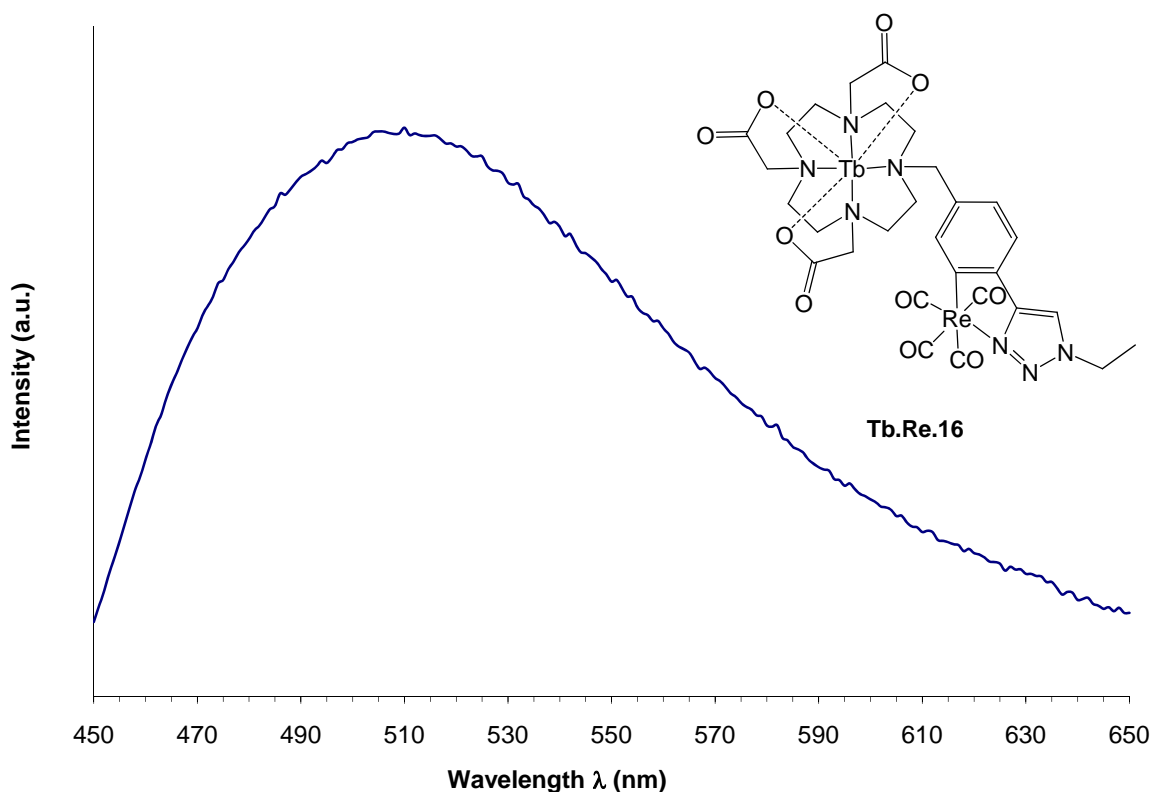


Figure 4.17 Luminescence emission spectrum for **Tb.Re.16**,  $\lambda_{\text{ex}} = 262$  nm,  $\text{H}_2\text{O}$ ,  $\text{pH} = 7$ .

As with **Eu.Re.16** there is no evidence of  $\text{Tb(III)}$  emission for **Tb.Re.16**, only  $\text{Re(I)}$  luminescence is observed with a maximum of  $\lambda = 508$  nm, when excited from the benzyl chromophore at  $\lambda = 262$  nm, this corresponds to the model compound **14**. This corresponds to the observation seen in Figure 4.14 for **Eu.Re.16**.

#### 4.4.3 Characterisation of **Y.Re.16**

**Y.Re.16** was synthesised from **Y.15** and  $\text{Re(CO)}_5\text{Cl}$ , in an 86% yield. The electronic absorption spectrum shows absorption at  $\lambda = 255$  nm, the peak at  $\lambda = 255$  nm corresponds to the  $\pi\text{-}\pi^*$  transition of the benzyl chromophore. The absence of an absorption around  $\lambda = 297$  nm suggests coordination of  $\text{Re(I)}$  to the 1,2,3-triazole as seen in Figure 4.17, which shows the various electronic absorption spectra for **Y.8** to **Y.Re.16**.

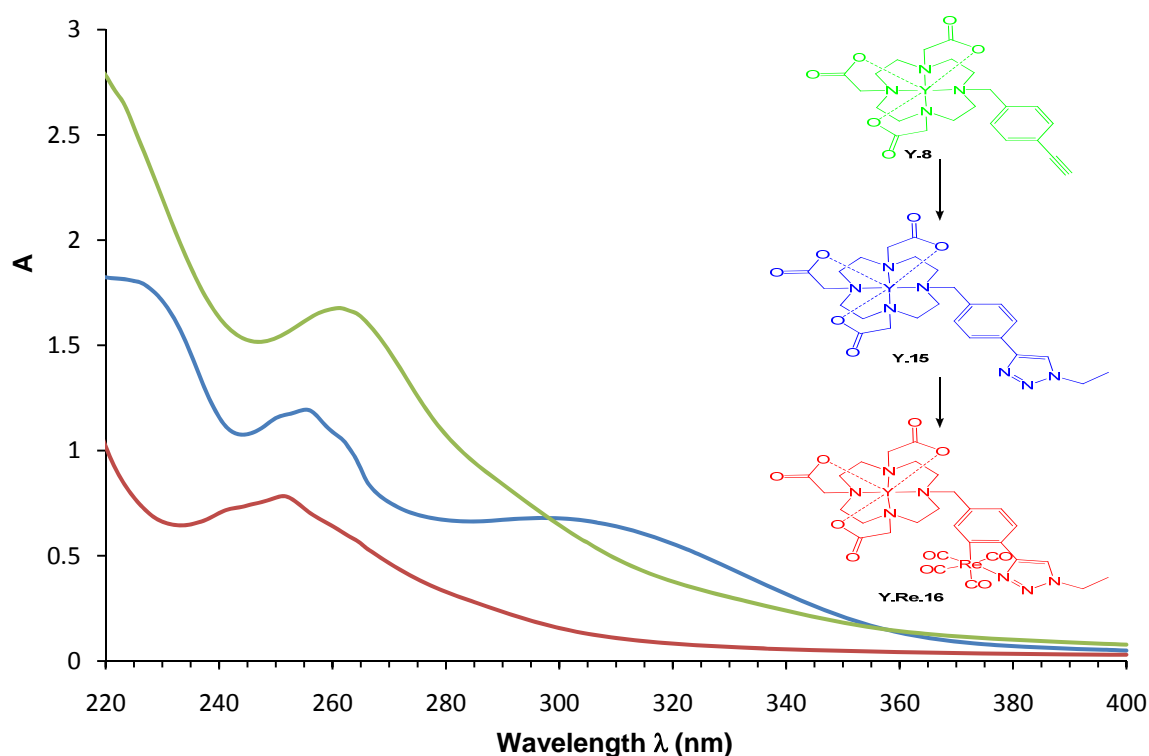


Figure 4.18 The electronic absorption spectra of **Y.8** (Green), **Y.15** (blue) and **Y.Re.16** (red) in H<sub>2</sub>O.

The emission spectra for **Y.Re.16**, shows luminescence from the Re(I) complex at  $\lambda = 450$  nm, when excited at  $\lambda = 262$  nm, this is similar to the maximum observed for both Eu(III) and Tb(III) compounds. The Re(I) emission observed is that of a complex, it is different to that of Re(CO)<sub>5</sub>Cl, the <sup>1</sup>H NMR spectra shows changes in the form of aromatic region of **Y.10** to **Y.Re.16**. Changes in the four 1H broadened doublets overlapping at 8.10-8.60 ppm which is typical of the aromatic para substituted benzyl ring, to three 1H broad multiplets between 7.90 and 8.75ppm. The broad 1H singlet at 8.75 ppm representing the CH of the 1,2,3-triazole shifts to 8.95 ppm. All this data suggests that **Y.Re.16** has been synthesised, although it could also be a mixture of Re(I) complexes; as shown from the model reaction, cyclometallated, double bridged and cyclometallated plus monodentate complexes can be formed.

#### 4.5 *p*-Benzyl Appended Gd(III) Complexes

**Gd.8**, **Gd.15** and **Gd.Re.16** were synthesised, all three complexes are expected to be seven-coordinate, just like the analogues Eu(III), Tb(III) and Y(III) complexes. This suggests that two waters will coordinate to the Gd(III) complex. No relaxivity data has been

obtained for the Gd(III) complexes; however, Re(I) luminescence has been observed for **Gd.11/Re.1**, with an emission maximum of  $\lambda = 457$  nm, when excited at  $\lambda = 262$  nm, this is in line with the observations for the **Ln.Re.16** complexes. Figure 4.18 shows the observed Re(I) luminescence of **Gd.Re.16**.

The electronic absorption spectrum shows absorption at  $\lambda = 262$  nm, the absorbance at  $\lambda = 262$  nm corresponds to the  $\pi$ - $\pi^*$  transition of the benzyl chromophore. The absence of an absorption around  $\lambda = 280$  nm suggests coordination of Re(I) to the 1,2,3-triazole.

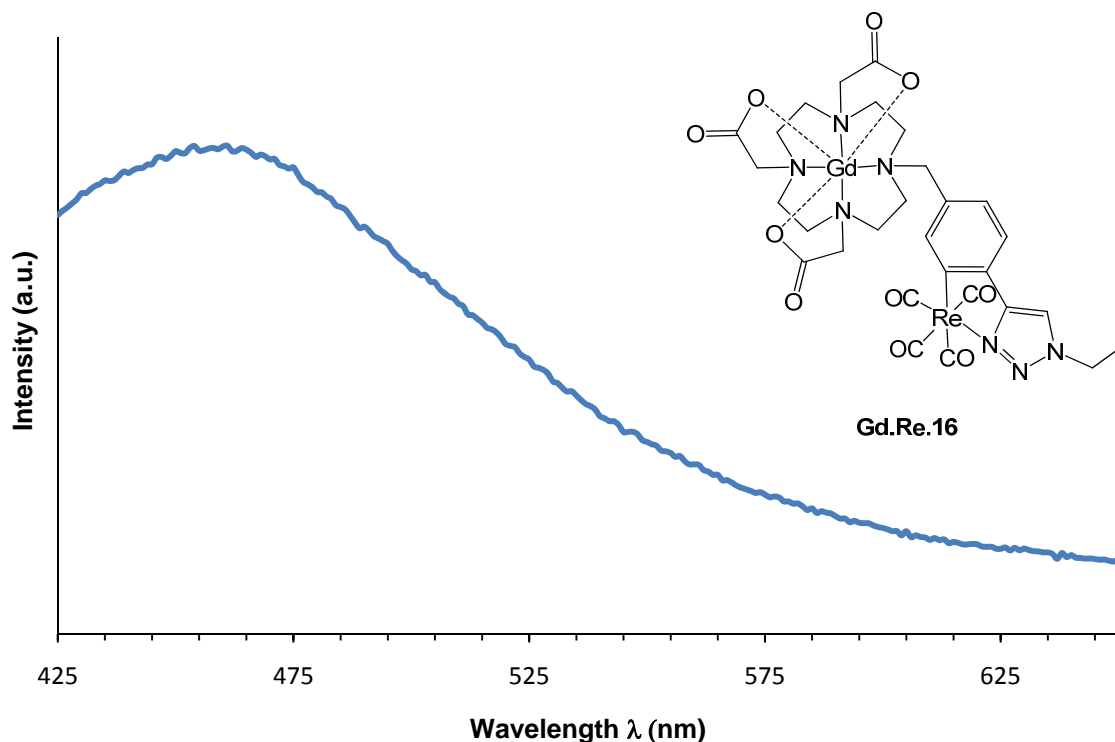


Figure 4.19 Luminescence emission spectrum of **Gd.Re.16**,  $\lambda_{ex} = 262$  nm, H<sub>2</sub>O, pH = 7.

#### 4.6 Summary and Conclusions

It has been demonstrated that *p*-benzyl-1,2,3-triazole appended Ln(III) complexes can be formed *via* the ‘Huisgen’ Cu(I) catalysed cycloaddition reaction between an alkyl halide and an alkyne appended lanthanide complex with *in situ* generation of the azide using sodium azide. The phenyltriazole that forms, can coordinate Re(I) to generate a bimetallic luminescent complex.

**Ln.15** has a hydration state  $q = 2$ , this can be formed from **Ln.8**, **Ln.15** has been shown to self-associate in solution, and this process is concentration dependent, above 10 mM the complex is fully dimerised and does not contain coordinated water, *i.e.* a hydration

state  $q = 0$ . It is postulated that  $\pi - \pi$  stacking of the phenyl rings acts as a driving force for self-association, with binding to the metal centre through either the N2 or N3 of the 1,2,3-triazole.

It was shown that Re(I) can be coordinated by phenyltriazole (**13**), in three different ways: cyclometallated between the N3 of the 1,2,3-triazole and the C5 of the benzene as in **14a**, secondly cyclometallated like **14a**, with a second phenyltriazole coordinating monodentate, **14b**. The third type of Re(I) coordination to **13** is through a di-Re-Cl bridged complex, coordinated to both the N2 and N3 of the 1,2,3-triazole as in **14c**, this has been verified by X-ray crystallography.

Bimetallic *d-f* hybrid molecules **Ln.Re.16**, were synthesised from **Ln.15** and  $\text{Re}(\text{CO})_5\text{Cl}$ , *via* microwave heating. Luminescence studies of **Eu.Re.16** and **Tb.Re.16** show only emission from coordinated Re(I). Irradiation of the chromophore now presumably means energy transfer to Eu/Tb is disfavoured. There is clearly no energy transfer from the  $^3\text{MLCT}$  of Re phenyltriazole to Eu(III). Studies of **Y.Re.16** show that Re is bound to the 1,2,3-triazole subunit, this is implied from the form of the  $^1\text{H}$  NMR spectra (cyclometallation of the phenyltriazole is suggested). Gd(III) Re(I) complexes can be formed; luminescent studies shows coordinated Re(I) emission, further tests on relaxivity must be done to test the efficiency of the potential dual modal contrast agent.

#### 4.7 References

1. L. E. Jennings and N. J. Long, *Chem. Commun.*, 2009, 3511.
2. A. Mishra, J. Pfeuffer, R. Mishra, J. Engelmann, A. K. Mishra, K. Ugurbil and N. K. Logothetis, *Bioconjugate Chem.*, 2006, **17**, 773.
3. M. Hueber, A. B. Staubli, K. Kustedjo, M. H. B. Gray, J. Shih, S. E. Fraser, R. E. Jacobs and T. J. Meade, *Bioconjugate Chem.*, 1998, **9**, 242.
4. T. Koullourou, L. S. Natrajan, H. Bhavsar, S. J. A. Pope, J. Feng, J. Narvainen, R. Shaw, E. Scales, R. Kauppinen, A. M. Kenwright and S. Faulkner, *J. Am. Chem. Soc.*, 2008, **130**, 2178.
5. B. Durham, J. V. Caspar, J. K. Nagle and T. J. Meyer, *J. Am. Chem. Soc.*, 1982, **104**, 4803.
6. V. C. Pierre, M. Botta, S. Aime and K. N. Raymond, *Inorg. Chem.*, 2006, **45**, 8355.

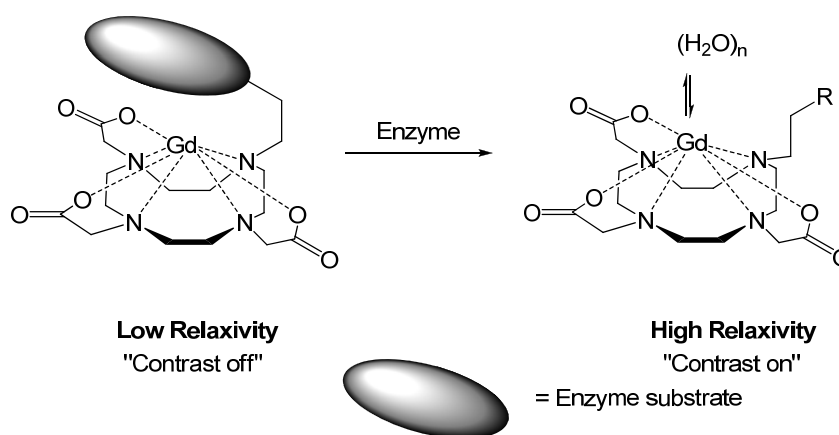
7. L. Moriggi, A. Aebischer, C. Cannizzo, A. Sour, A. Borel, J.-C. G. Bunzli and L. Helm, *Dalton Trans.*, 2009, 2088.
8. S. Aime, M. Botta, S. G. Crich, G. Giovenzana, R. Pagliarin, M. Sisti and E. Terreno, *Magn. Reson. Chem.*, 1998, **36**, S200.
9. K. Chen, Z. B. Li, H. Wang, W. Cai and X. Chen, *Eur. J. Nucl. Med. Mol. Imaging*, 2008, **35**, 2235.
10. P. Ray, A.M. Wu and S.S. Gambhir, *Cancer Res.*, 2003, **63**, 1160.
11. F.A. Cotton, G. Wilkinson, C.A. Murillo and M. Bochmann, *Advanced Inorganic Chemistry*, 6<sup>th</sup> Edition, Wiley, 1999.
12. P. J. Giordano and M. S. Wrighton, *J. Am. Chem. Soc.*, 1979, 2888.
13. T. L. Mindt, H. Struthers, L. Brans, T. Anguelov, C. Schweinsberg, V. Maes, D. Tourwe and R. Schibli, *J. Am. Chem. Soc.*, 2006, **128**, 15096.
14. P. Wu and V.V. Fokin, *Aldrichimica Acta*, 2007, **40**, 7.
15. M. Obata, A. Kitamura, A. Mori, C. Kameyama, J. A. Czaplewska, R. Tanaka, I. Kinoshita, T. Kusumoto, H. Hashimoto, M. Harada, Y. Mikata, T. Funabiki and S. Yano, *Dalton Trans.*, 2008, 3292.
16. S. R. Banerjee, A. Nagasawa and J. Zubieta, *Inorg. Chim. Acta*, 2002, **340**, 155.
17. R. Wilberger, C. Krinninger, H. Piotrowski, P. Mayer and I-P Lorenz, *Eur. J. Inorg. Chem.*, 2004, 2488.
18. D. Donghi, G. D'Alfonso, M. Mauro, M. Panigati, P. Mercandelli, A. Sironi, P. Mussini and L. D'Alfonso, *Inorg. Chem.*, 2008, **47**, 4243.
19. P. S. Donnelly, S. D. Zanatta, S. C. Zammit, J. M. White and S. J. Williams, *Chem. Commun.*, 2008, 2459.
20. S. Faulkner and B. Burton-Pye, *Chem. Commun.*, 2005, 259.
21. M. Jauregui, W. S. Perry, C. Allain, L. R. Vidler, M. C. Willis, A. M. Kenwright, J. S. Snaith, G. J. Stasiuk, M. P. Lowe and S. Faulkner, *Dalton Trans.*, 2009, 6283.
22. G.J. Stasiuk and M.P. Lowe, *Dalton Trans.*, 2009, 9725.

## Chapter 5

### Towards MR Contrast Agents for Imaging Gene Expressions

#### 5.1 Introduction

There has been great interest in the development of 'smart' contrast agents that respond to physiological processes, such as changes in pH,<sup>1</sup> changes in metal ion concentration<sup>2</sup> and the presence of an enzyme,<sup>3</sup> which may be associated with a particular disease state. Several contrast agents have been designed which contain the substrate for a given enzyme.<sup>3</sup> Such substrates are incorporated into the molecule and mask the relaxometric properties of the contrast agent, causing low MR image intensity. Enzymatic cleavage of the masking groups results in increased relaxivity of the contrast agent and an increase in the MR image intensity, effectively "switching on" the contrast agent, often changing hydration state (Scheme 5.1).

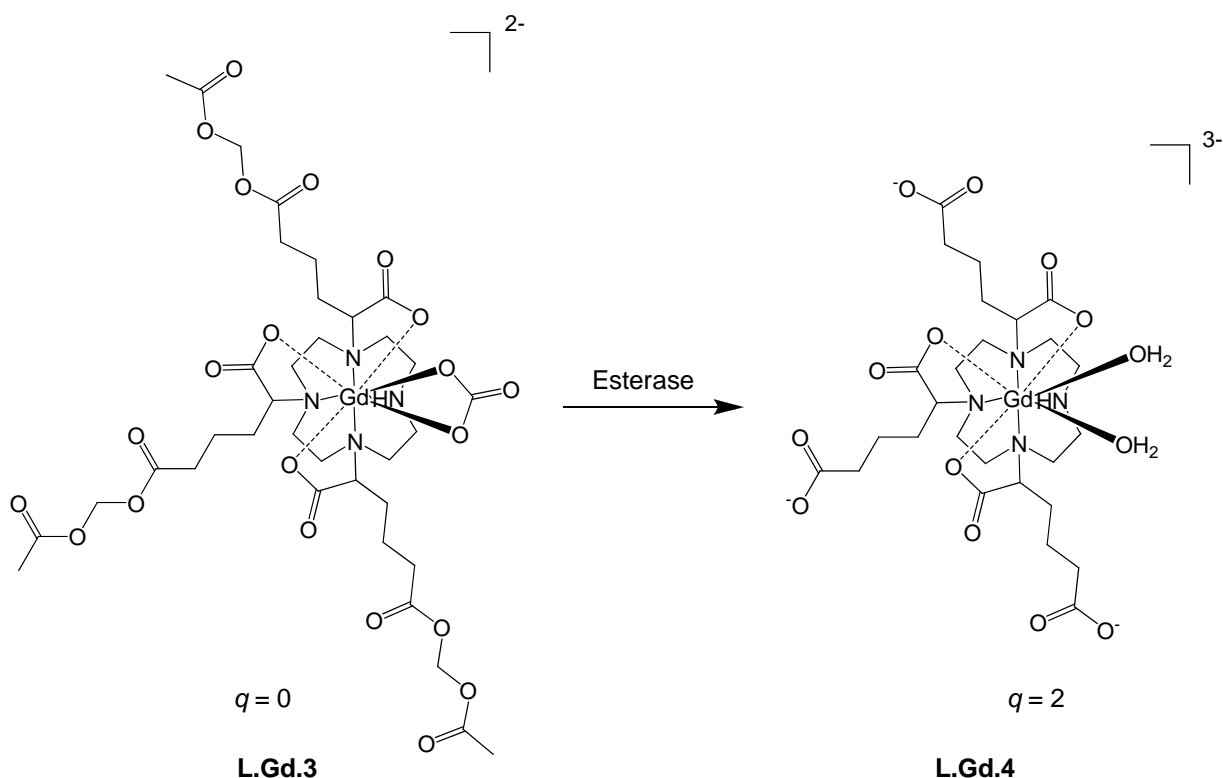


Scheme 5.1

In recent years the Lowe group has developed an enzyme activated agent that responds to the presence of esterase;<sup>3</sup> this is an enzyme that hydrolyses ester bonds. The neutral complex **L.Gd.3** (Scheme 5.2) is seven-coordinate with respect to ligand. Such complexes have a high affinity for binding anions such as carbonate (~ 20-30 mM), citrate (0.13 mM), lactate (2.3 mM) and phosphate (0.9 mM)<sup>4</sup> that are present in serum (approximate extracellular concentrations, shown in brackets). These all bind in a bidentate

manner (except phosphate which binds monodentate) to a  $q = 2$  neutral contrast agent, displacing the inner-sphere water.<sup>5</sup>

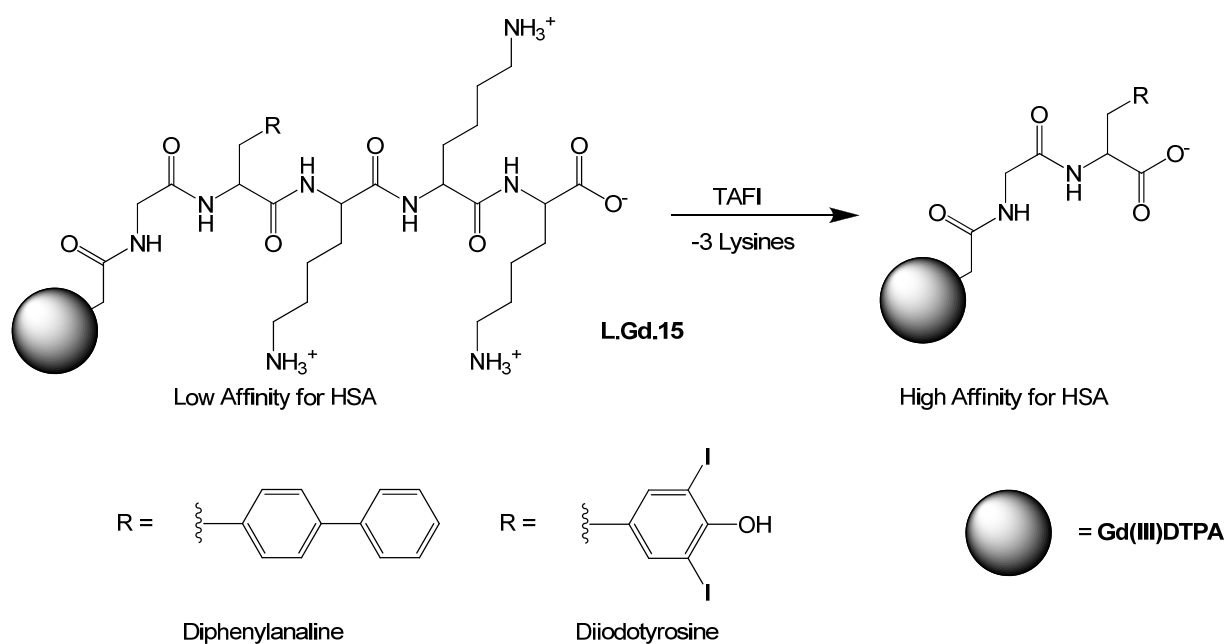
Under serum concentrations of carbonate **L.Gd.3** exists as a  $q = 0$  carbonate bound species in equilibrium with a  $q = 2$  species (at pH 7.4 ~ 60:40) and this has a lower than expected relaxivity. Upon interaction with the enzyme esterase the acetylmethoxy esters are cleaved, generating **[L.Gd.4]<sup>3-</sup>** which has a negative charge, this disfavours carbonate binding, giving a hydration state of  $q = 2$ , ‘switching’ on the contrast agent giving an 85% increase in relaxivity (Scheme 5.1). Relaxivities observed at physiological pH were measured as  $r_1 = \sim 10 \text{ mM}^{-1}\text{s}^{-1}$  and  $r_1 = \sim 6 \text{ mM}^{-1}\text{s}^{-1}$  for **[L.Gd.4]<sup>3-</sup>** and **L.Gd.3** respectively, suggesting a potential increase in MR image intensity upon enzyme activation.<sup>3</sup>



Scheme 5.2<sup>3</sup>

M<sup>c</sup>Murry and co-workers developed Gd(III)-DTPA based contrast agents incorporating either a diphenylalanine or a 3,5-diiodotyrosine group, **L.Gd.15**, both of which have a high affinity for human serum albumin (HSA).<sup>6</sup> Protein binding was suppressed by the incorporation of a tri-lysine peptide chain, known for its low affinity for HSA. These lysine residues are cleaved by carboxypeptidase B, thrombin-activatable fibrinolysis inhibitor (TAFI), which has been implicated in thrombotic disease. Enzymatic

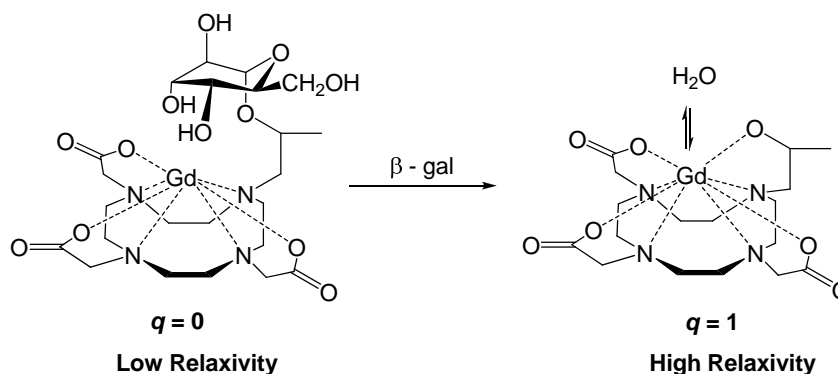
cleavage of the trilycine masking group results in the exposure of the moiety with an affinity for HSA binding. This leads to non-covalent attachment of the contrast agent to the slowly tumbling protein, resulting in a reduction of the rotational correlation time,  $\tau_R$ , and enhancement of relaxivity and thus MR image intensity (Scheme 5.3). Relaxivity was enhanced from  $r_1 = 11.1 \text{ mM}^{-1}\text{s}^{-1}$  to  $r_1 = 24.5 \text{ mM}^{-1}\text{s}^{-1}$  for the diphenylalanine derivative ( $\sim 120\%$  increase) and from  $r_1 = 9.8 \text{ mM}^{-1}\text{s}^{-1}$  to  $r_1 = 26.5 \text{ mM}^{-1}\text{s}^{-1}$  for the diiodotyrosine derivative ( $\sim 170\%$  increase) (4.5% w/v HSA, 20 MHz, pH 7.4 (PBS), 37°C).



Scheme 5.3

Meade and co-workers have developed an enzyme mediated MR gene expression agent; a  $\beta$ -galactose unit bound to a Gd(III) complex, that on entering the target cell expressing the reporter gene product,  $\beta$ -galactosidase, the  $\beta$ -galactose is cleaved from the probe, changing the nature of the probe and increasing signal intensity (Scheme 5.4).<sup>7</sup> The modulation of the hydration state,  $q$ , of a Gd-DO3A based contrast agent was achieved by the enzymatic cleavage of a galactopyranose, which was incorporated into the molecule to block the ninth Gd(III) coordination site from exchanging waters. The  $q = 0$  species will, therefore, have low relaxivity and hence low MR image intensity. Enzymatic cleavage of the galactopyranose results in the exposure of the final Gd(III) coordination site, which allows water exchange at the metal centre. Initial results showed a 20% increase in

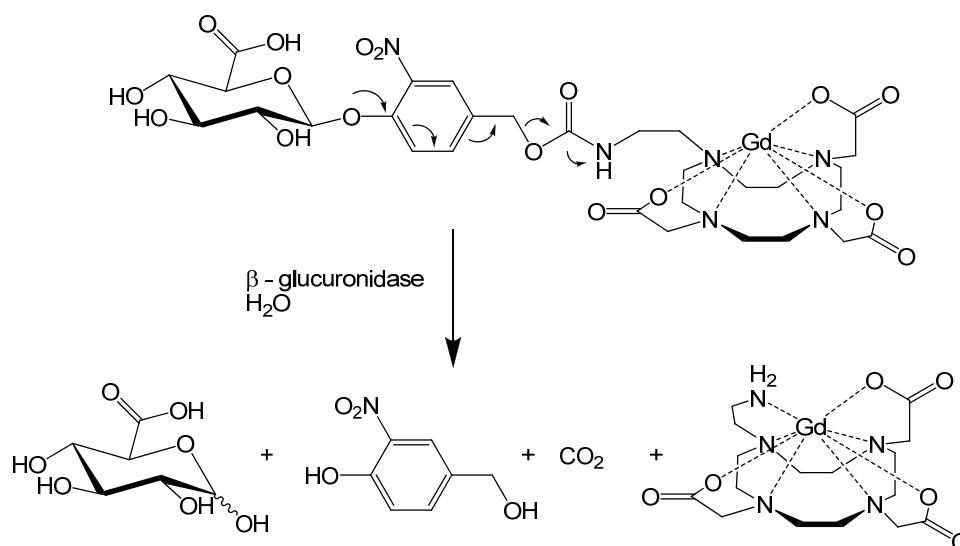
observed relaxivity upon  $\beta$ -gal activation.<sup>8</sup> The results were improved, however, by the addition of a  $\alpha$ -methyl to the sugar linkage arm, resulting in increased rigidity and steric hindrance to water exchange in the non-cleaved complex.



Scheme 5.4

The contrast agent has been used to detect *in vivo* transcription and translation in *Xenopus Laevis* embryos. One **L.Gd.16** labelled embryo was injected with a DNA construct carrying the lacZ gene, which encodes for  $\beta$ -gal, at the two-cell stage.<sup>7,8,9</sup> The subsequent MR image detected  $\beta$ -gal expression showing areas of enhanced MR image intensity, particularly in the eye, head and ventral regions. Initial experiments detected a 45-65% increase in relaxivity for embryos containing **L.Gd.L16** than for those that did not.

More recently the same group has adopted a similar strategy, incorporating a  $\beta$ -glucuronic acid moiety, a substrate for enzymatic cleavage by  $\beta$ -glucuronidase, which is found in high concentration in the proximity of cancer tumours.<sup>9</sup> Enzymatic hydrolysis of the pendant moiety, lead to the self-imolative generation of an eight-coordinate species, **L.Gd.17**. (Scheme 5.5). *In vitro* studies showed a non-cleaved species and the independently prepared cleaved species showed relaxivities of  $r_1 = 3.68 \text{ mM}^{-1}\text{s}^{-1}$  versus  $r_1 = 2.65 \text{ mM}^{-1}\text{s}^{-1}$  (pH 7.4, 10 mM MOPS buffer, 60 MHz, 37°C) respectively. The values were measured in a series of buffers and it was found that there was  $\sim 20\%$  difference in relaxivity between the two species. This was attributed to the higher hydration state of the non-cleaved complex. Upon addition of physiologically relevant carbonate concentrations (24 mM  $\text{NaHCO}_3$ ) to the buffered solutions a 20-30% drop in relaxivity was observed for the non-cleaved compound, while the cleaved species remained the same within error at  $r_1 = 2.64 \text{ mM}^{-1}\text{s}^{-1}$  and  $r_1 = 2.58 \text{ mM}^{-1}\text{s}^{-1}$  respectively (10 mM MOPS buffer, 60 MHz, 37°C).



Scheme 5.5

The seven-coordinate non-cleaved species, containing two vacant coordination sites, demonstrated almost an eight-fold higher affinity for carbonate binding than the eight-coordinate cleaved species. This displaces the inner-sphere waters and lowers relaxivity. Enzymatic hydrolysis using bovine liver  $\beta$ -glucuronidase was monitored *via* a continuous UV-visible assay, measuring the increased absorption of the 4-hydroxynitrobenzyl alcohol product.  $k_{cat}/K_m$  was measured as  $74.0 \pm 10.9 \text{ M}^{-1}\text{s}^{-1}$  using *p*-nitrophenyl- $\beta$ -D-glucuronide as a standard (1.0 mg/ml enzyme, 100 mM sodium phosphate, 0.01% (w/v) bovine serum albumin, pH 7.4, 37 °C). In human serum a 14% increase in relaxivity was observed after one hour in the presence of  $\beta$ -glucuronidase enzyme (60 MHz, 37 °C, pH 7.4).

### 5.1.1 Gene Therapy

Gene therapy is the insertions of genes into an individual's cells/tissue to treat a disease or hereditary disorder in which a defective mutant gene is replaced with a functional one.<sup>10</sup> A vector, which carries the gene, is used to implant it into the target cell *via* the process of transfection. Vectors in use are viruses, plasmids retroviruses and adenoviruses. The vector contains a gene construct, which is a length of DNA that is inserted into the vectors. This gene construct contains a specific promoter, transcription factors, the new gene, and a poly-A tail (splice site). Most vectors used are viruses, which

attack the host cell and introduce its genetic material into the host cell as part of their replication cycle. The genetic material contains instruction genes on how to replicate the virus by hijacking the host cells machinery, as shown in Figure 5.1.<sup>10</sup>

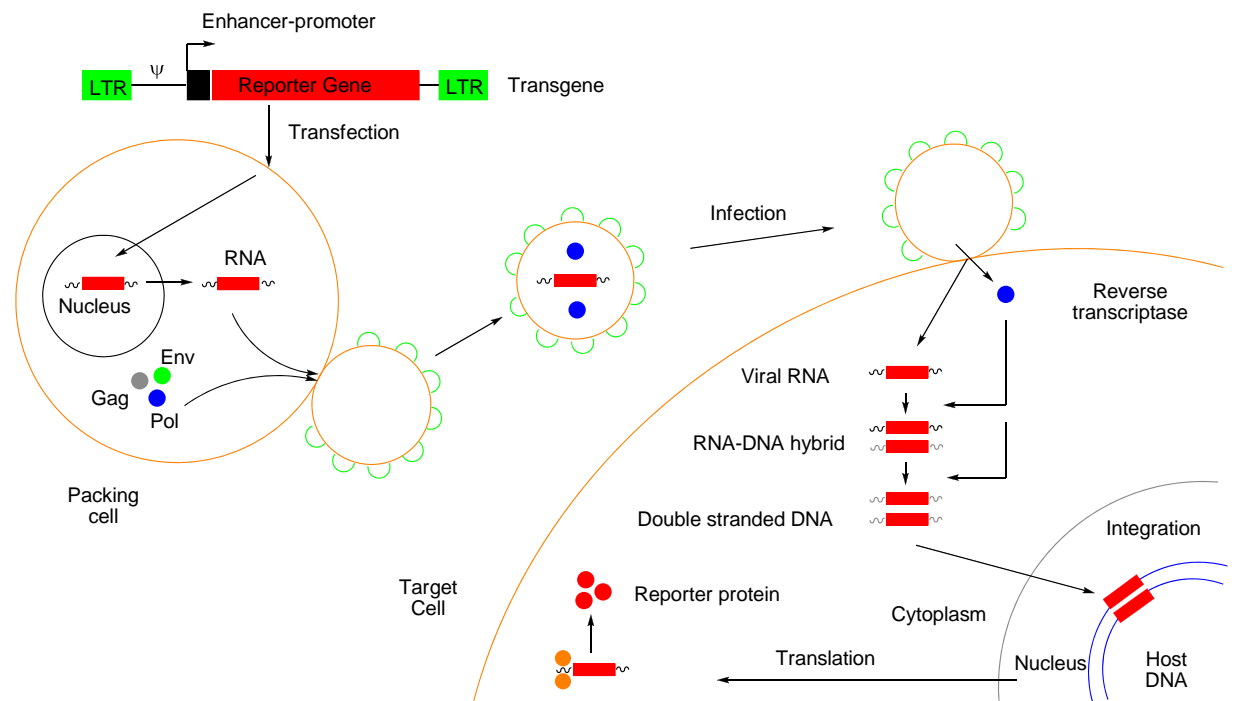


Figure 5.1 Infection, transfection and translation of virus genes into cells. For purposes of gene therapy.

Figure 5.1 show the lentivirus, a retrovirus, the process in which it transfects a reporter gene into the target cell. The reporter gene is transfects into the DNA of the packing cell, this cell produces a RNA template of the new recombined sequence containing the reporter gene construct. This is taken up in to the viral cell along with the enzyme reverse transcriptase, this enzyme turns the viral RNA into double stranded DNA once the vRNA has been introduced into the target cell. The double stranded DNA is then spliced into the target cells DNA and the new recombined DNA will be transcribed and translated giving the reporter gene product. The gene product is usually a protein that will stop cell proliferation, either stopping the cell signaling pathways or inducing the cell apoptosis pathways and terminating the cell. The reporter gene product is a protein that indicates whether the gene therapy has been taken up. The product will either be a visual probe like GFP or interact with a specific probe for PET or MR imaging.

### 5.1.2 Herpes Simplex Virus 1 Thymidine Kinase Reporter Gene

The Herpes Simplex Virus 1 Thymidine Kinase (HSV-TK) is a viral kinase enzyme that phosphorylates nucleoside analogues. The reporter gene construct contains an enhancer site and promoter site, which is at the 5' prime end of the construct, this is upstream of the gene encoding for HSV-TK. This is followed by a stop codon and a sequence of adenosine bases, which represents a splice site. For the purpose of gene therapy a second gene would be included downstream of the reporter gene, this gene would be the functional protein that replaces a faulty gene/protein. The HSV-TK reporter gene is the specific target for a PET imaging probe, containing thymidine analogues FIAU or FHBG, which will only be phosphorylated by the HSV-TK protein and not interact with endogenous mammalian TK1.<sup>11,12,13</sup>

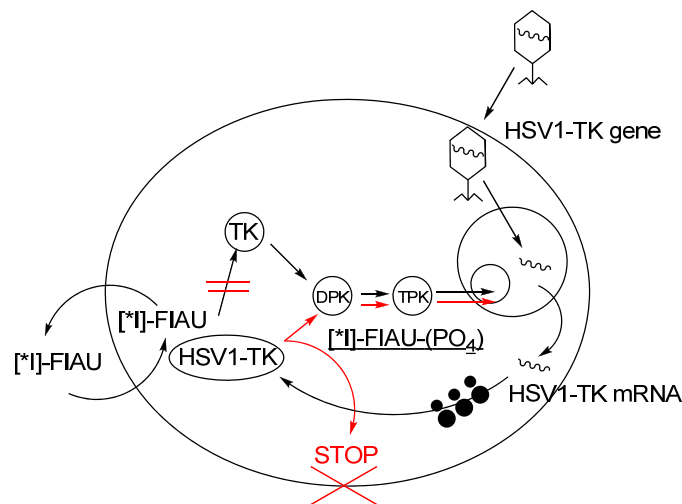
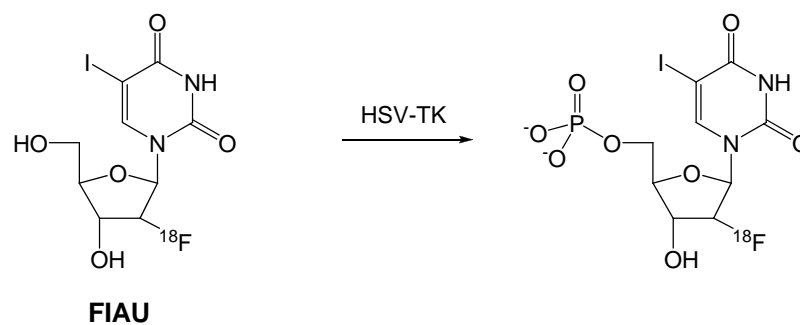


Figure 5.2 HSV1-TK gene being expressed in the cell and the gene product interacting with FIAU. Localising the PET agent within the cell.

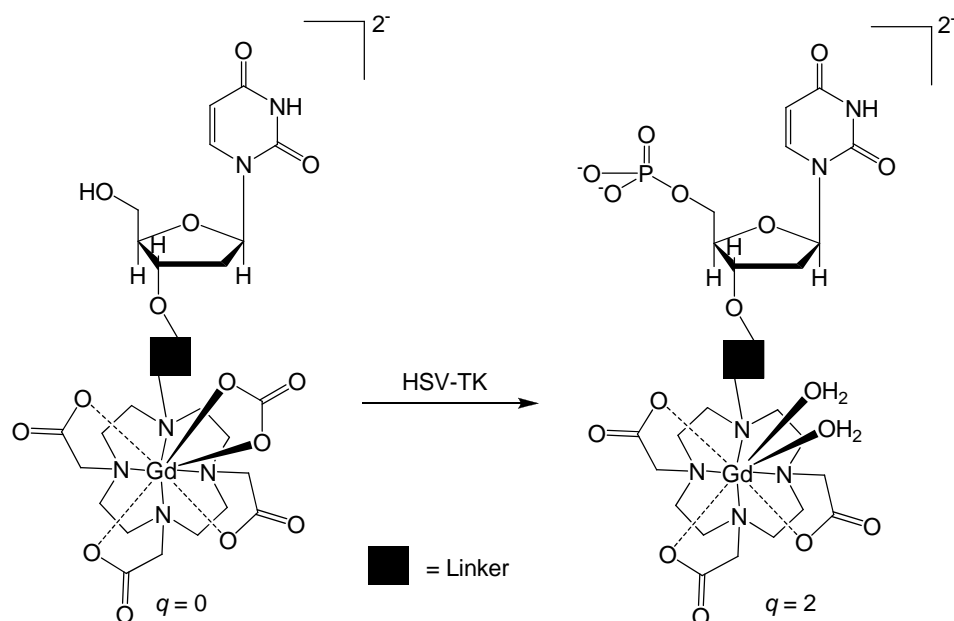
The probe moves freely in and out of cells/tissue until it reaches the target cell expressing the HSV-TK enzyme, HSV-TK phosphorylates the thymidine analogue part of the probe; this changes the nature and the charge of the molecule. The phosphorylated probe cannot pass through the cell membrane and is now trapped within the cell. This localisation of the probe is an increase of concentration within the cell and therefore increased signal intensity.<sup>11</sup>



Scheme 5.5 PET imaging agent 5-iodo-2'-fluoro-2'-deoxy-1-β-D-arabino-furanosyl-5-iodouracil (FIAU), which incorporate nucleoside bases, that enable imaging of HSV1-TK activity *in vivo*.

### 5.1.3 Target Complexes

The aim of this chapter was to develop an enzyme-activated MR contrast agent capable of imaging gene therapy. The hypothesis was: a uridine molecule (a non mammalian nucleoside) linked to a Gd(III)DO<sub>3</sub>A based complex will interact with the reporter gene enzyme, HSV1-TK. As with the PET agent FIAU, interaction with HSV1-TK would phosphorylate the uridine molecule changing the charge on the complex from neutral to negative. This would have two effects: localizing the agent within the cell undergoing gene therapy and potentially changing the hydration state of the agent. Gd(III)DO<sub>3</sub>A is a seven-coordinate complex, with respect to the ligand, allowing two water molecules to bind; however, within the body this will allow the endogenous anion carbonate to bind to the metal centre, displacing the inner-sphere water molecules. In an analogous manner to that discussed earlier as **L.Gd.3**, this will result in a reduction in MR signal intensity.<sup>3</sup> Interaction with the enzyme, in this case HSV1-TK, will phosphorylate the agent, changing the charge of the complex to -2, disfavouring carbonate binding, allowing two inner-sphere waters to occupy the metal centre, *i.e.* 'switching' on the agent. The 'smart' MR contrast agent would be accumulated and activated upon interaction with HSV1-TK (Scheme 5.6).



Scheme 5.6

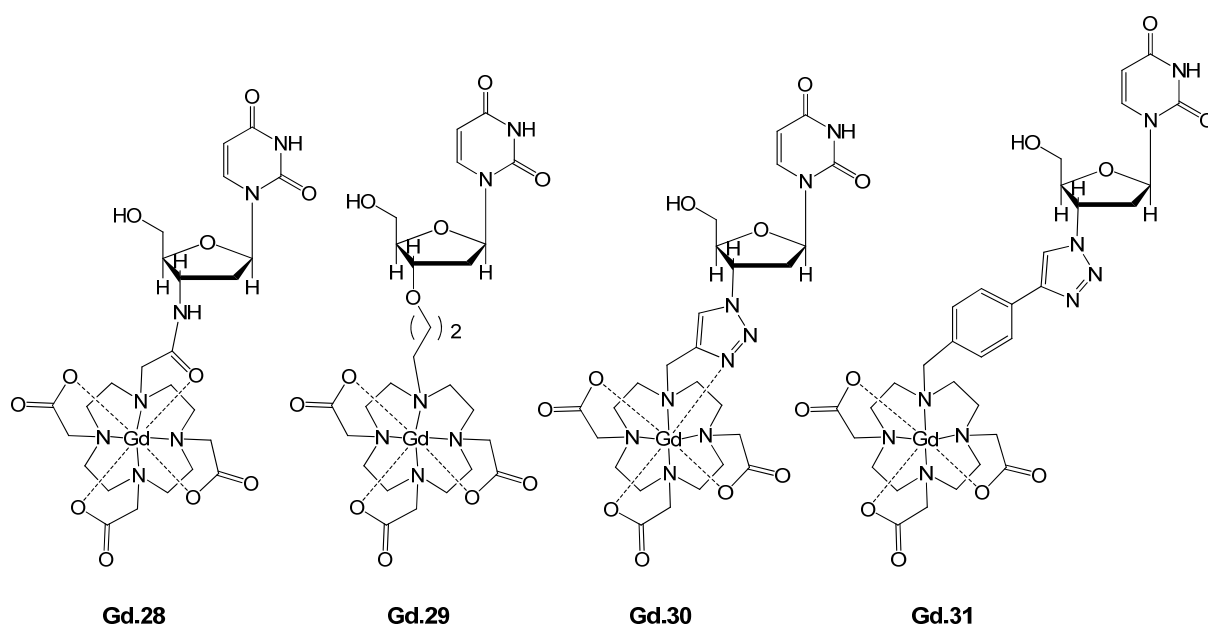


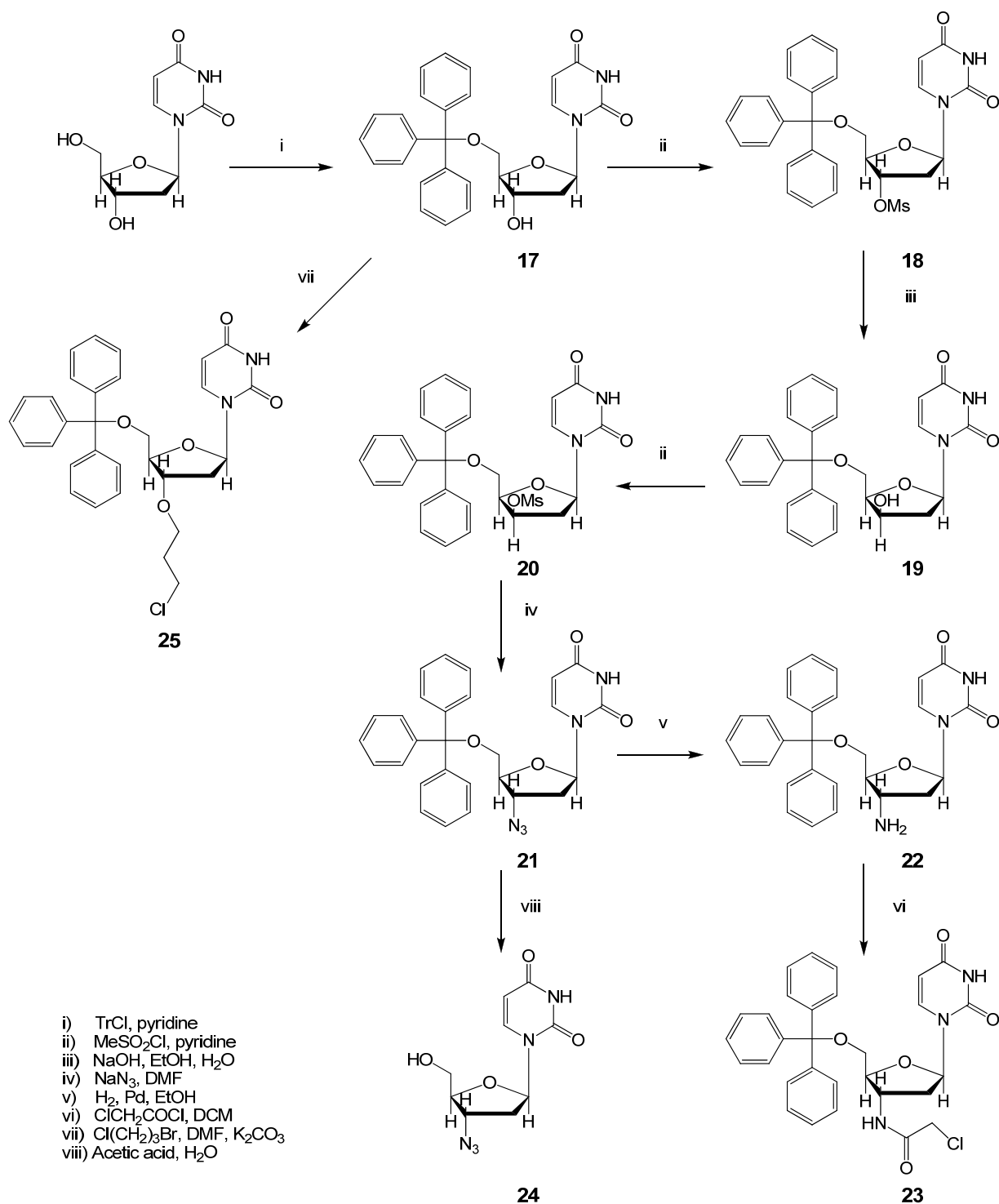
Figure 5.3 Proposed uridine linked, HSV1-TK activated MRI contrast agents

Figure 5.3 shows four different Gd(III) complexes of interest, showing the multiple linking strategies for attaching uridine to a Gd(III)DO3A-based chelate. The complexes were linked to a uridine molecule *via*: an amide, a propyl ether, or a 1,2,3-triazole generated by the ‘click’ reaction, either from a propargyl or *p*-benzylolethynyl-appended Gd(III)DO3A. **Gd.29** and **Gd.31** were expected to be seven-coordinate complexes and thus

be able to bind carbonate, hence, phosphorylation *via* HSV1-TK would change the charge of the complexes, potentially switching them on (as anion binding is disfavoured) and accumulating in the cell undergoing gene therapy. **Gd.28** and **Gd.30** are both eight-coordinate complexes and would be expected to act in a similar manner to the PET agent FIAU, *i.e.* upon phosphorylation *via* HSV1-TK they are expected to accumulate within the cell undergoing gene therapy.

To synthesise these compounds, multiple protection and transformations were used to retain uridine stereochemistry, about the O5 on the ribose sugar. Stereochemistry must be retained on uridine for biological activity, to allow the agent to fit into the active site of the HSV1-TK enzyme. If the macrocycle sits above the sugar in the same plane as the pyridinic base and the O3 on the ribose, the agent will not fit into the active site of the kinase preventing phosphorylation.

## 5.2 Uridine Transformations



Scheme 5.7

There are multiple synthetic steps to form **Ln.28 – Ln.31**, starting from uridine before linking to macrocycle, **1**. Scheme 5.7 shows all the uridine transformations before

attaching to a macrocycle, these synthetic steps are based on a paper by Mancini and Lin, whom synthesized compounds **17** to **22** and compound **24**.<sup>14</sup>

### 5.2.1 Formation of 5-Trityl-2-Deoxyuridine (**17**)

**17** was synthesised from uridine and trityl chloride in anhydrous pyridine (Scheme 5.7) as described by Horwitz *et al.*,<sup>15</sup> it was obtained as a white solid in 83% yield. Formation was indicated by ESMS(-) with a peak at  $m/z$  469 [M - H], and the <sup>1</sup>H NMR spectrum shows a 15H multiplet at 7.25 ppm corresponding to the hydrogens of the three phenyl rings of the trityl group. The yields are lower if there is any water present in the reaction, trityl hydroxide forms, which can be removed by washing with petrol ether 40-60. To increase the yield a catalytic amount of strong base can be added such as DMAP, as described by Hernades *et al.*<sup>16</sup> (synthesising a similar compound involved as an inhibitor of human mitochondrial thymidine kinase), the introduction of DMAP, takes the yield from 60% to 80%. There is also evidence of a second tritylation on the N2 of the uridine; this does not impede further reactions upon the uridine as there is no substitution at the O3 on the ribose ring.

### 5.2.2 Retention of Stereochemistry of the Uridine

For biological activity, stereochemistry must be retained around the ribose sugar, to allow the agent to fit into the active site of the HSV1-TK enzyme. This requires multiple synthetic steps from compound **17** to **21**. **17** to **18**, the transformation of O3 to a mesylate group, which is a significantly better leaving group than OH, is followed by a S<sub>N</sub>2 nucleophilic substitution (**18** to **19**), with hydroxide, inverting the stereochemistry around the ribose ring. Now with a different stereochemistry, the hydroxyl is mesylated again (**19** to **20**), followed by an S<sub>N</sub>2 nucleophilic substitution using azide, inverting the stereochemistry around the C3 of the ribose ring (**20** to **21**). This sequence of substitution reactions allows introduction of a functional group, which can be reacted further, whilst retaining the 'starting' stereochemistry around the ribose ring of uridine. This apparently convoluted synthesis enables the macrocycle to sit below the plane of the sugar, in theory unable to inhibit binding to the active site of the kinase, allowing phosphorylation, of the O5 by the enzyme.

### 5.2.3 Formation of 3'-O-Methanesulfonyl-5'-O-Trityl-2'-Deoxyuridine (**18**)

**18** was synthesised from **17** and mesolate chloride in anhydrous pyridine<sup>14</sup> (Scheme 5.7), it was obtained as a white solid in 72% yield. Formation was indicated by ESMS(+) with a peak at  $m/z$  571  $[M + Na]^+$  and the <sup>1</sup>H NMR spectrum shows a 3H singlet at 2.91 ppm corresponding to the methyl resonance of the mesylate group. This creates a better leaving group for the next step which is a S<sub>N</sub>2 substitution, inverting the stereochemistry around the C3 of the ribose sugar.

### 5.2.4 Formation of 1-[2-deoxy-5-O-(triphenylmethyl)-β-D-threo-pento-furanosyl]-uracil (**19**)

**19** was synthesised from **18** and NaOH in absolute EtOH (scheme 5.7)<sup>14</sup> it was obtained as a white solid in 99% yield. Formation was indicated by ESMS (-) with a peak at  $m/z$  469  $[M - H]^-$  the <sup>1</sup>H NMR spectrum shows the absence of the 3H singlet of the mesylate at 2.91 ppm, confirming substitution has occurred, the 1H doublet of doublets resonance at 4.42 ppm represents the CH of C3 which has shifted from 5.29 ppm in compound **18**. This represents the formation of the OH on the C3 of the ribose ring, in an inverted stereochemistry to that of **17**. This is a S<sub>N</sub>2 nucleophilic substitution reaction, inverting the stereochemistry around the C3; a second S<sub>N</sub>2 reaction is then required to reinstate the original stereochemistry about the ribose ring.

### 5.2.5 Formation of 1-[2-deoxy-3-O-methanesulfonyl-5-O-(triphenylmethyl)-β-D-threo-pentofuranosyl]uracil (**20**)

**20** was synthesised from **19** and mesyl chloride in anhydrous pyridine (as in Scheme 5.7),<sup>14</sup> it was obtained as a white solid in 98% yield. Formation was indicated by ESMS(+) with a peak at  $m/z$  571  $[M + Na]^+$  and the <sup>1</sup>H NMR spectrum shows a 3H singlet at 2.68 ppm corresponding the methyl resonance of the mesyl group. The shift from 2.91 ppm in **18** to 2.68 ppm in **20**, confirms that there has been inversion of the stereochemistry around the C3 of the ribose ring.

### 5.2.6 Formation of 3-azido-5-O-trityl-2,3-dideoxyuridine uracil (**21**)

**21** was synthesised from **20** and sodium azide in DMF (Scheme 5.7),<sup>14</sup> it was obtained as a white solid in 64% yield. Formation was indicated by ESMS(-) with a peak at  $m/z$  494  $[M - H]^-$  the <sup>1</sup>H NMR spectrum shows the disappearance of the 3H singlet at 2.91 ppm, of the mesylate group. The 1H doublet of doublets resonance at 4.25 ppm corresponding to the CH of C3, this is shifted to 5.17 ppm in compound **20**. This confirms the presence of azide on the C3 of the ribose ring, with stereochemistry inverted to that of **19**. The spectrum now resembles that of **17** which also possesses this stereochemistry. This is a S<sub>N</sub>2 nucleophilic substitution reaction, inverting the stereochemistry of C3, reinstating the original stereochemistry about the ribose ring.

### 5.2.7 Formation of 3-amino-5-O-trityl-2,3-dideoxyuridine uracil (**22**)

**22** was synthesised from **21** *via* hydrogenation in absolute EtOH (Scheme 5.7), with catalytic amount of Pd on carbon.<sup>14,17</sup> **22** was obtained as a white solid in low yield (17%). Formation was indicated by ESMS(+) with a peak at  $m/z$  470  $[M + H]^+$ . The yield is particularly low for hydrogenation, as the relatively harsh conditions also remove the trityl group, freeing the hydroxyl of the O5. This is a facile separation from **22** by washing with dry methanol giving a lower yield.

## 5.3 Linking Uridine to Macrocycles

Compounds **23**, **24** and **25** were all synthesised by linking modified uridine to the macrocycle **1** or **Ln.4/Ln.8**. **23** is an chloroacetamide appended uridine which will attach to **1** as an amide linker, in the same manner as Parker and co-workers appending amino acids to Ln(III)DO3A.<sup>5</sup> **24** is an azide appended uridine which can be used in the Cu(I) catalysed cycloaddition ‘click’ reaction as discussed in Chapter 2.1. **25** is a propyl chloride appended uridine which will attaches to **1** *via* alkyl linker (Figure 5.4).

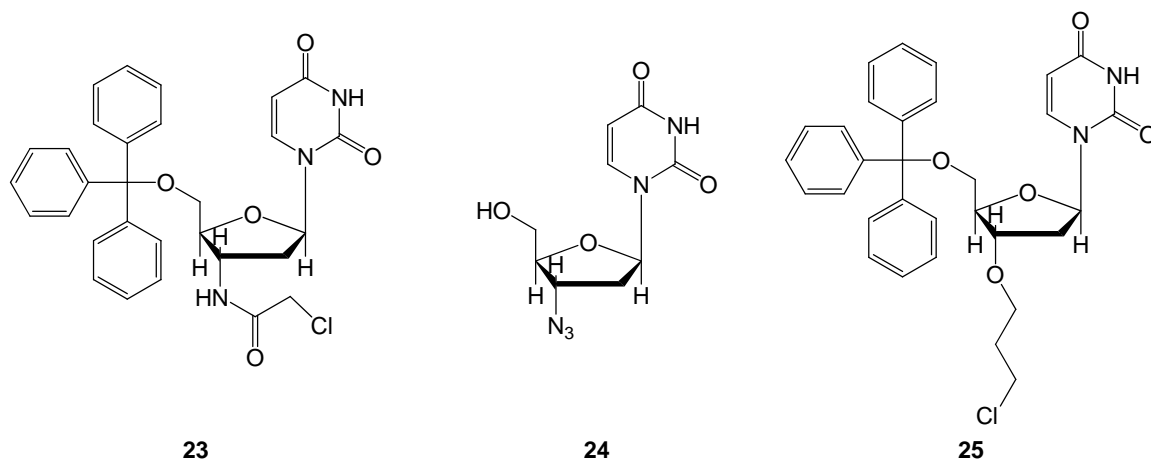


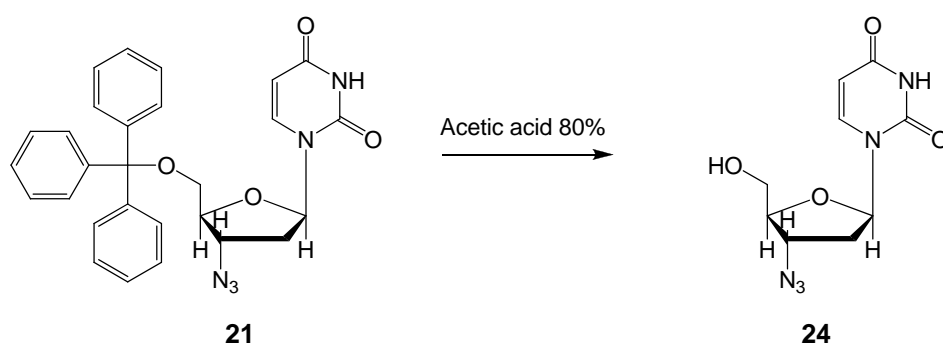
Figure 5.4

### 5.3.1 Formation of 3-chloroacetamide-5-O-trityl-2,3-dideoxyuridine (**23**)

**23** was synthesised from **22** and chloroacetyl chloride in DCM,<sup>5</sup> it was obtained as an orange oil in 57% yield. Formation was indicated by ESMS(-) with a peak at  $m/z$  544 [ $M - H$ ]<sup>-</sup> the <sup>1</sup>H NMR spectrum shows the appearance of a 2H singlet at 4.00 ppm, corresponding to the CH<sub>2</sub> resonance of the chloroacetamide. **23** was attached to **1** to form a macrocycle appended with a uridine linked *via* an amide through the C3 of the ribose ring. When deprotected and complexed, this was expected to form an eight-coordinate macrocycle for lanthanide coordination, allowing one solvent molecule to bind to the metal centre.

### 5.3.2 Formation of 3-azido-2,3-dideoxyuridine (**24**)

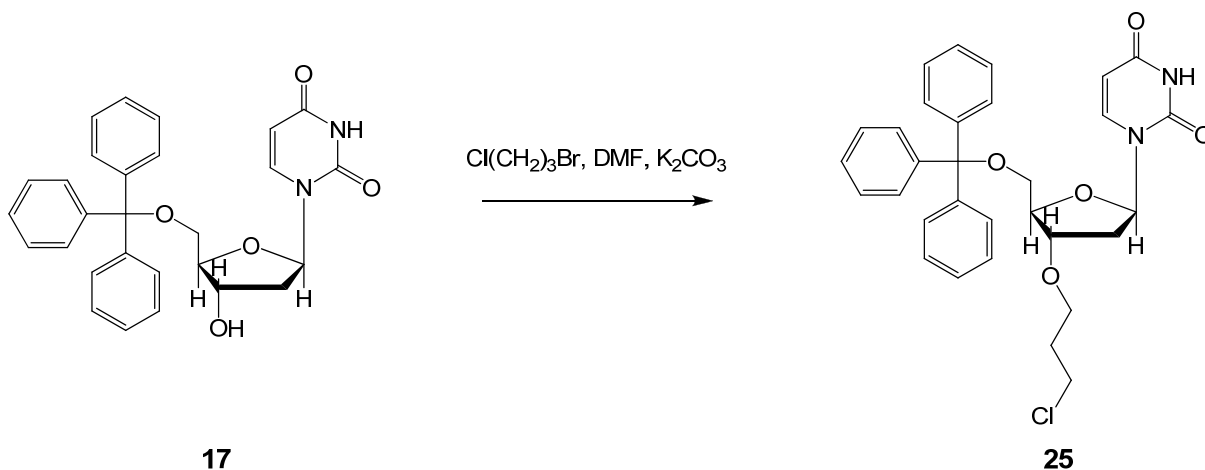
The trityl group in **21** was removed with 80% acetic acid (Scheme 5.9) to generate **24**,<sup>14</sup> it was obtained as a white solid in 42% yield. Formation was indicated by ESMS(-) with a peak at  $m/z$  252 [ $M - H$ ]<sup>-</sup> the <sup>1</sup>H NMR spectrum shows the absence of the 15H multiplet of the trityl group at 7.25 ppm. The azido-uridine **24** was used as a substrate for the ‘click’ reaction to form uridine appended Ln(III)DO3A complexes (Scheme 5.11).



Scheme 5.8

### 5.3.3 Formation of 5-trityl-2-(-3-chloropropoxy)-uridine (**25**)

**25** was synthesised from **17** and 1-bromo-3-chloropropane in DMF (Scheme 5.9) which has been developed from Gong and co-workers,<sup>18</sup> who use 1-bromo-3-chloropropane to synthesise novel tricyclic 1-anilino-5-H-pyridazino[4,5-b]indoles, as potential anti-tumour compounds. They show that only the bromide is substituted by a secondary alcohol, creating an ether bond, under these conditions the chloro-end of the molecule does not react. This is then amenable for nucleophilic substitutions in later reactions. **25** was obtained as a white solid in 77% yield. Formation was indicated by ESMS(+) with a peak at  $m/z$  548  $[M + H]^+$ , the  $^1\text{H}$  NMR spectrum shows three 2H peaks at 2.04, 3.49 and 4.40 ppm a triplet, multiplet and a triplet respectively, representing the propyl chain appended to the O3 of the ribose ring, the latter peak is shifted downfield due to the appended chloride. Confirmation of reaction at the O3 of the ribose ring, (rather than *e.g.* at the amide on the uridine) was determined *via* NOE  $^1\text{H}$  NMR experiments. The NOE experiment shows cross peaks *i.e.* correlations for protons within close proximity to each other, the NOE experiment shows an NOE for the  $\text{CH}_2$  of the propyl chain to that of the  $\text{CH}_2$  (2) on the ribose ring, shown in Figure 5.5.



Scheme 5.9

The NOE experiment in Figure 5.6 is overlapped by the COSY experiment, any cross peaks that occur in both are just for protons directly linked through a alkyl chain, the cross peaks that only occur in the NOE indicate protons in close proximity that are not directly connected. The cross peak between the  $\text{CH}_2$  at 4.40 ppm representing the  $\text{CH}_2$  on

the propyl chain and the CH<sub>2</sub> at 3.00 ppm representing the CH<sub>2</sub> (C4) on the ribose ring, suggests the propyl chain has reacted with the O(3) of the ribose ring.

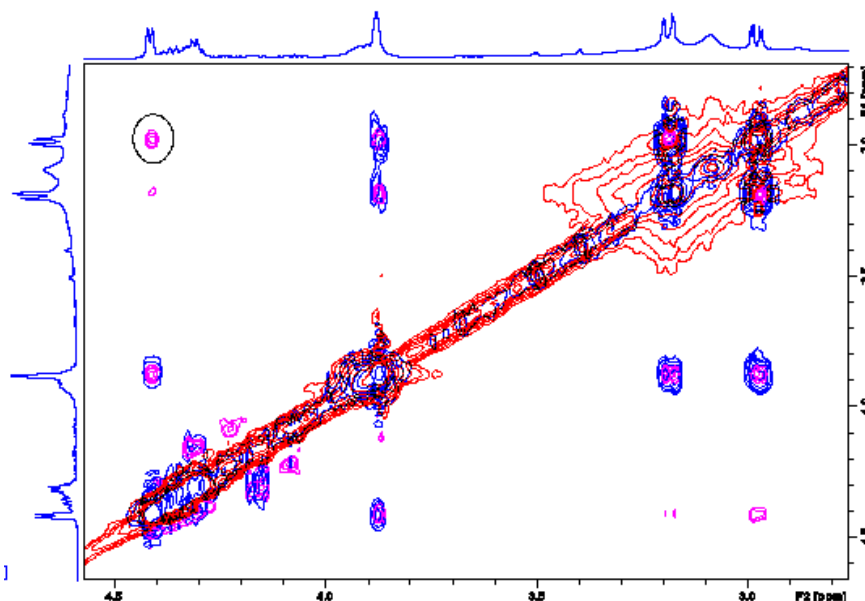
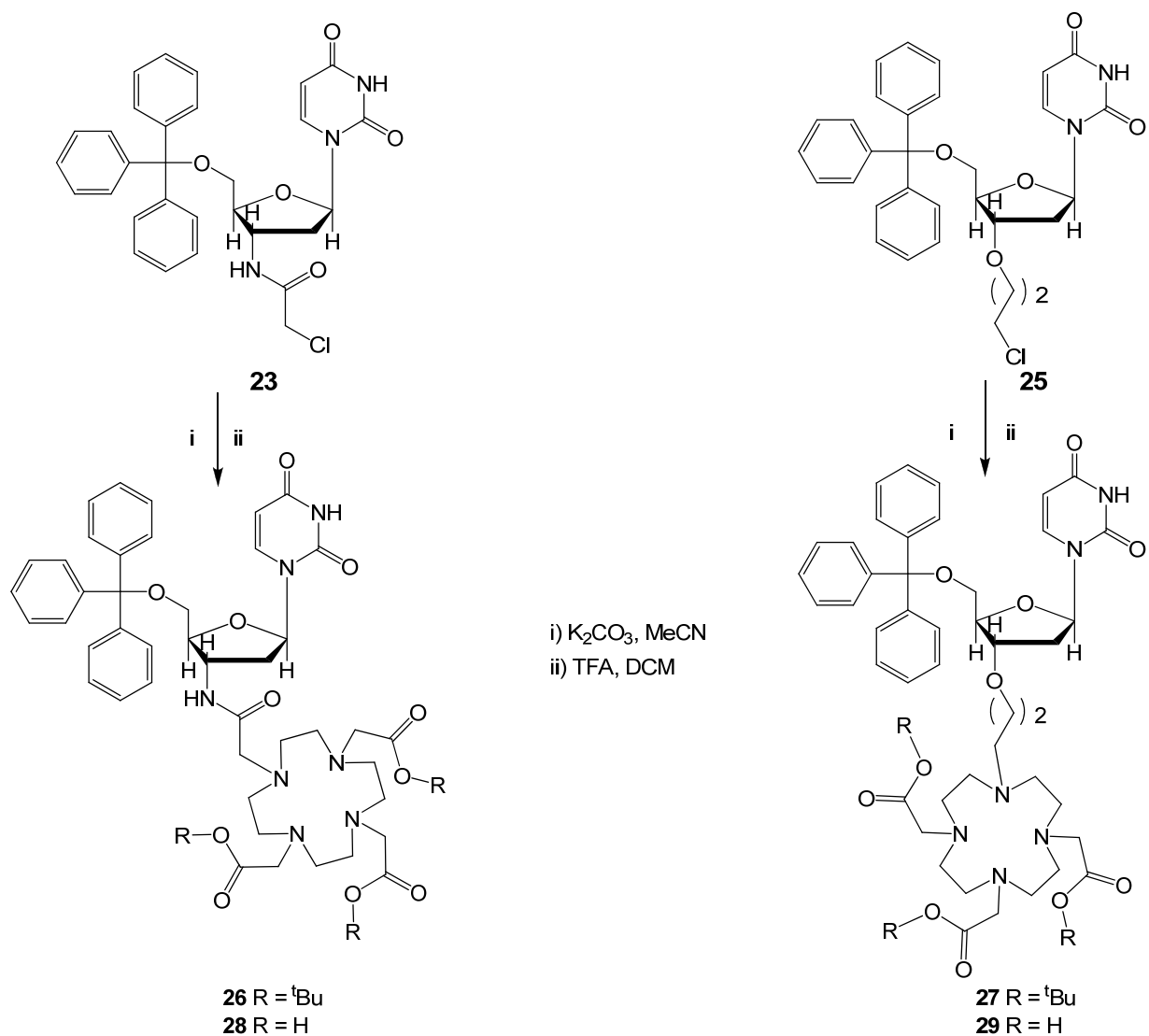


Figure 5.5 NOE and COSY <sup>1</sup>H NMR, for **25**

The NMR spectroscopy and the mass spectrometric evidence suggests that **25** has been synthesised, with the alkyl chain forming an ether linker to the O(3) of the ribose ring.

#### 5.4 Macrocyclic Synthesis

**26** and **27** were synthesised from **23** and **25** respectively using **1** as a common starting material (Scheme 5.10), they were then deprotected as described in Chapter 2 forming **28** and **29**, these are the proligands for uridine appended Ln(III) complexes.



Scheme 5.10

#### 5.4.1 Formation 1,4,7-tris(carbonylmethyl)-10-(3-acetamide-5-hydroxy-2,3-dideoxyuridine)-1,4,7,10-tetraazacyclododecane (**28**)

**26** was synthesised from **23** and **1** in MeCN.<sup>5</sup> The crude product was purified on silica using a DCM: Methanol (97:3) giving a colourless oil, in 95% yield. Formation was confirmed by ESMS(+) with a peak at  $m/z$  1024  $[M + H]^+$ , the  $^1H$  NMR spectrum shows the presence of the 27H singlet at 1.39 ppm, which corresponds to the *tert*-butyl ester groups.

The *tert*-butyl ester cleavage as described in Chapter 2 using TFA/DCM, yields **28** as a white hygroscopic solid in 76% yield. Analysis by  $^1H$  NMR spectrum showed an absence of the  $C(CH_3)_3$  peaks at 1.39 ppm, indicating cleavage of the *tert*-butyl esters.

#### 5.4.2 Formation 1,4,7-tris(carbonylmethyl)-10-(5-hydroxy-2-(3-chloropropoxy)-uridine)-1,4,7,10-tetraazacyclododecane (**29**)

**27** was synthesised from **25** and **1** in MeCN. The crude product was purified on silica using a DCM: Methanol (97:3) solvent system giving a yellow oil, 50% yield. Formation was confirmed by ESMS(+) with a peak at  $m/z$  1026  $[M + H]^+$  the  $^1H$  NMR spectrum shows the presence of the 27H singlet at 1.42 ppm, which represent the t-butyl ester groups. The yield is much lower in the formation of **27** compared with **26**, this is could be due to hydrolysis of the chloride on **25**, under the reaction condition the hydroxyl group can be formed and is seen in the ESMS at  $m/z$  529  $[M + H]^+$ .

**29** was synthesised *via* hydrolysis of the t-butyl esters in **27** in TFA/DCM, yielding a white hydroscopic solid in 76%. Analysis by  $^1H$  NMR spectroscopy confirmed the t-butyl esters were hydrolyzed due to the absence of the C(CH<sub>3</sub>) peaks at 1.42 ppm. NOE experiments show that the uridine is linked to the DO3A, CH<sub>2</sub> resonance at 3.82 ppm, has a NOE with the CH<sub>2</sub> resonance on the cyclen ring at 3.24 ppm.

### 5.5 Synthesis of Lanthanide Complexes

The lanthanide compounds **Ln.28** and **Ln.29** where synthesised in the same way, using **28** and **29**, respectively with LnCl<sub>3</sub>.6H<sub>2</sub>O in H<sub>2</sub>O at pH 6. The reactions were monitored by ES mass spectrometry for the specific mass and lanthanide isotope pattern for the complex and the depletion of starting material. Any unreacted lanthanide salts were removed using DOWEX MAC-3<sup>®</sup> weak acid cation exchange resin. The solutions were then tested for the presence of uncomplexed lanthanide ions using urotropine buffered solutions of xylenol orange at pH 5. If the solutions remained orange no free lanthanide ions were left in the solution.

#### 5.5.1 Luminescence studies of **Eu.28**

**Eu.28** was synthesised from **28** and EuCl<sub>3</sub>.6H<sub>2</sub>O, the reaction gave a white solid in 65% yield. **Eu.28** is an eight-coordinate complex, with seven-coordinating molecules from the DO3A macrocycle, and one from the oxygen of the amide. The hydration state  $q$ , of the complex was determined and its luminescent properties investigated.

The complex was excited at a wavelength of 293 nm giving the Eu(III) emission spectrum in Figure 5.6, showing the various  ${}^5D_0$  to  ${}^7F_J$  transitions of **Eu.28**. The spectral form is very different compared to **Eu.29** in Figure 5.6 and is typical of DO3A-monoamide derivatives. The spectrum shows the  $\Delta J = 2$  transition,  $\lambda = 618$  nm at relatively similar intensity to that of the  $\Delta J = 1$  transition  $\lambda = 595$  nm. This is indicative of an eight-coordinate complex, compared to that of **Eu.29** in Figure 5.7, which shows an increase in intensity of the hypersensitive  $\Delta J = 2$  transition, compared to the  $\Delta J = 1$  transition, which is typical of a seven-coordinate complex.

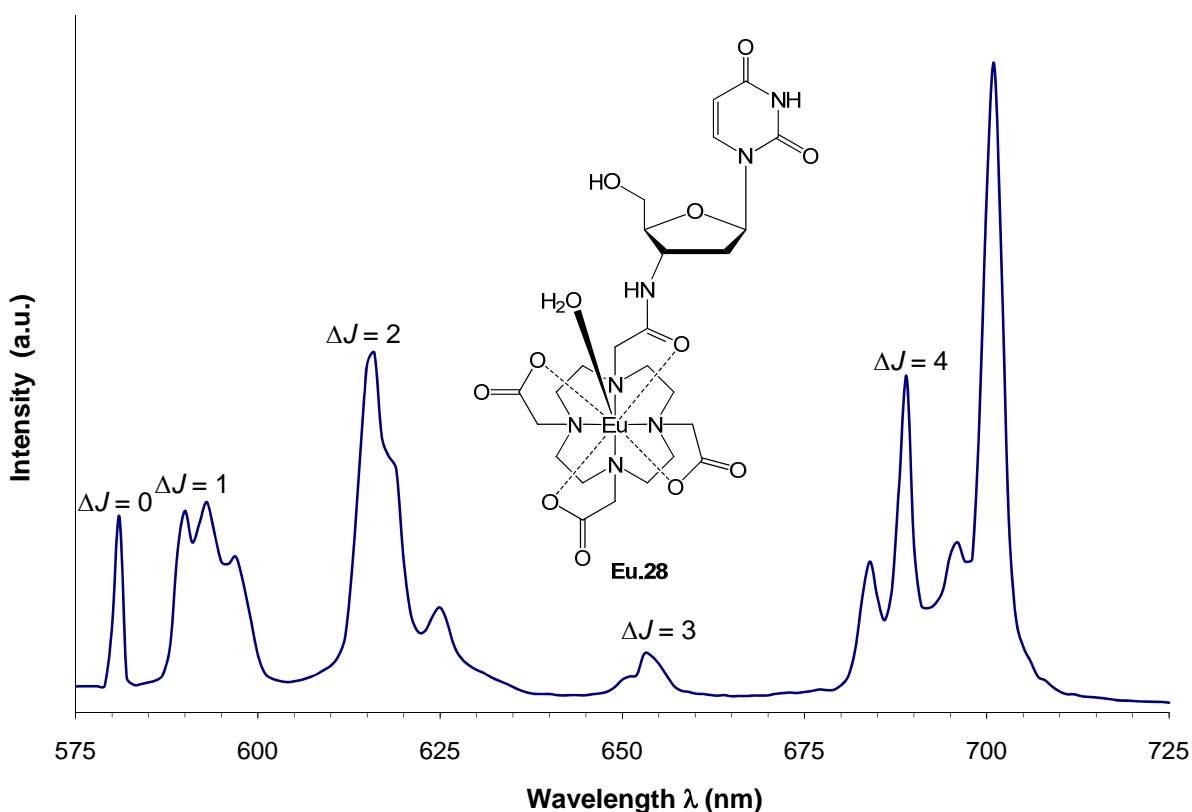


Figure 5.6 Luminescence emission spectrum of **Eu.28** ( $\lambda_{\text{ex}} = 293$  nm,  $\text{H}_2\text{O}$ , pH 7.4, 298K ).

The excitation spectrum monitors the emission at  $\lambda = 618$  nm,  $\Delta J = 2$  transition. This shows weak maxima at  $\lambda = 293$  nm,  $\lambda = 370$  nm and  $\lambda = 395$  nm. The maximum observed at  $\lambda = 395$  nm represents direct excitation of the Eu(III) ion, the maximum at  $\lambda = 293$  nm, could be sensitisation from the nucleoside base to the Eu(III) ion, or the LMCT band which occurs between  $\lambda = 260 - 290$  nm. The  $\Delta J = 2$  transition, at 618 nm is the wavelength that was monitored during lifetime studies showing the radiative decay carried out in  $\text{H}_2\text{O}/\text{D}_2\text{O}$  to determined  $q$  (Equation 42), taking account for the N-H oscillator

quenching from the amide.<sup>19</sup>  $k_{\text{H}_2\text{O}} = 2.14 \text{ ms}^{-1}$  and  $k_{\text{D}_2\text{O}} = 0.99 \text{ ms}^{-1}$ , for all three excitation wavelengths, this give a hydration state,  $q = 1$ .

$$q_{\text{Eu}} = 1.2[(k_{\text{H}_2\text{O}} - k_{\text{D}_2\text{O}}) - 0.25 - (0.075)] \quad (42)$$

The data suggests that **Eu.28** under physiological conditions, pH 7.4, will bind one water molecule, *i.e.*  $q = 1$ . This suggests that **Eu.28** is eight-coordinate and will not bind carbonate. Linking a uridine to a Eu(III)DO3A *via* an amide, creates an eight-coordinate complex the binds one solvent molecule. This suggests that Gd(III) analogue, will not bind carbonate and will not act as a ‘smart’ contrast agent, and it will act more like the FIAU, PET agent, upon interaction with HSV1-TK enzyme, *i.e.* it will accumulate, but not activate.

### 5.5.2 Luminescence studies of **Eu.29**

**Eu.29** was synthesised as for **Eu.28** from **29** and  $\text{EuCl}_3 \cdot 6\text{H}_2\text{O}$ , the reaction gave a white solid in 31% yield. **Eu.29** is a seven-coordinate complex with respect to ligand **29**, the  $^1\text{H}$  NMR spectrum is consistent with those observed for unsymmetrically substituted cyclen derivatives,<sup>20</sup> in which all protons are non-equivalent. The resonances only start to become resolved at low temperature ( $\sim 278\text{K}$ ), implying a relatively low barrier to arm rotation in the complex allowing intermediate (with respect to the timescale of the NMR experiment) exchange between diastereoisomers. This behaviour is to be expected given that the substituent cannot coordinate to the metal centre. The hydration state  $q$ , of the complex was determined and its photophysical properties investigated, including carbonate binding affinities.

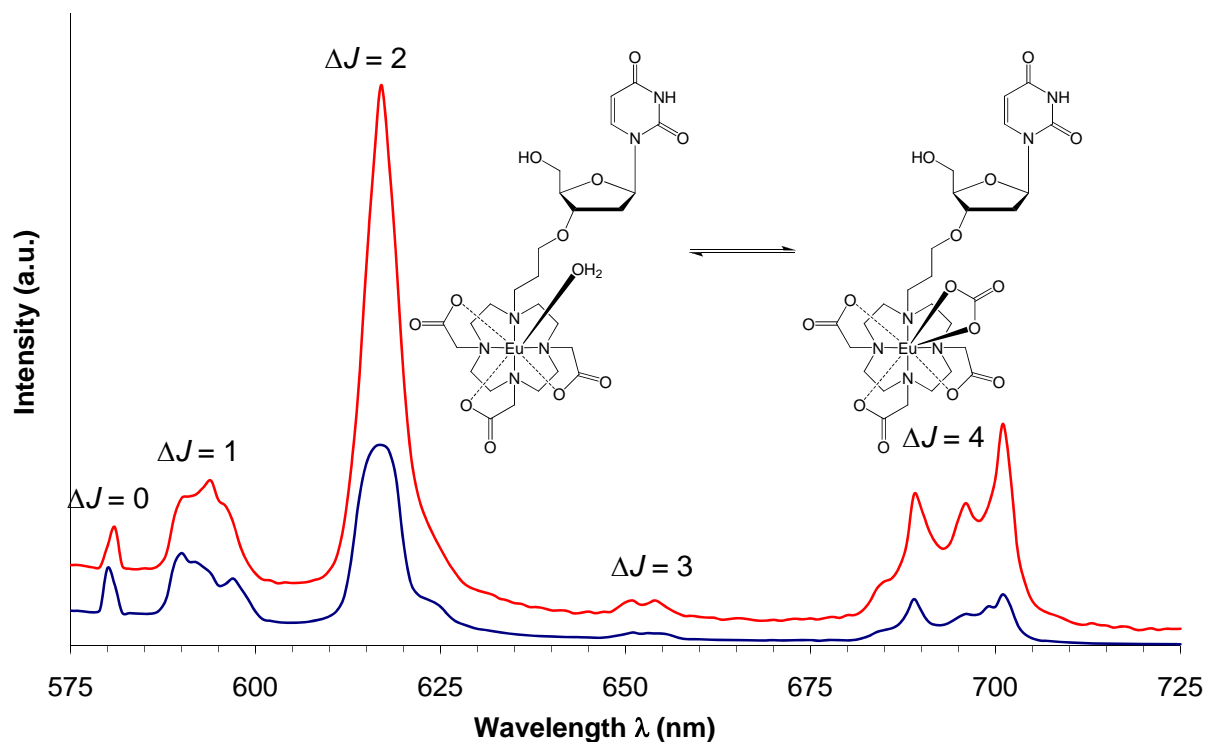


Figure 5.7 Luminescence emission spectra of **Eu.29** (blue), ( $\lambda_{\text{ex}} = 286$  nm, H<sub>2</sub>O, pH7.4, 298K) and **Eu.29**, + NaHCO<sub>3</sub> (30 mM), pH 7.4 (red) showing the change in intensity of the hypersensitive  $^5D_0$ - $^7F_2$  transition (618 nm).

The complex was excited at a wavelength of 286 nm, indirect sensitisation from the uridine, giving the Eu(III) emission spectrum in Figure 5.7, showing the various  $^5D_0$  to  $^7F_J$  transitions of **Eu.29** (blue) compared to **Eu.29** in the presence of 30 mM NaHCO<sub>3</sub>, (298K, pH 7.4) (red). The spectra show an increase in intensity of the hypersensitive  $\Delta J = 2$  transition, compared to that of the  $\Delta J = 1$  transition, this corresponds to a change in local coordination environment. The form of the **Eu.29** spectrum + 30 mM NaHCO<sub>3</sub>, is typical for carbonate binding to the Eu(III) centre and resembles similar compounds reported by Giardiello *et al.*<sup>3</sup> Carbonate displaces the inner-sphere water molecules, therefore there is no longer quenching O-H oscillators and changes the polarisability of the axial donor atom.<sup>19</sup> This can be seen by the increased intensity of the  $\Delta J = 2$  transition at  $\lambda = 618$  nm. The ratio of  $\Delta J = 2 / \Delta J = 1$  changes from 1:2.4 in the absence of carbonate to 1:3.7 in the presence of carbonate. The change in spectral form suggests that endogenous anions such as carbonate at intracellular concentrations will bind to the seven-coordinate **Eu.29** complex.

The excitation spectrum monitors the emission at  $\lambda = 618$  nm,  $\Delta J = 2$  transition. This shows weak maxima at  $\lambda = 286$  nm and  $\lambda = 395$  nm. The maximum observed at  $\lambda = 395$  nm represents direct excitation of the Eu(III) ion, the maximum at  $\lambda = 286$  nm, could

be sensitisation from the nucleoside base to the Eu(III) ion, or the LMCT band which occurs between  $\lambda = 260 - 290$  nm. The  $\Delta J = 2$  transition, at 618 nm is the wavelength that is monitored during luminescence lifetime studies out in H<sub>2</sub>O/D<sub>2</sub>O to determine  $q$ . The lifetime data is shown in Table 5.1

Complex	$\lambda_{em} / \text{nm}$	$\lambda_{ex} / \text{nm}$	$k_{\text{H}_2\text{O}}$	$k_{\text{D}_2\text{O}}$	$q$
<b>Eu.29</b>	286, 395	618	1.83	0.72	1
<b>Eu.29 + 30mM NaHCO<sub>3</sub></b>	286, 396	618	1.62	0.63	0.8

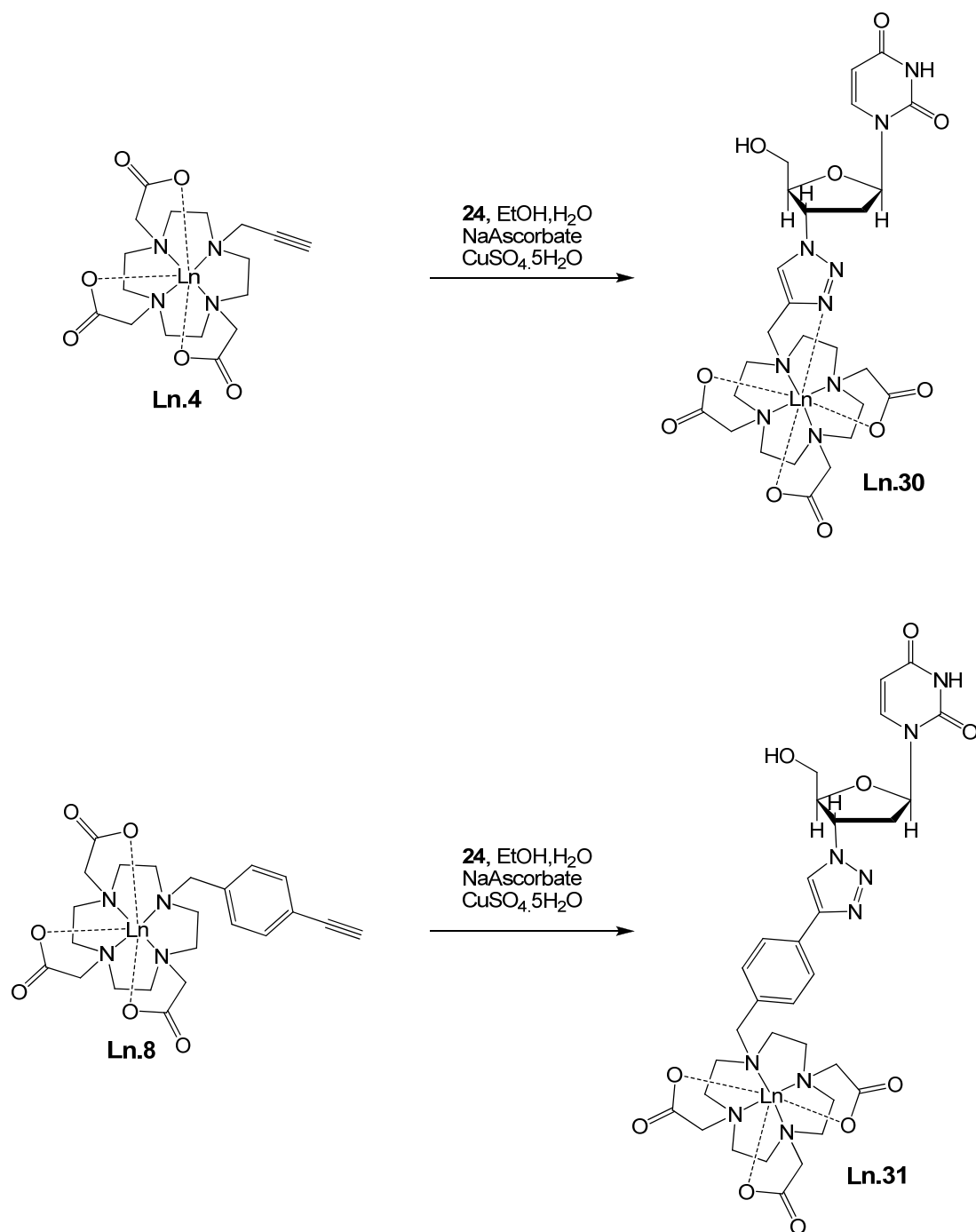
Table 5.1 Rate constants,  $k$ , and calculated hydration states,  $q$ , for **Eu.29** and **Eu.29 + 30mM NaHCO<sub>3</sub>**

The data in Table 5.1 suggests that **Eu.29** under physiological conditions, pH 7.4 carbonate (30 mmol) that a proportion of complex will bind carbonate. The lifetime is a ratio of two species a proportion with carbonate bound and a proportion of complex without carbonate bound, although from these results it suggests that **Eu.29** remains with a  $q = 1$ , in the presence and absence of carbonate. This is not unprecedented Parker and co-workers have also shown a  $q = 1$  complex while still binding carbonate.<sup>5</sup> Given the change in spectral form, a larger change in  $q$  would be expect. The emission spectrum in Figure 5.7 is typical of a seven-coordinate complex (blue) the second spectrum shows spectral form consistent with binding of carbonate (red). The ratio of  $\Delta J = 1: \Delta J = 2$ , in both spectra suggest that carbonate binds. This suggests that **Gd.29** will bind carbonate and upon interaction with HSV1-TK enzyme, the carbonate should be displaced, like in **LGd.3**.<sup>3</sup>

## 5.6 Click Chemistry with Nucleosides

The ‘Huisgen’ Cu(I) catalysed cycloaddition reaction between an organic azide and a substituted alkyne, offers a facile technique in order to append lanthanide chelates to biological molecules.<sup>21</sup> The basis for this has been demonstrated by Hulme and Romain, linking a dansyl group to a Eu(III)DO3A amide appended alkyne.<sup>22</sup> Work reported earlier in this thesis highlights the applications of this technique (Chapter 2 using **Ln.4** and in Chapter 3 and 4 using **Ln.8**). Two uridine appended lanthanide complexes were synthesized from **Ln.4** and **Ln.8** and **24** using the Cu(I) cycloaddition ‘click’ reaction,

using the standard conditions outlined in Chapter 2, providing **Ln.30** and **Ln.31** (Scheme 5.11).



Scheme 5.11

### 5.6.1 Luminescent studies of **Eu.30**

**Eu.30** was synthesised as in Scheme 5.12 from **24** and **Eu.4**, the reaction gave a white solid in 32% yield. **Eu.30** is an eight-coordinate complex with respect to ligand, with

seven-DO3A donors, the 8th from the triazole (N2), *cf.* **Ln.4**.<sup>23</sup> The hydration state  $q$ , of the complex was determined and its photophysical properties investigated.

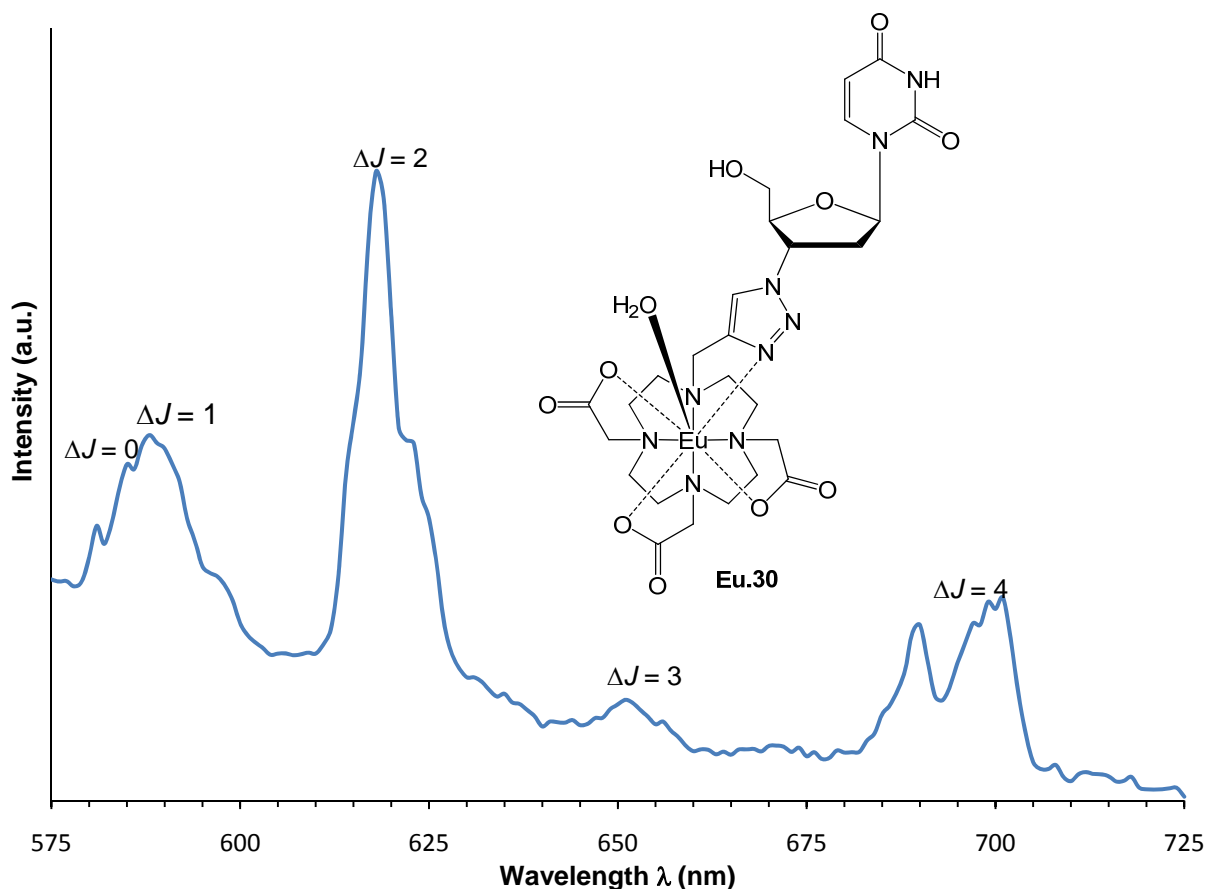


Figure 5.8 Luminescent emission spectrum of **Eu.30** ( $\lambda_{\text{ex}} = 283$  nm, H<sub>2</sub>O, pH 7.4, 298K).

The complex was excited at a wavelength of 283 nm giving the Eu(III) emission spectrum in Figure 5.8, showing the various  $^5D_0$  to  $^7F_J$  transitions of **Eu.30**. The spectral form is very different compared to **Eu.29** in Figure 5.7. The spectrum shows the  $\Delta J = 2$  transition,  $\lambda = 618$  nm at a relatively similar intensity to that of the  $\Delta J = 1$  transition  $\lambda = 588$  nm. This is indicative of an eight coordinate complex, compared that of **Eu.29** in Figure 5.7, which shows an increase in intensity of the hypersensitive  $\Delta J = 2$  transition, compared to the  $\Delta J = 1$  transition, which is typical of a seven-coordinate complex.

The excitation spectrum monitors the emission at  $\lambda = 618$  nm,  $\Delta J = 2$  transition. This shows weak maxima at  $\lambda = 293$  nm,  $\lambda = 370$  nm and  $\lambda = 395$  nm. The peak observed at  $\lambda = 395$  nm represents direct excitation of the Eu(III) ion, the maximum at  $\lambda = 293$  nm, could be sensitisation from the nucleoside base to the Eu(III) ion, or the LMCT band which occurs between  $\lambda = 260 - 290$  nm. The  $\Delta J = 2$  transition, at 618 nm is the wavelength that

was monitored during luminescence lifetime studies carried out in H<sub>2</sub>O/D<sub>2</sub>O to determine  $q$ . The lifetime studies are shown in Table 5.2.

The data in Table 5.2 suggests that **Eu.30** under physiological conditions, pH 7.4, will bind one water molecule, *i.e.*  $q = 1$ . This suggests that **Eu.30** is eight-coordinate and will not bind carbonate. Linking a uridine to a Eu(III)DO3A *via* a triazole, creates an eight-coordinate complex with respect to ligand, with one water molecule occupying the last binding site. This suggests that the **Gd.30** analogue, will not bind carbonate, and this will therefore not be a ‘smart’ contrast agent, it will act more like the FIAU, PET agent, upon interaction with HSV1-TK enzyme.

Complex	$\lambda_{em} / \text{nm}$	$\lambda_{ex} / \text{nm}$	$k_{\text{H}_2\text{O}}$	$k_{\text{D}_2\text{O}}$	$q$
<b>Eu.30</b>	283, 370, 395	618	2.91	1.99	1
<b>Eu.31</b>	262, 290, 355, 395	618	4.46	3.36	1

Table 5.2 Rate constants,  $k$ , and derived hydration states,  $q$ , for the decay of **Eu.30** and **Eu.31**.

### 5.6.2 Luminescence studies of **Eu.31**

**Eu.31** was synthesised from **24** and **Eu.8**, the reaction gave a white solid in 50% yield. **Eu.31** is a seven-coordinate complex with respect to the ligand, with seven DO3A donors. The hydration state  $q$ , of the complex was determined and its photophysical properties investigated.

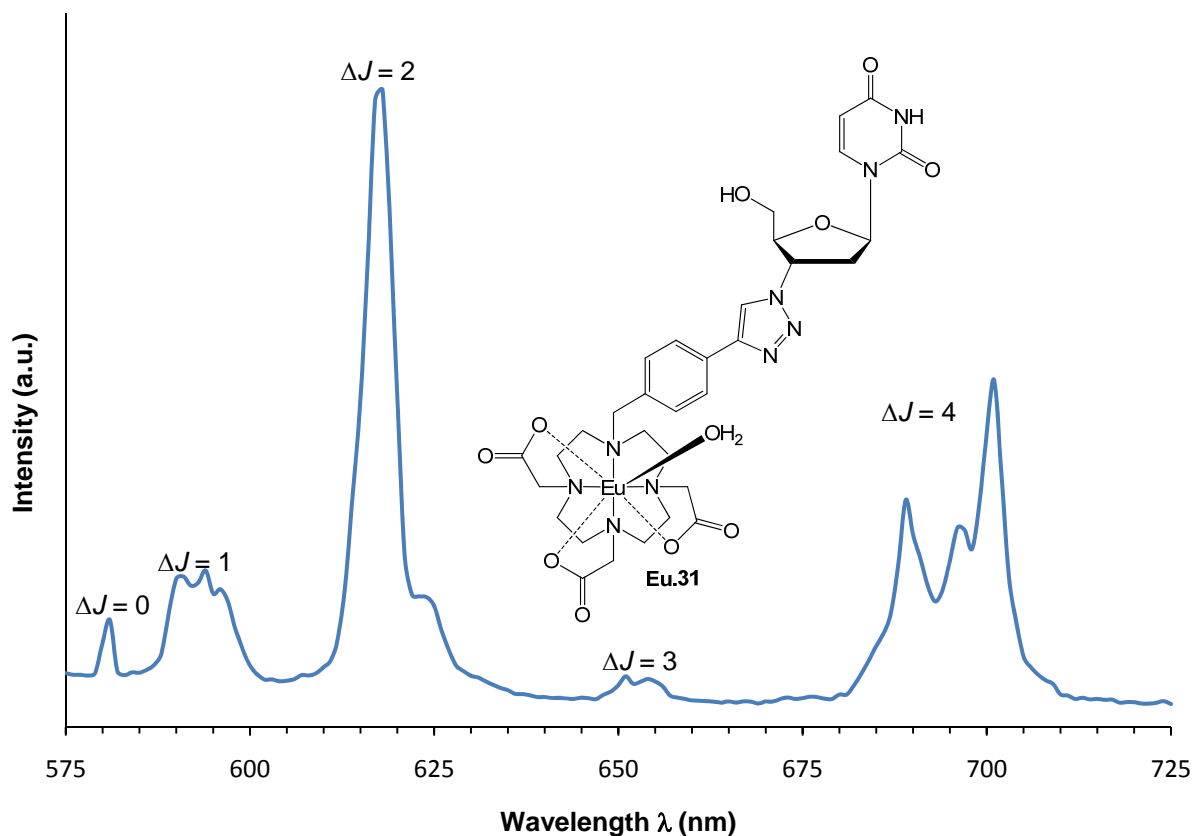


Figure 5.9 Luminescence emission spectrum of **Eu.31** ( $\lambda_{\text{exc}} = 262$  nm,  $\text{H}_2\text{O}$ , pH 7.4, 298K).

The complex was excited at a wavelength of 262 nm giving the Eu (III) emission spectrum in Figure 5.9, showing the various  $^5\text{D}_0$  to  $^7\text{F}_J$  transitions of **Eu.31**. The spectral form is very different *c.f.* **Eu.31** in Figure 5.9. The spectrum shows the  $\Delta J = 2$  transition,  $\lambda = 618$  nm at a significantly higher intensity than that of the  $\Delta J = 1$  transition  $\lambda = 595$  nm. This is comparable to the seven-coordinate complex, **Eu.29** in Figure 5.7, the spectral form is very similar to that of **Eu.12** in Figure 3.8, the model compound for the ‘click’ reaction, which shows an increase in intensity of the hypersensitive  $\Delta J = 2$  transition, compared to the  $\Delta J = 1$  transition, also very similar to the form of the spectrum for **Eu.15** as a monomer.

The excitation spectrum monitors the emission at  $\lambda = 618$  nm,  $\Delta J = 2$  transition. This shows weak maxima at  $\lambda = 262$  nm,  $\lambda = 290$  nm,  $\lambda = 355$  nm and  $\lambda = 395$  nm. The maximum observed at  $\lambda = 395$  nm represents direct excitation of the Eu(III) ion, the more intense maximum at  $\lambda = 262$  nm, is the sensitization from  $\pi\text{-}\pi^*$  transitions of the phenyl group. The peak at  $\lambda = 290$  nm, could be sensitisation from the nucleoside base to the Eu(III) ion, or more likely sensitization from the triazole, this is discussed in Chapters 3 and 4. The  $\Delta J = 2$  transition, at 618 nm is the wavelength that is monitored during

luminescence lifetime studies carried out in H<sub>2</sub>O/D<sub>2</sub>O to determine  $q$ . The Lifetime data is shown in Table 5.2.

The data in Table 5.2 suggests that **Eu.31** under physiological conditions, pH 7.4, will bind one solvent molecule, with a hydration state,  $q = 1$ , it is likely that the bulky substituent blocks access of a second solvent molecule. This suggests that **Eu.31** is seven-coordinate and could possibly bind endogenous carbonate; further studies are required to confirm this. Linking a uridine to a Eu(III)DO3A *via* a *p*-benzyltriazole, creates a seven-coordinate complex the binds one inner-sphere water molecule. This suggests that the **Gd.31** analogue could bind carbonate and act as a ‘smart’ contrast agent, upon interaction with HSV1-TK enzyme.

## 5.7 Summary and Conclusions

It has been demonstrated that uridine can be transformed and linked to Ln(III)DO3A chelates *via* three different methods. Uridine compounds **17** to **24** excluding **23**, developed by Mancini and co-worker,<sup>14</sup> have been reproduced in comparable yields. Compounds **23**, **24** and **25**, have been synthesized in respectable yields as precursors for linking uridine to Ln(III)DO3A complexes, either *via* an ether, amide or triazole linker. **23** and **25** have been successfully appended to **1**, appending the uridine through the O3 on the ribose ring, to the N10 of the cyclen ring.

Four europium(III) uridine appended complexes have been synthesized, **Eu.28**, **Eu.29**, **Eu.30** and **Eu.31**. **Eu.29** is an ether linked uridine Eu(III)DO3A complex, with hydration state of  $q = 1$ . **Eu.28** is an amide linked uridine Eu(III) DO3A complex, with a hydration state of  $q = 1$ . The emission spectrum is typical of an eight-coordinate complex, binding through seven molecules from the DO3A macrocycle, and one from the oxygen on the amide. **Eu.28** will not bind carbonate, therefore it can be assumed that the Gd(III) analogue will not, this does not rule it out as a contrast agent for visualizing gene therapy, it may well interact with HSV1-TK in the same manner as the PET agent FIAU.<sup>11</sup> Further tests on the Gd(III) complex analogues, upon interaction with HSV1-TK enzyme and localization within a cell are needed.

It has been shown that **Eu.29** will bind carbonate at physiological concentrations of NaHCO<sub>3</sub>. This suggests that with interaction with HSV1-TK, the Gd(III) complex would act as a ‘smart’ contrast agent. Further studies into phosphorylated form of the complexes and relaxivity studies in the presence of carbonate and the HSV1-TK enzyme, must be

performed to prove that interaction with HSV1-TK will change the local hydration state of the Gd(III) complex.

It has been demonstrated that 1,2,3-triazole linkers can be used to append Ln(III) complexes to a uridine molecule *via* the 'Huisgen' Cu(I) catalysed cycloaddition reaction between an azide and an alkyne. **Eu.30** is a 1,2,3-triazole linked uridine DO3A complex, with a hydration state  $q = 1$ . The emission spectrum is typical of an eight-coordinate complex, binding through seven donor atoms from the DO3A macrocycle, and one from the N2 on the triazole, in a pyridinic manner such as **Eu.5**.<sup>24</sup> **Eu.30** will not bind endogenous carbonate, therefore the Gd(III) analogue is not expected to, this does not rule it out as a contrast agent for visualizing gene therapy, it should interact with HSV1-TK in the same manner as the PET agent FIAU.<sup>11</sup> Further tests on the Gd(III) complex analogues, upon interaction with HSV1-TK enzyme and localization within a cell are needed.

**Eu.31** is a *p*-benzyl-1,2,3-triazole linked uridine DO3A complex, with a hydration state  $q = 1$ . The emission spectrum is typical of a seven-coordinate complex, binding through seven DO3A donor atoms. Further studies into binding carbonate at physiological concentrations and interactions with HSV1-TK enzyme are needed. Relaxivity studies need to be carried out on the Gd(III) analogues; it is hypothesized that it will act as a 'smart' contrast agent, in the same manner as **L.Gd.3**.<sup>3</sup>

The most facile route to a uridine appended Ln(III) complex is *via* the ether linker as it has fewer synthetic steps to **Ln.29**, so far this has proven the most promising in developing a 'smart' contrast agent, showing that carbonate will bind at physiological concentrations. Further tests with Gd(III) analogues, phosphorylated analogues and the HSV1-TK enzyme, are required in order to show that **Ln.31** can be utilized as a smart contrast agent for imaging gene therapy.

## 5.8 References

1. S. Amie, A. Barge, M. Botta, J. A. K. Howard, R. Katakya, M. P. Lowe, J. M. Moloney, D. Parker and A. S. de Sousa, *Chem. Commun.*, 1999, 1047.
2. W. Li, S. E. Fraser and T. J. Meade, *J. Am. Chem. Soc.*, 1999, **121**, 1413.
3. M. Gardiello, M. P. Lowe and M. Botta, *Chem. Commun.*, 2007, **39**, 4044.
4. D. Parker, 'Crown Compounds: Towards Future Applications; Tailoring Macrocycles for Medical Applications', ed. S. E. Cooper, VHC Publisher Inc., 1992.

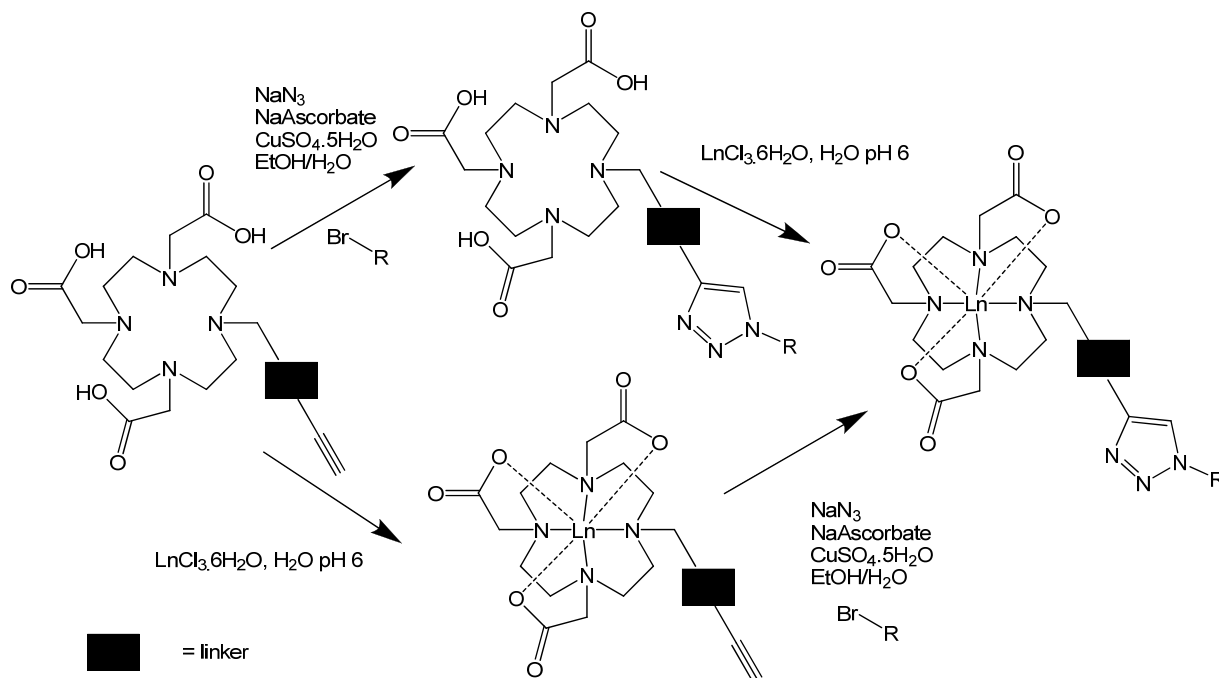
5. J. I. Bruce, R. S. Dickins, L. J. Govenlock, T. Gunnlaugsson, S. Lopinski, M. P. Lowe, D. Parker, R. D. Peacock, J. J. B. Perry, S. Aime and M. Botta, *J. Am. Chem. Soc.*, 2000, **122**, 9674.
6. A. L. Nivorozhkin, A. F. Kolodziej, P. Caravan, M. T. Greenfield, R. B. Lauffer and T. J. McMurry, *Angew. Chem. Int. Ed.*, 2001, **40**, 2903.
7. A. Y. Louie, M. M. Hüber, E.T. Ahrens, U. Rothbacher, R. Moats, R. E. Jacobs, S. E. Fraser and T. J. Meade, *Nat. Biotechnol.*, 2000, **18**, 321.
8. R. A. Moats, S. E. Fraser and T. J. Meade, *Angew. Chem. Int. Ed.*, 1997, **36**, 726.
9. J. A. Duimstra, F. J. Femia and T. J. Meade, *J. Am. Chem. Soc.*, 2005, **127**, 12847.
10. B. Alberts, A. Johnson, J. Lewis, M. Raff, K. Roberts and P. Walter, 'Molecular Biology of the Cell' fourth Edition, 2002.
11. A. A. Gilad, P. T. Winnard Jr, P. C. M. van Zijl and J. W. M. Bulte, *NMR Biomed.*, 2007, **20**, 275.
12. J. G. Tjuvajeve, G. Stockhammer, R. Desai, H. Uehara, K. Watanabe, B. Gansbacher and R. G. Blasberg, *Cancer Res.*, 1995, **55**, 6126.
13. S. S. Yaghoubi and S. S. Gambir, *Nature Protocols*, 2006, 3069.
14. T. Lin and W. R. Mancini, *J. Med. Chem.*, 1983, **26**, 54.
15. J. P. Horwitz, M. Noel and M. A. DaRooge, *J. Med. Chem.*, 1964, **7**, 385.
16. A. I. Hernandez, J. Balzarini, A. Karlsson, M. J. Camarasa and M. J. Perez-Perez, *J. Med. Chem.*, 2002, **45**, 4254.
17. R. Griffin, PhD Thesis, University of Leicester, 2007.
18. R. D. Li, X. Zhai, Y. F. Zhao, S. Yu and P. Gong, *Arch. Pharm. Chem. Life Sci.*, 2007, **340**, 424.
19. J. I. Bruce, M. P. Lowe and D. Parker, 'The Chemistry of Contrast Agents in Magnetic Resonance Imaging; Phototypical Aspects of Lanthanide(III) Complexes', ed. A. E. Merbach and E. Toth, Wiley, 2001.
20. J. P. Andre, C. F. G. C. Geraldes, J.A. Martins, A.E. Merbach, M. I. M. Prata, A. C. Santos, J. J. P. De Lima and E. Toth, *Chem. Eur. J.*, 2004, **10**, 5804.
21. V. V. Rostovtsev, L. G. Green, V. V. Fokin and B. Sharpless, *Angew. Chem. Int. Ed.*, 2002, **41**, 2597.
22. F. H. Romain and A. N. Hulme, *J. Am. Chem. Soc.*, 2006, **128**, 11370.
23. G.J. Stasiuk and M.P. Lowe, *Dalton Trans.*, 2009, 9725.
24. M. Jauregui, W. S. Perry, C. Allain, L. R. Vidler, M. C. Willis, A. M. Kenwright, J. S. Snaith, G. J. Stasiuk, M. P. Lowe and S. Faulkner, *Dalton Trans.*, 2009, 6283.

# Chapter 6

## Conclusions and Future Work

### 6.1 Click Chemistry with Lanthanide Chelates

It has been demonstrated that 1,2,3-triazole appended Ln(III) complexes can be formed *via* the ‘Huisgen’ Cu(I) catalysed cycloaddition reaction between an azide and an alkyne. The desired product can be formed *via* two routes: chelating a Ln(III) metal ion with an alkyne-appended complex followed by ‘clicking’, or clicking the alkyne appended proligand then chelating a Ln(III) metal ion. The former route is the most desirable as it requires a catalytic amount of Cu(I) for the ‘click’ reaction to occur. The latter needs more than one equivalent of Cu(I) as no reaction occurs until the macrocycle is filled. The removal of the copper from the macrocycle is not facile, and lowers yields for the Cu(I) cycloaddition reaction. Scheme 6.1 showing the two routes to 1,2,3-triazole appended LnDO3A complexes.



Scheme 6.1

**Ln.4** has a hydration state  $q = 2$ , this is a precursor for the 1,2,3-triazole. N<sub>3</sub><sup>-</sup> binds to **Ln.4** with a  $K = 2.3 \text{ M}^{-1}$ , this is weak binding, with only 2% of azide bound under ‘click’

chemistry conditions; however, the ‘click’ reaction, is still sufficient enough to allow the formation of the 1,2,3-triazole. The ‘click’ reaction is not supposed to work with  $N_3^-$  but shown in Chapter 2 that it does. Azide binding studies suggest coordinated  $N_3^-$  must be important in this unusual, unprecedented reaction.

The 1,2,3-triazole that is formed **Ln.5a**, provides a stable linker, which remains coordinated to the lanthanide in the pH range 4 - 12, this is unsurprising and mirrors the behaviour of pyridyl and tetrazole appended lanthanide complexes. **Ln.5a** has a hydration state  $q = 1$  cf. **Ln.4** which is  $q = 2$ . The change in local coordination environment from the preformed complex **Ln.4**, was demonstrated by the change in form of luminescence and  $^1\text{H}$  NMR spectra, shows that the Cu(I) cycloaddition reaction to form 1,2,3-triazoles is an effective method for linking molecules of interest to lanthanide chelates, forming a stable linker that can coordinate to the metal centre.

The formation of **Ln.5a** demonstrated using a propargyl-appended DO3A as a means of coupling lanthanide chelates *via* click chemistry is only suitable if the organic azide involved in the click reaction is pre-formed and the solution is free of  $\text{NaN}_3$ . The unexpected product of this click reaction **Ln.5c** showed interesting protonation behaviour, switching from triazole bound to Ln(III) in an N-deprotonated anionic form in basic media, to an N-H protonated ‘pyridyl’ form in acidic media, this change of coordination mode does not change the hydration state with  $q = 1$ . This pH-dependent switch, demonstrated by both  $^1\text{H}$  NMR and luminescence studies occurs in the physiological pH range, with an apparent  $\text{pK}_a = 7.5$ .

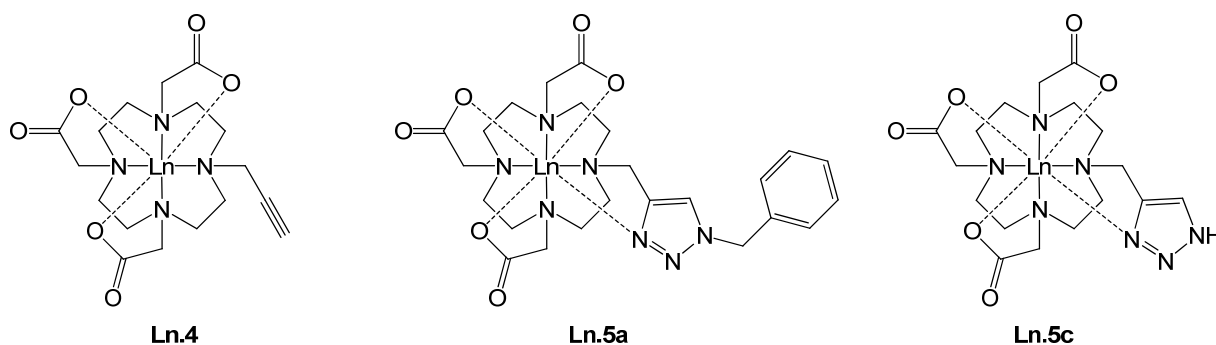
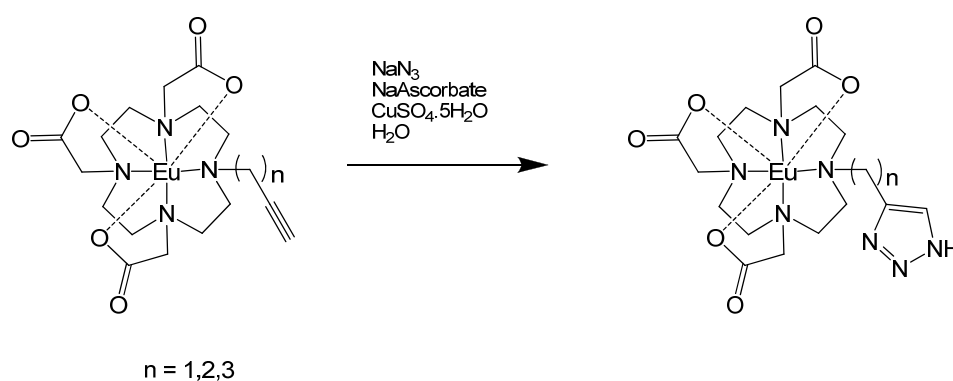


Figure 6.1 **Ln.4,5a** and **5c**.

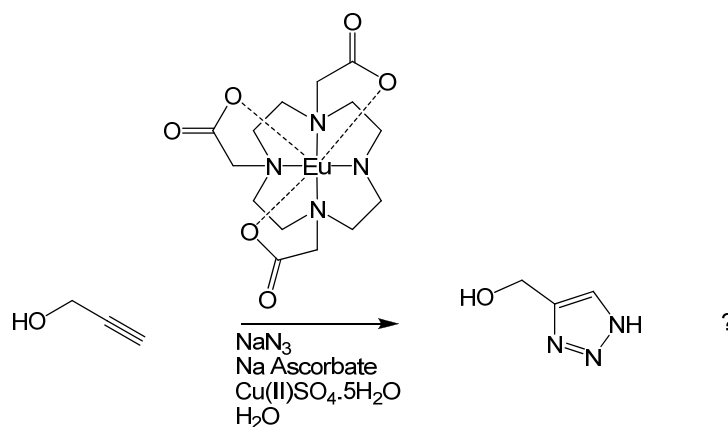
Studies on various lanthanide complexes of **5c** (Eu, Tb and Gd) confirm that the 1,2,3-triazole provides a robust coordinating linker for Ln(III) complexes to biomolecules of interest.

Future investigations should determine if changing the length of the alkyne appended to a Eu(III)DO3A chelate, from one methylene between the macrocyclic nitrogen and alkyne (propargyl)  $n = 1$ , to *e.g.* two or three, *e.g.*  $n = 2, 3$ , will also result in the formation of an unsubstituted triazole (Scheme 6.2). As the length of the linker is extended, the activated alkyne will be held more remote from the N<sub>3</sub>-bound Eu. If formation of the NH-triazole is no longer possible in these examples, then it will provide some evidence to support the hypothesis that it is the proximity of the azide-bound to the Cu-bound alkyne, that unexpectedly drives this reaction.



Scheme 6.2

The unsubstituted 1,2,3-triazole is a much sought after compound in drug discovery, as it is an analogue for histidine. The formation of the stereo selective unsubstituted triazole upon a Ln macrocycle with sodium azide, is unique and very important. Is the formation due to the proximity of the alkyne to the Ln(III) centre or can a Ln(III) DO3A complex act as a catalyst for the formation of unsubstituted 1,2,3-triazoles? Further investigation is required, using simple alkynes such as propargyl alcohol, reacted with sodium azide, in the presence of Eu(III)DO3A and Cu(I) (Scheme 6.3), to determine if this could be used to form unsubstituted 1,2,3 triazoles, without long protection deprotection synthesis.



Scheme 6.3

## 6.2 'Click' Chemistry as a Route to Multimeric MRI Contrast Agents

In Chapter 3 it was demonstrated that *p*-ethynylbenzyl appended Ln(III) complexes (**Ln.8**) can be used to form multimeric lanthanide complexes, *via* the 'Huisgen' Cu(I) catalysed cycloaddition reaction. The desired products **Ln.13** and **Ln.14** were synthesised *via in situ* generation of azides from the central bromide methyl hub and sodium azide. This reaction avoided isolation of compounds bearing multiple azides, and avoids production of NH-triazoles *cf.* **Ln.4**.

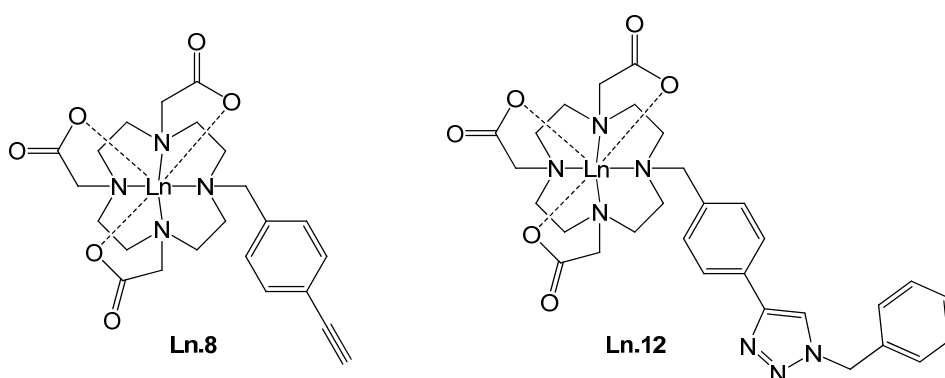


Figure 6.2 **Ln.8** and **Ln.12**

Luminescent lifetime studies indicate that **Ln.8** has a hydration state  $q = 2$ , this is the precursor for the synthesis of 1,2,3-triazole substituted complexes **Ln.12**, **Ln.13** and **Ln.14**. **Ln.12** has a hydration state  $q = 2$ , there are three routes to **Ln.12**: firstly by the 'click' reaction with **Ln.8** and benzyl bromide, the desired route; secondly *via* the 'click' reaction with 4-ethynyl(hydroxymethyl)benzene, followed by chlorination and reaction with **1**, giving **11**, the precursor for **Ln.12**. The third is the Cu(I) cycloaddition reaction with **7** to form **11**, which requires an excess of copper and removal from the macrocycle, which is not facile, and the least desirable route to **Ln.12**. The use of 'click' chemistry *via in situ* generation of azides enables safe preparation of 1,2,3-triazole complexes.

The trimeric complex based on a mesitylene hub, **Ln.13** has a hydration state  $q = 1$ . This shows that the Cu(I) cycloaddition reaction to form 1,2,3-triazoles is an efficient way of linking multiple lanthanide chelates together, forming a viable linker. **Ln.13** has  $q = 1$ , presumably due to steric congestion around the metal centre, or a result of aggregation or folding due to the hydrophobic nature of the complex.

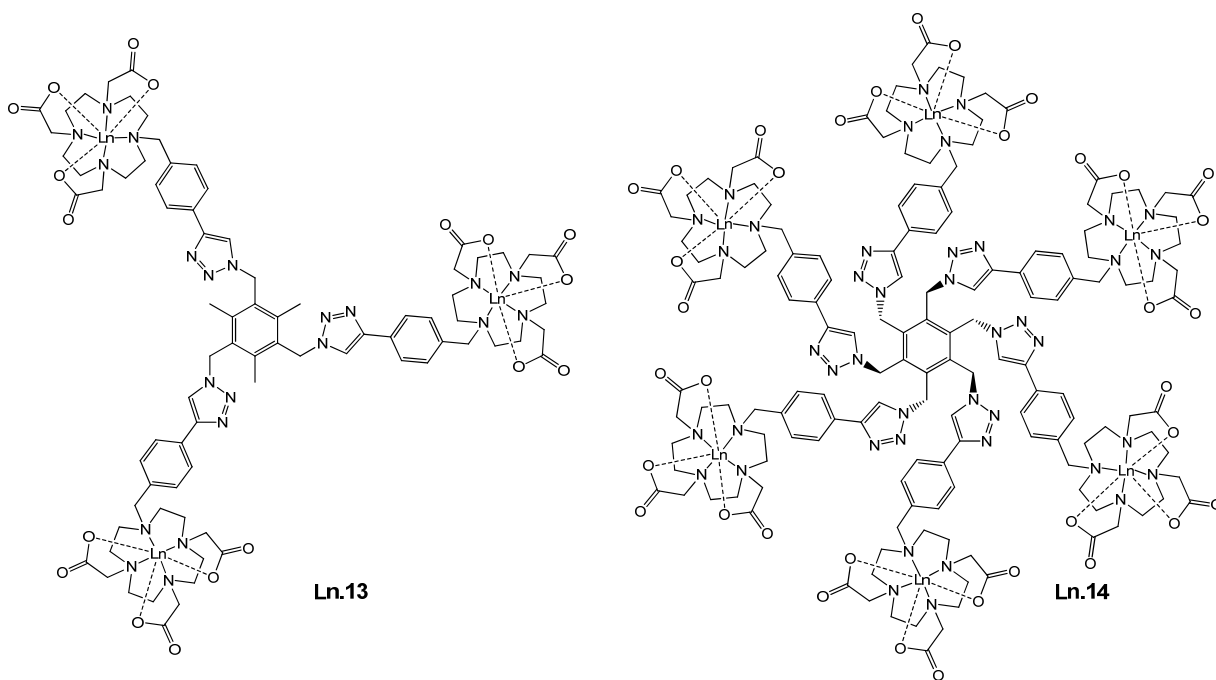


Figure 6.3 **Ln.13/14**

The possible formation of **Ln.14** or the isolation of a pure complex that has ‘clicked’ based upon the hexakis(azidomethyl)benzene hub, again demonstrated that multimeric lanthanide complexes, can be formed via the Cu(I) catalysed cycloaddition reaction. The possible **Ln.14** compound has a hydration state  $q = 1$ . Purification of a pure sample was not facile and requires extensive HPLC, the complex itself was not amenable to mass spectrometric techniques. **Gd.14** was not synthesised due to the constraints in characterisation. It is postulated that **Gd.14** would have a higher relaxivity than Meades **L.Gd.9**, further work on developing techniques to purify and characterise multimeric complexes are necessary.

Studies on a variety of lanthanide complexes (Eu(III) and Tb(III)), show that it is possible to make various multimeric compounds *via* the Cu (I) catalysed cycloaddition reaction. The *in situ* generation of the azide allowed for safe preparation of the potentially explosive multi-azide benzyl hubs without the need for isolation. Despite this there are many limitations to this technique, *i.e.* characterisation and isolation of pure products, this method is not ideal for the synthesis of multimeric lanthanide compounds.

### 6.3 'Click' Chemistry as a Route to Dual Modal Contrast Agents

The work in Chapter 4 demonstrated that *p*-benzyl-1,2,3-triazole appended Ln(III) complexes can be formed *via* the 'Huisgen' Cu(I) catalysed cycloaddition reaction between an alkyl halide and an alkyne appended lanthanide complex with *in situ* generation of the azide using sodium azide. The phenyltriazole moiety generated in **Ln.15** can coordinate Re(I) to generate a bimetallic luminescent complex.

**Ln.15** has a hydration state  $q = 2$ , this can be formed from **Ln.8**. It was shown to self-associate in aqueous solution, and the process is concentration dependent. Above 10 mM, the complex is fully dimerised and does not contain coordinated water, *i.e.* a hydration state  $q = 0$ . It is postulated that  $\pi - \pi$  stacking of the phenyl rings acts as a driving force for self-association, with coordination to an adjacent metal centre through the N2 or N3 of the 1,2,3-triazole.

Re(I) was shown to be coordinated by the model compound ethyl-1,2,3-triazole-benzene (**13**), in three different ways; cyclometallated between the N2 of the 1,2,3-triazole and the C5 of the benzene as in **14a**, secondly cyclometallated as **14a**, with a second phenyltriazole coordinating in a monodentate manner, **14b**. Thirdly Re(I) coordination to **13** is through a di-bridged complex, one Re coordinated to the N2 and another to the N3 of the 1,2,3-triazole (**14c**), this has been verified by X-ray crystallography.

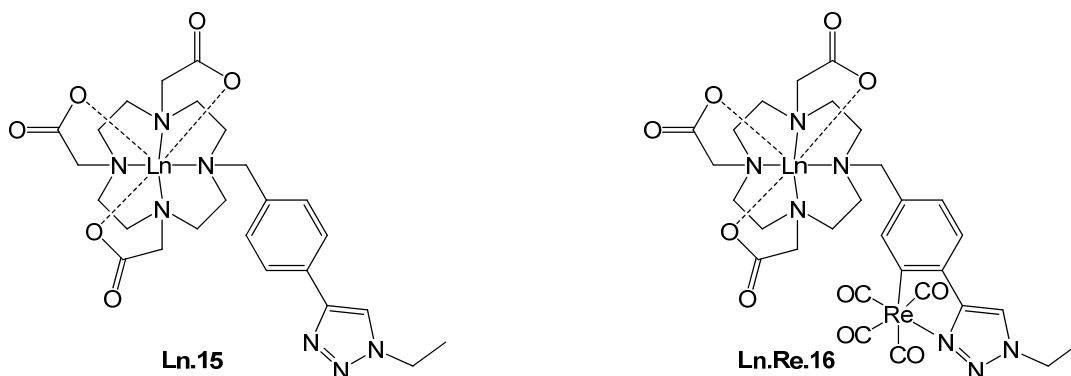


Figure 6.4 **Ln.15** and **Ln.Re.16**

Bimetallic *d-f* hybrid molecules **Ln.Re.16**, were synthesised from **Ln.15** and  $\text{Re}(\text{CO})_5\text{Cl}$ , *via* microwave heating. Luminescence studies of **Eu.Re.16** and **Tb.Re.16** show only emission from coordinated Re(I). The phenyltriazole chromophore acted as moderate sensitizers for Ln emission in **Ln.15**; however this moiety is coordinated to Re(I) *via* cyclometallation, in **Ln.Re.16**, this coordinated phenyltriazole no longer sensitises Eu/Tb emission. There is clearly no energy transfer from the  $^3\text{MLCT}$  state of Re phenyltriazole to

Eu(III). Studies on **Y.Re.16** show that Re is bound to the 1,2,3-triazole subunit, (the form of the  $^1\text{H}$  NMR spectra suggests cyclometallation of the phenyltriazole). **Gd.Re.16** complex was formed; luminescent studies shows Re(I) emission, further tests on relaxivity must be done to test the efficiency of this potential dual modal contrast agent.

If relaxivity studies prove promising, there are three potential uses for the Gd(III) moieties: **Gd.Re.16** could act a dual modal contrast agent that can be used firstly as a MR imaging for pre-operation localization and directed fluorescence imaging during surgery. A second use would utilize the  $^{186}\text{Re}$  isotope that could be incorporated for cancer therapy as it is a  $\beta$ -emitter penetrating up to 5mm, this could be used as a diagnostic and therapeutic contrast agent. A third potential application for the phenyl triazole moiety is coordination to other transition metals, the most useful metal for the purposes of imaging would be  $^{94\text{m}}\text{Tc}$  the isotope which can be used in PET imaging. Tc lies above Re in the periodic table and should be coordinated in a similar manner as Re(I) to the phenyltriazole. **Gd. $^{94\text{m}}\text{Tc.16}$**  would likely be a useful MR / PET contrast agent; overcoming the limitations of the two techniques.

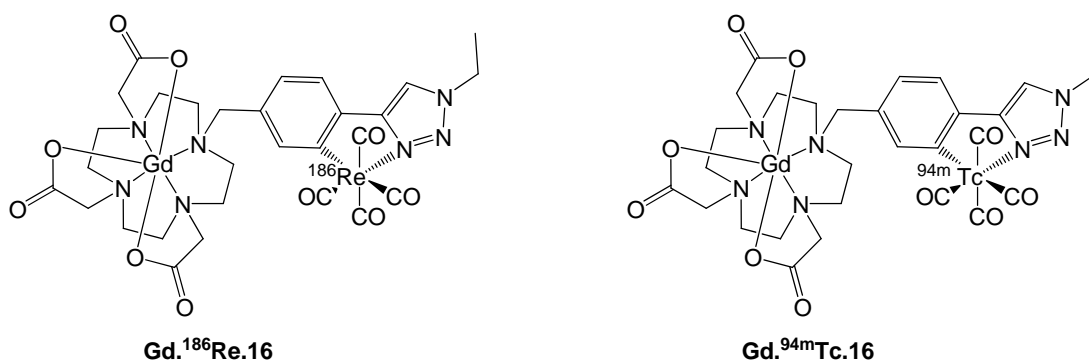


Figure 6.5 Radioisotope analogues of Gd(III) DO3A phenyltriazole appended complexes

#### 6.4 Enzyme Activated Contrast Agents

It was demonstrated in Chapter 5 that uridine can be transformed and linked to Ln(III)DO3A chelates *via* three different methods. Uridine compounds **23**, **24** and **25**, were synthesized in respectable yields as precursors for linking uridine to Ln(III)DO3A complexes, either *via* an ether, amide or triazole linker. **23** and **25** were been successfully appended to **1**, *via* the O3 on the ribose ring, to the N10 of the cyclen ring.

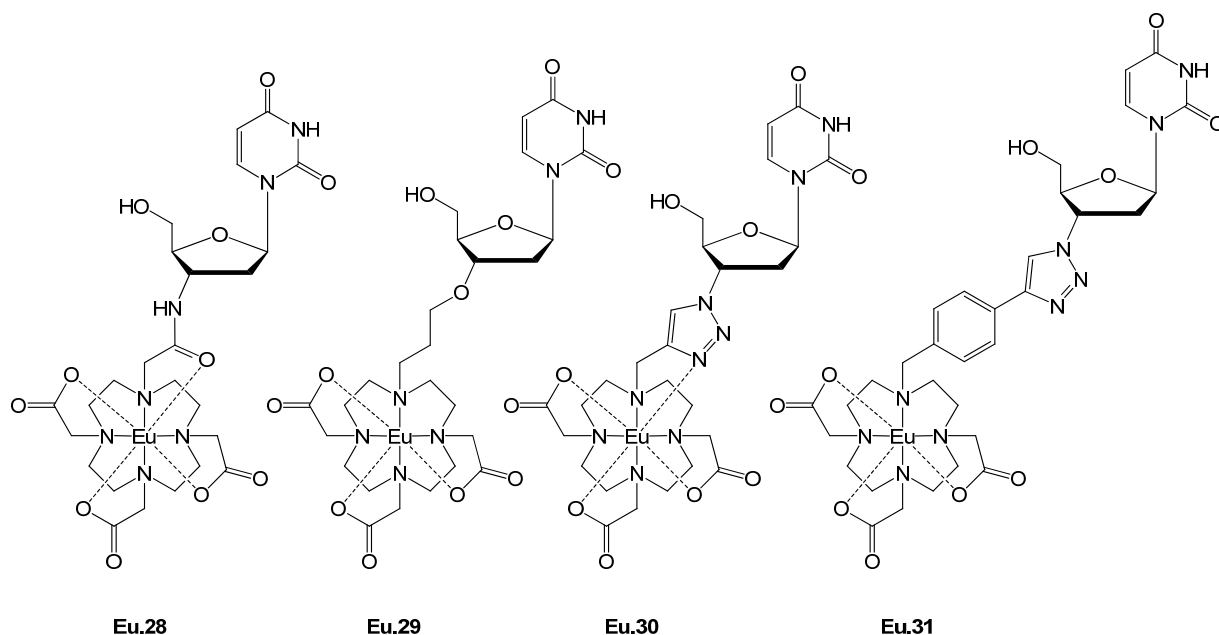


Figure 6.6 Eu(III) Uridine appended complexes

Four Eu(III) uridine appended complexes were synthesized, **Eu.28**, **Eu.29**, **Eu.30** and **Eu.31**. **Eu.29** is an ether linked uridine Eu(III)DO3A complex, with hydration state of  $q = 1$ . **Eu.28** is an amide linked uridine Eu(III) DO3A complex, with a hydration state of  $q = 1$ . **Eu.28** does not bind carbonate, therefore it can be assumed that the Gd(III) analogue will not, this does not rule it out as a contrast agent for visualizing gene therapy, it may well interact with HSV1-TK in the same manner as the PET agent FIAU.<sup>11</sup> Further tests on the Gd(III) complex analogues, upon interaction with HSV1-TK enzyme and localization within a cell are needed.

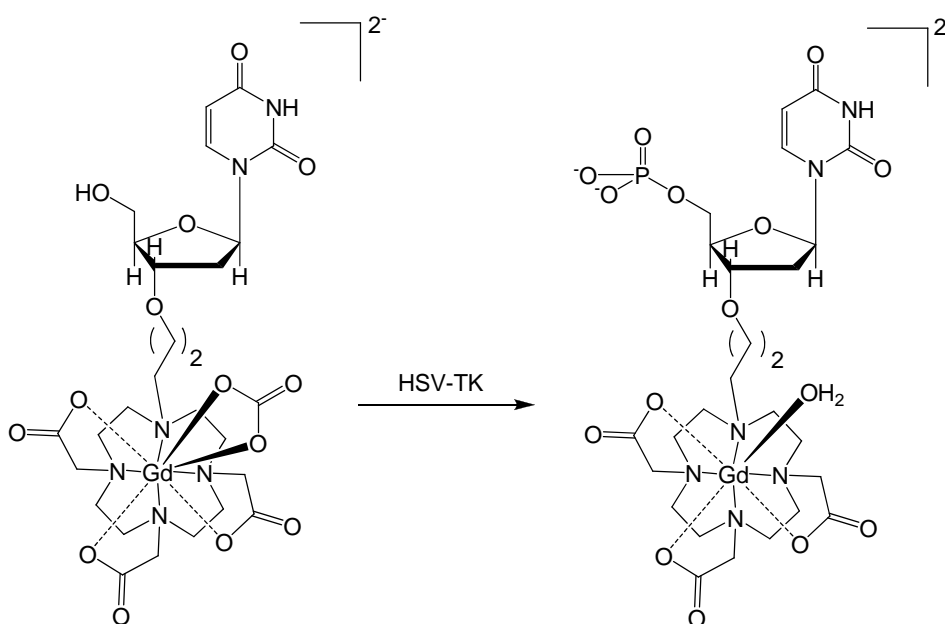
It was shown that **Eu.29** binds carbonate at physiological concentrations of  $\text{NaHCO}_3$ . This suggests that an interaction with HSV1-TK, the Gd(III) complex could act as a ‘smart’ contrast agent. Further studies into the phosphorylated form of the complexes and relaxivity studies in the presence of carbonate and the HSV1-TK enzyme, must be performed to prove that interaction with HSV1-TK will change the local hydration state of the Gd(III) complex.

It was demonstrated that 1,2,3-triazole linkers can be used to append Ln(III) complexes to a uridine molecule *via* the ‘Huisgen’ Cu(I) catalysed cycloaddition reaction between an azide and an alkyne. **Eu.30** is a 1,2,3-triazole linked uridine DO3A complex, with a hydration state  $q = 1$ . The emission spectrum is typical of an eight-coordinate complex, binding through seven molecules from the DO3A macrocycle, and one from the

N2 on the triazole, in a pyridinic manner such as **Eu.5**. **Eu.30** does not bind endogenous carbonate, therefore the Gd(III) analogue is not expected to. Further studies on the Gd(III) complex analogues, including interaction with HSV1-TK enzyme and cell localization studies are needed.

**Eu.31** is a *p*-benzyltriazole linked uridine DO3A complex, with a hydration state  $q = 1$ . Despite the lower than expected hydration state, the emission spectrum is typical of a seven-coordinate complex, binding through seven molecules from the DO3A macrocycle. Further studies into binding carbonate at physiological concentrations, interactions with HSV1-TK enzyme and relaxivity studies need to be carried out on the Gd(III) analogues, it is hypothesized that it will act as a ‘smart’ contrast agent, in the same manner as **L.Gd.3**.

The most facile route to a uridine appended Ln(III) complex is *via* the ether linker as it has fewer synthetic steps to **Ln.29**, so far this has proven the most promising in search for a ‘smart’ contrast agent, showing that carbonate will bind at physiological concentrations. Further studies on the Gd(III) analogues, phosphorylated analogues and the HSV1-TK enzyme, are required in order to show that **Gd.29** or **Gd.31** can be utilized as a smart contrast agent for imaging gene therapy (Scheme 6.4).



Scheme 6.4

# Chapter 7

## Experimental

### 7.1 Materials and Methods

#### 7.1.1 Reagents

All reagents and solvents were purchased from Alfa Aesar, Strem, Acros or Sigma Aldrich. Dichloromethane and acetonitrile were dried over calcium hydride using an Innovative Technology inc. PureSolv solvent purification system. THF was dried over sodium benzophenone. Methanol was preliminarily dried over magnesium and distilled onto 3 Å sieves. Triethylamine was preliminarily dried over calcium hydride and distilled onto 4 Å sieves.

#### 7.1.2 Chromatography

Flash column chromatography was carried out using silica gel 60. Cation exchange chromatography was carried out using Dowex 50W 50 x 4 – 200 strong ion-exchange resin, prepared with 5 M HCl, Dowex MAC-3 weak acid-cation exchange resin, prepared with 1% HCl and Amberlite XAD-16 resin, prepared with water, where stated. Analytical HPLC was carried out on a Perkin Elmer series 200, using a C12 reverse phase column (Sigma), preparative HPLC was carried out on Shimadzu LC-4A using H<sub>2</sub>O and HPLC grade MeOH (Fluka).

#### 7.1.3 Spectroscopy

<sup>1</sup>H and <sup>13</sup>C NMR spectra were recorded using Bruker, 300 MHz, 400 MHz and 500 MHz spectrometers using deuterated chloroform (CDCl<sub>3</sub>), deuterated methanol (CD<sub>3</sub>OD) and deuterium oxide (D<sub>2</sub>O) where stated, referenced to residual solvent peaks. All chemical shifts are recorded in ppm. Electrospray mass spectra (ESMS) were recorded using a Micromass Quatro mass spectrometer using MeOH as solvent. FAB mass spectra were recorded using a Kratos Concept mass spectrometer with a NBA matrix. Accurate masses

were determined at the EPSRC National MS Service at Swansea. IR measurements were carried out using a Perkin Elmer Spectrum One FT-IR spectrometer. Electronic absorption spectra were measured with a Shimadzu UV 180 spectrometer using a 10x10 mm or 10x2 mm quartz Hellma cuvette.

#### 7.1.4 Luminescence Spectroscopy

Luminescence data was recorded using a Jobin Yvon Horiba FluoroMax-P spectrometer (using DataMax for Windows v2.2). Samples were held in a 10x10 mm or 10x2 mm quartz Hellma cuvette and a cut-off filter (typically 450 nm) was used to avoid second-order diffraction effects. Excitation and emission slits were typically 10:1 nm for emission spectra. Eu(III) excitation was either direct ( $\lambda_{ex} = 395$  nm) or sensitised *via* a chromophore (typically  $\lambda_{ex} \sim 260$  nm). Eu(III) excitation spectra monitored the  $\Delta J = 2$  band. Excitation and emission slits were 5:5 nm with a 1.0 s integration time.

#### 7.1.5 Hydration State, $q$ , Determination

Lifetimes were measured by excitation (395 nm direct unless stated) of the sample with a short 40 ms pulse of light (500 pulses per point) followed by monitoring the integrated intensity of light ( $\Delta J = 2$ ) emitted during a fixed gate time of 0.1 ms, at a delay time later. Delay times were set at 0.1 ms intervals, covering 4 or more lifetimes. Excitation and emission slits were set to 5:5 nm. The data is then applied to the standard first order decay Equation 43, minimised in terms of  $k$  by iterative least-square fitting operation in Microsoft Excel, where  $I_{obs}$  is the observed intensity,  $I_o$  is the initial intensity of the excited state Eu(III) and  $t$  is the time (ms). The calculated  $k$  values are then applied to Equation 34 to calculate the hydration state,  $q$ .

$$I_{obs} = I_o e^{-kt} + offset \quad (43)$$

$$q = 1.2[(K_{H_2O} - K_{D_2O}) - 0.25] \quad (34)$$

### 7.1.6 $^1\text{H}$ Relaxation Data

The observed longitudinal water proton relaxation times ( $T_{1obs}$ ) were measured on a Stellar Spinmaster spectrometer (Stellar, Mede (PV) Italy) operating at 20 MHz, by means of the standard inversion-recovery technique (16 experiments, 2 scans). A typical  $90^\circ$  pulse width was  $3.5 \mu\text{s}$  and the reproducibility of the  $T_{1obs}$  data was  $\pm 0.5\%$ . The paramagnetic water proton relaxation rate,  $R_{1p}$  and relaxivity,  $r_1$  were determined following Equations 19, 44 and 45, where 0.38 is the diamagnetic contribution of the bulk water molecules. Complex concentrations were estimated *via* mineralization with nitric acid.

$$R_{1obs} = \frac{1}{T_{1obs}} \quad (44)$$

$$R_{1p} = R_{1obs} - 0.38 \quad (45)$$

$$r_1 = R_{1p} / [\text{Gd}] \quad (19)$$

The  $1/T_1$  nuclear magnetic relaxation dispersion (NMRD) profiles of water protons were measured over a continuum of magnetic field strength from 0.00024 to 0.7 T (corresponding to 0.01 – 30 MHz proton Larmor frequency) on a fast field-cycling Stellar Spinmaster FFC 2000 relaxometer equipped with a silver magnet. The relaxometer operates under complete computer control with an absolute uncertainty in the  $1/T_1$  values of  $\pm 1\%$ . The typical field sequences used were the NP sequence between 30 and 8 MHz and the PP sequence between 8 and 0.01MHz. The observation field was set at 13 MHz. 16 experiments of 2 scans were used for the observed longitudinal relaxation time  $T_1$  determination at each field.

Variable-temperature  $^{17}\text{O}$  NMR measurements were recorded on a JEOL EX-90 (2.1 T and 9.4 T) spectrometer, equipped with a 5 mm probe, by using  $\text{D}_2\text{O}$  as external lock. Experimental settings were: spectral width 10,000 Hz, pulse width  $7 \mu\text{s}$ , acquisition time 10 ms, 1,200 scans and no sample spinning. Solutions containing 2.6% of  $^{17}\text{O}$  isotope (Yeda,

Israel) were used. The observed transverse relaxation rates,  $R_{2obs}^O$ , were calculated from the signal width at half height.

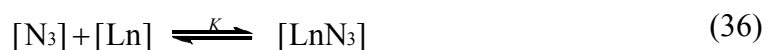
### 7.1.7 pH Titrations

pH measurements were recorded using a Jenway 3510 pH meter with a BDH probe, model 309-1025-02 calibrated at pH 4, 7 and 10. Both luminescence and relaxivity pH titrations were carried out in a background of constant ionic strength ( $I = 0.1$  NaCl, 298 K). Aqueous solutions were made basic by addition of 1 M or 0.1 M NaOH and titrated to acid pH by addition of small aliquots of 1 M or 0.1 M HCl. For each titration 20-25 points were recorded. Equation 46 and 47 were minimized in terms of  $K_a$ , where  $I_{obs}$  is the observed  $I/I_o$  ratio ( $\Delta J = 1$ ) of Eu(III) emission intensity and  $I_{Htri}$  and  $I_{tri^-}$  are the  $I/I_o$  ( $\Delta J = 1$ ) Eu(III) emission intensity ratios of the fully protonated and fully deprotonated triazole. Data analysis was performed using an iterative least-squares fitting procedure, operating in Microsoft Excel.

$$I_{obs} = \frac{[H^+]I_{Htri} + K_a I_{tri^-}}{[H^+] + K_a} \quad (46)$$

### 7.1.8 Azide Binding Studies

Aqueous solutions were adjusted to pH 5 using HCl solution. Titrations were carried out using a fixed complex concentration (1 mM) with varied  $[N_3]$  at 25 °C. 14 points were recorded for each titration. The Eu(III) complexes were excited directly, at  $\lambda_{ex} = 395$  nm and the variations in intensity of the  $\Delta J = 4$  band was recorded. The equilibrium Equation 36 was assumed, where  $K$  is the affinity constant and  $[Ln]$  represents the Ln-alkyne complex. The concentration of bound complex,  $[LnN_3]$ , is determined from Equation 37, where  $[N_3]_T$  and  $[Ln]_T$  are the total concentrations of sodium azide and the Ln-alkyne complex.



$$[\text{LnN}_3] = \frac{([\text{N}_3]_T + [\text{Ln}]_T + 1/K) - \sqrt{([\text{N}_3]_T + [\text{Ln}]_T + 1/K)^2 - 4[\text{N}_3]_T[\text{Ln}]_T}}{2} \quad (37)$$

Concentrations were substituted for Eu(III) emission intensity as in Equation 38, where  $I_{calc}$  is the calculated Eu(III) emission intensity (to be compared with the experimentally observed intensity),  $I_{Eu}$  is the intensity of the Eu(III) complex when in the absence of  $\text{N}_3$  (*i.e.* at the start of the titration) and  $I_{Eu\text{N}_3}$  is the intensity of the Eu(III) complex when  $\text{N}_3$  is entirely bound (*i.e.* at the end of the titration).

$$I_{calc} = \frac{1}{[\text{Eu}]_T} ([\text{Eu}]_T I_{Eu} + (I_{Eu\text{N}_3} - I_{Eu}) [\text{EuN}_3]) \quad (38)$$

Equations 37 and 38 and were combined to give Equation 36, which was minimized in terms of  $K$ . Data analysis was performed using an iterative least-squares fitting procedure, assuming a 1:1 binding stoichiometry, operating in Microsoft Excel.

$$I_{calc} = \frac{1}{[\text{Eu}]_T} \left( \left( \frac{(I_{Eu} \times [\text{Eu}]_T) + \left( \frac{([\text{N}_3]_T + [\text{Eu}]_T + 1/K) - \sqrt{([\text{N}_3]_T + [\text{Eu}]_T + 1/K)^2 - 4[\text{N}_3]_T[\text{Eu}]_T}}{2} \right)}{(I_{Eu\text{N}_3} - I_{Eu})} \right) \right) \quad (48)$$

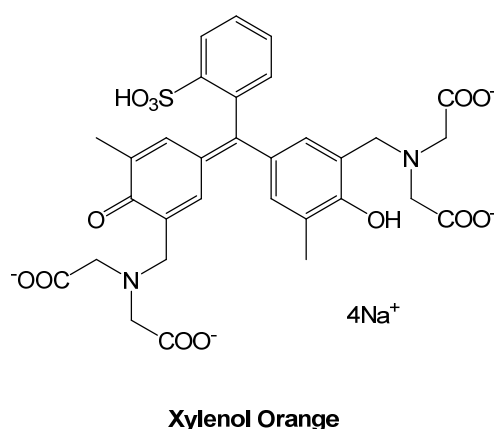
### 7.1.9 Concentration Determination via Mineralisation with Nitric Acid

In order to estimate the concentration of the Gd(III) in solution, complexes were dissolved in water and 70% nitric acid in a 1:1 ratio and left in a sealed ampule at 120 °C overnight, destroying the complex leaving free Gd(III) in solution. The observed relaxation rates for this solution were measured and applied to Equation 64 (determined from previous calibrations using atomic absorption standard solutions, 1005  $\mu\text{g ml}^{-1}$  Gd in 1 wt. %  $\text{HNO}_3$ ), where 0.4 is the corrected diamagnetic contribution of nitric acid and 13.99  $\text{mM}^{-1}\text{s}^{-1}$  is the relaxivity of Gd(III) in 45%  $\text{HNO}_3$ . Note: values are multiplied by two as solutions were diluted 50:50.

$$[\text{Gd}] = 2 \times \left( \frac{R_{1obs} - 0.40}{13.99} \right) \quad (49)$$

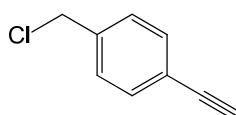
### 7.1.10 Xylenol Orange Calibrations

Xylenol orange is used as a metal ion indicator not only for the lanthanides but for various other metal ions including lead, aluminium and zinc. In acidic conditions the solutions of xylenol orange are yellow as phenolic oxygen remains protonated. Deprotonation of the hydroxyl group in basic media results in an extended electronic delocalisation, resulting in an increase of the absorption wavelength at  $\lambda_{max} \sim 580$  nm with the solution colour changing to purple. Metal ion coordination occurs through both the iminodiacetic moiety and the phenolic hydroxyl group, resulting in its deprotonation. The presence of metal ions has, therefore, the same resulting colour change effects as variation of pH. When the solutions are buffered to pH 5, colour change can be entirely attributed to the presence of metal ions in solution.



## 7.2 Phenyl Triazole synthesis

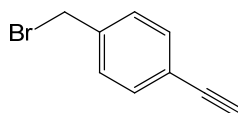
### 7.2.1 1-(Chloromethyl)-4-ethynylbenzene (**6a**)<sup>1</sup>



Thionyl chloride (10 cm<sup>3</sup>) was added slowly to 1-(hydroxymethyl)-4-ethynylbenzene (0.500 g, 3.79 mmol) at 0 °C and then heated at reflux for 1 hour. The solution was reduced, giving a colourless oil (0.560 g, 98%).  $\delta_{\text{H}}$  (400 MHz, CDCl<sub>3</sub>): 3.02 (1H, s, ~CCH~), 4.48 (2H, s, ~ClCH<sub>2</sub>C~), 7.25 (2H, d, <sup>3</sup>J<sub>HHa</sub> 8.6Hz, ~CCHCHC~), 7.39

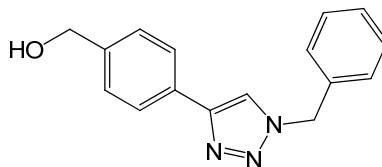
(2H, d,  $^3J_{HHa}$  8.6Hz, ~CCHCHC~).  $\delta_C$  (100 MHz,  $CDCl_3$ ): 138.0 (~CCHCHC~), 132.4 (~CCHCHC~), 128.5 (~CCHCHC~), 122.2 (~CCHCHC~), 83.1 (~CCH~), 77.9 (~CCH~), 45.6 (~CH<sub>2</sub>C~).  $m/z$  (ESMS+) 151 [M + H]<sup>+</sup>. The data was consistent with that found in ref. [1].

### 7.2.2 1-(Bromomethyl)-4-ethynylbenzene (**6b**)<sup>2</sup>



1-(hydroxymethyl)-4-ethynylbenzene (0.500 g, 3.67 mmol) and carbon tetrabromide (1.518 g, 4.587 mmol) were dissolved in diethyl ether (100 cm<sup>3</sup>), to this triphenylphosphine (1.200 g, 4.587 mmol) dissolved in diethyl ether (60 cm<sup>3</sup>) was added drop wise. The solution was stirred for 3 hours at room temperature, forming a white precipitate that formed was filtered, the filtrate is concentrated giving a yellow solid. The compound was purified on silica with hexane, giving a yellow oil (0.156 g, 22%). Rf 0.38,  $\delta_H$  (400 MHz,  $CDCl_3$ ): 3.02 (1H, s, ~CCH~), 4.38 (2H, s, ~BrCH<sub>2</sub>C~), 7.25 (2H, d,  $^3J_{HHa}$  8.6Hz, ~CCHCHC~), 7.37 (2H, d,  $^3J_{HHa}$  8.6Hz, ~CCHCHC~).  $\delta_C$  (100 MHz,  $CDCl_3$ ): 138.4 (~CCHCHC~), 132.5 (~CCHCHC~), 129 (~CCHCHC~), 122.2 (~CCHCHC~), 83.1 (~CCH~), 78.0 (~CCH~), 32.7 (~BrCH<sub>2</sub>C~).  $m/z$  (ESMS+) 195 [M + H]<sup>+</sup>. The data was consistent with that found in ref. [2].

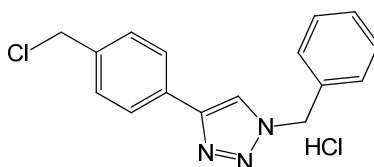
### 7.2.3 1-(Hydroxymethyl)-4-(1-phenyl-1,2,3-triazo-4-yl)-benzene (**9**)<sup>3</sup>



1-(hydroxymethyl)-4-ethynylbenzene (0.100 g, 0.833 mmol), benzyl bromide (0.156 g, 0.109 cm<sup>3</sup>, 0.916 mmol) and sodium azide (0.108 g 1.66 mmol) were dissolved in THF/H<sub>2</sub>O (25 cm<sup>3</sup>). To this sodium ascorbate (0.016 g, 0.0833 mmol) and CuSO<sub>4</sub>·5H<sub>2</sub>O (0.010 g, 0.041 mmol) were added sequentially, and the solution was stirred at room temperature for 24 hours. After this period 12% ammonia solution followed by water (50

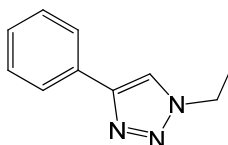
cm<sup>3</sup>), precipitating a white solid which was purified on silica using DCM:ethyl acetate (70:30), giving a white solid (0.071 g, 32%). Rf. 0.68.  $\delta_{\text{H}}$  (400 MHz, CDCl<sub>3</sub>): 1.80 (1H, bs, ~OHCH<sub>2</sub>C~), 4.63 (2H, s, ~OHCH<sub>2</sub>C~), 5.49 (2H, s, ~NCH<sub>2</sub>C~), 7.22-7.30 (5H, m, ~CH<sub>2</sub>Ph~) 7.31 (2H, d, <sup>3</sup>J<sub>HHa</sub> 8.6Hz, ~CCHCHC~), 7.57 (1H, s, ~CCHN~), 7.70 (2H, d, <sup>3</sup>J<sub>HHa</sub> 8.6Hz, ~CCHCHC~).  $\delta_{\text{C}}$  (100 MHz, CDCl<sub>3</sub>): 148.5 (~NCCH~), 140.9 (~CCHCHC~), 134.6 (~CCHCHC~), 129.8 (~CH<sub>2</sub>CCH~), 129.1, 128.8, 128.1 (~CPh~), 127.3 (~CCHCHC~), 125.8 (~CCHCHC~), 119.1 (~CCHN~), 65.0 (~OHCH<sub>2</sub>C~), 54.2 (~CCH<sub>2</sub>N~). *m/z* (ESMS+) 266 [M + H]<sup>+</sup>. The data was consistent with that found in ref. [3].

#### 7.2.4 1-(Chloromethyl)-4-(1-phenyl-1,2,3-triazo-4-yl)-benzene (hydrochloride salt)(10)



Thionyl chloride (10 cm<sup>3</sup>) was carefully added to **9** (0.071 g, 0.267 mmol) at 0°C and then heated at 70 °C for 1 hour. The solution was reduced, giving a white solid (0.08 g, 93%).  $\delta_{\text{H}}$  (400 MHz, CDCl<sub>3</sub>): 4.43 (2H, bs, ~ClCH<sub>2</sub>C~), 5.72 (2H, bs, ~NCH<sub>2</sub>C~) 7.25 (5H, bm, ~CH<sub>2</sub>Ph~) 7.41 (2H, bd, <sup>3</sup>J<sub>HHa</sub> 8.6Hz, ~CCHCHC~), 7.85 (2H, bd, <sup>3</sup>J<sub>HHa</sub> 8.6Hz, ~CCHCHC~), 8.87 (1H, bs, ~CCHN~).  $\delta_{\text{C}}$  (100 MHz, CDCl<sub>3</sub>): 142.7 (~CCHCHC~), 141 (~CCHCHC~), 131.6 (~CH<sub>2</sub>CCH~), 130.0, 129.8, 129.6 (~CPh~), 129.3 (~CCHCHC~), 127.6 (~CCHCHC~), 125.1 (~CCHN~), 122.8 (~NCCH~), 57.5 (~CCH<sub>2</sub>N~), 47.2 (~ClCH<sub>2</sub>C~). *m/z* (ESMS+) 284 [M + H]<sup>+</sup>.

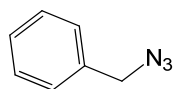
#### 7.2.5 1-Ethyl-4-phenyl-1,2,3-triazole (13)<sup>4</sup>



Phenyl acetylene (1.000 g, 1.075 cm<sup>3</sup>, 9.8 mmol), ethyl bromide (2.970 g, 2.034 cm<sup>3</sup>, 29.41 mmol) and sodium azide (1.900 g, 29.41 mmol) were dissolved in EtOH/H<sub>2</sub>O

(25 cm<sup>3</sup>). To this sodium ascorbate (0.194 g, 0.98 mmol) and CuSO<sub>4</sub>·5H<sub>2</sub>O (0.122 g, 0.49 mmol) were added sequentially, and the solution was stirred at room temperature for 24 hours. After this period 35% ammonia solution (0.5 cm<sup>3</sup>) was added followed by water (50 cm<sup>3</sup>), which was extracted with CHCl<sub>3</sub> (3 x 50 cm<sup>3</sup>). The combined organic fractions were washed with water (50 cm<sup>3</sup>) and saturated NaCl solution (50 cm<sup>3</sup>), dried over MgSO<sub>4</sub>, filtered and concentrated *in vacuo*, giving a yellow oil (1.540 g) which was purified on silica (DCM:ethyl acetate (70:30)), yielding a yellow solid (0.793 g, 47%). δ<sub>H</sub> (400 MHz, CDCl<sub>3</sub>): 1.52 (3H, t, <sup>3</sup>J<sub>HH</sub> 7.4Hz, ~NCH<sub>2</sub>CH<sub>3</sub>~), 4.73 (2H, q, <sup>3</sup>J<sub>HH</sub> 7.4Hz, ~NCH<sub>2</sub>CH<sub>3</sub>~), 7.25 (1H, t, <sup>3</sup>J<sub>HH</sub> 7.4Hz ~CHCHCHCHCH~), 7.34 (2H, t, <sup>3</sup>J<sub>HH</sub> 7.4Hz, ~CHCHCHC~), 7.70 (1H, s, ~CCHN~), 7.74 (2H, d, <sup>3</sup>J<sub>HH</sub> 7.0Hz, ~CHCHC~). δ<sub>C</sub> (100 MHz, CDCl<sub>3</sub>): 148.7 (~CC(N)CH~), 130.7 (~CHCHCHC~), 128.8 (~CHCHCHC~), 128 (~CHCHCHCHCH~), 125.2 (~CHCHC~), 119.1 (~CCHN~), 45.4 (~NCH<sub>2</sub>CH<sub>3</sub>~), 15.5 (~NCH<sub>2</sub>CH<sub>3</sub>~). *m/z* (ESMS+) 173 [M + H]<sup>+</sup>. The data was consistent with that found in ref. [4].

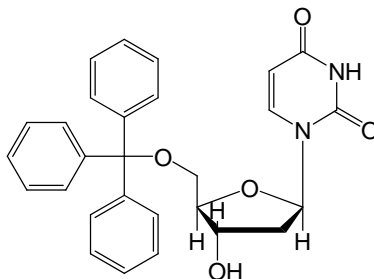
#### 7.2.6 Benzyl Azide<sup>5</sup>



Benzyl bromide (0.1 g, 0.069 cm<sup>3</sup>, 0.58 mmol) and sodium azide (0.19 g, 2.9 mmol) were taken up in MeCN (10 cm<sup>3</sup>) and heated at 80°C for 12 hours. The solution was taken up in diethyl ether (25 cm<sup>3</sup>) washed with water (3 x 50 cm<sup>3</sup>) and saturated NaCl (50 cm<sup>3</sup>), the organic layer wash dried over MgSO<sub>4</sub>, filtered and concentrated under reduced pressure giving an orange oil (0.068 g, 96%). δ<sub>H</sub> (400 MHz, CDCl<sub>3</sub>): 4.3 (2H, s, ~N<sub>3</sub>CH<sub>2</sub>C~), 7.28 – 7.35 (5H, m, ~Ph~). *m/z* (ESMS+) 134 [M + H]<sup>+</sup>. The data was consistent with that found in ref. [5].

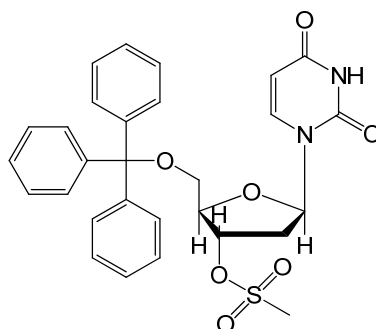
## 7.3 Uridine Transformations

### 7.3.1 5-Trytyl-2-deoxyuridine (**17**)<sup>6</sup>



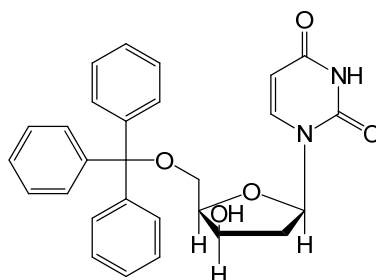
Deoxy-uridine (0.100 g, 0.438 mmol) was dissolved in anhydrous pyridine (5 cm<sup>3</sup>) with trityl chloride (0.134 g, 0.482 mmol) and DMAP (0.0013 g, 0.0109 mmol). After stirring at room temperature under nitrogen for 18 hours, the solution was then heated at 70°C for 3 hours and poured over ice water (100 cm<sup>3</sup>). The gummy precipitate was filtered and taken up in DCM (50 cm<sup>3</sup>), dried over MgSO<sub>4</sub> and concentrated *in vacuo* giving a white solid (0.249 g). The solid was washed with petroleum ether 40-60°C (3 x 50 cm<sup>3</sup>) to remove impurities giving a white solid (0.171 g, 83%).  $\delta_{\text{H}}$  (400 MHz, CDCl<sub>3</sub>): 2.12 (1H, m, ~CH(OH)CH<sub>2</sub>CHN~), 2.35 (1H, m, ~CH(OH)CH<sub>2</sub>CHN~), 3.34 (2H, d, <sup>3</sup>J<sub>HH</sub> 3.1Hz ~OCH<sub>2</sub>CH~), 3.66 (1H, bs, ~CHOH~), 3.95 (1H, dd, <sup>3</sup>J<sub>HHa</sub> 3.9Hz, <sup>3</sup>J<sub>HHb</sub> 3.1Hz, ~CH<sub>2</sub>CHCH(OH)~), 4.46 (1H, dd, <sup>3</sup>J<sub>HHa</sub> 5.8Hz, <sup>3</sup>J<sub>HHb</sub> 4.3Hz, ~CHCH(OH)CH<sub>2</sub>~), 5.26 (1H, d, <sup>3</sup>J<sub>HH</sub> 8.2Hz, ~NCH=CH~), 6.21 (1H, t, <sup>3</sup>J<sub>HH</sub> 6.2Hz, ~NCHCH<sub>2</sub>~), 7.25 (15H, m, ~benzyl ring~), 7.66 (1H, d, <sup>3</sup>J<sub>HH</sub> 7.8Hz, ~NCH=CH~), 9.75 (1H, bs, ~NH~).  $\delta_{\text{C}}$  (100 MHz, CDCl<sub>3</sub>): 163.3, 143.2 (~CO~), 140.2 (~NCH=CH~), 128.6-127.2 (~benzyl ring~), 123.9 (~C(Ph)<sub>3</sub>~), 102.2 (~NCH=CH~), 86.1 (~CH<sub>2</sub>CHCH(OH)~), 85.1 (~NCHCH<sub>2</sub>~), 71.2 (~CHCH(OH)CH<sub>2</sub>~), 63.1 (~CH(OH)CH<sub>2</sub>CHN~), 41.2 (~CH<sub>2</sub>CHCH(OH)CH<sub>2</sub>~). *m/z* (ESMS-) 469 [M - H]<sup>-</sup>. The data was consistent with that found in ref. [6].

### 7.3.2 3'-O-Methanesulfonyl-5'-O-trityl-2'-deoxyuridine (**18**)<sup>6</sup>



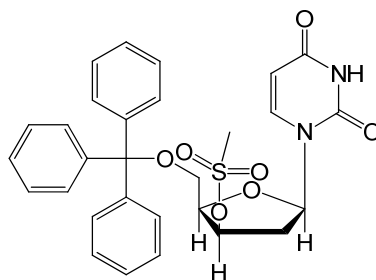
**17** (0.300 g, 0.638 mmol) was dissolved at room temperature in pyridine (5 cm<sup>3</sup>). The solution was put into an ice bath and methane sulfonyl chloride (0.145 g, 0.0983 cm<sup>3</sup>, 1.276 mmol) was added dropwise. The resulting solution was stirred at 4°C for 24 hours, the reaction mixture was then added to ice water (2:3) (150 cm<sup>3</sup>), stirred for 20 minutes and a pale solid formed, which was collected by filtration and washed with water (500 cm<sup>3</sup>). The solid was taken up in DCM (50 cm<sup>3</sup>), dried over MgSO<sub>4</sub> and concentrated, giving a white solid (0.253 g, 72%).  $\delta_{\text{H}}$  (400 MHz, CDCl<sub>3</sub>): 2.32 (1H, m, ~CH(OS)CH<sub>2</sub>CHN~), 2.62 (1H, m, ~CH(OS)CH<sub>2</sub>CHN~), 2.91 (3H, s, ~OS(O<sub>2</sub>)CH<sub>3</sub>~) 3.43 (2H, dd, <sup>3</sup>J<sub>HHa</sub> 2.7Hz, <sup>2</sup>J<sub>HHb</sub> 0.7Hz ~OCH<sub>2</sub>CH~), 3.22 (1H, q, <sup>3</sup>J<sub>HHa</sub> 2.7Hz, <sup>3</sup>J<sub>HHb</sub> 2.7Hz, ~CH<sub>2</sub>CHCH(OS)~), 5.29 (1H, dt, <sup>3</sup>J<sub>HHa</sub> 6.2Hz, <sup>3</sup>J<sub>HHb</sub> 2.7Hz, ~CHCH(OS)CH<sub>2</sub>~), 5.32 (1H, d, <sup>3</sup>J<sub>HH</sub> 8.2Hz, ~NCH=CH~), 6.26 (1H, t, <sup>3</sup>J<sub>HH</sub> 6.2Hz, ~NCHCH<sub>2</sub>~), 7.24 (15H, m, ~benzyl ring~), 7.57 (1H, d, <sup>3</sup>J<sub>HH</sub> 7.8Hz, ~NCH=CH~), 9.75 (1H, bs, ~NH~).  $\delta_{\text{C}}$  (100 MHz, CDCl<sub>3</sub>): 146.9, 142.8 (~CO~), 139.5(~NCH=CH~), 128.7-127.2 (~benzyl ring~), 123.7 (~C(Ph)<sub>3</sub>~), 102.7 (~NCH=CH~), 84.7 (~NCHCH<sub>2</sub>~), 83.8 (~CH<sub>2</sub>CHCH(OS)~), 79.2 (~CHCH(OS)CH<sub>2</sub>~), 62.7 (~CH(OS)CH<sub>2</sub>CHN~), 41.2 (~OCH<sub>2</sub>CH~), 38.6 (~OS(O<sub>2</sub>)CH<sub>3</sub>~). *m/z* (ESMS+) 571 [M + Na]<sup>+</sup>. The data was consistent with that found in ref. [6].

### 7.3.3 1-[2-Deoxy-5-O-(triphenylmethyl)- $\beta$ -D-threo-pento-furanosyl]-uracil (**19**)<sup>6</sup>



A solution of **18** (0.23 g, 0.419 mmol) in absolute EtOH (4.5 cm<sup>3</sup>), 1M NaOH (1.5 cm<sup>3</sup>) and water (2 cm<sup>3</sup>) was heated at 130°C for 4 hours. The solution was transferred to a 400 cm<sup>3</sup> beaker and diluted with ice water (100 cm<sup>3</sup>), while vigorously stirring, the solution was acidified to pH 3 with concentrated HCl, after stirring for 20 minutes the precipitate was filtered and washed with water (500 cm<sup>3</sup>). The precipitate was taken up in DCM (50 cm<sup>3</sup>), dried over MgSO<sub>4</sub> and concentrated, giving a white solid (0.195 g, 99%).  $\delta_{\text{H}}$  (400 MHz, CDCl<sub>3</sub>): 2.12 (1H, m, ~CH(OH)CH<sub>2</sub>CHN~), 2.37 (1H, m, ~CH(OH)CH<sub>2</sub>CHN~), 3.07 (1H, bs, ~CHOH~), 3.38 - 3.58 (2H, m, ~OCH<sub>2</sub>CH~), 3.99 (1H, m, ~CH<sub>2</sub>CHCH(OH)~), 4.42 (1H, m, ~CHCH(OH)CH<sub>2</sub>~), 5.33 (1H, d, <sup>3</sup>J<sub>HH</sub> 8.1Hz, ~NCH=CH~), 5.98 (1H, d, <sup>3</sup>J<sub>HH</sub> 7.6Hz, ~NCHCH<sub>2</sub>~), 7.25 (15H, m, ~benzyl ring~), 7.60 (1H, d, <sup>3</sup>J<sub>HH</sub> 8.1Hz, ~NCH=CH~), 9.77 (1H, bs, ~NH~).  $\delta_{\text{C}}$  (100 MHz, CDCl<sub>3</sub>): 163.3, 143.2 (~CO~), 140.2 (~NCH=CH~), 128.6-127.2 (~benzyl ring~), 123.9 (~C(Ph)<sub>3</sub>~), 102.2 (~NCH=CH~), 83.1 (~CH<sub>2</sub>CHCH(OH)~), 82.1 (~NCHCH<sub>2</sub>~), 71.2 (~CHCH(OH)CH<sub>2</sub>~), 61.9 (~CH(OH)CH<sub>2</sub>CHN~), 40.9 (~CH(OH)CH<sub>2</sub>CHN~). *m/z* (ESMS<sup>-</sup>) 469 [M - H]<sup>-</sup>. The data was consistent with that found in ref. [6].

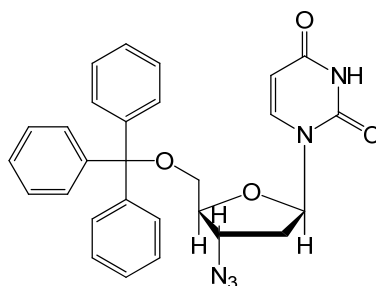
7.3.4 *1-[2-Deoxy-3-O-methanesulfonyl-5-O-(triphenylmethyl)-β-D-threo-pentofuranosyl]uracil (20)*<sup>6</sup>



**19** (0.158 g, 0.336 mmol) was dissolved at room temperature in pyridine (5 cm<sup>3</sup>). The solution was put into an ice bath and methane sulfonyl chloride (0.076 g, 0.051 cm<sup>3</sup>, 0.672 mmol) was added dropwise. The resulting solution was stirred at 4°C for 24 hours, the reaction mixture was then added to ice water (2:3) (150 cm<sup>3</sup>), this was stirred for 20 minutes and a pale solid formed, which was collected by filtration and washed with water (500 cm<sup>3</sup>). The solid was taken up in DCM (50 cm<sup>3</sup>), dried over MgSO<sub>4</sub> and concentrated, giving a white solid (0.180 g, 98%).  $\delta_{\text{H}}$  (400 MHz, CDCl<sub>3</sub>): 2.41 (1H, m, ~CH(OS)CH<sub>2</sub>CHN~), 2.69 (1H, m, ~CH(OS)CH<sub>2</sub>CHN~), 2.68 (3H, s, ~OS(O<sub>2</sub>)CH<sub>3</sub>~) 3.38

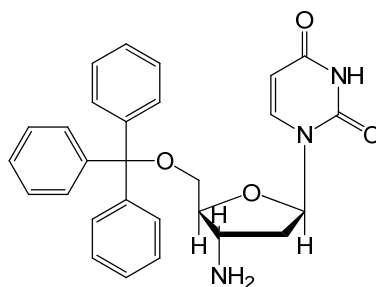
- 3.58 (2H, m,  $\sim\text{OCH}_2\text{CH}\sim$ ), 4.16 (1H, m,  $\sim\text{CH}_2\text{CHCH}(\text{OS})\sim$ ), 5.17 (1H, m,  $\sim\text{CHCH}(\text{OS})\text{CH}_2\sim$ ), 5.54 (1H, d,  $^3J_{\text{HH}}$  8.1Hz,  $\sim\text{NCH}=\text{CH}\sim$ ), 6.12 (1H, d,  $^3J_{\text{HH}}$  7.6Hz,  $\sim\text{NCHCH}_2\sim$ ), 7.25 – 7.40 (16H, m,  $\sim\text{benzyl ring}\sim$ ,  $\sim\text{NCH}=\text{CH}\sim$ ), 9.77 (1H, bs,  $\sim\text{NH}\sim$ ), 9.75 (1H, bs,  $\sim\text{NH}\sim$ ).  $\delta_{\text{C}}$  (100 MHz,  $\text{CDCl}_3$ ): 146.9, 142.8 ( $\sim\text{CO}\sim$ ), 139.5( $\sim\text{NCH}=\text{CH}\sim$ ), 128.7-127.2 ( $\sim\text{benzyl ring}\sim$ ), 123.7 ( $\sim\text{C}(\text{Ph})_3\sim$ ), 102.7 ( $\sim\text{NCH}=\text{CH}\sim$ ), 84.7 ( $\sim\text{NCHCH}_2\sim$ ), 83.8 ( $\sim\text{CH}_2\text{CHCH}(\text{OS})\sim$ ), 79.2 ( $\sim\text{CHCH}(\text{OS})\text{CH}_2\sim$ ), 62.7 ( $\sim\text{CH}(\text{OS})\text{CH}_2\text{CHN}\sim$ ), 41.2 ( $\sim\text{OCH}_2\text{CH}\sim$ ), 28.6 ( $\sim\text{OS}(\text{O}_2)\text{CH}_3\sim$ ).  $m/z$  (ESMS+) 571  $[\text{M} + \text{Na}]^+$ . The data was consistent with that found in ref. [6].

### 7.3.5 3-Azido-5-O-trityl-2,3-dideoxyuridine (**21**)<sup>6</sup>



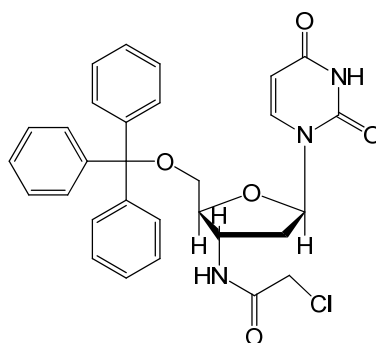
**20** (0.157 g, 0.286 mmol) was dissolved in DMF (5 cm<sup>3</sup>) with sodium azide (0.074 g, 1.145 mmol), this solution was heated at 85°C for 2 hours and poured over ice water (100 cm<sup>3</sup>). The gummy precipitate was then filtered and taken up in DCM (50 cm<sup>3</sup>), dried over  $\text{MgSO}_4$  and concentrated, giving a white solid (0.091 g, 64%).  $\delta_{\text{H}}$  (400 MHz,  $\text{CDCl}_3$ ): 2.30 (1H, m,  $\sim\text{CH}(\text{N}_3)\text{CH}_2\text{CHN}\sim$ ), 2.40 (1H, m,  $\sim\text{CH}(\text{N}_3)\text{CH}_2\text{CHN}\sim$ ), 3.34 – 3.48 (2H, m,  $\sim\text{OCH}_2\text{CH}\sim$ ), 3.85 (1H, m,  $\sim\text{CH}_2\text{CHCH}(\text{N}_3)\sim$ ), 4.25 (1H, dd,  $^3J_{\text{HHa}}$  6.2Hz,  $^3J_{\text{HHb}}$  6.6Hz,  $\sim\text{CHCH}(\text{N}_3)\text{CH}_2\sim$ ), 5.26 (1H, d,  $^3J_{\text{HH}}$  8.2Hz,  $\sim\text{NCH}=\text{CH}\sim$ ), 6.11 (1H, t,  $^3J_{\text{HH}}$  6.2Hz,  $\sim\text{NCHCH}_2\sim$ ), 7.25 (15H, m,  $\sim\text{benzyl ring}\sim$ ), 7.73 (1H, d,  $^3J_{\text{HH}}$  7.8Hz,  $\sim\text{NCH}=\text{CH}\sim$ ), 8.83 (1H, bs,  $\sim\text{NH}\sim$ ).  $\delta_{\text{C}}$  (100 MHz,  $\text{CDCl}_3$ ): 163.3, 143.2 ( $\sim\text{CO}\sim$ ), 140.2 ( $\sim\text{NCH}=\text{CH}\sim$ ), 128.6-127.2 ( $\sim\text{benzyl ring}\sim$ ), 123.9 ( $\sim\text{C}(\text{Ph})_3\sim$ ), 102.2 ( $\sim\text{NCH}=\text{CH}\sim$ ), 86.1 ( $\sim\text{CH}_2\text{CHCH}(\text{N}_3)\sim$ ), 85.1 ( $\sim\text{NCHCH}_2\sim$ ), 71.2 ( $\sim\text{CHCH}(\text{N}_3)\text{CH}_2\sim$ ), 53.1 ( $\sim\text{CH}(\text{N}_3)\text{CH}_2\text{CHN}\sim$ ), 29.2 ( $\sim\text{CH}_2\text{CHCH}(\text{N}_3)\text{CH}_2\sim$ ).  $m/z$  (ESMS-) 494  $[\text{M} - \text{H}]^-$ . The data was consistent with that found in ref. [6].

### 7.3.6 3-Amino-5-O-trityl-2,3-dideoxyuridine (**22**)<sup>6,7</sup>



**21** (0.055 g, 0.111 mmol) was dissolved in absolute EtOH (50 cm<sup>3</sup>) to this palladium on carbon (0.010 g) was added, the mixture was stirred for 2 hours at room temperature under an atmosphere of hydrogen (balloon). The solution was then filtered through celite and concentrated. The white solid, was recrystallised from methanol:chloroform to give white crystals (0.009 g, 17%).  $\delta_{\text{H}}$  (500 MHz, MeOD): 2.61 (2H, m,  $\sim\text{CH}(\text{NH}_2)\text{CH}_2\text{CHN}\sim$ ), 3.55 (2H, m,  $\sim\text{OCH}_2\text{CH}\sim$ ), 4.05 (1H, m,  $\sim\text{CHCH}(\text{NH}_2)\text{CH}_2\sim$ ), 4.27 (1H, m,  $\sim\text{CH}_2\text{CHCH}(\text{NH}_2)\sim$ ), 5.43 (1H, d,  $^3J_{\text{HH}}$  8.2Hz,  $\sim\text{NCH}=\text{CH}\sim$ ), 6.26 (1H, t,  $^3J_{\text{HH}}$  6.2Hz,  $\sim\text{NCHCH}_2\sim$ ), 7.23 -7.48 (15H, m,  $\sim\text{C}(\text{Ph})_3\sim$ ), 7.79 (1H, d,  $^3J_{\text{HH}}$  8.2Hz,  $\sim\text{NCH}=\text{CH}\sim$ ).  $\delta_{\text{C}}$  (125 MHz, MeOD): 166.3, 142.5 ( $\sim\text{CO}\sim$ ), 144.8 ( $\sim\text{NCH}=\text{CH}\sim$ ), 128.6-127.2 ( $\sim\text{benzyl ring}\sim$ ), 123.9 ( $\sim\text{C}(\text{Ph})_3\sim$ ), 103.2 ( $\sim\text{NCH}=\text{CH}\sim$ ), 87.3 ( $\sim\text{CH}_2\text{CHCH}(\text{NH}_2)\sim$ ), 84.2 ( $\sim\text{NCHCH}_2\sim$ ), 65.2 ( $\sim\text{CH}_2\text{CHCH}(\text{NH}_2)\text{CH}_2\sim$ ), 52.1 ( $\sim\text{CHCH}(\text{NH}_2)\text{CH}_2\sim$ ), 37.1 ( $\sim\text{CH}(\text{NH}_2)\text{CH}_2\text{CHN}\sim$ ).  $m/z$  (ESMS+) 470 [M + H]<sup>+</sup>. The data was consistent with that found in ref. [6].

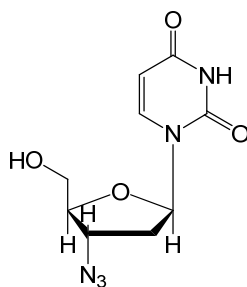
### 7.3.7 3-Chloroacetamide-5-O-trityl-2,3-dideoxyuridine (**23**)



**22** (0.012 g, 0.0256 mmol) was dissolved in DCM (5 cm<sup>3</sup>) at 0 °C to this triethylamine (2.8 mg, 3.9  $\mu\text{l}$ , 0.0282 mmol) was added, followed by chloroacetate chloride (3.15 mg, 2.22  $\mu\text{l}$ , 0.0282 mmol) in a solution of DCM (1 cm<sup>3</sup>) dropwise. After 30 minutes the solution was warmed to room temperature. The solution was washed with water (4 x 25 cm<sup>3</sup>) and saturated NaCl solution (2 x 25 cm<sup>3</sup>); the organic layer was dried over MgSO<sub>4</sub>,

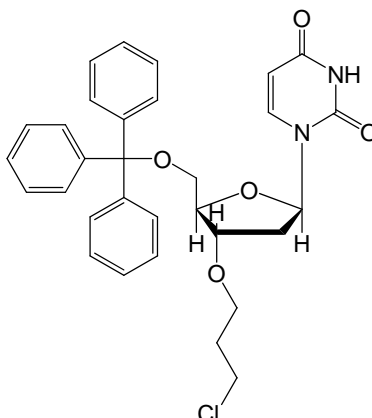
filtered and concentrated, yielding a yellow oil (8 mg, 57%).  $\delta_{\text{H}}$  (400 MHz,  $\text{CDCl}_3$ ): 2.39 (2H, m,  $\sim\text{CH}(\text{NH})\text{CH}_2\text{CHN}\sim$ ), 3.42 (2H, bd,  $^3J_{\text{HH}}$  3.1Hz,  $\sim\text{OCH}_2\text{CH}\sim$ ), 3.92 (1H, m,  $\sim\text{CH}_2\text{CHCH}(\text{NH})\sim$ ), 4.00 (2H, s,  $\sim\text{NHC}(\text{O})\text{CH}_2\text{Cl}\sim$ ) 4.64 (1H, m,  $\sim\text{CHCH}(\text{NH})\text{CH}_2\sim$ ), 5.30 (1H, d,  $^3J_{\text{HH}}$  8.2Hz,  $\sim\text{NCH}=\text{CH}\sim$ ), 6.18 (1H, t,  $^3J_{\text{HH}}$  6.2Hz,  $\sim\text{NCHCH}_2\sim$ ), 6.56 (1H, bd,  $^3J_{\text{HH}}$  7.0Hz,  $\sim\text{CH}(\text{NH})\text{CH}_2\sim$ ) 7.15 -7.48 (15H, m,  $\sim\text{C}(\text{Ph})_3\sim$ ), 7.72 (1H, d,  $^3J_{\text{HH}}$  8.2Hz,  $\sim\text{NCH}=\text{CH}\sim$ ) 8.24 (1H, bs,  $\sim\text{NH}\sim$ ).  $\delta_{\text{C}}$  (100 MHz,  $\text{CDCl}_3$ ): 166.3, 142.5 ( $\sim\text{CO}\sim$ ), 144.8 ( $\sim\text{NCH}=\text{CH}\sim$ ), 128.6-127.2 ( $\sim\text{phenyl ring}\sim$ ), 123.9 ( $\sim\text{C}(\text{Ph})_3\sim$ ), 103.2 ( $\sim\text{NCH}=\text{CH}\sim$ ), 87.3 ( $\sim\text{CH}_2\text{CHCH}(\text{NH})\sim$ ), 84.2 ( $\sim\text{NCHCH}_2\sim$ ), 61.2 ( $\sim\text{CH}_2\text{CHCH}(\text{NH})\text{CH}_2\sim$ ), 52.1 ( $\sim\text{CHCH}(\text{NH})\text{CH}_2\sim$ ), 41.1 ( $\sim\text{CH}(\text{NH})\text{CH}_2\text{CHN}\sim$ ) 37.1 ( $\sim\text{NHC}(\text{O})\text{CH}_2\text{Cl}\sim$ ).  $m/z$  (ESMS-) 544 [M - H]<sup>-</sup>.

### 7.3.8 3-Azido-2,3-dideoxyuridine (**24**)<sup>6</sup>



A suspension of **21** (0.065 g, 0.131 mmol) in 80% acetic acid (10 cm<sup>3</sup>) was heated at 110°C for 20 minutes. The solution was permitted to cool to room temperature at which the trityl alcohol precipitated out, water (5 cm<sup>3</sup>) was added to aid precipitation and the mixture was filtered. The filtrate was clarified using activated charcoal and stirred for 20 minutes. After two filtrations the filtrate was concentrated, the excess water was lyophilised yielding a white solid (0.014 g, 42%).  $\delta_{\text{H}}$  (400 MHz,  $\text{D}_2\text{O}$ ): 2.29 (1H, m,  $\sim\text{CH}(\text{N}_3)\text{CH}_2\text{CHN}\sim$ ), 2.45 (1H, m,  $\sim\text{CH}(\text{N}_3)\text{CH}_2\text{CHN}\sim$ ), 3.73 (2H, m,  $\sim\text{OCH}_2\text{CH}\sim$ ), 3.97 (1H, m,  $\sim\text{CH}_2\text{CHCH}(\text{N}_3)\sim$ ), 4.38 (1H, dd,  $^3J_{\text{HHa}}$  6.2Hz,  $^3J_{\text{HHb}}$  6.6Hz,  $\sim\text{CHCH}(\text{N}_3)\text{CH}_2\sim$ ), 5.81 (1H, d,  $^3J_{\text{HH}}$  8.2Hz,  $\sim\text{NCH}=\text{CH}\sim$ ), 6.20 (1H, t,  $^3J_{\text{HH}}$  6.2Hz,  $\sim\text{NCHCH}_2\sim$ ), 7.76 (1H, d,  $^3J_{\text{HH}}$  7.8Hz,  $\sim\text{NCH}=\text{CH}\sim$ ).  $m/z$  (ESMS-) 252 [M - H]<sup>-</sup>. The data was consistent with that found in ref. [6].

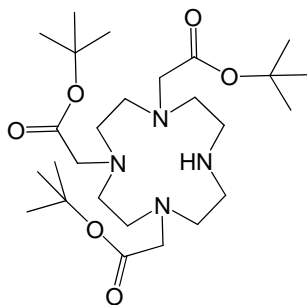
### 7.3.9 5-Trityl-2-(-3-chloropropoxy)-uridine (25)



To a solution of **17** (0.100 g, 0.213 mmol) in DMF (5 cm<sup>3</sup>) containing K<sub>2</sub>CO<sub>3</sub> (0.032 g, 0.234 mmol), 1-bromo-3-chloropropane (0.036 g, 0.023 cm<sup>3</sup>, 0.234 mmol) was added, this was heated at 70°C for 4 hours. After this the solution was added to water (20 cm<sup>3</sup>), a white precipitate was collected and taken up in DCM (30 cm<sup>3</sup>), dried with MgSO<sub>4</sub> and concentrated, giving a yellow oil (0.17 g). The oil was taken up in DCM (50 cm<sup>3</sup>) and washed with water (3 x 50 cm<sup>3</sup>), the organic layer was dried with MgSO<sub>4</sub> and concentrated, giving a colourless oil (0.09 g, 77%).  $\delta_{\text{H}}$  (400 MHz, CDCl<sub>3</sub>): 2.04 (2H, t, <sup>3</sup>*J*<sub>HH</sub> 6.7Hz ~OCH<sub>2</sub>CH<sub>2</sub>CH<sub>2</sub>Cl~), 2.17 (1H, m, ~CH(OCH<sub>2</sub>)CH<sub>2</sub>CHN~), 2.37 (1H, m, ~CH(OCH<sub>2</sub>)CH<sub>2</sub>CHN~), 3.40 (2H, d, <sup>3</sup>*J*<sub>HH</sub> 3.1Hz ~OCH<sub>2</sub>CH~), 3.49 (2H, m, ~OCH<sub>2</sub>CH<sub>2</sub>CH<sub>2</sub>Cl~), 3.95 (1H, dd, <sup>3</sup>*J*<sub>HHa</sub> 3.9Hz, <sup>3</sup>*J*<sub>HHb</sub> 3.1Hz, ~CH<sub>2</sub>CHCH(O)~), 3.98 (2H, t, <sup>3</sup>*J*<sub>HH</sub> 6.7Hz ~OCH<sub>2</sub>CH<sub>2</sub>CH<sub>2</sub>Cl~), 4.47 (1H, dd, <sup>3</sup>*J*<sub>HHa</sub> 6.3Hz, <sup>3</sup>*J*<sub>HHb</sub> 4.7Hz, ~CHCH(O)CH<sub>2</sub>~), 5.36 (1H, d, <sup>3</sup>*J*<sub>HH</sub> 8.2Hz, ~NCH=CH~), 6.22 (1H, t, <sup>3</sup>*J*<sub>HH</sub> 6.3Hz, ~NCHCH<sub>2</sub>~), 7.25 (15H, m, ~benzyl ring~), 7.66 (1H, d, <sup>3</sup>*J*<sub>HH</sub> 7.8Hz, ~NCH=CH~), 9.75 (1H, bs, ~NH~).  $\delta_{\text{C}}$  (100 MHz, CDCl<sub>3</sub>): 163.3, 143.2 (~CO~), 137.3 (~NCH=CH~), 128.6-127.2 (~phenyl ring~), 125.9 (~C(Ph)<sub>3</sub>~), 102.2 (~NCH=CH~), 85.1 (~CH<sub>2</sub>CHCH(OCH<sub>2</sub>)~), 84.7 (~NCHCH<sub>2</sub>~), 69.7 (~CHCH(OCH<sub>2</sub>)CH<sub>2</sub>~), 62.1 (~CH(OCH<sub>2</sub>)CH<sub>2</sub>~), 41.5 (~CH<sub>2</sub>CHCH(OCH<sub>2</sub>)~), 40.3 (~OCH<sub>2</sub>CH<sub>2</sub>CH<sub>2</sub>Cl~), 37.8 (~OCH<sub>2</sub>CH<sub>2</sub>CH<sub>2</sub>Cl~), 30.4 (~OCH<sub>2</sub>CH<sub>2</sub>CH<sub>2</sub>Cl~). *m/z* (ESMS+) 548 [M + H]<sup>+</sup>.

## 7.4 Macrocycle Synthesis

### 7.4.1 1,4,7-Tris(*tert*-butoxycarbonylmethyl)-1,4,7,10-tetraazacyclododecane, (*t*BuDO3A) (**1**)<sup>8,9</sup>

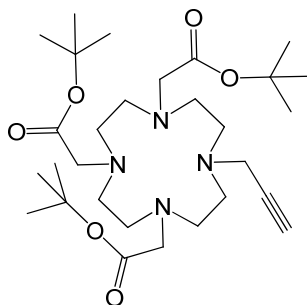


Method 1: *tert*-butyl bromoacetate (11.9 g, 9 cm<sup>3</sup>, 0.061 mol) was dissolved in dimethylacetamide (15 cm<sup>3</sup>) and added dropwise under nitrogen over 4 hours at room temperature to a stirred solution of 1,4,7,10-tetraazacyclododecane (3.0 g, 0.2 mol) and sodium acetate (5.0 g, 0.061 mol) in DMA (60 cm<sup>3</sup>). After the addition was complete the mixture was stirred for 19 days at room temperature. After this the precipitate was collected and the filtrate was concentrated to afford a second crop. The crops were dissolved in CHCl<sub>3</sub> (100 cm<sup>3</sup>) and washed with water (3 x 50 cm<sup>3</sup>), the CHCl<sub>3</sub> was concentrated to give a yellow oil, addition of ethyl acetate gave a white solid (7.34 g, 61%) which was collected and washed with ether.

Method 2: *tert*-butyl bromoacetate (1.689 g, 1.285 cm<sup>3</sup>, 8.707 mmol) was dissolved in chloroform (50 cm<sup>3</sup>) and added dropwise under nitrogen over 4 hours at room temperature to a stirred solution of 1,4,7,10-tetraazacyclododecane (0.5 g, 2.902 mmol) and K<sub>2</sub>CO<sub>3</sub> (0.401 g, 2.902 mmol) in CHCl<sub>3</sub> (125 cm<sup>3</sup>). After the addition was complete the mixture was stirred for 3 days. After this the inorganic salts were filtered off and the solution was concentrated in *vacuo*. The crude product was purified by silica column chromatography, with a gradient DCM 100% to MeOH 10%, 1% ammonia and DCM 89% giving a white solid (0.794 g, 53%).

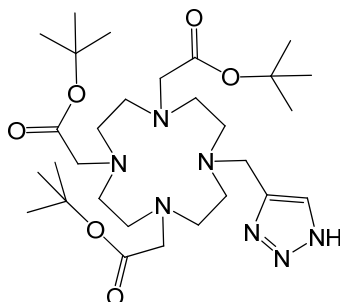
$\delta_{\text{H}}$  (300 MHz, CDCl<sub>3</sub>): 1.39 (27H, s, ~C(CH<sub>3</sub>)<sub>3</sub>~) 2.85 (12H, bm, ~NCH<sub>2</sub>CH<sub>2</sub>N~) 3.03 (4H, bs, ~CH<sub>2</sub>NCH<sub>2</sub>~) 3.22 (2H, s, ~NCH<sub>2</sub>CO<sub>2</sub>~) 3.31 (4H, s, ~NCH<sub>2</sub>CO<sub>2</sub>~).  $\delta_{\text{C}}$  (75.4 MHz, CDCl<sub>3</sub>): 170.5, 169.6 (~CO~), 81.8, 81.6 (~C(CH<sub>3</sub>)<sub>3</sub>~) 58.1(~NCH<sub>2</sub>CO<sub>2</sub>~), 48.7 (~NCH<sub>2</sub>CO<sub>2</sub>~), 51.3, 51.2, 49.1, 47.4 (~NCH<sub>2</sub>~), 28.1 (~C(CH<sub>3</sub>)<sub>3</sub>~). *m/z* (ESMS+) 515 [M + H]<sup>+</sup>. The data was consistent with that found in ref. [8,9].

7.4.2 1,4,7-Tris(*tert*-butoxycarbonylmethyl)-10-(*prop*-2-ynyl)-1,4,7,10-tetraazacyclododecane (**2**)



A solution of **1** (0.100 g, 0.194 mmol), propargyl bromide (0.022 g, 0.0164 cm<sup>3</sup>, 0.194 mmol) and K<sub>2</sub>CO<sub>3</sub> (0.026 g, 0.194 mmol) in MeCN (2 cm<sup>3</sup>) was stirred under nitrogen for 2 hours at room temperature. The inorganic salts were filtered off and the solvent was concentrated, giving a pale yellow oil (0.100 g, 86%)  $\delta_{\text{H}}$  (400 MHz, CDCl<sub>3</sub>): 1.38 (27H, s,  $\sim\text{C}(\text{CH}_3)_3\sim$ ), 2.07 (1H, t,  $^4J_{\text{HH}}$  2.3Hz,  $\sim\text{C}\equiv\text{CH}$ ), 2.61-2.63 (4H, bm,  $\sim\text{CH}_2\text{NCH}_2\sim$ ), 2.72-2.75 (12H, bm,  $\sim\text{NCH}_2\text{CH}_2\text{N}\sim$ ), 3.21 (6H, bm,  $\sim\text{NCH}_2\text{CO}_2\sim$ ), 3.36 (2H, bm,  $\sim\text{NCH}_2\text{C}\equiv\text{CH}$ ).  $\delta_{\text{C}}$  (75.4 MHz, CDCl<sub>3</sub>): 173.4, 172.7, 169.4 ( $\sim\text{CO}\sim$ ), 82.8, 82.6 ( $\sim\text{C}(\text{CH}_3)_3\sim$ ), 78.9 ( $\sim\text{C}\equiv\text{CH}\sim$ ), 72.6 ( $\sim\text{C}\equiv\text{CH}$ ), 56.7( $\sim\text{NCH}_2\text{C}\equiv\text{CH}$ ), 56.4( $\sim\text{NCH}_2\text{CO}_2\sim$ ), 55.7( $\sim\text{NCH}_2\text{CO}_2\sim$ ), 51.0, 50.5, 49.8, 49.7 ( $\sim\text{NCH}_2\sim$ ), 27.8 ( $\sim\text{C}(\text{CH}_3)_3\sim$ ).  $m/z$  (ESMS+) 553 [M + H]<sup>+</sup>.

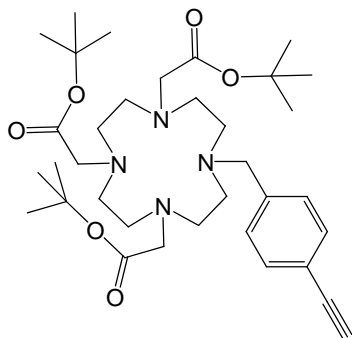
7.4.3 1,4,7-Tris(*tert*-butoxycarbonylmethyl)-10-((1*H*-1,2,3-triazol-4-yl)methyl)-,)-1,4,7,10-tetraazacyclododecane (**3c**)



**2** (0.100 g, 0.18 mmol) and sodium azide (0.011 g, 0.18 mmol) were dissolved in DMF:H<sub>2</sub>O (25 cm<sup>3</sup>). To this sodium ascorbate (0.071 g, 0.36 mmol) and CuSO<sub>4</sub>·5H<sub>2</sub>O (0.67 g, 0.198 mmol) were added sequentially. The solution was stirred at room temperature for 18 hours. The DMF was removed and the water layer was passed down a Dowex-50W exchange resin column. The ammonia was removed *in vacuo* and the water was lyophilised to give a hygroscopic white solid (0.046 g, 42%).  $\delta_{\text{H}}$  (300 MHz, CDCl<sub>3</sub>): 1.45 (27H, s,  $\sim\text{C}(\text{CH}_3)_3\sim$ ), 2.21-2.93 (16H, bm,  $\sim\text{NCH}_2\text{CH}_2\sim$ ), 3.39-3.71 (6H, bm,

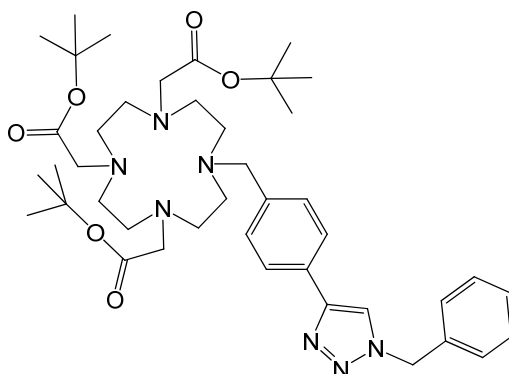
$\sim\text{NCH}_2\text{CO}_2\sim$ ), 3.90 (2H, bs,  $\sim\text{NCH}_2\text{C}=\text{CH}\sim$ ), 8.39 (1H, bs,  $\sim\text{C}=\text{CHNH}\sim$ ).  $m/z$  (ESMS+) 595  $[\text{M} + \text{H}]^+$ .

7.4.4 1,4,7-Tris(*tert*-butoxycarbonylmethyl)-10-(1-methyl-4-ethynylbenzene)-1,4,7,10-tetraazacyclododecane (**7**)



A solution of **1** (1.735 g, 2.916 mmol), 1-(chloromethyl)-4-ethynylbenzene (0.525 g, 3.5 mmol) and  $\text{K}_2\text{CO}_3$  (0.805 g, 5.83 mmol) in MeCN (25 cm<sup>3</sup>) was stirred under nitrogen for 18 hours at room temperature. The inorganic salts were filtered off and the solvent was concentrated, giving a yellow oil (2.13 g). Purified on silica (3% MeOH and 1% ammonia in DCM), yielding a yellow oil (1.291 g, 70%).  $\delta_{\text{H}}$  (400 MHz,  $\text{CDCl}_3$ ): 1.38 (27H, s,  $\sim\text{C}(\text{CH}_3)_3\sim$ ), 2.14 (1H, s,  $\sim\text{C}\equiv\text{CH}\sim$ ), 2.61-2.63 (4H, bm,  $\sim\text{CH}_2\text{NCH}_2\sim$ ), 2.70-2.90 (12H, bm,  $\sim\text{NCH}_2\text{CH}_2\text{N}\sim$ ), 3.31 (6H, bm,  $\sim\text{NCH}_2\text{CO}_2\sim$ ), 4.45 (2H, bm,  $\sim\text{NCH}_2\text{C}\sim$ ), 7.25 (2H, d,  $^3J_{\text{HHa}}$  8.6Hz,  $\sim\text{CCHCHC}\sim$ ), 7.39 (2H, d,  $^3J_{\text{HHa}}$  8.6Hz,  $\sim\text{CCHCHC}\sim$ ).  $\delta_{\text{C}}$  (100 MHz,  $\text{CDCl}_3$ ): 173.4, 172.7, 169.4 ( $\sim\text{CO}\sim$ ), 138.4 ( $\sim\text{CCHCHC}\sim$ ), 132.5 ( $\sim\text{CCHCHC}\sim$ ), 129 ( $\sim\text{CCHCHC}\sim$ ), 122.2 ( $\sim\text{CCHCHC}\sim$ ), 83.1 ( $\sim\text{CCH}\sim$ ), 78.0 ( $\sim\text{CCH}\sim$ ), 82.8, 82.6 ( $\sim\text{C}(\text{CH}_3)_3\sim$ ), 56.7 ( $\sim\text{NCH}_2\text{C}\equiv\text{CH}\sim$ ), 56.4 ( $\sim\text{NCH}_2\text{CO}_2\sim$ ), 55.7 ( $\sim\text{NCH}_2\text{CO}_2\sim$ ), 54.7 ( $\sim\text{NCH}_2\text{C}\sim$ ), 51.0, 50.5, 49.8, 49.7 ( $\sim\text{NCH}_2\sim$ ), 27.8 ( $\sim\text{C}(\text{CH}_3)_3\sim$ ).  $m/z$  (ESMS+) 628  $[\text{M} + \text{H}]^+$ .

7.4.5 1,4,7-Tris(tert-butoxycarbonylmethyl)-10-(1-methyl-4-(1-phenyl-1,2,3-triazo-4-yl)-benzene)-1,4,7,10-tetraazacyclododecane (**11**)

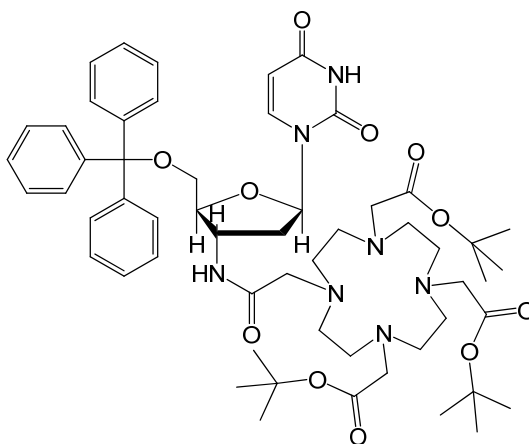


Method 1: A solution of **1** (0.098 g, 0.165 mmol), **10** (0.056 g, 0.1978 mmol) and  $\text{K}_2\text{CO}_3$  (0.045 g, 0.329 mmol) in MeCN ( $10 \text{ cm}^3$ ) was heated at  $80^\circ\text{C}$  for 18 hours. The inorganic salts were filtered off and the solvent was concentrated, giving a yellow oil (0.126 g). Which was purified on silica (3% MeOH and 1% ammonia in DCM), yielding a yellow oil (0.091 g, 72%).

Method 2: **7** (0.041 g, 0.0625 mmol), benzyl bromide (0.012 g, 0.0087  $\text{cm}^3$ , 0.0718 mmol) and sodium azide (0.013 g, 0.195 mmol) were dissolved in EtOH/ $\text{H}_2\text{O}$  ( $5 \text{ cm}^3$ ). To this sodium ascorbate (0.025 g, 0.13 mmol) and  $\text{CuSO}_4 \cdot 5\text{H}_2\text{O}$  (0.018 g, 0.0718 mmol) were added sequentially, and the solution was stirred at room temperature for 24 hours. After this period the solution was passed down a strong cation exchange resin Dowex-50W to remove the excess Cu, the compound was eluted with 12% ammonia solution, which was concentrated, giving a yellow oil (0.02 g, 42%).

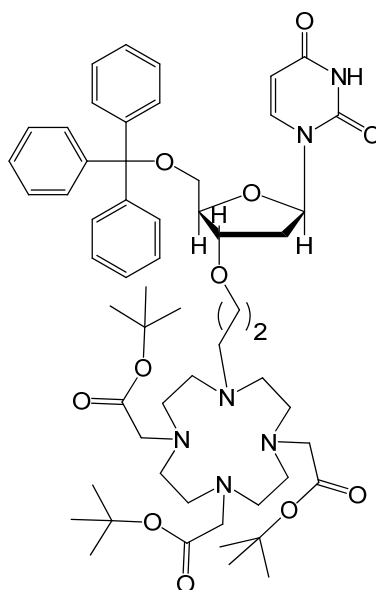
$\delta_{\text{H}}$  (400 MHz,  $\text{CDCl}_3$ ): 1.38 (27H, s,  $\sim\text{C}(\text{CH}_3)_3\sim$ ), 2.61-2.63 (4H, bm,  $\sim\text{CH}_2\text{NCH}_2\sim$ ), 2.70-2.90 (12H, bm,  $\sim\text{NCH}_2\text{CH}_2\text{N}\sim$ ), 3.31 (6H, bm,  $\sim\text{NCH}_2\text{CO}_2\sim$ ), 4.35 (2H, bs,  $\sim\text{NCH}_2\text{C}\sim$ ), 5.52 (2H, s,  $\sim\text{NCH}_2\text{C}\sim$ ) 7.29 (5H, m,  $\sim\text{CH}_2\text{Ph}\sim$ ) 7.47 (2H, d,  $^3J_{\text{HHa}}$  8.2Hz,  $\sim\text{CCHCHC}\sim$ ), 7.67 (1H, s,  $\sim\text{CCHN}\sim$ ), 7.77 (2H, d,  $^3J_{\text{HHa}}$  8.2Hz,  $\sim\text{CCHCHC}\sim$ ), 57.5 ( $\sim\text{CCH}_2\text{N}\sim$ ),  $\delta_{\text{C}}$  (100 MHz,  $\text{CDCl}_3$ ): 173.4, 172.7, 169.4 ( $\sim\text{CO}\sim$ ), 142.4 ( $\sim\text{CCHCHC}\sim$ ), 141.5 ( $\sim\text{CCHCHC}\sim$ ), 131.6 ( $\sim\text{CH}_2\text{CCH}\sim$ ), 130.0, 129.8, 129.6 ( $\sim\text{CPh}\sim$ ) 129 ( $\sim\text{CCHCHC}\sim$ ), 125.1 ( $\sim\text{CCHN}\sim$ ), 122.8 ( $\sim\text{NCCH}\sim$ ), 122.2 ( $\sim\text{CCHCHC}\sim$ ), 83.1 ( $\sim\text{CCH}\sim$ ), 78.0 ( $\sim\text{CCH}\sim$ ) 82.8, 82.6 ( $\sim\text{C}(\text{CH}_3)_3\sim$ ), 56.4 ( $\sim\text{NCH}_2\text{CO}_2\sim$ ), 55.7 ( $\sim\text{NCH}_2\text{CO}_2\sim$ ), 54.7 ( $\sim\text{NCH}_2\text{C}\sim$ ), 51.0, 50.5, 49.8, 49.7 ( $\sim\text{NCH}_2\sim$ ), 27.8 ( $\sim\text{C}(\text{CH}_3)_3\sim$ ).  $m/z$  (ESMS+) 762 [ $\text{M} + \text{H}$ ] $^+$ .

7.4.6 1,4,7-Tris(*tert*-butoxycarbonylmethyl)-10-(3-acetamide-5-*O*-trityl-2,3-dideoxyuridine)-1,4,7,10-tetraazacyclododecane (**26**)



A solution of **1** (0.0079 g, 0.0146 mmol), **23** (0.008 g, 0.0133 mmol) and  $K_2CO_3$  (0.004 g, 0.0266 mmol) in MeCN (2 cm<sup>3</sup>) was heated at 80°C for 72 hours. The inorganic salts were filtered off and the solvent was concentrated, giving a yellow oil, which was purified on silica (3% MeOH in DCM), giving a colourless oil (0.013 g, 95%).  $\delta_H$  (400 MHz,  $CDCl_3$ ): 1.39 (27H, s,  $\sim C(CH_3)_3\sim$ ), 2.23 (2H, m,  $\sim CH(NH)CH_2CHN\sim$ ), 2.64-2.91 (8H, bm,  $\sim CH_2NCH_2\sim$ ), 2.98- 3.08 (4H, bm,  $\sim NCH_2CH_2N\sim$ ), 3.22 (6H, bm,  $\sim NCH_2CO_2\sim$ ), 3.29 (4H, bm,  $\sim NCH_2CH_2N\sim$ ) 3.40 (2H, s,  $\sim NHC(O)CH_2N\sim$ ) 3.42 (2H, bd,  $^3J_{HH}$  3.1Hz,  $\sim OCH_2CH\sim$ ), 3.85 (1H, m,  $\sim CH_2CHCH(NH)\sim$ ), 4.14 (1H, m,  $\sim CHCH(NH)CH_2\sim$ ), 5.28 (1H, d,  $^3J_{HH}$  8.2Hz,  $\sim NCH=CH\sim$ ), 6.18 (1H, t,  $^3J_{HH}$  6.2Hz,  $\sim NCHCH_2\sim$ ), 6.9 (1H, bs,  $\sim CH(NH)CH_2\sim$ ) 7.14 -7.48 (16H, m,  $\sim C(Ph)_3\sim, \sim NCH=CH\sim$ ).  $\delta_C$  (100 MHz,  $CDCl_3$ ): 173.4, 169.4 ( $\sim CO\sim$ ) 166.3, 142.5 ( $\sim CO\sim$ ), 144.8 ( $\sim NCH=CH\sim$ ), 128.6-127.2 ( $\sim phenyl ring\sim$ ), 123.9 ( $\sim C(Ph)_3\sim$ ), 103.2 ( $\sim NCH=CH\sim$ ), 87.3 ( $\sim CH_2CHCH(NH)\sim$ ), 84.2 ( $\sim NCHCH_2\sim$ ), 82.8, 82.6 ( $\sim C(CH_3)_3\sim$ ), 61.2 ( $\sim CH_2CHCH(NH)CH_2\sim$ ) 56.4 ( $\sim NCH_2CO_2\sim$ ), 55.7 ( $\sim NCH_2CO_2\sim$ ), 52.1 ( $\sim CHCH(NH)CH_2\sim$ ), 51.0, 50.5, 49.8, 49.7 ( $\sim NCH_2\sim$ ), 41.1 ( $\sim CH(NH)CH_2CHN\sim$ ) 37.1 ( $\sim NHC(O)CH_2N\sim$ ), 27.8 ( $\sim C(CH_3)_3\sim$ ).  $m/z$  (ESMS+) 1024 [M + H]<sup>+</sup>.

7.4.7 1,4,7-Tris(*tert*-butoxycarbonylmethyl)-10-(5-trityl-2-(3-chloropropoxy)-uridine)-1,4,7,10-tetraazacyclododecane (**27**)

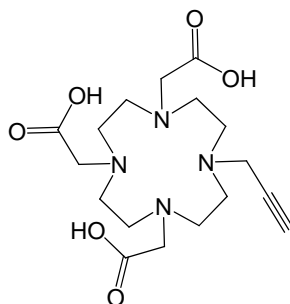


A solution of **1** (0.087 g, 0.147 mmol), **25** (0.089 g, 0.163 mmol) and  $K_2CO_3$  (0.04 g, 0.296 mmol) in MeCN (5 cm<sup>3</sup>) was heated at reflux for 72 hours. The inorganic salts were filtered off and the solvent was concentrated, giving a yellow oil, which was purified on silica with 3% MeOH in DCM giving a yellow oil (0.077 g, 50%).  $\delta_H$  (500 MHz,  $CDCl_3$ ): 1.42 (27H, s,  $\sim C(CH_3)_3$ ), 1.71 (2H, t,  $^3J_{HH}$  6.7Hz,  $\sim OCH_2CH_2CH_2N$ ), 1.87 (1H, m,  $\sim CH(OCH_2)CH_2CHN$ ), 1.91 (1H, m,  $\sim CH(OCH_2)CH_2CHN$ ), 2.15-2.39 (8H, bm,  $\sim CH_2NCH_2$ ), 2.85 (4H, bm,  $\sim NCH_2CH_2N$ ), 2.92 (6H, bm,  $\sim NCH_2CO_2$ ), 3.12 (4H, bm,  $\sim NCH_2CH_2N$ ), 3.40 (2H, d,  $^3J_{HHa}$  3.1Hz,  $\sim OCH_2CH$ ), 3.67 (2H, m,  $\sim OCH_2CH_2CH_2N$ ), 3.72 (1H, dd,  $^3J_{HHa}$  3.9Hz,  $^3J_{HHb}$  3.1Hz,  $\sim CH_2CHCH(O)$ ), 4.25 (2H, t,  $^3J_{HH}$  6.7Hz,  $\sim OCH_2CH_2CH_2N$ ), 4.47 (1H, dd,  $^3J_{HHa}$  6.3Hz,  $^3J_{HHb}$  4.7Hz,  $\sim CHCH(O)CH_2$ ), 5.24 (1H, d,  $^3J_{HH}$  8.2Hz,  $\sim NCH=CH$ ), 6.32 (1H, t,  $^3J_{HH}$  6.3Hz,  $\sim NCHCH_2$ ), 7.25 (15H, m,  $\sim$ benzyl ring), 7.46 (1H, d,  $^3J_{HH}$  7.8Hz,  $\sim NCH=CH$ ), 9.75 (1H, bs,  $\sim NH$ ).  $\delta_C$  (125 MHz,  $CDCl_3$ ): 173.4, 169.4 ( $\sim CO$ ), 163.3, 143.2 ( $\sim CO$ ), 137.3 ( $\sim NCH=CH$ ), 128.6-127.2 ( $\sim$ phenyl ring), 125.9 ( $\sim C(Ph)_3$ ), 102.2 ( $\sim NCH=CH$ ), 89.1 ( $\sim CH_2CHCH(OCH_2)$ ), 85.7 ( $\sim NCHCH_2$ ), 82.8, 82.6 ( $\sim C(CH_3)_3$ ), 76.7 ( $\sim CHCH(OCH_2)CH_2$ ), 66.3 ( $\sim OCH_2CH_2CH_2N$ ), 62.1 ( $\sim CH(OCH_2)CH_2$ ), 56.4 ( $\sim NCH_2CO_2$ ), 55.7 ( $\sim NCH_2CO_2$ ), 51.0, 50.5, 49.8, 49.7 ( $\sim NCH_2$ ), 41.5 ( $\sim CH_2CHCH(OCH_2)$ ), 40.3 ( $\sim OCH_2CH_2CH_2N$ ), 30.4 ( $\sim OCH_2CH_2CH_2N$ ), 27.8 ( $\sim C(CH_3)_3$ ).  $m/z$  (ESMS+) 1026 [M + H]<sup>+</sup>.

## 7.5 Proligand Synthesis

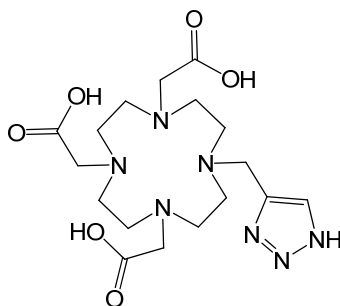
The following compounds were prepared in the same manner; t-butyl containing compound, was dissolved in DCM (2.5 cm<sup>3</sup>), to this trifluoroacetic acid (2.5 cm<sup>3</sup>) was added and the solution was stirred at room temperature for 24 h. The solvent was removed *in vacuo*. DCM (2 x 5 cm<sup>3</sup>) was added and concentrated, followed by diethylether (2 x 5 cm<sup>3</sup>) and concentrated, yielding a hygroscopic white solid.

### 7.5.1 1,4,7-Tris(carbonylmethyl)-10-(prop-2-ynyl)-1,4,7,10-tetraazacyclododecane (**4**)



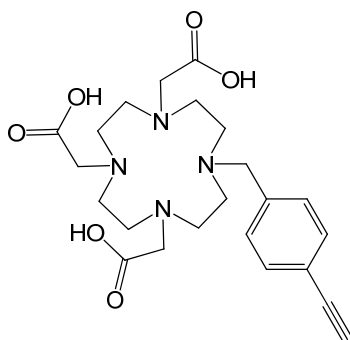
**2** (0.100 g, 0.18 mmol), gave a hygroscopic white solid **4** (0.060 g, 89%).  $\delta_{\text{H}}$  (400 MHz, D<sub>2</sub>O): 2.95 (1H, bm,  $\sim\text{C}\equiv\text{CH}$ ), 3.16 (8H, bm,  $\sim\text{NCH}_2\text{CH}_2\text{N}\sim$ ) 3.34 (8H, bm,  $\sim\text{NCH}_2\text{CH}_2\text{N}\sim$ ), 3.73 (2H, bs,  $\sim\text{NCH}_2\text{C}\equiv\text{CH}\sim$ ), 3.95 (6H, bm,  $\sim\text{NCH}_2\text{CO}_2\sim$ ).  $\delta_{\text{C}}$  (75.4 MHz, CDCl<sub>3</sub>): 163.3, 163.1, 162.7 ( $\sim\text{CO}\sim$ ), 54.7 ( $\sim\text{C}\equiv\text{CH}\sim$ ), 53.7 ( $\sim\text{C}\equiv\text{CH}$ ), 52.9 ( $\sim\text{NCH}_2\text{C}\equiv\text{CH}$ ), 51.7 ( $\sim\text{NCH}_2\text{CO}_2\sim$ ), 50.1 ( $\sim\text{NCH}_2\text{CO}_2\sim$ ), 49.1, 48.2, 47.8, 42.9 ( $\sim\text{NCH}_2\sim$ ).  $m/z$  (ESMS+) 385 [M + H]<sup>+</sup>.

### 7.5.2 1,4,7-Tris(carbonylmethyl)-10-((1H-1,2,3-triazol-4-yl)methyl)-1,4,7,10-tetraazacyclododecane (**5c**)



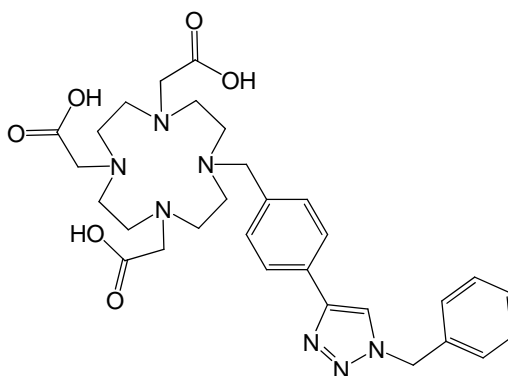
**3c** (0.035 g, 0.058 mmol), gave an orange solid **5c**, (0.023 g, 93%).  $\delta_{\text{H}}$  (300 MHz, D<sub>2</sub>O): 2.81-3.37 (16H, bm,  $\sim\text{NCH}_2\text{CH}_2\sim$ ), 3.44-3.71 (6H, bm,  $\sim\text{NCH}_2\text{CO}_2\sim$ ), 3.80 (2H, bs,  $\sim\text{NCH}_2\text{C}=\text{CH}\sim$ ), 8.37 (1H, bs,  $\sim\text{C}=\text{CHNH}\sim$ ).  $m/z$  (ESMS+) 427 [M + H]<sup>+</sup>.

7.5.3 *1,4,7-Tris(carboxymethyl)-10-(1-methyl-4-ethynylbenzene)-1,4,7,10-tetraazacyclododecane (8)*



**7** (0.444 g, 0.707 mmol), gave an orange oil, **8** (0.320 g, 98 %).  $\delta_{\text{H}}$  (400 MHz,  $\text{D}_2\text{O}$ ): 2.14 (1H, s,  $\sim\text{C}\equiv\text{CH}\sim$ ), 2.61-2.63 (4H, bm,  $\sim\text{CH}_2\text{NCH}_2\sim$ ), 2.70-2.90 (12H, bm,  $\sim\text{NCH}_2\text{CH}_2\text{N}\sim$ ), 3.31 (6H, bm,  $\sim\text{NCH}_2\text{CO}_2\sim$ ), 4.45 (2H, bm,  $\sim\text{NCH}_2\text{C}\sim$ ), 7.25 (2H, bd,  $^3J_{\text{HHa}}$  8.6Hz,  $\sim\text{CCHCHC}\sim$ ), 7.39 (2H, bd,  $^3J_{\text{HHa}}$  8.6Hz,  $\sim\text{CCHCHC}\sim$ ).  $\delta_{\text{C}}$  (100 MHz,  $\text{D}_2\text{O}$ ): 173.4, 172.7, 169.4 ( $\sim\text{CO}\sim$ ), 138.4 ( $\sim\text{CCHCHC}\sim$ ), 132.5 ( $\sim\text{CCHCHC}\sim$ ), 129 ( $\sim\text{CCHCHC}\sim$ ), 122.2 ( $\sim\text{CCHCHC}\sim$ ), 83.1 ( $\sim\text{CCH}\sim$ ), 78.0 ( $\sim\text{CCH}\sim$ ), 56.7 ( $\sim\text{NCH}_2\text{C}\equiv\text{CH}\sim$ ), 56.4 ( $\sim\text{NCH}_2\text{CO}_2\sim$ ), 55.7 ( $\sim\text{NCH}_2\text{CO}_2\sim$ ), 54.7 ( $\sim\text{NCH}_2\text{C}\sim$ ), 51.0, 50.5, 49.8, 49.7 ( $\sim\text{NCH}_2\sim$ ).  $m/z$  (ESMS+) 461  $[\text{M} + \text{H}]^+$ .

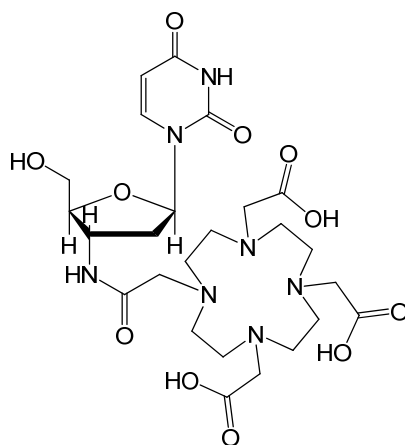
7.5.4 *1,4,7-tris(carboxymethyl)-10-(1-methyl-4-(1-phenyl-1,2,3-triazo-4-yl)-benzene)-1,4,7,10-tetraazacyclododecane (12)*



**11** (0.020 g, 0.0262 mmol) gave a brown solid, **12** (0.014 g, 90 %).  $\delta_{\text{H}}$  (400 MHz,  $\text{D}_2\text{O}$ ): 2.61-2.63 (4H, bm,  $\sim\text{CH}_2\text{NCH}_2\sim$ ), 2.70-2.90 (12H, bm,  $\sim\text{NCH}_2\text{CH}_2\text{N}\sim$ ), 3.31 (6H, bm,  $\sim\text{NCH}_2\text{CO}_2\sim$ ), 3.35 (2H, bs,  $\sim\text{NCH}_2\text{C}\sim$ ), 5.42 (2H, s,  $\sim\text{NCH}_2\text{C}\sim$ ) 7.26 (5H, m,

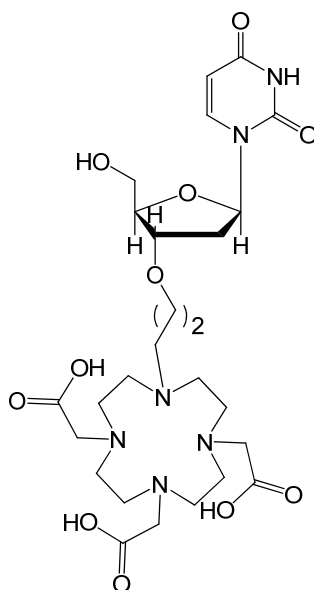
~CH<sub>2</sub>Ph~) 7.47 (2H, d, <sup>3</sup>J<sub>HHa</sub> 8.2Hz, ~CCHCHC~), 7.67 (1H, s, ~CCHN~), 7.77 (2H, d, <sup>3</sup>J<sub>HHa</sub> 8.2Hz, ~CCHCHC~), 57.5 (~CCH<sub>2</sub>N~). δ<sub>C</sub> (100 MHz, D<sub>2</sub>O): 173.4, 172.7, 169.4 (~CO~), 142.4 (~CCHCHC~), 141.5 (~CCHCHC~), 131.6 (~CH<sub>2</sub>CCH~), 130.0, 129.8, 129.6 (~CPh~) 129 (~CCHCHC~), 125.1 (~CCHN~), 122.8 (~NCCH~), 122.2 (~CCHCHC~), 83.1 (~CCH~), 78.0 (~CCH~), 56.4 (~NCH<sub>2</sub>CO<sub>2</sub>~), 55.7 (~NCH<sub>2</sub>CO<sub>2</sub>~), 54.7 (~NCH<sub>2</sub>C~), 51.0, 50.5, 49.8, 49.7 (~NCH<sub>2</sub>~). *m/z* (ESMS+) 595 [M + H]<sup>+</sup>.

7.5.5 1,4,7-Tris(carbonylmethyl)-10-(3-acetamide-5-hydroxy-2,3-dideoxyuridine)-1,4,7,10-tetraazacyclododecane (**28**)



**26** (0.011 g, 0.0107 mmol), gave a hyroscopic white solid, **28** (0.005 g, 76 %). δ<sub>H</sub> (400 MHz, MeOD): 2.23 (2H, m, ~CH(NH)CH<sub>2</sub>CHN~), 2.64-2.91 (8H, bm, ~CH<sub>2</sub>NCH<sub>2</sub>~), 2.98- 3.08 (4H, bm, ~NCH<sub>2</sub>CH<sub>2</sub>N~), 3.22 (6H, bm, ~NCH<sub>2</sub>CO<sub>2</sub>~), 3.29 (4H, bm, ~NCH<sub>2</sub>CH<sub>2</sub>N~) 3.40 (2H, s, ~NHC(O)CH<sub>2</sub>N~) 3.42 (2H, bd, <sup>3</sup>J<sub>HH</sub> 3.1Hz, ~OCH<sub>2</sub>CH~), 3.85 (1H, m, ~CH<sub>2</sub>CHCH(NH)~), 4.54 (1H, m, ~CHCH(NH)CH<sub>2</sub>~), 5.66 (1H, d, <sup>3</sup>J<sub>HH</sub> 8.2Hz, ~NCH=CH~), 6.15 (1H, bt, <sup>3</sup>J<sub>HH</sub> 6.2Hz, ~NCHCH<sub>2</sub>~), 7.28 (1H, d, <sup>3</sup>J<sub>HH</sub> 8.2Hz, ~NCH=CH~).

7.5.6 1,4,7-Tris(carbonylmethyl)-10-(5-hydroxy-2-(-3-chloropropoxy)-uridine)-1,4,7,10-tetraazacyclododecane (**29**)



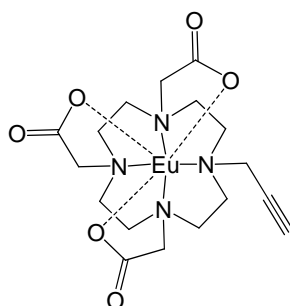
**27** (0.020 g, 0.0195 mmol), gave a hygroscopic white solid, **29** (0.011 g, 92 %).  $\delta_{\text{H}}$  (500 MHz,  $\text{D}_2\text{O}$ ): 1.96 (2H, m,  $\sim\text{OCH}_2\text{CH}_2\text{CH}_2\text{N}\sim$ ), 2.23 (2H, m,  $\sim\text{CH}(\text{OCH}_2)\text{CH}_2\text{CHN}\sim$ ), 2.85-3.01 (8H, bm,  $\sim\text{NCH}_2\text{CH}_2\text{N}\sim$ ), 3.19 (2H, m,  $\sim\text{OCH}_2\text{CH}_2\text{CH}_2\text{N}\sim$ ), 3.24-3.35 (8H, bm,  $\sim\text{NCH}_2\text{CH}_2\text{N}\sim$ ), 3.63 (2H, dd,  $^3J_{\text{HHa}}$  17.1Hz,  $^3J_{\text{HHb}}$  8.9Hz  $\sim\text{OHCH}_2\text{CH}\sim$ ), 3.83 (2H, m,  $\sim\text{OCH}_2\text{CH}_2\text{CH}_2\text{N}\sim$ ), 3.90 (1H, dd,  $^3J_{\text{HHa}}$  5Hz,  $^3J_{\text{HHb}}$  3.9Hz,  $\sim\text{CH}_2\text{CHCH}(\text{OCH}_2)\sim$ ), 3.92 (6H, bm,  $\sim\text{NCH}_2\text{CO}_2\sim$ ), 4.29 (1H, dd,  $^3J_{\text{HHa}}$  6.2Hz,  $^3J_{\text{HHb}}$  3.9Hz,  $\sim\text{CHCH}(\text{O})\text{CH}_2\sim$ ), 5.79 (1H, d,  $^3J_{\text{HH}}$  8.2Hz,  $\sim\text{NCH}=\text{CH}\sim$ ), 6.14 (1H, t,  $^3J_{\text{HH}}$  6.5Hz,  $\sim\text{NCHCH}_2\sim$ ), 7.68 (1H, d,  $^3J_{\text{HH}}$  8.2Hz,  $\sim\text{NCH}=\text{CH}\sim$ ).  $\delta_{\text{C}}$  (125 MHz,  $\text{D}_2\text{O}$ ): 163.4, 162.9 ( $\sim\text{CO}\sim$ ), 159.9, 117.2 ( $\sim\text{CO}\sim$ ), 140.3 ( $\sim\text{NCH}=\text{CH}\sim$ ), 101.2 ( $\sim\text{NCH}=\text{CH}\sim$ ), 86.9 ( $\sim\text{CH}_2\text{CHCH}(\text{OCH}_2)\sim$ ), 86.3 ( $\sim\text{NCHCH}_2\sim$ ), 70.7 ( $\sim\text{CHCH}(\text{OCH}_2)\text{CH}_2\sim$ ), 61.1 ( $\sim\text{CH}_2\text{CHCH}(\text{OCH}_2)\sim$ ), 55.4 ( $\sim\text{NCH}_2\text{CO}_2\sim$ ), 51.9 ( $\sim\text{OCH}_2\text{CH}_2\text{CH}_2\text{N}\sim$ ), 53.2, 51.5, 49.8, 48.7 ( $\sim\text{NCH}_2\sim$ ), 38.9 ( $\sim\text{CH}(\text{OCH}_2)\text{CH}_2\sim$ ), 38.6 ( $\sim\text{OCH}_2\text{CH}_2\text{CH}_2\text{N}\sim$ ), 21.4 ( $\sim\text{OCH}_2\text{CH}_2\text{CH}_2\text{N}\sim$ ).

## 7.6 Lanthanide Complexation

All lanthanide compounds in this section were prepared in a similar manner: **4**, **5** or **8** and  $\text{LnCl}_3 \cdot 6\text{H}_2\text{O}$  were dissolved in water (5  $\text{cm}^3$ ) and adjusted to pH 7 by addition of NaOH. On mixing the pH fell to  $\sim 5$ , due to the release of protons on complexation. The solution was adjusted to pH 6 using NaOH and was stirred at room temperature for 72 hours. The solution was then added to Dowex Mac-3 cation exchange resin at pH 5.

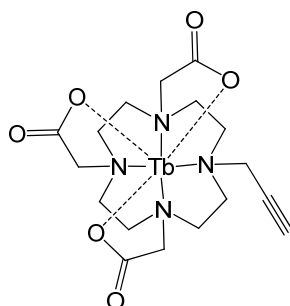
Xylenol orange was used to test for free lanthanide, upon all free metal ions being taken up; the solution filtered and lyophilised giving a white hygroscopic solid.

7.6.1 *Europium (III) 1,4,7-tris(carboxymethyl)-10-(prop-2-ynyl)-1,4,7,10-tetraazacyclododecane, (Eu.4)*



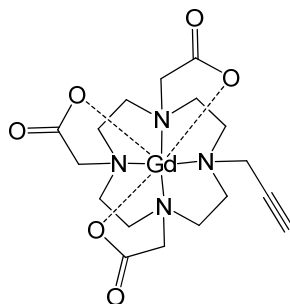
**4** (0.173 g, 0.452 mmol) and  $\text{EuCl}_3 \cdot 6\text{H}_2\text{O}$  (0.198 g, 0.544 mmol). Giving a white hygroscopic solid, **Eu.4** (0.275 g, 86%).  $m/z$  (ESMS+) 533  $[\text{M} + \text{H}]^+$  ( $^{151}\text{Eu}$ ), (HR-ESMS+)  $[\text{M} + \text{H}]^+$  calcd for  $\text{C}_{17}\text{H}_{26}\text{N}_4\text{O}_6 \text{ Eu}$ ; 533.1045, found; 533.1039 ( $^{151}\text{Eu}$ ). The  $^1\text{H}$  NMR spectrum showed broad resonances that were not sufficiently resolved at 273 K.

7.6.2 *Terbium (III) 1,4,7-tris(carboxymethyl)-10-(prop-2-ynyl)-1,4,7,10-tetraazacyclododecane, (Tb.4)*



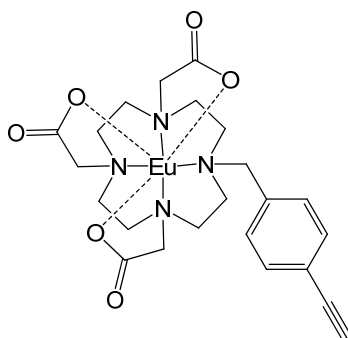
**4** (0.050 g, 0.130 mmol) and  $\text{TbCl}_3 \cdot 6\text{H}_2\text{O}$  (0.058 g, 0.156 mmol). Giving a white hygroscopic solid, **Tb.4** (0.068 g, 97%).  $m/z$  (ESMS+) 541  $[\text{M} + \text{H}]^+$   $^1\text{H}$  NMR broad resonances were not sufficiently resolved at 273 K.

7.6.3 Gadolinium (III) 1,4,7-tris(carboxymethyl)-10-(prop-2-ynyl)-1,4,7,10-tetraazacyclododecane, (**Gd.4**)



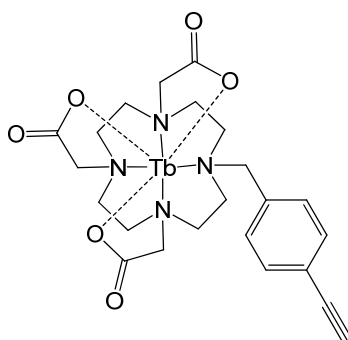
**4** (0.500 g, 1.30 mmol) and  $\text{GdCl}_3 \cdot 6\text{H}_2\text{O}$  (0.579 g, 1.562 mmol). Giving a white hygroscopic solid, **Gd.4** (0.487 g, 69%).  $m/z$  (ESMS+) 540  $[\text{M} + \text{H}]^+$  ( $^{158}\text{Gd}$ ), (HR-ESMS+)  $[\text{M} + \text{H}]^+$  calcd for  $\text{C}_{17}\text{H}_{26}\text{N}_4\text{O}_6 \text{Gd}$ ; 540.1092, found; 540.1084 ( $^{158}\text{Gd}$ ).

7.6.4 Europium (III) 1,4,7-tris(carboxymethyl)-10-(1-methyl-4-ethynylbenzene)-1,4,7,10-tetraazacyclododecane (**Eu.8**)



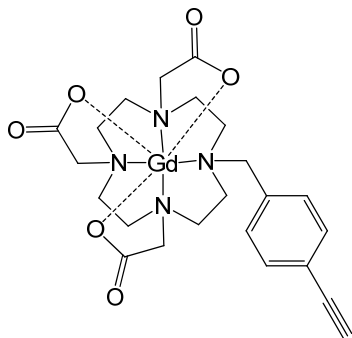
**8** (0.200 g, 0.437 mmol) and  $\text{EuCl}_3 \cdot 6\text{H}_2\text{O}$  (0.206 g, 0.565 mmol). **Eu.8** (0.221 g, 83%) was obtained as a white powder.  $\lambda_{\text{max}}$  ( $\text{H}_2\text{O}$ ): 208 and 251 nm. The  $^1\text{H}$  NMR spectrum showed broad resonances that were not sufficiently resolved at 273 K.

7.6.5 Terbium (III) 1,4,7-tris(carboxymethyl)-10-(1-methyl-4-ethynylbenzene)-1,4,7,10-tetraazacyclododecane (**Tb.8**)



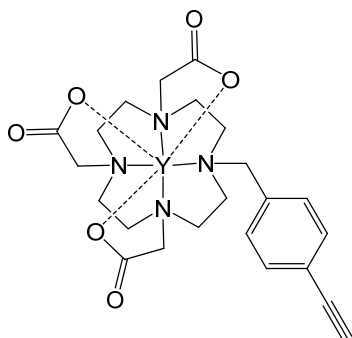
**8** (0.200 g, 0.437 mmol) and  $\text{TbCl}_3 \cdot 6\text{H}_2\text{O}$  (0.210 g, 0.565 mmol). **Tb.8** (0.217 g, 80%) was obtained as a white powder.  $\lambda_{\text{max}}$  ( $\text{H}_2\text{O}$ ): 208 and 252 nm.  $^1\text{H}$  NMR broad resonances were not sufficiently resolved at 273 K.

7.6.6 *Gadolinium (III) 1,4,7-tris(carboxymethyl)-10-(1-methyl-4-ethynylbenzene)-1,4,7,10-tetraazacyclododecane (Gd.8)*



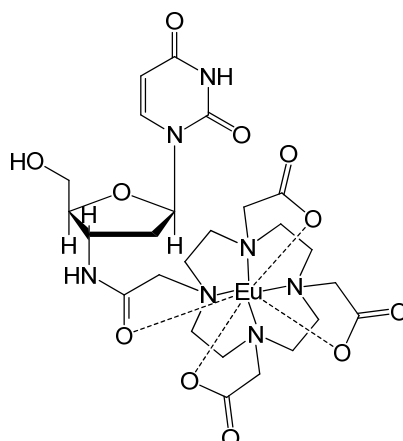
**8** (0.282 g, 0.617 mmol) and  $\text{GdCl}_3 \cdot 6\text{H}_2\text{O}$  (0.251 g, 0.678 mmol). **Gd.8** (0.375 g, 98%) was obtained as a white powder.  $\lambda_{\text{max}}$  ( $\text{H}_2\text{O}$ ): 208 and 252 nm.

7.6.7 *Yttrium (III) 1,4,7-tris(carboxymethyl)-10-(1-methyl-4-ethynylbenzene)-1,4,7,10-tetraazacyclododecane (Y.8)*



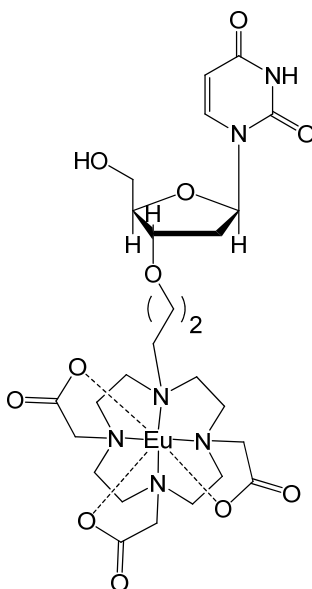
**8** (0.300 g, 0.656 mmol) and  $\text{YCl}_3 \cdot 6\text{H}_2\text{O}$  (0.218 g, 0.722 mmol). **Y.8** (0.301 g, 84%) was obtained as a white powder.  $\lambda_{\text{max}}$  ( $\text{H}_2\text{O}$ ): 206, 251 nm.  $\delta_{\text{H}}$  (400 MHz;  $\text{D}_2\text{O}$ ): 1.9 (1H, s,  $\sim\text{CCCH}\sim$ ), 2.4 – 3.4 (16 H, bm, ring H) 3.5 (8H, bm,  $\sim\text{NCH}_2\sim$ ) 7.10-7.65 (4H, bm,  $\sim\text{CCHCHC}\sim$ ).

7.6.8 *Europium (III) 1,4,7-tris(carbonylmethyl)-10-(3-acetamide-5-hydroxy-2,3-dideoxyuridine)-1,4,7,10-tetraazacyclododecane (Eu.28)*



**28** (0.010 g, 0.016 mmol) and  $\text{EuCl}_3 \cdot 6\text{H}_2\text{O}$  (0.0071 g, 0.0319 mmol) giving a white hygroscopic solid (0.008 g, 65%).

7.6.9 *Europium (III) 1,4,7-tris(carbonylmethyl)-10-(5-hydroxy-2-(3-chloropropoxy)-uridine)-1,4,7,10-tetraazacyclododecane (Eu.29)*

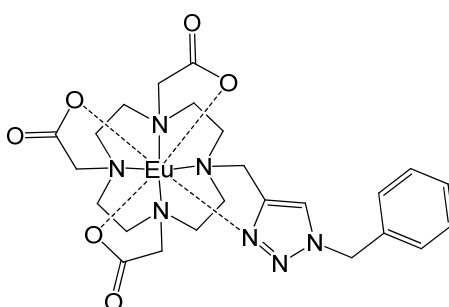


**29** (0.019 g, 0.033 mmol) and  $\text{EuCl}_3 \cdot 6\text{H}_2\text{O}$  (0.012 g, 0.034 mmol), giving a white hygroscopic solid (0.008 g, 31%).

## 7.7 'Click' Chemistry Synthesis

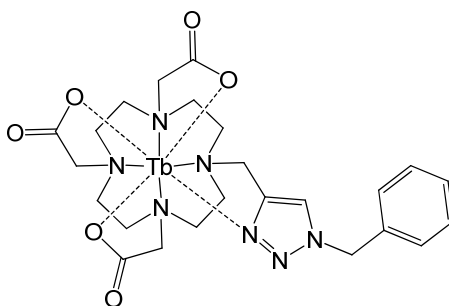
The following lanthanide compounds were prepared in this manner; **Ln.4** and sodium/alkyl azide were dissolved in EtOH/H<sub>2</sub>O (5 cm<sup>3</sup>). To this sodium ascorbate and CuSO<sub>4</sub>·5H<sub>2</sub>O were added sequentially. The solution was stirred at room temperature for 24 hours. The solution was passed down an Amberlite XAD-16 resin column. The fractions containing the complex were lyophilised to give a hygroscopic white solid.

### 7.7.1 Europium (III) 1,4,7-tris(carbonylmethyl)-10-((1-benzyl-1,2,3-triazol-4-yl)methyl)-,)-1,4,7,10-tetraazacyclododecane (**Eu.5a**)



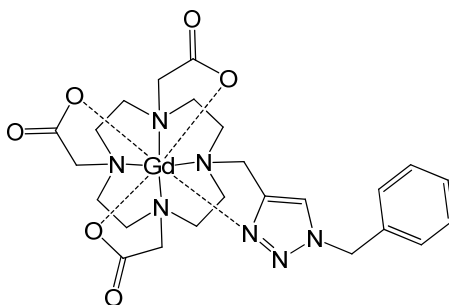
**Eu.4** (0.030 g, 0.056 mmol) benzyl azide (8.67 mg, 0.0652 mmol), sodium ascorbate (1 mg, 0.0056 mmol) and CuSO<sub>4</sub>·5H<sub>2</sub>O (0.7 mg, 0.0023 mmol). giving a hygroscopic white solid **Eu.5a** (0.021 g, 53 %).  $\delta_{\text{H}}$  (400 MHz, D<sub>2</sub>O) multiple resonances from  $\delta$  -20 to +40 ppm indicative of DOTA-like complexes of Eu(III). The four resonances shifted to highest frequency correspond to four axial ring hydrogens of the square antiprismatic geometry ( $\Delta(\lambda\lambda\lambda\lambda)/\Lambda(\delta\delta\delta\delta)$ ),  $\delta$  29.68, 27.31, 26.95, 26.29 ppm. The resonances corresponding to four axial ring hydrogens of the twisted square antiprismatic geometry; ( $\Delta(\lambda\lambda\lambda\lambda)/\Lambda(\delta\delta\delta\delta)$ ),  $\delta$  13.12, 11.34, 11.07, 10.17 ppm.  $m/z$  (ESMS+) 667 [M + H]<sup>+</sup> (<sup>151</sup>Eu).

### 7.7.2 Terbium (III) 1,4,7-tris(carbonylmethyl)-10-((1-benzyl-1,2,3-triazol-4-yl)methyl)-,)-1,4,7,10-tetraazacyclododecane (**Tb.5a**)



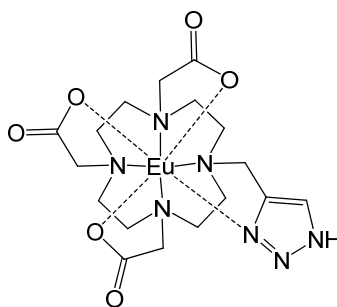
**Tb.4** (0.030 g, 0.0556 mmol) benzyl azide (8.8 mg, 0.066 mmol), sodium ascorbate (1.1 mg, 0.0056 mmol) and CuSO<sub>4</sub>·5H<sub>2</sub>O (0.7 mg, 0.0028 mmol). Giving a hygroscopic white solid **Tb.5a** (0.025 g, 66 %). *m/z* (ESMS+) 674 [M + H]<sup>+</sup>.

7.7.3 *Gadolinium (III) 1,4,7-tris(carbonylmethyl)-10-((1-benzyl-1,2,3-triazol-4-yl)methyl)-,)-1,4,7,10-tetraazacyclododecane (Gd.5a)*



**Gd.1** (0.100 g, 0.185 mmol), benzyl azide (0.029 g, 0.233 mmol), sodium ascorbate (3.6 mg, 0.0185 mmol) and CuSO<sub>4</sub>·5H<sub>2</sub>O (2.3 mg, 0.0092 mmol). Giving a hygroscopic white solid **Gd.5a** (0.074 g, 60 %). *m/z* (ESMS+) 673 [M + H]<sup>+</sup> (<sup>158</sup>Gd), (HR-ESMS-) [M - H]<sup>-</sup> calcd for C<sub>24</sub>H<sub>32</sub>N<sub>7</sub>O<sub>6</sub>Gd; 673.1733, found; 673.1730 (<sup>158</sup>Gd).

7.7.4 *Europium (III) 1,4,7-tris(carbonylmethyl)-10-((1H-1,2,3-triazol-4-yl)methyl)-,)-1,4,7,10-tetraazacyclododecane (Eu.5c)*



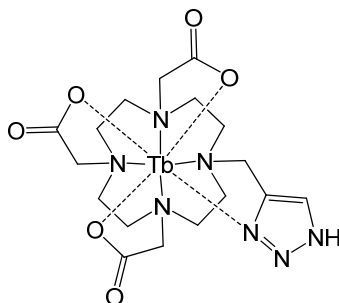
Method 1: **Eu.4** (0.030 g, 0.056 mmol) and sodium azide (0.004 g, 0.062 mmol) were dissolved in H<sub>2</sub>O (5 cm<sup>3</sup>), sodium ascorbate (1 mg, 0.0056 mmol) and CuSO<sub>4</sub>·5H<sub>2</sub>O (0.7 mg, 0.0023 mmol). Gave a hygroscopic white solid **Eu.5c** (0.022 g, 68 %).

Method 2: **5c** (25 mg, 64.9 Nmol) and EuCl<sub>3</sub>·6H<sub>2</sub>O (36 mg, 97.4 Nmol) Giving a white hygroscopic solid, **Eu.5c** (4 mg, 11%)

$\delta_{\text{H}}$  (400 MHz, D<sub>2</sub>O) multiple resonances from  $\delta$  -20 to +40 ppm indicative of DOTA-like complexes of Eu(III). The four resonances shifted to highest frequency correspond to four axial ring hydrogens of the square antiprismatic geometry

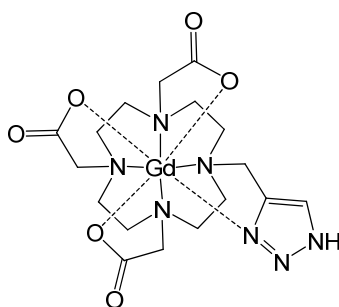
( $\Delta(\lambda\lambda\lambda\lambda)/\Lambda(\delta\delta\delta\delta)$ ),  $\delta$  33.38, 33.14, 32.58, 31.29 ppm. The resonances corresponding to four axial ring hydrogens of the twisted square antiprismatic geometry; ( $\Delta(\lambda\lambda\lambda\lambda)/\Lambda(\delta\delta\delta\delta)$ ),  $\delta$  13.55, 13.31, 11.29, 9.87 ppm.  $m/z$  (ESMS-) 574 [M - H]<sup>-</sup> (<sup>151</sup>Eu), (HR-ESMS<sup>-</sup>) [M-H]<sup>-</sup> calcd for C<sub>17</sub>H<sub>25</sub>N<sub>7</sub>O<sub>6</sub>Eu; 574.1070, found; 574.1060 (<sup>151</sup>Eu).

7.7.5 *Terbium (III) 1,4,7-tris(carbonylmethyl)-10-((1H-1,2,3-triazol-4-yl)methyl)-,)-1,4,7,10-tetraazacyclododecane (Tb.5c)*



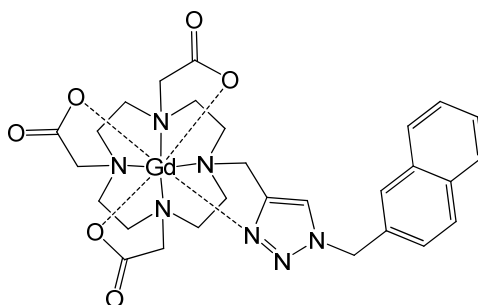
**Tb.4** (0.0341 g, 0.078 mmol) and sodium azide (5.5 mg, 0.0858 mmol) were dissolved in H<sub>2</sub>O (5 cm<sup>3</sup>), sodium ascorbate (1.54 mg, 0.0078 mmol) and CuSO<sub>4</sub>·5H<sub>2</sub>O (0.97 mg, 0.0039 mmol). Giving a hydroscopic white solid **Tb.5c** (0.027 g, 59 %).  $m/z$  (ESMS<sup>+</sup>) 582 [M + H]<sup>+</sup>.

7.7.6 *Gadolinium (III) 1,4,7-tris(carbonylmethyl)-10-((1H-1,2,3-triazol-4-yl)methyl)-,)-1,4,7,10-tetraazacyclododecane (Gd.5c)*



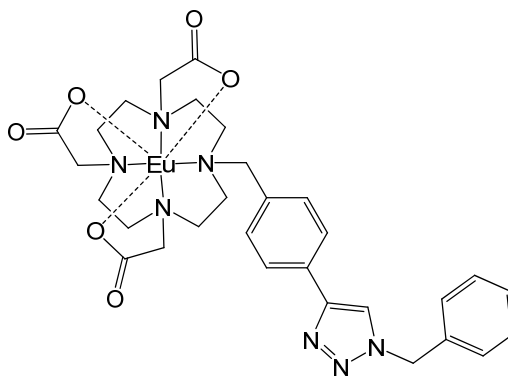
**Gd.4** (0.100 g, 0.185 mmol) and sodium azide (0.014 g, 0.223 mmol) were dissolved in H<sub>2</sub>O (5 cm<sup>3</sup>), sodium ascorbate (3.6 mg, 0.0185 mmol) and CuSO<sub>4</sub>·5H<sub>2</sub>O (3.6 mg, 0.0092 mmol). Gave a hydroscopic white solid **Gd.5c** (0.078 g, 73 %).  $m/z$  (ESMS-) 579 [M - H]<sup>-</sup> (<sup>157</sup>Gd).

7.7.7 Gadolinium (III) 1,4,7-tris(carboxymethyl)-10-((1-naphthyl-1,2,3-triazol-4-yl)methyl)-,)-1,4,7,10-tetraazacyclododecane (**Gd.5d**)



**Gd.4** (0.100 g, 0.185 mmol) naphthyl azide (0.04 g, 0.223 mmol), sodium ascorbate (3.6 mg, 0.0185 mmol) and  $\text{CuSO}_4 \cdot 5\text{H}_2\text{O}$  (2.3 mg, 0.0092 mmol). Gave a hygroscopic white solid **Gd.5d** (0.03 g, 22%).  $m/z$  (ESMS+) 723  $[\text{M} + \text{H}]^+$  ( $^{157}\text{Gd}$ ).

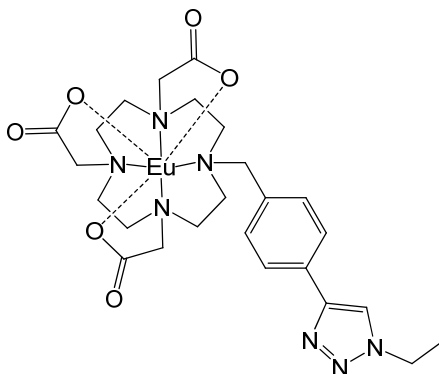
7.7.8 Europium (III) 1,4,7-tris(carboxymethyl)-10-(1-methyl-4-(1-phenyl-1,2,3-triazol-4-yl)-benzene)-1,4,7,10-tetraazacyclododecane (**Eu.12**)



**12** (0.030 g, 0.0505 mmol) and  $\text{EuCl}_3 \cdot 6\text{H}_2\text{O}$  (0.02 g, 0.0556 mmol). **Eu.12** (0.031 g, 82%) was obtained as a white powder.  $m/z$  (ESMS+) 781  $[\text{M} + \text{K}]^+$ , with Eu isotope pattern ( $^{151}\text{Eu}$ ).

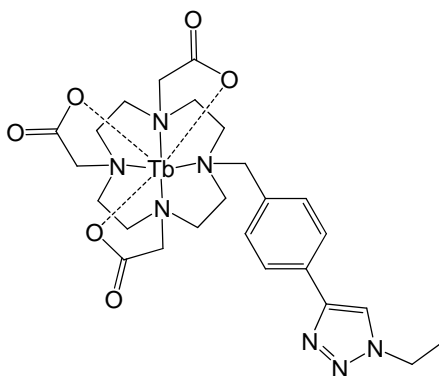
**Eu.8** (0.020 g, 0.0328 mmol), sodium azide (2.56 mg, 0.039 mmol) and benzyl bromide (6.17 mg, 4.2  $\mu\text{l}$ , 0.0361 mmol) were dissolved in  $\text{EtOH}/\text{H}_2\text{O}$  (5  $\text{cm}^3$ ). To this sodium ascorbate (0.65 mg, 0.0032 mmol) and  $\text{CuSO}_4 \cdot 5\text{H}_2\text{O}$  (0.4m g, 0.0016 mmol) were added sequentially, to give a hygroscopic white solid (0.02 g, 82 %).

7.7.9 *Europium (III) 1,4,7-tris(carboxymethyl)-10-(1-methyl-4-(1-ethyl-1,2,3-triazo-4-yl)-benzene)-1,4,7,10-tetraazacyclododecane. (Eu.15)*



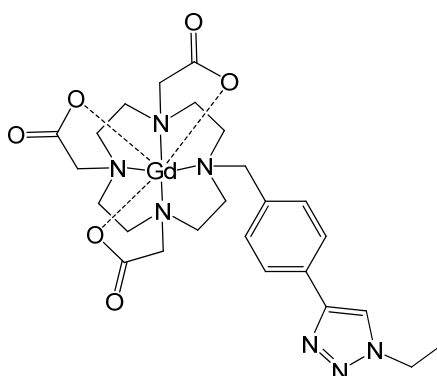
**Eu.8** (0.03 g, 49.3  $\mu\text{mol}$ ), ethyl bromide (6.39 mg, 4.3  $\mu\text{l}$ , 59.2  $\mu\text{mol}$ ), sodium azide (3.8 mg, 59.2  $\mu\text{mol}$ ), sodium ascorbate (0.97 mg, 4.9  $\mu\text{mol}$ ) and  $\text{CuSO}_4 \cdot 5\text{H}_2\text{O}$  (0.61 mg, 2.4  $\mu\text{mol}$ ). **Eu.15** (0.022 g, 65%) was obtained as a white powder.  $\lambda_{\text{max}}$  ( $\text{H}_2\text{O}$ ); 213, 249 and 297 nm.

7.7.10 *Terbium (III) 1,4,7-tris(carboxymethyl)-10-(1-methyl-4-(1-ethyl-1,2,3-triazo-4-yl)-benzene)-1,4,7,10-tetraazacyclododecane (Tb.15)*



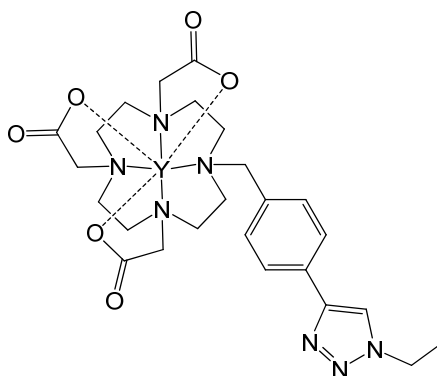
**Tb.8** (0.030 g, 48.7  $\mu\text{mol}$ ), ethyl bromide (6.32 mg, 4.3  $\mu\text{mol}$ , 58.5  $\mu\text{mol}$ ), sodium azide (3.8 mg, 58.5  $\mu\text{mol}$ ), sodium ascorbate (0.96 mg, 4.87  $\mu\text{mol}$ ) and  $\text{CuSO}_4 \cdot 5\text{H}_2\text{O}$  (0.6 mg, 2.4  $\mu\text{mol}$ ). **Tb.15** (14 mg, 42%) was obtained as a white powder.  $\lambda_{\text{max}}$  ( $\text{H}_2\text{O}$ ); 198, 255 and 294 nm

7.7.11 Gadolinium (III) 1,4,7-tris(carboxymethyl)-10-(1-methyl-4-(1-ethyl-1,2,3-triazo-4-yl)-benzene)-1,4,7,10-tetraazacyclododecane (**Gd.15**)



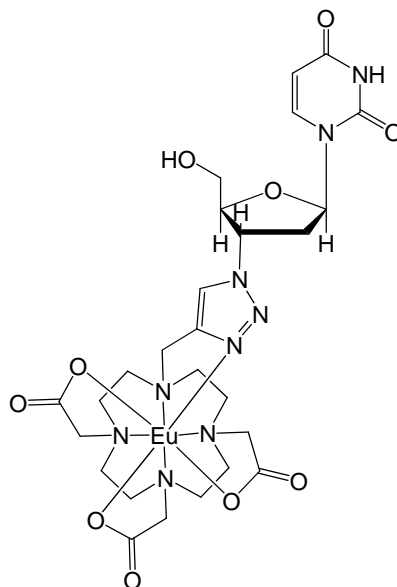
**Gd.8** (0.100 g, 0.162 mmol), ethyl bromide (0.0193 g, 13.57  $\mu$ l, 0.179 mmol), sodium azide (11.6 mg, 0.179 mmol), sodium ascorbate (3.2 g, 16.2  $\mu$ mol) and  $\text{CuSO}_4 \cdot 5\text{H}_2\text{O}$  (2 mg, 8.1  $\mu$ mol). **Gd.15** (0.018 g, 16%) was obtained as a white powder.  $\lambda_{\text{max}}$  ( $\text{H}_2\text{O}$ ); 195, 250 and 298 nm.

7.7.12 Yttrium (III) 1,4,7-tris(carboxymethyl)-10-(1-methyl-4-(1-ethyl-1,2,3-triazo-4-yl)-benzene)-1,4,7,10-tetraazacyclododecane (**Y.15**)



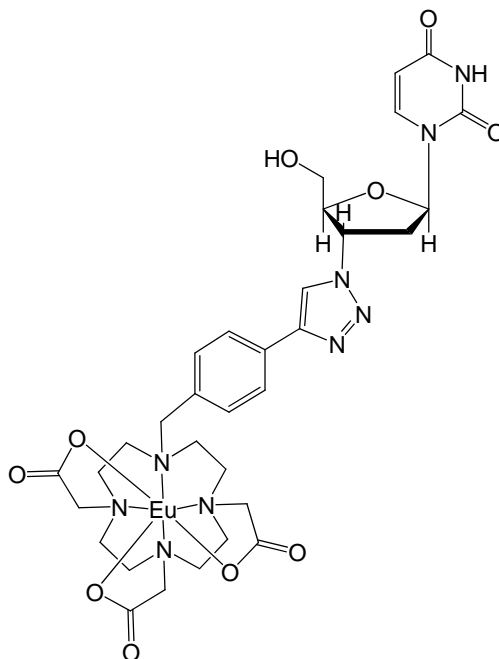
**Y.8** (0.100 g, 0.183 mmol), ethyl bromide (0.0217 g, 15  $\mu$ l, 0.201 mmol), sodium azide (0.013 g, 0.201 mmol), sodium ascorbate (3.6 mg, 18  $\mu$ mol) and  $\text{CuSO}_4 \cdot 5\text{H}_2\text{O}$  (2.2 mg, 9  $\mu$ mol). **Y.18** (0.041 g, 36%) was obtained as a white powder.  $\lambda_{\text{max}}$  ( $\text{H}_2\text{O}$ ); 197, 255 and 297 nm.  $\delta_{\text{H}}$  (400 MHz;  $\text{D}_2\text{O}$ ) 1.15 (3H, d,  $\sim\text{NCH}_2\text{CH}_3$ ), 2.4 – 3.4 (16 H, bm, ring H) 3.5 (8H, bm,  $\sim\text{NCH}_2$ ), 4.05 (2H, m,  $\sim\text{NCH}_2\text{CH}_3$ ) 8.10-8.65 (4H, bm,  $\sim\text{CCHCHC}$ ), 8.59 (1H, s,  $\sim\text{CCHN}$ ).

7.7.13 *Europium(III)1,4,7-tris(carbonylmethyl)-10-((1-2,3-dideoxyuridine-1,2,3-triazol-4-yl)methyl)-,)-1,4,7,10-tetraazacyclododecane (Eu.30)*



**Eu.4** (0.021 g, 0.039 mmol), **24** (0.01 g, 0.039 mmol), sodium ascorbate (0.8 mg, 0.0039 mmol) and  $\text{CuSO}_4 \cdot 5\text{H}_2\text{O}$  (0.5m g, 0.0019 mmol), gave a hygroscopic white solid (0.01 g, 32%).

7.7.14 *Europium(III)1,4,7-tris(carbonylmethyl)-10-(4-(2,3-dideoxyuridine-1,2,3-triazol-4-yl)-1-methyl-benzene)-,)-1,4,7,10-tetraazacyclododecane (Eu.31)*

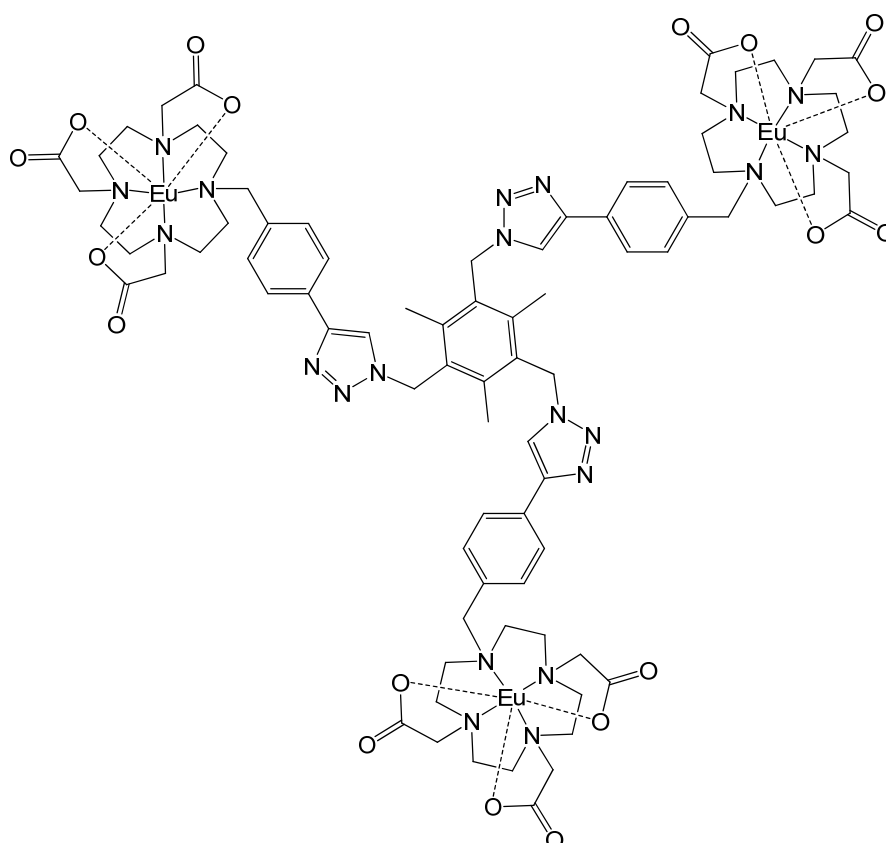


**Eu.8** (0.024 g, 0.039 mmol), **24** (0.010 g, 0.039 mmol), sodium ascorbate (0.8 mg, 0.0039 mmol) and  $\text{CuSO}_4 \cdot 5\text{H}_2\text{O}$  (0.5 mg, 0.0019 mmol), gave a hygroscopic white solid (0.017 g, 50%).

## 7.8 Synthesis of Multimeric Compounds

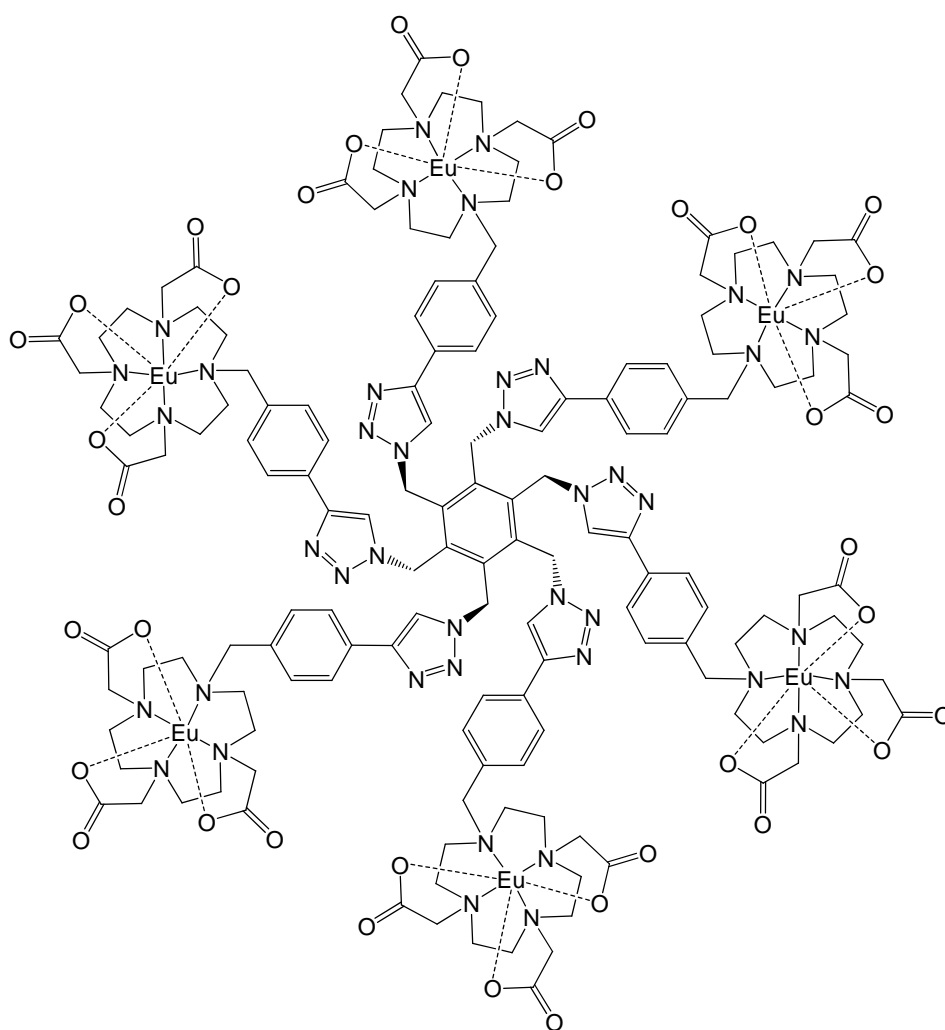
The following compounds were prepared in the same manner: **Ln.8**, sodium azide and alkyl bromide were dissolved in THF/ $\text{H}_2\text{O}$  ( $25 \text{ cm}^3$ ). To this sodium ascorbate and  $\text{CuSO}_4 \cdot 5\text{H}_2\text{O}$  were added sequentially. The solution was heated at  $60^\circ\text{C}$  for 24 hours. The THF was removed under reduced pressure and water ( $25 \text{ cm}^3$ ) was added to precipitate any unreacted alkyl bromide. The solution was filtered and lyophilised to give a green solid, which was purified by HPLC. The fractions containing the complex were lyophilised to give a hygroscopic white solid.

7.8.1 *1,3,5-Tris((Europium (III) 1,4,7-tris(carboxymethyl)-10-(1-methyl-4-(1,2,3-triazolo-4-yl)-benzene)-1,4,7,10-tetraazacyclododecane)-methyl)-2,4,6-tris (methyl), benzene (Eu.13)*



**Eu.8** (0.061 g, 0.1 mmol), 1,3,5,-tris-(bromomethyl)-2,4,6,-tris-(methyl)-benzene (0.010 g, 0.025 mmol), sodium azide (8.6 mg, 0.125 mmol), sodium ascorbate (1.49 mg, 7.5  $\mu$ mol) and CuSO<sub>4</sub>.5H<sub>2</sub>O (0.93 mg, 3.7  $\mu$ mol). The sample was purified by HPLC water: MeOH (25%, 20 mins - 100%, 35 mins). **Eu.13** (0.010 g, 19%) was obtained as a white powder. HPLC: elution time 21.4 mins,  $\lambda_{\max}$  (H<sub>2</sub>O); 213, 249 and 297 nm.

7.8.2 *1,2,3,4,5,6-Hexa-((Europium (III) 1,4,7-tris(carboxymethyl)-10-(1-methyl-4-(1,2,3-triazo-4-yl)-benzene)-1,4,7,10-tetraazacyclododecane)-methyl)-benzene. (Eu.14)*



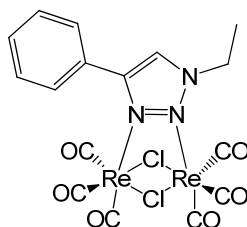
**Eu.8** (0.067 g, 0.11 mmol), hexakis-(bromomethyl)-benzene (10 mg, 0.0157 mmol), sodium azide (8.18 mg, 0.125 mmol), sodium ascorbate (1.8 mg, 9.4  $\mu$ mol) and CuSO<sub>4</sub>.5H<sub>2</sub>O (1.17 mg, 4.7  $\mu$ mol). The sample was purified by HPLC water: MeOH (20%,

25 mins - 100%, 40 mins). **Eu.14** (0.004 g, 6%) was obtained as a white powder. HPLC: elution time 26.35 mins,  $\lambda_{\max}$  (H<sub>2</sub>O); 194, 251 and 299 nm.

## 7.9 Rhenium Complexation

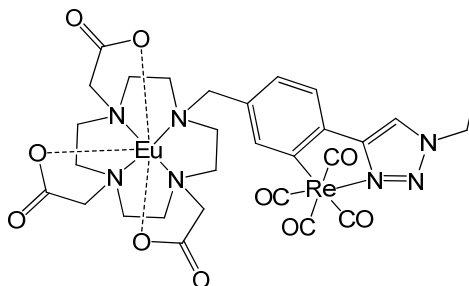
The following compounds were all prepared in the same manner: **Ln.15** and Rhenium penta-carbonyl chloride were taken up in isopropanol:water (3:1) (2 cm<sup>3</sup>) and heated *via* microwave radiation at 90°C for 30 mins (100W), the solution was concentrated, giving a orange solid.

### 7.9.1 Synthesis of **14c**



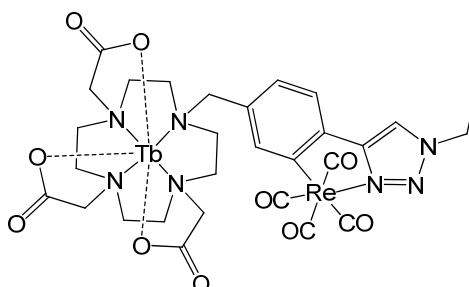
**13** (0.020 g, 0.115 mmol), Re(CO)<sub>5</sub>Cl (0.041 g, 0.115 mmol). Gave an orange solid (54 mg) that was crystallised from CHCl<sub>3</sub>, yielding colourless crystals, (20 mg, 22%).  $\delta_{\text{H}}$  (400 MHz, CDCl<sub>3</sub>): 1.79 (3H, t,  $^3J_{\text{HH}}$  7.4Hz, ~NCH<sub>2</sub>CH<sub>3</sub>~), 4.3 (2H, q,  $^3J_{\text{HH}}$  7.4Hz, ~NCH<sub>2</sub>CH<sub>3</sub>~), 7.12 (2H, d,  $^3J_{\text{HH}}$  7.0Hz, ~CHCHC~), 7.25 (1H, t,  $^3J_{\text{HH}}$  7.4Hz ~CHCHCHCHCH~), 7.34 (2H, t,  $^3J_{\text{HH}}$  7.4Hz, ~CHCHCHC~), 7.81(1H, s, ~CCHN~). *m/z* (ESMS+) 785 [M + H]<sup>+</sup>.

7.9.2 *Europium (III) 1,4,7-tris(carboxymethyl)-10-(1-methyl-4-(1-ethyl-2,3-rhenium-hexacarbonyl-dichloride-1,2,3-triazo-4-yl)-benzene)-1,4,7,10-tetraazacyclododecane. (Eu.Re.16)*



**Eu.15** (0.005 g, 7.34  $\mu\text{mol}$ ),  $\text{Re}(\text{CO})_5\text{Cl}$  (0.0026 g, 7.34  $\mu\text{mol}$ ). Giving an orange solid, **Eu.Re.16** (5 mg, 53%).  $\lambda_{\text{max}}$  ( $\text{H}_2\text{O}$ ); 210 and 263 nm.

7.9.3 *Terbium (III) 1,4,7-tris(carboxymethyl)-10-(1-methyl-4-(1-ethyl-2,3-rhenium-hexacarbonyl-dichloride-1,2,3-triazo-4-yl)-benzene)-1,4,7,10-tetraazacyclododecane (Tb.Re.16)*



**Tb.15** (0.010 g, 14.5  $\mu\text{mol}$ ),  $\text{Re}(\text{CO})_5\text{Cl}$  (5.25 mg, 14.5  $\mu\text{mol}$ ). Giving an orange solid, **Tb.Re.16** (8 mg, 42%).  $\lambda_{\text{max}}$  ( $\text{H}_2\text{O}$ ); 208 and 262 nm.



## 7.10 References

1. L.-Y. Wu, Z.-Y. Yan, Y.-X. Xie, Y.-N. Niu and Y.-M. Liang, *Tetrahedron Asymmetry*, 2007, **18**, 2086.
2. V. Aucagne, J. Berna, J. D. Crowley, S. M. Goldup, K. D. Hanni, D. A. Leigh, P. J. Lusby, V. E. Ronaldson, A. M. Z. Slawin, A. Viterisi and D. B. Walker, *J. Am. Chem. Soc.*, 2007, **129**, 11950.
3. Q. Zhang and J. M. Takacs, *Organic Letters*, 2008, **10**, 545.
4. P. Mathew, A. Neels and M. Albrecht, *J. Am. Chem. Soc.*, 2008, **130**, 13534.
5. K. Nishiyama and H. Karigomi, *Chem. Lett.*, 1982, 1477.
6. T. Lin and W. R. Mancini, *J. Med. Chem.*, 1983, **26**, 54.
7. R. Griffin, PhD Thesis, University of Leicester, 2007.
8. A. Beeby, L. M. Bushby, D. Maffeo and J. A. G. Williams, *J. Chem. Soc., Dalton Trans.*, **2002**, 48.
9. L. M. Shultze and A. R. Bulls, U. S. patent 5,631,368, **1997**; *Chem. Abstr.*, **1996**, 125, 315328.patent

## Chapter 8

### Appendix

#### 8.1 Courses and Conferences

##### 8.1.1 Lecture Courses

Metals in Medicine, 5 credits, 2.2

Pharmaceutical Chemistry, 10 credits, 2.1

##### 8.1.2 Training Courses

###### *Induction*

03/10/06 Departmental induction

04/10/06 Graduate school induction

05/10/06 Cross-faculty general scientific induction

###### *Information skills*

09/10/06 Introduction to techniques

12/10/06 Introduction to using Bibliographic Software Packages

08/11/06 Introduction to chemical information database

15/11/06 1D NMR spectroscopy

22/11/06 2D NMR spectroscopy

14/02/07 The nOe Effect

30/05/07 Presentation of NMR data

###### *Study skills*

21/02/07 Project managing PhD

28/02/07 More efficient reading and note taking

28/03/07 Presentation skills

##### 8.1.3 Conferences Attended

###### 8.1.3.1 Oral Communication

“Applications of click chemistry within lanthanide complexes: a Word of Caution”

**G. J. Stasiuk**, M. P. Lowe, *August 2009*, ICFE-Conference, Cologne (Germany)

#### 8.1.3.2 Posters Presentations

“Click chemistry within lanthanide complexes: a Word of Caution” **G. J. Stasiuk**, M. P. Lowe, *August 2009*, ICFE-Conference, Cologne (Germany)

“Click Chemistry with Lanthanide complexes: a Word of Caution” **G. J. Stasiuk**, M. P. Lowe, *June 2009*, CCDG-meeting, Leeds (UK)

“Incorporation of ‘Click’ chemistry into lanthanide chelates” **G. J. Stasiuk**, M. P. Lowe, *September 2008*, D-38 COST, working group 1 and 6 Meeting Trinity College, Dublin. (Ireland)

“Incorporation of ‘Click’ chemistry into lanthanide chelates” **G. J. Stasiuk**, M. P. Lowe, *May 2008*, D-38 COST Meeting Lisbon (Portugal)

“Incorporation of ‘Click’ chemistry into lanthanide chelates” **G. J. Stasiuk**, M. P. Lowe, *April 2008*, Daltons Meeting midlands section, Warwick (UK).

#### 8.1.4 Publications

“Click Chemistry with Lanthanide complexes: a Word of Caution” **G.J. Stasiuk** and M.P. Lowe, *Dalton Trans.*, 2009, 9725 – 9727

“Changing the local coordination environment in mono- and bi- metallic lanthanide complexes through “click” chemistry” M. Jauregui, W. S. Perry, C. Allain, L. R. Vidler, M. C. Willis, A. M. Kenwright, J. S. Snaith, **G. J. Stasiuk**, M. P. Lowe and S. Faulkner, *Dalton Trans.*, 2009, 6283 – 6285.

#### 8.1.5 Demonstrating

31/10/06 – 12/12/06 3<sup>rd</sup> Year advanced Inorganic Practical

31/10/07 – 15/12/07 3<sup>rd</sup> Year advanced Inorganic Practical

31/01/09 – 02/03/09 3<sup>rd</sup> Year advanced Inorganic Practical

### 8.1.6 Seminars Attended

22/11/06 Mini symposium "Aspects of Green Chemistry"

Dr Neil Winterton (University of Liverpool)

*"Ionic Liquids: Hype or Help"*

Dr Peter Licence (University of Nottingham)

*"Ionic Liquids in-vacuo"*

Dr Paul Watts (University of Hull)

*"The application of micro reactors for improving atom efficient chemical reactions"*

30/04/07 Mini symposium "Metals in Medicine"

Dr Sofia Pascu (University of Oxford)

*"Designing Small Molecule-based Probes for In Vitro Fluorescence Imaging"*

Prof. Nils Metzler-Nolte (Rhur-Universitaet Bochum, Germany)

*"Labelling of Bioactive Peptide with organometallic Compounds: From Basic Chemistry to Biomedical Application"*

Dr Gareth Williams (Durham University)

*"Sensing and Imaging with Cell-permeable Luminescent Platinum and Iridium Complexes"*

Prof. Chris Orvig (University of British Columbia, Canada)

*"Carbohydrate Conjugates in Medicinal Inorganic Chemistry"*

09/05/07 Mini-symposium "Aspects of catalysis"

Dr Ian Fairlamb (University of York)

*"Ligand effects in Pd catalysed processes: Importance of conformational flexibility and the exploitation of non-innocent alkene ligands"*

Prof. Simon Woodward (University of Nottingham)

*“Organic ‘Couplings’ via New Metallic Chemistry of Al, Ni, Cu and Zn”*

Dr David Willock (University of Cardiff)

*“Simulation of adsorption and Reaction at catalyst surfaces”*

- 06/05/08 Prof. T. Don Tilley  
*“New stoichiometric and catalytic transformations involving transition metal- silicon systems”*
- 29/10/08 Dr George Britovsek (Imperial College)  
*“Tuning the Reactivity of Non-heme Iron Catalysts for the Oxidation of Alkanes”*
- 05/11/08 Dr Paul Davies (Birmingham)  
*“Organic Synthesis by Gold Catalysed Alkyne Activation”*
- 19/11/08 Prof. Rudolf Allemann (Cardiff)  
*“Generation of structural diversity in class 1 terpenoid synthesis”*
- 01/12/08 Prof. Andrea T. Vasella (Zurich) RSC Haworth Lecture  
*“Inspiration from carbohydrates”*
- 25/02/09 Prof. Martin Willis  
*“Asymmetric catalysis for the asymmetric reduction of ketones to imines”*
- 09/03/09 Prof. Joe Harity (Sheffield)  
*“development of new strategies for the synthesis of functionalised synthetic intermediates”*
- 18/03/09 Mini symposium “Synthetic Chemistry for Synthetic Biology. Is This the Path to Take?”  
Prof. Anthony Davis (Bristol)  
*“Synthetic Lectins: Receptors for Carbohydrates in Aqueous Media”*  
Dr. Michael Gait (MRC Laboratory of Molecular Biology, Cambridge)  
*“Synthetic Approaches on Enhancing Therapeutic Oligonucleotide Delivery”*  
Prof. Steve Howdle (Nottingham)  
*“Supercritical Fluids: A Clean Approach to Polymers, Biomaterials and Drug Delivery”*
- 06/05/09 Prof. James Clark (York)  
*“Green Chemistry and the biorefinery”*

## 8.2 X-ray Crystallography Data

### 8.2.1 X ray Data for 3c

Table 8.1 Crystal data and structure refinement for 08019.

Identification code	08019	
Empirical formula	C <sub>29</sub> H <sub>59</sub> N <sub>7</sub> O <sub>9</sub>	
Formula weight	649.83	
Temperature	150(2) K	
Wavelength	0.71073 Å	
Crystal system	Monoclinic	
Space group	P2(1)	
Unit cell dimensions	a = 9.5329(15) Å	α = 90°.
	b = 10.5318(17) Å	β = 100.029(3)°.
	c = 18.128(3) Å	γ = 90°.
Volume	1792.2(5) Å <sup>3</sup>	
Z	2	
Density (calculated)	1.204 Mg/m <sup>3</sup>	
Absorption coefficient	0.089 mm <sup>-1</sup>	
F(000)	708	
Crystal size	0.35 x 0.21 x 0.18 mm <sup>3</sup>	
Theta range for data collection	2.17 to 25.00°.	
Index ranges	-11 ≤ h ≤ 11, -12 ≤ k ≤ 12, -21 ≤ l ≤ 21	
Reflections collected	12992	
Independent reflections	3342 [R(int) = 0.0372]	
Completeness to theta = 25.00°	99.9 %	
Absorption correction	None	
Refinement method	Full-matrix least-squares on F <sup>2</sup>	
Data / restraints / parameters	3342 / 1 / 421	
Goodness-of-fit on F <sup>2</sup>	1.019	
Final R indices [I > 2σ(I)]	R1 = 0.0395, wR2 = 0.0922	
R indices (all data)	R1 = 0.0458, wR2 = 0.0947	
Absolute structure parameter	-10(10)	
Largest diff. peak and hole	0.401 and -0.260 e.Å <sup>-3</sup>	

O(1)-C(10)	1.331(4)	C(1)-H(1A)	0.99	C(12)-H(12C)	0.98	C(23)-C(25)	1.514(5)
O(1)-C(11)	1.489(4)	C(1)-H(1B)	0.99	C(13)-H(13A)	0.98	C(24)-H(24A)	0.98
O(2)-C(10)	1.193(4)	C(2)-H(2A)	0.99	C(13)-H(13B)	0.98	C(24)-H(24B)	0.98
O(3)-C(16)	1.346(4)	C(2)-H(2B)	0.99	C(13)-H(13C)	0.98	C(24)-H(24C)	0.98
O(3)-C(17)	1.478(3)	C(3)-C(4)	1.514(4)	C(14)-H(14A)	0.98	C(25)-H(25A)	0.98
O(4)-C(16)	1.207(3)	C(3)-H(3A)	0.99	C(14)-H(14B)	0.98	C(25)-H(25B)	0.98
O(5)-C(22)	1.328(4)	C(3)-H(3B)	0.99	C(14)-H(14C)	0.98	C(25)-H(25C)	0.98
O(5)-C(23)	1.496(3)	C(4)-H(4A)	0.99	C(15)-C(16)	1.521(4)	C(26)-H(26A)	0.98
O(6)-C(22)	1.211(4)	C(4)-H(4B)	0.99	C(15)-H(15A)	0.99	C(26)-H(26B)	0.98
N(1)-C(1)	1.514(4)	C(5)-C(6)	1.516(4)	C(15)-H(15B)	0.99	C(26)-H(26C)	0.98
N(1)-C(8)	1.515(4)	C(5)-H(5A)	0.99	C(17)-C(18)	1.513(5)	C(27)-C(28)	1.489(4)
N(1)-C(27)	1.526(3)	C(5)-H(5B)	0.99	C(17)-C(19)	1.516(4)	C(27)-H(27A)	0.99
N(2)-C(9)	1.454(4)	C(6)-H(6A)	0.99	C(17)-C(20)	1.518(4)	C(27)-H(27B)	0.99
N(2)-C(3)	1.461(4)	C(6)-H(6B)	0.99	C(18)-H(18A)	0.98	C(28)-C(29)	1.379(4)
N(2)-C(2)	1.472(4)	C(7)-C(8)	1.525(4)	C(18)-H(18B)	0.98	C(29)-H(29)	0.95
N(3)-C(15)	1.458(4)	C(7)-H(7A)	0.99	C(18)-H(18C)	0.98	O(7)-H(7C)	0.867
N(3)-C(4)	1.470(4)	C(7)-H(7B)	0.99	C(19)-H(19A)	0.98	O(7)-H(7D)	0.8708
N(3)-C(5)	1.474(4)	C(8)-H(8A)	0.99	C(19)-H(19B)	0.98	O(8)-H(8C)	0.8727
N(4)-C(7)	1.457(4)	C(8)-H(8B)	0.99	C(19)-H(19C)	0.98	O(8)-H(8D)	0.8696
N(4)-C(21)	1.463(4)	C(9)-C(10)	1.521(4)	C(20)-H(20A)	0.98	O(9)-H(9C)	0.668
N(4)-C(6)	1.479(3)	C(9)-H(9A)	0.99	C(20)-H(20B)	0.98	O(9)-H(9D)	1.0347
N(5)-N(6)	1.340(3)	C(9)-H(9B)	0.99	C(20)-H(20C)	0.98		
N(5)-C(28)	1.344(4)	C(11)-C(12)	1.492(5)	C(21)-C(22)	1.497(4)		
N(6)-N(7)	1.327(4)	C(11)-C(14)	1.505(5)	C(21)-H(21A)	0.99		
N(7)-C(29)	1.329(4)	C(11)-C(13)	1.506(6)	C(21)-H(21B)	0.99		
N(7)-H(7)	0.88	C(12)- H(12A)	0.98	C(23)-C(24)	1.510(5)		
C(1)-C(2)	1.505(4)	C(12)- H(12B)	0.98	C(23)-C(26)	1.512(5)		

Table 8.2 bond lengths for **3c**, Å

## 8.2.2 X ray Data for **14c**

Table 8.3 Crystal data and structure refinement for 09063.

Identification code	09063	
Empirical formula	C <sub>16</sub> H <sub>11</sub> Cl <sub>2</sub> N <sub>3</sub> O <sub>6</sub> Re <sub>2</sub>	
Formula weight	784.58	
Temperature	150(2) K	
Wavelength	0.71073 Å	
Crystal system	Monoclinic	
Space group	P2(1)/c	
Unit cell dimensions	a = 12.260(6) Å	α = 90°.
	b = 10.543(5) Å	β = 93.646(8)°.
	c = 16.118(8) Å	γ = 90°.
Volume	2079.2(17) Å <sup>3</sup>	
Z	4	
Density (calculated)	2.506 Mg/m <sup>3</sup>	
Absorption coefficient	11.928 mm <sup>-1</sup>	
F(000)	1440	
Crystal size	0.42 x 0.35 x 0.15 mm <sup>3</sup>	
Theta range for data collection	1.66 to 27.00°.	
Index ranges	-15 ≤ h ≤ 15, -13 ≤ k ≤ 13, -20 ≤ l ≤ 20	
Reflections collected	16809	
Independent reflections	4528 [R(int) = 0.0744]	
Completeness to theta = 27.00°	99.6 %	
Absorption correction	Empirical	
Max. and min. transmission	0.862 and 0.299	
Refinement method	Full-matrix least-squares on F <sup>2</sup>	
Data / restraints / parameters	4528 / 0 / 263	
Goodness-of-fit on F <sup>2</sup>	1.081	
Final R indices [I > 2σ(I)]	R1 = 0.0371, wR2 = 0.0883	
R indices (all data)	R1 = 0.0423, wR2 = 0.0906	
Largest diff. peak and hole	3.020 and -3.056 e.Å <sup>-3</sup>	

Re(1)-C(2)	1.915(7)	N(3)-C(15)	1.462(8)
Re(1)-C(1)	1.916(7)	C(7)-C(8)	1.368(8)
Re(1)-C(3)	1.922(7)	C(7)-H(7)	0.95
Re(1)-N(1)	2.205(5)	C(8)-C(9)	1.484(8)
Re(1)-Cl(2)	2.4924(19)	C(9)-C(14)	1.383(9)
Re(1)-Cl(1)	2.5092(19)	C(9)-C(10)	1.384(9)
Re(2)-C(4)	1.907(7)	C(10)-C(11)	1.377(9)
Re(2)-C(5)	1.913(7)	C(10)-H(10)	0.95
Re(2)-C(6)	1.929(7)	C(11)-C(12)	1.370(10)
Re(2)-N(2)	2.200(5)	C(11)-H(11)	0.95
Re(2)-Cl(2)	2.499(2)	C(12)-C(13)	1.381(11)
Re(2)-Cl(1)	2.5084(17)	C(12)-H(12)	0.95
O(1)-C(1)	1.139(8)	C(13)-C(14)	1.387(10)
O(2)-C(2)	1.146(8)	C(13)-H(13)	0.95
O(3)-C(3)	1.146(9)	C(14)-H(14)	0.95
O(4)-C(4)	1.136(8)	C(15)-C(16)	1.500(9)
O(5)-C(5)	1.139(8)	C(15)-H(15A)	0.99
O(6)-C(6)	1.140(8)	C(15)-H(15B)	0.99
N(1)-N(2)	1.334(7)	C(16)-H(16A)	0.98
N(1)-N(3)	1.341(7)	C(16)-H(16B)	0.98
N(2)-C(8)	1.364(8)	C(16)-H(16C)	0.98
N(3)-C(7)	1.343(8)		

Table 8.4 bond lengths for **14c**, Å